CRANFIELD UNIVERSITY

Andrew Martin Rolt

Enhancing Aero Engine Performance through Synergistic Combinations of Advanced Technologies

School of Aerospace, Transport and Manufacturing
PhD in Aerospace by Research

PhD Thesis
Academic Year: 2015 - 2018

Supervisor: Dr Vishal Sethi
Associate Supervisor: Dr Devaiah Nalianda
July 2019

CRANFIELD UNIVERSITY

School of Aerospace, Transport and Manufacturing
PhD in Aerospace by Research

PhD

Academic Year 2015 - 2018

Andrew Martin Rolt

Enhancing Aero Engine Performance through Synergistic Combinations of Advanced Technologies

Supervisor: Dr Vishal Sethi
Associate Supervisor: Dr Devaiah Nalianda
July 2019

ABSTRACT

By 2050 the evolutionary approach to aero engine research and development will no longer be able to maintain historic rates of performance improvement. Future geared fan and open rotor engines promise increased propulsive efficiency and reduced noise, but will need to incorporate new technologies to improve core thermal efficiency in order to meet the ambitious fuel-burn and emissions targets set by ACARE in Flightpath 2050. In the face of increasing air traffic, radical new approaches will be needed to minimize the impact of aviation on the environment. A long-term vision is required.

This PhD project investigates the potential of innovative propulsion technologies for civil aviation. Candidate technologies include topping and bottoming cycles, secondary combustion, intercooling and recuperation. The reported research investigates potential synergies between these advanced core technologies that when integrated together should give a significant fuel burn reduction relative to a more-conventional year-2050 ‘reference’ Brayton-cycle turbofan.

Spreadsheet models have been used to quantify performance and estimate the weight and fuel burn savings for each new engine cycle. Further models were created to investigate preferred topping and bottoming cycle arrangements. NOx emissions are estimated for engines with rich-quench-lean (RQL) or lean-direct-injection (LDI) combustors. The correlation for future LDI combustor NOx emissions was selected following a review of recent LDI combustor research and a detailed study of alternative options.

Increasingly aerodynamically efficient and lighter weight aircraft with more efficient engines will have lower thrust requirements. Advanced engine cycles also generally increase core specific power and reduce core mass flow, so future engines will have smaller turbo-machines that will tend to have lower component efficiencies. Therefore a preliminary study investigated the effects of thrust-scaling on the efficiency of the reference turbofan and possible high-OPR intercooled engines, since these could have very small core components.

Novel core-component designs and engine architectures can minimize these penalties. Positive-displacement topping-cycle machines and reverse-flow-core engine layouts should help to maintain component efficiency and improve SFC, but low weight and low drag are also essential to minimize fuel burn. Therefore weight assessments of the advanced engine designs were made, and fuel-burn exchange rates used to quantify expected mission-level CO_2 reductions.

Following a qualitative assessment of synergies between potential advanced technologies, an engine that combines intercooling, a topping cycle, secondary combustion and an open-air-cycle bottoming cycle was selected for detailed study. While each of these technologies has been researched previously, the contribution and value that each advanced core technology could bring to the whole in a large geared turbofan has not so far been reported. The approach initiated was to model a series of engines omitting each technology in turn and this scheme has been partially realized. The modelled topping-cycle technology uses six nutating-disc modules as a replacement for conventional combustors, high pressure compressors and turbines. A nutating-disc core module concept design led to the creation of a display model that was shown on the ULTIMATE project stand at the 2018 Farnborough International Air Show.

The selected cycle combining all four technologies should reduce SFC by about 15% relative to the reference year-2050 turbofan and is assessed to reduce fuel burn by up to 18.5% in a long-range aircraft. An engine with intercooling, intra-turbine combustion and a bottoming cycle reduces SFC by about 6%, and an engine that is simply intercooled reduces SFC by about 3%. The topping cycle gives the biggest potential thermal efficiency improvement, but nutating-disc technology presents very significant design challenges for large aero engines, particularly with regard to internal sealing and bearing loads. Therefore it is recommended that alternative topping-cycle technologies should be researched for long-term aero engine performance improvements. A further study shows the effect of the target 15% reduction in fuel burn on in-flight CO_2 emissions by the civil aviation fleet under various traffic-growth scenarios.

ACKNOWLEDGEMENTS

I am extremely grateful to Professor Pilidis and Cranfield University for the opportunity to carry-out this research, to Bobby Sethi and Devaiah Nalianda for co-supervising my studies, and to Gill Hargreaves for organising everything.

This project could not have been completed without the wholehearted support of my wife Jenny and advice and encouragement from many colleagues in Cranfield and in the ULTIMATE project partner organisations. Particular thanks are due to: Joshua Sebastiampillai, Florian Jacob, Francesco Mastropierro, Mathieu Belmonte and Diana Guiomar San Benito Pastor, with whom I sometimes shared an office; to Paul Newton, Lorenzo Raffaelli and John Whurr at Rolls-Royce; to Tomas Grönstedt, Carlos Xisto and Anders Lundbladh at Chalmers University and GKN in Sweden; to Stefan Donnerhack, formerly at MTU; to Nicolas Tantot at Safran, to Arne Seitz at BHL, and to many other participants in the ULTIMATE project, which would not have come together without Tomas's Grönstedt's leadership and the efforts of Martin Dietz, Tanja Oster, Sandra Annetzberger and Anna Yenokyan at Arttic.

Special thanks are due to Eleni Chatzidimitriou and Francesco Mastropierro for their work on the nutating-disc display-model. It has also been a pleasure to work with Pierre Gauthier, Cesar Celis and Xiaoxiao Sun, in providing advice to Cranfield MSc students in studies that related to the ULTIMATE project.

***

Figure 5 and Figure 6 are reproduced courtesy of the NEWAC Consortium and Figure 23 is reproduced courtesy of Rolls-Royce plc.

***

The ULTIMATE project has received funding from the *European Union's Horizon 2020 research and innovation programme* under Grant Agreement No. 633436.

TABLE OF CONTENTS

LIST OF FIGURES

LIST OF TABLES

LIST OF EQUATIONS

GLOSSARY

AATT	Advanced Air Transport Technology (NASA Programme/Study Cycle)
ABC	Air Bottoming Cycle
ABCHX	Air Bottoming Cycle Heat Exchanger
AC	Active Core (NEWAC study engine from MTU)
a/c	Aircraft
ACARE	Advisory Council for Aviation Research and Innovation in Europe
AEM3	Advanced Emission Model 3
AFR	Air/Fuel Ratio
AHEAD	Advanced Hybrid Engines for Aircraft Development (EU programme)
ALAQS	Airport Local Air Quality Studies (project and model)
ANTLE	Affordable Near-Term Low Emissions (EU programme)
App	Approach (engine thrust rating in LTO cycle)
APU	Auxiliary Power Unit
ASCR	Advanced Subsonic Combustion Rig
ASE	Advanced Subsonic Engine (NASA research programme)
ASK	Available Seat Kilometres
ATAG	Air Transport Action Group
ATC	Air Traffic Control
ATM	Air Transport Management
ATW	Advanced Tube and Wing (aircraft)
BFF2, BFFM2, or BM2	Boeing Fuel Flow Model 2 (for emissions assessment)
BHL	Bauhaus Luftfahrt
BLI	Boundary Layer Ingestion
BPR	Bypass Ratio

CAEP	Committee on Aviation Environmental Protection
CASK	Cost per Available Seat Kilometre
cc	Cubic Centimetres
CCA	Cooled Cooling Air
CCACA	Cooled-Cooling-Air Cooling Air
CCE	Composite Cycle Engine
CIMO	Commission for Instruments and Methods of Observation
C/O	Climb-out (engine thrust rating in LTO cycle)
COT	Combustor Outlet Temperature
CR	Cruise (typical or mid-cruise unless otherwise specified)
CRECK	Chemical Reaction Engineering and Chemical Kinetics (Modelling Group at Politecnico di Milano)
CU	Cranfield University
DOC	Direct Operating Cost
DHHS	(US) Department of Health and Human Services
EASA	European Aviation Safety Agency
ECS	Environmental Control System
EDB	Emissions Databank
EEFAE	Efficient and Environmentally Friendly Aero Engine
EGT	Exhaust Gas Temperature
EI	Emissions Index
EIS	Entry Into Service
ENOVAL	Engine Module Validators (EU research programme)
EOR	End of Runway
EPA	Environmental Protection Agency
ESA	European Space Agency
ETS	Emissions Trading Scheme
Foo	Sea-level Static Thrust (zero altitude and Mach number)
FANN	Full Annular (combustor test)

FAR	Fuel/Air Ratio
FB	Fuel Burn
FBN	Fuel-bound Nitrogen
FCC	Flow Controlled Core (study engine from Safran Aircraft Engines)
FF	Fuel Flow
FHV	Fuel (Lower) Heating Value
FN	Net Thrust
GOR2050	Geared Open Rotor engines for year 2050
GTF	Geared Turbofan
GWP_{100}	Global Warming Potential (over a 100-year timeframe)
Hephaestus	Software for combustor modelling developed at CU
HC	Hydrocarbons
HP	High Pressure
IATA	International Air Transport Association
IC	Intercooled or Intercooled Core (NEWAC study engine from RR)
ICAO	International Civil Aviation Organisation
IP	Intermediate Pressure
IRA	Intercooled and Recuperated Aero Engine (study engine from MTU)
ISA	International Standard Atmosphere
ISABE	International Symposium on Air Breathing Engines
ISAE	Institut Supérieur de l'Aéronautique et de l'Espace
ITB	Inter-Turbine Burning
ITR	Inter-Turbine Reheat (same as ITB)
LDI	Lean Direct Injection (combustor)
LEMCOTEC	Low Emissions Core Engine Technologies (EU research programme)
LES	Large Eddy Simulation

LP	Low Pressure
LPC	Low Pressure Compressor
LPP	Lean Pre-mixed Pre-vaporised (combustor)
LR	Long Range
LTO	Landing and Take-off (cycle)
MLDI	Multi-point Lean Direct Injection (combustor)
MTOW	Maximum Take-off Weight
MTU	MTU Aero Engines AG
NEPAIR	New Emissions Parameter Covering the Whole Aircraft Operation
NEWAC	New Aero Engine Core Concepts (EU research programme)
NDC	Nutating Disc Compressor
NGV	Nozzle Guide Vane
NIOSH	(US) National Institute for Occupational Safety and Health
NOx	Oxides of Nitrogen
NPSS	Numerical Propulsion System Simulation
nvPM	Non-volatile Particulate Matter
OPF	Oxy-poor-flame
OPR	Overall Pressure Ratio
P	Total Pressure
PAX	Number of Passengers
PDC	Pulse Detonation Combustor
PDE	Pulse Detonation Engine
PED	Price Elasticity of Demand
PERM	Partial Evaporation and Rapid Mixing (combustor)
PFR	Plug-Flow Reactor
PED	Price Elasticity of Demand
PLF	Passenger Load Factor
PM	Particulate Matter

ppb	Parts per billion (10^9) (by mass)
ppm	Parts per million (by mass)
PRECISE-UNS	Predictive-system for Real Engine Combustors with Improved Sub-models and Efficiency - UNStructured
Prometheus	A combustor modelling system
PROOSIS	Propulsion Object Oriented Simulation Software
QGIS	‘Quantum’ Geographic Information System
REL	Recommended Exposure Limit
RH	Relative Humidity
rms	Root Mean Square
RNDM	Recuperated Nutating-Disc Module
RPK	Revenue Passenger Kilometres
RQL	Rich–Quench–Lean (style of combustor)
RR	Rolls-Royce plc
RTK	Revenue Tonne Kilometres
SC	Secondary Combustor
S-CO_2	Supercritical Carbon Dioxide
SESAR	Single European Sky Air traffic management Research
SFC	Specific Fuel Consumption
SLS	Sea-Level Static
SMD	Sauter Mean Diameter (for fuel droplets)
SOx	Oxides of Sulphur
SR	Short Range
SRIA	Strategic Research and Innovation Agenda
SV	Swirl-Venturi
TAPS	Twin-Annular Premixing Swirler (combustor)
TAS	True Air Speed
TCA	Turbine Cooling Air (that is not cooled-cooling air)
TDC	Top Dead Centre

TEGT	Turbine Exhaust Gas Temperature
TERA	Techno-Economic and Environmental Risk Analysis
TET	Turbine Entry Temperature
TF2050	Reference turbofan engine for year 2050 (refers to the optimally-sized engine modelled by Jacob in [1] UOS)
THC	Total Hydrocarbons (same as HC)
TO or T/O	Take-off
TOC	Top of Climb
TRL	Technology Readiness Level (see section 10.3.1)
TROPOMI	Tropospheric Monitoring Instrument
UHC	Unburned Hydrocarbons (same as HC)
ULTIMATE	Ultra Low Emission Technology Innovations for Mid-century Aircraft Turbine Engines
UOS	Unless Otherwise Specified
USD	United States of America Dollars
VAFN	Variable Area Fan Nozzle
VGC	Variable Geometry Combustor
VIGV	Variable Inlet Guide Vane
VITAL	Environmentally Friendly Aero Engine (EU research programme)
VOC	Volatile Organic Compounds
WeiCo	Weight and Cost Estimation (TERA Program)
WSR	Well-Stirred Reactor

NOMENCLATURE

Symbols

a, b, c… etc.	Constants in emissions correlation equations
B	Time-constant (Hz)
c_1, c_2 … *etc.*	Constants in the saturation vapour pressure equation
C_0, C_1, C_2, C_3	Coefficients in a polynomial curve fit equation
CH_{ratio}	Ratio of carbon to hydrogen by mass
D_p	Mass of pollutant emitted per engine, over the LTO cycle (kg)
e *(or* ϵ*)*	Ratio of the Mole Weight of Water Vapour to Air (0.62198)
e	Partial pressure of water vapour (Pa)
e_L	Water vapour partial pressure saturated over liquid (Pa)
EICO	Emissions Index for Carbon Monoxide (g/kg fuel)
EI_{H_2O}	Emissions Index for Water Vapour
EIHC	Emissions Index for Unburned Hydrocarbons (g/kg fuel)
$EINO_x$	Emissions Index for NOx (g/kg fuel)
$e_{(P)}$	Price Elasticity of Demand
F	Net Thrust (kN or MN)
F_{oo}	Rated 100% sea-level static thrust for the LTO cycle (kN)
FAR	Fuel/Air Ratio
FAR_{ALT}	Fuel/Air Ratio at Altitude
FAR_{GL}	Fuel/Air Ratio at Ground Level
FAR_{ST}	Fuel/Air Ratio for stoichiometry
FF	Fuel Flow (g/s or kg/s)
h	Specific Humidity (kg H_2O / kg air) (the same as ω) *
h_{SL}	Specific Humidity (kg H_2O / kg air) at sea level *
H	Humidity Correction Factor
m, n	Exponents
M	Flight Mach Number

M	Mass Flow (kg/s)
P	Total Pressure (pa or kPa) or Price
p	Ambient or Static Pressure (Pa)
$P_{3_{ALT}}$	Combustor Entry Pressure at Altitude (Pa, UOS)
$P_{3_{GL}}$	Combustor Entry Pressure at Ground Level (Pa, UOS)
P_a	Absolute Water Vapour Pressure in Air (Pa)
p_v	Saturation Water Vapour Pressure in Air (Pa)
Q	Quantity Demanded
Q	Proportion of Combustor Inlet Air Used for Wall Cooling
R^2	Coefficient of Determination in Regression Analysis
R_{CO_2}	The fraction of CO_2 remaining after time *t* years
REICO	Reference Emissions Index for Carbon Monoxide (g/kg fuel)
REIHC	Ditto for Unburned Hydrocarbons (g/kg fuel)
$REINO_x$	Ditto for NOx (g/kg fuel)
T	Time (s or years)
$t_{1/2}$	Half-life (years)
t_e	Evaporation Time (s)
t_r	Residence Time (s)
T	Temperature (K)
T_{ad}	Equilibrium Adiabatic Flame Temperature (K)
$T_{ad,l}$	Local Adiabatic Flame Temperature (K)
T_c	Combustion Temperature *or* CCA Temperature (K)
T_{cref}	Reference CCA Temperature (K)
TF	Technology Factor Exponent for NOx Emissions Estimates
T_{gref}	HP Turbine Reference Relative Inlet Gas Temperature
T_{grel}	HP Turbine Relative Inlet Gas Temperature
T_{pz}	Primary Zone Temperature (K)
T_{st}	Stoichiometric Combustion Temperature (K)

U	Ambient Air Relative Humidity
V_c	Combustor Volume (m^3)
W	Mass Flow (kg/s)
W_4	Combustor Exit Mass Flow (kg/s)
W_{4ref}	Reference Combustor Exit Mass Flow (kg/s)
W_c	Cooling-Air Mass Flow (kg/s)
W_{cref}	Reference Cooling-Air Mass Flow (kg/s)
W_f	Corrected Fuel Flow (kg/s)
W_{ff}	Modified Fuel Flow (kg/s)
x	A known quantity
y	A quantity to be determined

Subscripts

3	At HP compressor Exit
31	At combustor inlet
4	At combustor exit
a, ALT	At altitude
ad	Adiabatic
amb	Ambient condition
design	At the design case
GL	At ground level
is	Isentropic
ISA	International Standard Atmosphere
ref	Reference value
SLS	Sea-level static

Greek

B	Index to Correlate Water Vapour Saturation Pressure with Temperature
Δ	Efficiency Correction
δ_{amb}	Ambient Pressure Correction Factor
ϵ *or* e	Ratio of the Specific Gas Constants of Water Vapour to Air (0.62198)
Θ_{amb}	Ambient Temperature Correction Factor
λ	Air/Fuel Equivalence ratio or Excess Air Ratio or HP Compressor Last-stage Blade-height (mm)
π_{oo}	OPR at max SLS take-off thrust
T	Residence Time (s)
τ_L	Effective Residence Time (years in the Atmosphere)
Φ	Relative Humidity or Fuel/Air Equivalence Ratio
Φ_{pilot}	Equivalence Ratio for the pilot burner
Φ_{m1}	Equivalence Ratio for first set of main burners
$\Phi_{m2,3}$	Equivalence Ratio for second and third set of main burners
$\boldsymbol{\omega}$	Specific Humidity (sometimes also written as *h*) *

* Note specific humidity can either be defined as kg of water vapour per kg of moist air, or as kg of water vapour per kg of dry air, though in most cases the difference between these figures is practically negligible. See section 3.8.3.

1 RESEARCH SCOPE AND CONTEXT

1.1 Introduction

For over sixty years most large civil aircraft have used engines with propellers, or ducted fans, driven by Brayton cycle gas turbines. These engines with gas turbine cores had higher power/weight ratios than the highly developed piston engines that preceded them, and they improved productivity by enabling aircraft to fly higher and faster. They also offered lower maintenance costs, and, as fuel was relatively inexpensive, their lower cycle efficiencies resulting from reduced peak cycle pressures and temperatures were acceptable. Subsequent aero engine developments have progressively improved fuel burn (FB), but the demand for further improvements remains strong because of the continuing growth in air travel and its environmental impact. Major concerns relate to global warming resulting from CO_2 and the effects of other emissions, particularly NOx and particulates, on local air quality and human health. Aircraft noise is also still a significant issue.

Typical engines for year 2050 are expected to have geared fans for faster long-range aircraft and geared open rotors for shorter-range aircraft [2]. Ducted fans could have variable-pitch fan blades to enable reduced specific thrust and higher propulsive efficiency. Open-rotors with highly efficient contra-rotating propeller blades could have a ‘pusher’ configuration and be rear-fuselage mounted to minimise cabin noise. These propulsion systems are considered preferred candidates for efficient future short-range ‘narrowbody’ aircraft, but turbofan engines are considered more realistic for heavier long-range aircraft, on account of their higher cruise speeds, the installation challenges of large open rotors and their noise footprints. Nevertheless the 2050 aero engine fuel-burn targets will not be met by either type without further radical changes to core engine design. Thus the ULTIMATE project has investigated breakthrough technologies for aircraft propulsion to meet the ambitious Advisory Council for Aviation Research and Innovation (ACARE) Strategic Research and Innovation Agenda (SRIA) Flightpath 2050 targets for CO_2, noise and emissions [3] [4] [5].

The overall efficiency of a propulsion system can be analysed as the product of propulsive efficiency, transfer efficiency and core thermal efficiency [6]. The propulsive efficiency of turbofan engines has been increased by increasing fan sizes and bypass ratios to increase air flow and reduce specific thrust and jet velocities. In coming years, this trend will be taken further by introducing geared fans to enable the use of higher-speed and more-compact low pressure (LP) turbines, but increases in powerplant weight and nacelle drag place upper limits on potential improvements in propulsive efficiency. These limits can however be shifted by adopting open rotor propulsor systems to reduce nacelle drag or by improving engine/airframe integration, e.g. by exploiting boundary layer ingestion (BLI) to increase propulsive efficiency [6].

Transfer efficiency states how-efficiently power is transferred from the core engine to the propulsion system. Turbojets have very high transfer efficiency, but increasing bypass ratios in turbofan and open rotor engines tends to reduce transfer efficiency. However, the trend can be offset by raising the component efficiencies of low-pressure turbines and fans or propellers. Using gearboxes to enable the speeds of different components to be optimised can also help to improve transfer efficiency, even after accounting for the gearbox transmission losses and cooling requirements.

The potential for further improvements in propulsive and transfer efficiency in turbofans is relatively limited, but larger improvements in core thermal efficiency are possible. This is because in gas turbines the biggest increase in entropy (i.e. loss of available energy or exergy) occurs when the fuel burns at constant pressure. Incorporation of constant volume or pressure-rise combustion will greatly reduce the exergy loss and improve core thermal efficiency [5].

Historically, thermal efficiency in gas turbines has been improved by raising turbine entry temperature (TET), overall pressure ratio (OPR) and component efficiencies. However, attaining higher thermal efficiency by increasing TET is reaching its practical limits due to material limitations in the high pressure (HP) turbine and the adiabatic flame temperature of kerosene. Industry targets and

legislation limiting NOx emissions will also curb flame temperatures, which tend to increase with increasing combustor inlet temperature and pressure. Also, higher OPR leads to smaller blades in the HP compressor and HP turbine, tending to reduce their component efficiencies. Alternative approaches to the current trends of increasing TET and OPR are needed in order to make significant progress on improving thermal efficiency.

One reason for the modest thermal efficiency of existing aero engines is failure to extract more energy from the heat exported in their hot core-exhaust gasses. This heat may be extracted by a recuperator to pre-heat air entering the combustor, or to drive a bottoming cycle. Intercooled and recuperated engine cycles have been investigated in previous EU-funded programmes including EEFAE, NEWAC, LEMCOTEC and ULTIMATE [7]. Recuperator designs have been researched to increase effectiveness and reduce installation losses [8]. Bottoming cycles for aero engines have been relatively under-researched until recently. These can be closed-circuit [9] or open-circuit [10] systems.

1.1.1 Project Outline, Aims, Objectives and Overall Methodology

Several unconventional engine technologies have been researched in recent years. Intercooling, recuperation, inter-turbine combustion, topping cycles and bottoming cycles have all demonstrated potential to improve core thermal efficiency. While some of these technologies can be combined to give useful synergies, other combinations will not work so well together.

The study aims to close gaps in the knowledge regarding combinations of advanced-cycle aero-engine core technologies that would be either synergistic, or antagonistic to each other. The research objectives include:

- Determining the pros and cons of the novel technologies and combinations of technologies that could improve the thermal efficiency of future engines.
- Investigating the effects of scaling-down thrust requirements and core turbomachinery components on engine efficiency and cycle matching.

- Creating a concept design for a nutating-disc topping-cycle module and assessing its performance and mechanical limitations,
- Identifying a realistic large commercial turbofan engine performance cycle and architecture with potential for a 15% step-change reduction in fuel-burn together with reduced NOx emissions,
- Quantifying the incremental benefits from potential technologies including intercooling, secondary combustion and topping and bottoming cycles,
- Selecting a method for predicting the NOx emissions of future-engine lean-burn combustion systems,
- Estimating the likely impact of technology improvements on civil-aviation CO_2 emissions for a number of different air-traffic growth and economic scenarios up to 2075 and beyond.
- Comparing predicted year-2050 engine emissions with industry targets

In the first part of this study various technology combinations were reviewed. Comparing possible engine cycles highlighted the performance parameters limiting their potential, and technology combinations that either might overcome the constraints, or be in conflict with each other. The study gave a qualitative down-selection of the most promising cycles. The assessment considered potential thermal efficiency benefits and likely cost and weight implications, based on core specific power and overall complexity.

For the selected top-level performance cycle, further design choices were made. Topping cycles for example could have been implemented using pulse-detonation, wave-rotors or piston engines, but it was decided to focus on the relatively under-researched option of nutating-disc machinery and its potential application to turbofans for larger longer-range aircraft. It was considered that more-complex cycles combining multiple core technologies would be easier to justify in such an application because of more-favourable fuel-burn exchange rates and relatively lower sensitivity to acquisition costs. However, the effects of scaling-down the thrust requirements for future aircraft and reducing component sizes in advanced-cycle engine cores have also been considered.

In the last part of the project the selected design concept has been holistically assessed using quantitative models and new methods. Maximising overall efficiency requires that losses of available energy (exergy) are minimised.

Temperature-entropy diagrams show how the performance cycles affect overall engine thermal efficiency. They also show where the losses occur and where improvements in component technology would minimise these losses.

Figure 1 summarises the major steps taken through the PhD project, from the initial literature survey and other inputs (in the left-hand column) to the final publications and other dissemination materials (in the right-hand column).

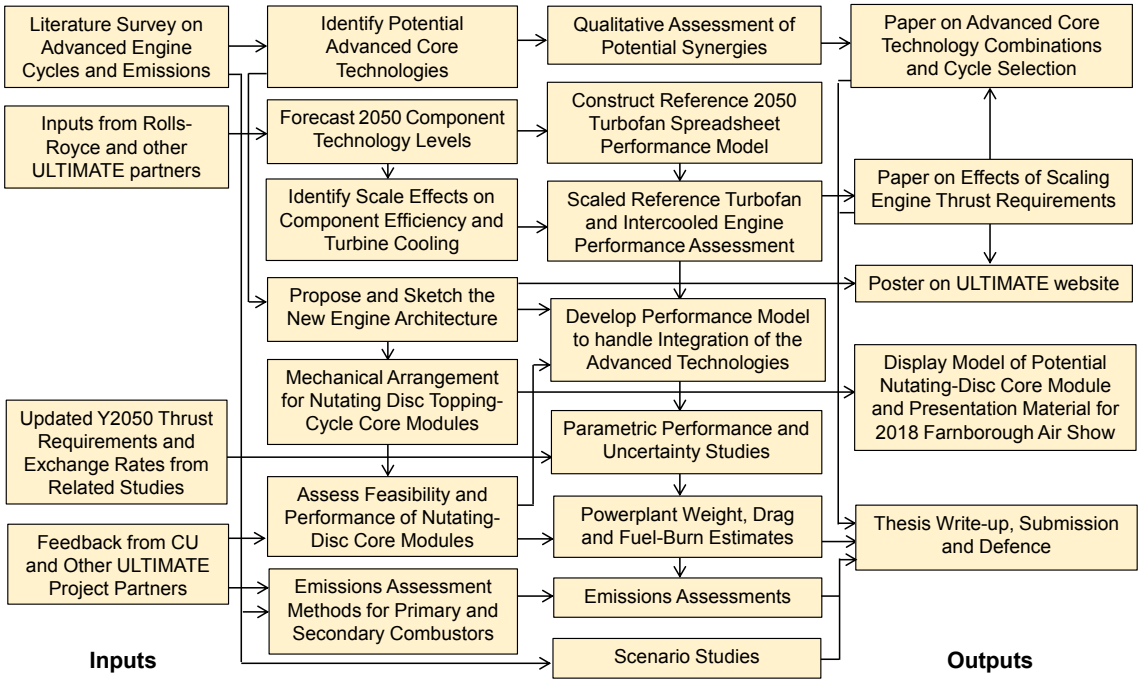

Figure 1 – Overall Methodology for the PhD Study

1.1.2 The ULTIMATE Project

Over the course of these studies the author has worked with Rolls-Royce plc and other partners in the European Commission's Horizon 2020 ULTIMATE project [5]. See www.ultimate.aero for details.

The project aimed first to quantify reference levels for long-term improvements in more-established aircraft and engine technologies and in ongoing enabling

technologies, such as developments in high temperature materials and heat exchanger design. Then future reference engines with conventional cycles were modelled prior to making comparisons with the radical engine cycle concepts investigated in the main part of the project.

ULTIMATE has investigated combinations of advanced technologies with the potential to greatly improve the fuel burn and emissions of aero engines for aircraft entering service from 2050 onwards [5]. It has modelled ‘advanced tube and wing’ (ATW) commercial aircraft, flying Airbus A320-like and A330-like missions, that together represent about 90% of current commercial air traffic [11]. These aircraft were modelled with projected 2050 entry-into-service (EIS) ‘reference engines’ having conventional Brayton-cycle gas-turbine cores. The aircraft and engine designs and thrust requirements were then iterated to give the lowest fuel burn. The final reference engine designs anticipate mid-century technology improvements, including the trend towards higher component, core-thermal, and propulsive efficiencies. For the larger ‘intercontinental’ aircraft a geared turbofan is assumed. For the smaller ‘intra-European’ aircraft a geared ‘open rotor’ engine is assumed.

This thesis and the ULTIMATE project assume that engines entering service in 2050 would still use kerosene, or a drop-in-replacement bio-fuel or synthetic fuel. Nevertheless, to meet the ‘emissions-free taxiing’ objective, it has been assumed that auxiliary power for ground use would normally be provided by a hydrogen-fuelled auxiliary power unit (APU) or fuel cells. Therefore, since future aircraft would possess these systems, they could also be used to provide auxiliary power in flight to further reduce mission-level CO_2 emissions. However, the use of hydrogen might not always be possible, so it was further assumed that engine-mounted electric starter-generators should be able to take-over supplying all of the demanded electrical power, as and when necessary. This includes power to drive the environmental control system (ECS) in the ‘more-electric’ year-2050 aircraft. Table 1 lists key characteristics assumed for the year-2000 and year-2050 long-range (intercontinental) study aircraft modelled by Bauhaus Luftfahrt (BHL) as reported in [11] and [12].

Table 1 –Year-2000 Baseline and Year-2050 Reference Aircraft Data

Parameter	Units	Baseline (2000)	Reference (2050)
Number of Passengers (PAX)	–	277	300
Design Range	NM	4867*	7000
Maximum Take-off Weight (MTOW)	kg	212000**	190600
Operating Empty Weight (OEW)	kg	–	91100
Relative to Year-2000 Aircraft	–	–	73.7% (-26.3%)
Wingspan	m	60.3	61.564
Wing Aspect Ratio	–	c. 11	13.0
Mid-cruise Lift/Drag Ratio	–	c. 21	24.7
Design Cruise Mach number	–	0.82	0.80
Engine Type	–	Turbofan	Geared turbofan
Study Engine Designation	–	LRTF2000	TF2050
Engine Installation	–	Under-wing pylon	Under-wing pylon
Engine Fan Diameter	m	2.47	2.84
Engine Bypass Ratio for Aircraft Model	–	5	17
Take-off Thrust 0.2 M Sea Level ISA+15 K	kN	183.5	183.5
Top of Climb Thrust	kN	73.0	50.0
Design Mission Fuel Burn / Passenger***	g/NM	41.16	22.64
Design Mission Fuel Burn / Passenger***	g/km	22.23	12.22
Relative to Year-2000 Aircraft	–	–	55.0% (-45.0%)

* Original range including cargo as well as passengers
** Original maximum take-off weight
*** Assuming 100% passenger load factor (PLF)

The ULTIMATE project year-2050 reference aircraft has a conventional tube and wing configuration, but incorporates advanced technologies and materials. The engines are developments of Brayton-cycle gas-turbine-cored aero-engines that also use advanced materials and cooling technologies. The study engines aim to demonstrate further step-change improvements over the Brayton-cycle reference engines. Assessments of the performance of the baseline and reference aircraft and engines were reported in ULTIMATE project deliverables D2.1 [12] and D2.6 [13], but the final assessment of the performance of the year-2050 long-range reference turbofan engine ‘TF2050’ was provided in an

internal memorandum ULTIMATE-CU-ECM-005 [1]. Dissemination of the aircraft study results was in [11] and the engine results will be provided in [14].

1.2 Motivation

The author has a long-standing interest in radical designs for commercial aero engines because these seem to have the potential for significant improvements in fuel economy and reduced emissions. At Rolls-Royce plc and in EU research programmes he has studied advanced technologies including cooled cooling air, intercooling and recuperation, which have the potential to improve aero engine performance. However, it has been difficult to make business cases for further development of these technologies while improvements in more conventional technologies have offered more immediate benefits.

Nevertheless it is clear that diminishing returns from conventional aero engine developments will make more radical design solutions essential if historic rates of engine performance improvement are to be maintained much beyond 2035. The author's main objective has been to identify synergies between emerging and unconventional engine technologies to see if they genuinely could create significant step-change improvements in the fuel-burn, emissions and cost of ownership of aero engines for future commercial aircraft.

1.2.1 Minimising the Environmental Impact of Civil Aviation

Ambitious targets for reducing aviation emissions have been set by several industry-led bodies, including the 'Air Transport Action Group' (ATAG) and the 'Advisory Council for Aviation Research and Innovation in Europe' (ACARE). Some inputs for setting the ACARE targets were provided by the 'ACARE Goals Progress Evaluation' (AGAPE) project. The targets have the objective of driving research and technology programmes with potential to mitigate environmental impacts from the ongoing rapid growth of the global civil aviation fleet.

In accordance with its 'Commitment to Action on Climate Change' [15], ATAG has defined a set of goals aimed at tackling aviation's impact on climate change. Medium and long-term the goals include stabilising emissions from

2020 onwards with carbon-neutral growth and the goal of reducing emissions from aviation by 50% by 2050 compared to 2005 levels. Realistically *the only way* these goals can be met is by 'offsetting' much of the commercial and business aviation fleets' CO_2 emissions.

Long-term goals from ACARE are defined in its Strategic Research and Innovation Agenda (SRIA). These include targets for year 2050 in Flightpath 2050 [4], and intermediate targets for years 2020 and 2035. The most ambitious targets include 75% reduction in CO_2 emissions and 90% reduction in NOx emissions per passenger kilometre for new aircraft in 2050, relative to new aircraft in year 2000. The 75% reduction in CO_2 emissions is supposed to be achieved by a combination of improvements in airframe and engine technologies, air traffic management, airline operations and infrastructure.

Table 2 shows the breakdown of the SRIA targets. The AGAPE assessment of a target overall CO_2 reduction for year 2020 is less ambitious than the SRIA target and much less ambitious than the original Vision 2020 ACARE target. Note the improved technologies for application in these aircraft and engines would need to be demonstrated to Technology Readiness Level 6 (TRL 6)[1] about five years ahead of the date for earliest EIS.

Table 2 – SRIA Improvement Targets for CO_2 Emissions

(relative to year-2000 technology levels)

Improvement Targets for EIS Year	**2020**	**2035**	**2050**
Attributable to the Propulsion System	0.80 (-20%)	0.70 (-30%)	0.32 (-68%)
Attributable to the Airframe	0.80 (-20%)	0.70 (-30%)	
Attributable to ATM and Infrastructure	0.93 (-7%)	0.88 (-12%)	0.88 (-12%)
Otherwise Attributable to Airline Operations	0.96 (-4%)	0.93 (-7%)	0.88 (-12%)
Overall Improvement	0.57 (-43%)	0.40 (-60%)	0.25 (-75%)

[1] Technology readiness levels on a scale from zero to nine were invented by NASA and are now used across the industry. TRL 6 implies sufficient maturity to launch product development.

The improvement factors and reduction targets in Table 2 are assumed to apply equally across all civil aircraft types, though in practice they will not be equally easy to achieve for all types of aircraft and aircraft operations. It is further assumed that kerosene or a 'drop-in' replacement fuel will continue to be used and the component target improvements are independent and commutative (which can only be approximately true).

1.3 Advanced-cycle Engine Concepts

Various technological advances have the potential to improve the performance of future propulsion systems, including improvements in propulsive efficiency resulting from reduced specific thrust and increased engine-airframe integration.

Open rotor powerplants already have very high propulsive efficiencies, and for engines with geared fans the potential for further improvements is limited by cost, weight and installation issues. There is more scope for substantial improvements in thermal efficiency with advanced cycles, because the biggest increases in entropy and the biggest exergy losses in existing engines occur in their core streams. Therefore the reported research has focused on advanced cycles and technologies that can improve core thermal efficiency, and on engine designs that will also enable NOx and other noxious emissions around airports to be kept to a minimum. Technologies assessed include topping and bottoming cycles, intercooling, recuperation and secondary combustion.

Figure 2 shows a schematic combination of intercooling, nutating-disc topping cycle modules, secondary combustion and an open-circuit bottoming cycle in a reverse-flow geared turbofan engine architecture and Figure 3 shows a concept for a nutating-disc topping-cycle module. Typically, six nutating-disc modules might be arranged around the core of the engine. Figure 4 is a schematic cross-section looking aft, cut ahead of the nutating disc modules and the secondary combustor and just behind the reverse-flow high pressure turbine.

More details of the proposed designs are given in Chapter 6 and Chapter 8. For year-2050 this engine configuration has been assessed with the potential for a

15% reduction in fuel burn and CO_2 emissions relative to the more-conventional Brayton-cycle reference engine.

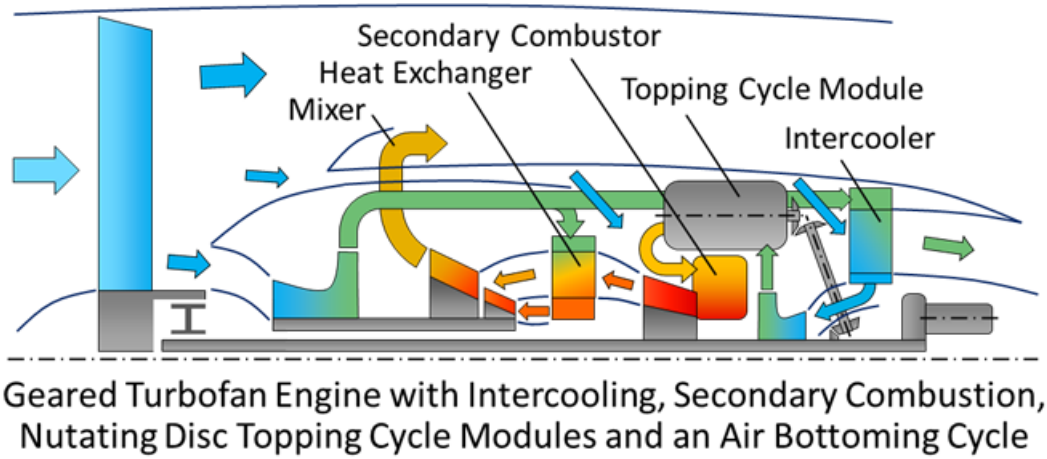

Figure 2 – Turbofan Engine Design Concept for EIS in 2050
(colour-coding is indicative of cycle temperatures with red being hottest)

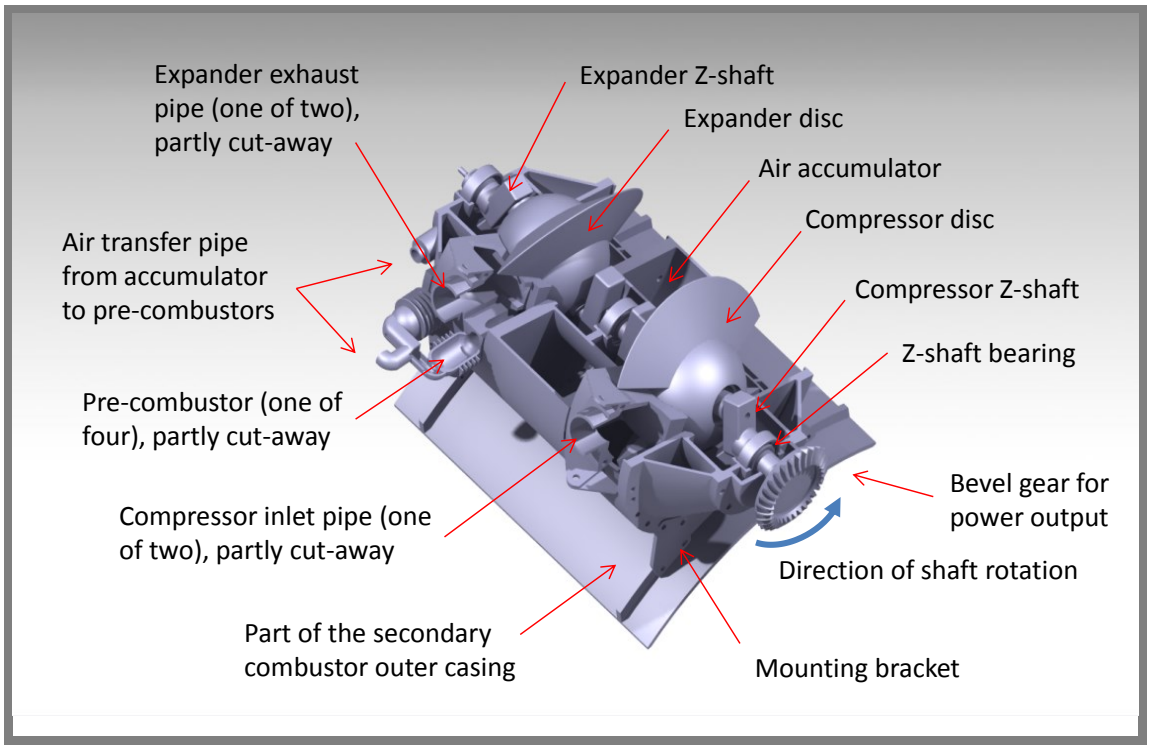

Figure 3 – Concept for a Nutating-disc Topping-cycle Module
(3-D solid model courtesy of Francesco Mastropierro)

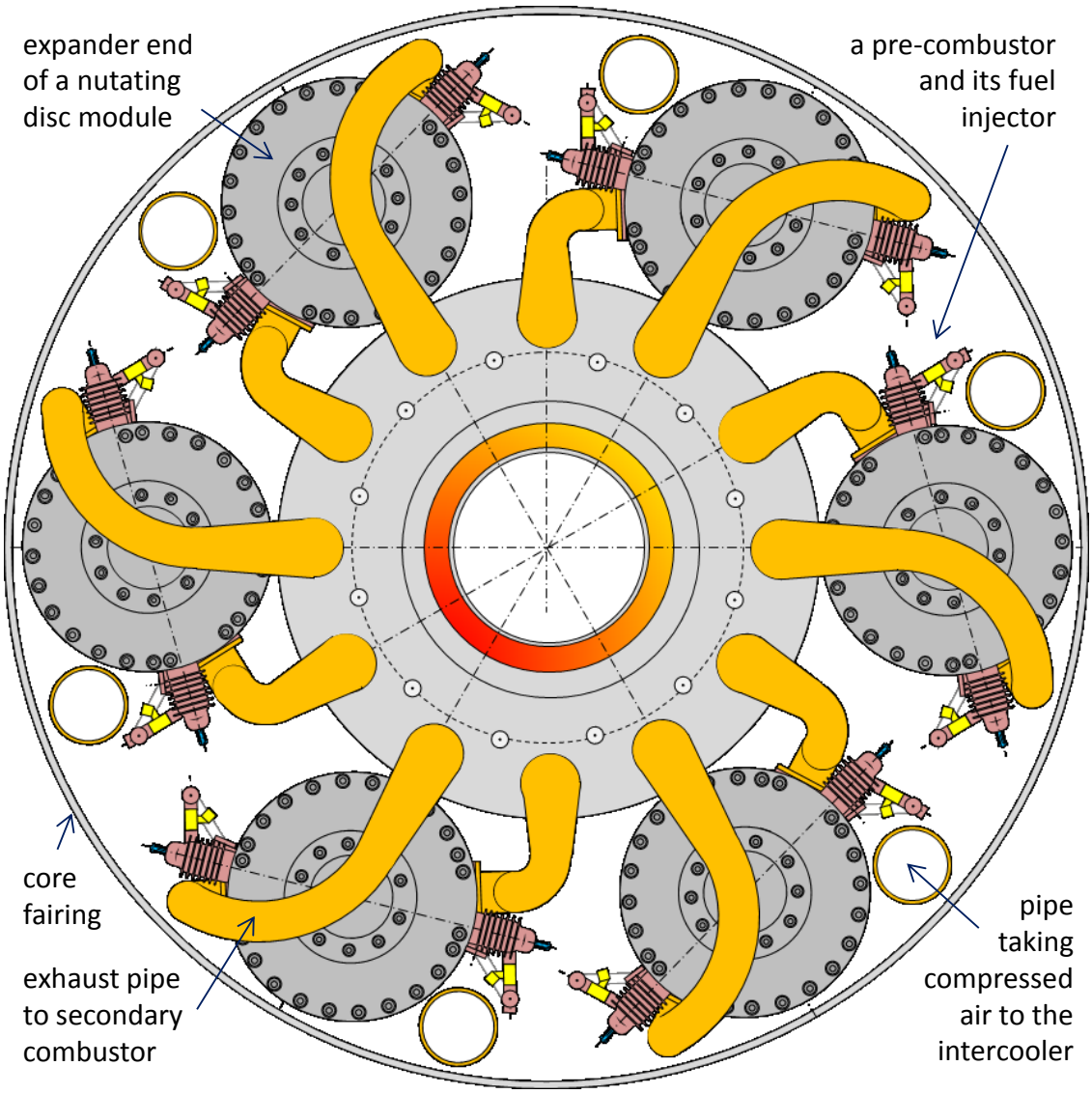

Figure 4 – Proposed Arrangement of Six Nutating-disc Modules (each one having two exhausts feeding into a secondary combustor upstream of the high pressure turbine)

1.4 Contribution to Knowledge

This project has made a substantial contribution to knowledge by exploring combinations of technologies not so far reported in the literature, identifying potential synergies, quantifying the benefits and investigating the challenges associated with realizing the novel engine cycles and configurations.

The literature survey highlights those technology combinations that have been studied previously and it identifies gaps in the knowledge of how candidate technologies in new combinations can benefit integrated engine cycles and powerplant designs. The survey recalls a substantial literature on intercooling and recuperation and on intercooled and recuperated aero engine design. The integration of pressure-rise combustion systems with turbine aero engines has also been widely studied and there is abundant material on turbocharged and turbocompounded piston engines. The addition of a closed-circuit bottoming cycle that would extract heat from the core exhaust and reject it to an air-cooled or fuel-cooled pre-cooler has been studied at Cranfield with supercritical-CO_2 recommended as the working fluid [16]. An open, air bottoming cycle (ABC) has also been investigated by Anders Lundbladh in Sweden [10]. Novel pressure-rise combustion systems have been designed, manufactured and tested, and even flown on light aircraft, but only one patent application is known that considers combining up to five of these technologies in an aero engine [17]. Thus there exists considerable scope to investigate integrating and optimising different combinations of the above technologies and quantifying their costs and benefits. The reported study has made a good start on this.

The reverse-flow-core architecture studied in the LEMCOTEC project [18] has been revisited as a framework for various advanced cycle engines. The engine configuration selected for detailed evaluation combines topping and bottoming cycles with secondary combustion and intercooling in a reverse-flow-core geared turbofan architecture. It is contended that this novel combination of technologies has the potential to achieve very high thermal efficiency with acceptable levels of NOx emissions, powerplant weight and nacelle-drag.

The potential to use nutating-disc core modules in a topping cycle has been the subject of a detailed study and critical analysis. The author has proposed some novel features including integrating the accumulator in double-walled casings to provide regenerative cooling. Construction of a display model helped to clarify details of its operation, but realization of the concept in a highly-turbocharged

engine was shown to present very significant design challenges. Simpler free-piston arrangements probably offer a more attractive topping-cycle solution.

Topping-cycles are shown to offer large SFC improvements and significant fuel-burn reductions when combined with intercooling. Adding an ABC further improves SFC and fuel burn when combined with secondary combustion.

An investigation of known correlations to estimate the NOx emissions of future lean-burn combustors has shown that none of them can be expected to give accurate predictions. Some existing correlations from rig testing were shown to have been misapplied when predicting engine emissions. It was concluded that an established simple correlation from NASA was the least-worst option, so it was used in the rest of the study. Unlike some other correlations, it should work as well for intercooled engines as for conventional engines.

Potential new formulations for emissions correlations were also investigated, but there was no evidence that trying to emulate the underlying physics and chemistry would increase accuracy. Some of the available data that might be used to validate new correlations were shown to have errors or inconsistencies.

An investigation of the impact of advanced cycle engines on civil aerospace global CO_2 emissions in the second half of the century also provided new insight into the feasibility of achieving the ATAG target of a 50% reduction in CO_2 emissions. It was shown that the 'market based measures' needed to offset CO_2 emissions after 2050 could be significantly reduced.

1.5 Thesis Structure

The thesis follows a conventional layout and incorporates and updates material from the author's publications, rather than attaching the original papers.

The introduction to the study covering the research scope and context and contribution to knowledge is followed by a literature survey in Chapter 2 that reviews the state of the art regarding research into advanced engine cycles and technologies, and into associated efforts to minimise engine exhaust emissions.

Research gaps are identified to show where this study has been able to make useful contributions to knowledge.

The main methods adopted in this study are described in Chapter 3. These include performance modelling tools and emissions estimation methodologies. Considerable efforts were made to identify the most appropriate emissions assessments methods for future aero engines incorporating lean direct ingestion (LDI), but ultimately it was concluded that a widely-quoted existing correlation from NASA should continue to be used. (Details of the alternative methods reviewed for estimating emissions are included in Appendix B.)

Chapter 4 covers the initial concept selection for combinations of technologies for the advanced-cycle year-2050 turbofan engines. Technologies considered include intercooling, recuperation, secondary combustion, open-circuit and closed-circuit bottoming cycles, and alternative topping cycles. A rationale is established for qualitatively selecting combinations of advanced core-engine technologies with potential to help meet ACARE 'Flightpath 2050' targets for CO_2, noise and emissions. Systematic assessment of technology combinations led to the down-selection of a preferred engine configuration combining topping and bottoming cycles with intercooling and secondary combustion.

Chapter 5 describes design studies and performance modelling of a possible nutating-disc topping-cycle module for the selected engine configuration. It is proposed to use a bank of six highly-turbocharged modules, each of which has separate compressor and expander discs and four pre-combustors. This novel topping-cycle technology provides an alternative to more-conventional piston engines or Wankel rotary engines that might otherwise have been used. The modules provide a pressure-rise from inlet to outlet and also generate extra shaft-power for the engine. The studies identify outstanding design challenges that would need to be addressed through improved materials and bearing technology. The display model of the concept design for a nutating-disc core module is also described.

Design requirements and enabling technologies for other novel components for the preferred engine configuration are reviewed in Chapter 6. The studies include the heat exchangers, the secondary combustion systems and the open-circuit bottoming-cycle components.

Chapter 7 describes the detailed whole-engine performance modelling work to quantify the benefits of the novel technologies. This starts by investigating a conventional Brayton-cycle geared turbofan reference engine with materials and component technologies appropriate to year 2050. A sensitivity study on engine scale-effects and intercooling quantifies the adverse effects of reduced core-size resulting from the reduced thrust requirements of the lighter and more aerodynamically efficient aircraft anticipated in year 2050. The potential benefits of secondary combustion and open-circuit bottoming cycles are assessed and used to refine the preferred engine cycle combining intercooling, nutating-disc topping-cycle modules, secondary combustion and an open-circuit bottoming cycle. A parametric study then compares the performance and SFC of this relatively-complex engine cycle with simpler variants and also quantifies sensitivity to the efficiencies of the enabling component technologies.

Chapter 8 provides further assessments of the candidate year-2050 advanced engine configurations. These integrate estimates of engine SFC and weight to estimate fuel burn and overall emissions. Modelling uncertainties are reviewed. The potential environmental costs and benefits relative to existing engines and to year-2050 ACARE SRIA Flightpath 2050 targets are also assessed.

Chapter 9 describes scenario studies to show the effects of air-traffic growth and technology improvements on the civil aviation fleet's CO_2 emissions. These studies demonstrate the potential reduction in CO_2 emissions from realizing the ULTIMATE project's goal of delivering an extra 15% reduction in fuel burn for new aircraft from year-2050 onwards.

Chapter 10 summarises the conclusions from the research and makes some recommendations for follow-on studies.

The extensive bibliography is followed by four appendices.

Appendix A reviews the impact of engine exhaust emissions

Appendix B provides more details of potential alternative existing and potential new NOx emissions correlations for year-2050 engines.

Appendix C gives more details of the whole-engine performance spreadsheet.

Appendix D describes the true motion of a nutating disc subject to the proposed anti-rotation constraint.

1.6 Publications

The author presented two papers arising from this PhD study at the 2017 ISABE conference and one of the papers was published in the Aeronautical Journal of the Royal Aeronautical Society. Contributions have also been made as a co-author to several papers on related studies.

A poster was presented at Cranfield University Aerospace PhD students' 2017 annual review, and then published on-line on the ULTIMATE project's public website [19]. The author also provided materials for the ULTIMATE project stand at the 2018 Farnborough International Air Show, These included a poster presenting Cranfield University's ULTIMATE project study engines [20] and a datasheet describing the display-model of a nutating-disc topping-cycle module.

As a participant in the ULTIMATE project, several project deliverable reports were written or co-written and edited by the author. These documents are referenced in this thesis, but they remain confidential to the partners in the project. However, most of the material that the author contributed to them is included herein.

The author's most-relevant publications are listed in Table 3.

Table 3 – Publications Related to the Current Thesis

Publications as the lead author
Rolt A., Sethi V., Jacob F., Sebastiampillai J., Xisto C., Grönstedt T., et al. ISABE 2017-22659 Scale effects on conventional and intercooled turbofan engine performance. ISABE. Manchester, UK; 2017.
Rolt A., Sethi V., Jacob F., Sebastiampillai J., Xisto C., Grönstedt T., et al. Scale effects on conventional and intercooled turbofan engine performance. The Aeronautical Journal. 2017; (October 2016): 1–24. Available at: DOI:10.1017/aer.2017.38
Rolt A., Sebastiampillai J., Jacob F., Sethi V. ISABE-2017-22660: Selecting Combinations of Advanced Aero Engine Technologies. Proceedings of the 27th ISABE Conference. 2017. pp. 1–17.
Publications as a co-author
Grönstedt T., Xisto C., Sethi V., Rolt A., Garcia Rosa N., Seitz A., et al. GT2016-56123: Ultra Low Emission Technology Innovations for Mid-Century Aircraft Turbine Engines. Proceedings of ASME Turbo Expo 2016. Seoul, South Korea: ASME; 2016. pp. 1–13.
Xisto C., Ali F., Petit O., Grönstedt T., Rolt A., Lundbladh A. GT2017-63776: Analytical model for the performance estimation of pre-cooled pulse detonation turbofan engines. Proceedings of the ASME Turbo Expo 2017. Charlotte, NC, USA; 2017. Available at: DOI:10.1115/GT2017-63776
Jacob F., Rolt AM., Sebastiampillai JM., Sethi V., Belmonte M., Cobas P. Performance of a supercritical CO2 bottoming cycle for aero applications. Applied Sciences (Switzerland). 2017; 7(3). Available at: DOI:10.3390/app7030255
Sebastiampillai J., Jacob F., Mastropierro FS., Rolt A. GT 2019-90775: Modelling Geared Turbofan and Open Rotor Engine Performance for Year-2050 Long-Range and Short-Range Aircraft. ASME 2019 Turbo Expo. 2019. pp. 1–14.

2 LITERATURE SURVEY

The literature survey starts by considering how aircraft designs may develop over the next thirty years, since improvements in aircraft structures, systems and aerodynamics will affect future engine thrust requirements. The survey then reviews the historical development of piston and compound aero engines for increased thermal efficiency, and more-recent research into novel technologies to improve aero engine performance and reduce emissions. NASA predictions for future turbofan engine performance are assessed, and research from recent EU programmes is reviewed. The potential for open rotors and topping and bottoming cycles to improve engine efficiency are addressed. Some specific topping and bottoming cycle technologies are introduced, including nutating-disc technology, but discussion of the use of nutating discs in topping cycles for large aero engines is deferred to Chapter 5. Finally the scope of the ULTIMATE project is reviewed.

2.1 Projected Aircraft Developments to Year 2050

Year-2050 reference aircraft designs have been worked-up by BHL for the ULTIMATE project as described in [11] and in ULTIMATE deliverable D2.1 [12]. A summary of the key characteristics of the year-2050 long-range ATW aircraft has already been provided in Table 1. A modest increase of c.8% in average passenger capacity is assumed relative to the year-2000 baseline aircraft.

The year-2050 aircraft's reduced take-off weight benefits from a significant reduction in the amount of fuel the aircraft needs to carry, but this benefit is offset by a significant increase in the assumed range with the design payload.

The 45% reduction in fuel burn per passenger kilometre with the year-2050 reference engine, while impressive, still falls well-short of the ambitious SRIA target of 68% reduction. Even the 45% figure depends on some questionable assumptions; notably that a lower cruise Mach number will be acceptable and that hydrogen fuel cells will be used to meet secondary power requirements. Arguably the latter benefit should be attributable to airline operational

improvements, rather than to engine and airframe technologies, since it is assumed that the engines would need to be capable of generating auxiliary power for the aircraft if hydrogen would not be available.

The advanced technologies and systems assumed to be included in the year-2050 reference aircraft are listed in Table 4.

Table 4 – Advanced Technologies in the Year-2050 Reference Aircraft

Category	**Technology**
Aerodynamics	Active flow control on vertical stabilizer using suction
	Riblets on fuselage
	Natural laminar flow nacelle
	Hybrid laminar flow control wing/tail
	High aspect ratio wings with manoeuvre and gust-load alleviation
	Variable camber wings
Weight	Advanced carbon-fibre-reinforced-polymer structures
	Cabin furnishing weight reduction
Systems	All-electric subsystems powered by hydrogen fuel cells
	Fly-by-light control systems
Propulsion	Advanced geared fan engines

For further details of the long-range and short-range study aircraft, including general arrangements, payload range diagrams, approach speeds, take-off and landing field lengths, hydrogen tank capacities etc., refer to [11].

The ULTIMATE project aimed to demonstrate the potential for 15% fuel-burn reduction beyond the reduction anticipated from a conventional year-2050 reference turbofan by the incorporation of radical engine technologies. This would give an overall 53% reduction for the long-range aircraft relative to the year-2000 baseline. Even the short-range study-aircraft, which benefits from open rotors and seems closer to meeting the SRIA target, will not meet it with

this further 15% target reduction. The conclusion is that achieving the SRIA fuel-burn target for 2050 with a kerosene-fuelled and conventionally-configured aircraft will be extremely challenging.

Several concepts for more radical airframe designs have been promoted in recent years that may help to meet the SRIA targets, but a discussion of these concepts is beyond the scope of the current thesis.

2.2 A Brief Summary of Piston Aero Engine Development

None of the advanced core cycle concepts currently being researched is of very recent origin and it can be argued that some are nearly two hundred years old. The intercooled, supercharged and turbocharged piston engines of the 1940s and turbocompound engines in the 1950s had thermal efficiencies exceeding those of contemporary turbine engines, so it is instructive to review their development and understand why these designs were superseded. There are lessons to be learned regarding the challenges facing the proposed advanced cycle core engines for the 2050s.

The earliest engines used to propel dirigibles in the 19th Century were steam engines and electric motors, but in 1900 Daimler was manufacturing 10 kW internal combustion engines for the original Zeppelin [21]. Up to the end of the First World War various piston aero engine designs were developed. After 1918, supercharging and turbocharging were introduced to increase engine power, especially for higher altitudes. As boost pressures rose, intercooling (between compressors) and/or aftercooling (just before the piston engine) were added to help increase the charge density and mass-flow of air through the cylinders. This cooling helped limit peak temperatures and avoid knocking. Intercooling improved fuel economy by enabling the engines to run less rich, when higher fuel-flow would otherwise have been needed to avoid overheating. Fuel additives were developed to raise the spontaneous ignition temperature (SIT) and so enable higher compression ratios for improved thermal efficiency.

Two piston engine arrangements proved popular. The radial engines were mostly air-cooled with three to nine cylinders having their axes in a common plane perpendicular to the axis of the propeller. When higher powers were needed, up to four additional cylinder-banks were added. The other common arrangement was to have up to six cylinders arranged in-line fore and aft. Most of these engines were liquid cooled 4-stroke designs, and when more power was demanded, V-12 and horizontally-opposed arrangements were developed. The most powerful variants had 24 cylinders, typically configured as two 12-cylinder engines geared together in an “H” arrangement. Most engines ran on gasoline, but a few diesel engines were designed, notably the 2-stroke Junkers Jumo 205 and subsequent Jumo designs. These had an opposed-piston arrangement, which eliminated cylinder-heads and therefore reduced cooling requirements. Side-porting was essential for opposed piston engines and was also used on other aero engines. Side-port sleeve-valves were developed for the large Bristol radial engines and for the Rolls-Royce Crecy [22]. The sleeves slide between the piston and cylinder to control opening and closing of the ports. The motion of the sleeves is not purely axial – they also oscillate about the cylinder axis, so unlike the pistons the sleeves never come to rest while the engine is running. This helps to maintain hydrodynamic oil-film lubrication of the piston rings, and because the sleeves slide at intermediate velocities, higher piston speeds were possible while maintaining acceptable component lives.

The highly supercharged and turbocharged piston engines of the Second World War improved power/weight ratios and thermal efficiency. Turbo-compounding was a further development, where additional power was extracted from exhaust turbines and fed back through gearing to the propeller shaft. The two-stroke Rolls-Royce Crecy [22] and the four-stroke Wright R-3350 Duplex Cyclone turbo-compound engines were early examples, the latter going on to power long-range 1940s and 50s airliners like the Lockheed Super Constellation.

The Napier Nomad turbo-compound engines had very high boost pressures (7:1) and produced relatively greater power from their turbomachinery. The Nomad I, and the somewhat-simpler Nomad II, were horizontally-opposed

12-cylinder two-stroke diesel engines. The Nomad II claimed 30% lower SFC than then state-of-the-art aero engines [23], but like the Rolls-Royce Crecy, the Napier Nomad never entered service.

Napier also built a highly turbocharged prototype engine based on its 36-piston 18-cylinder Deltic diesel engine, but this suffered a crankshaft failure on test before reaching its targeted 6,000 hp power output. Like the Junkers Jumo 205, the Deltic diesels had opposed-piston arrangements.

These high-power turbocompound engine developments were superseded by turbo-prop and turbojet engines in the 1950s and by turbofans in the 1960s. Turbocompound engines were more complex than gas turbines and could not match their power/weight ratios. Their better SFC was outweighed by the lower weight of gas turbines and the latter's higher reliability and lower maintenance costs. Turbine powered aircraft also improved productivity by flying higher and faster and offered smoother flights with less engine noise and vibration.

2.3 More-Recent Research into Advanced-Cycle Aero Engines

The section focuses on the advanced cycle technologies of intercooling, recuperation, pressure-rise combustion, secondary combustion, topping cycles and bottoming cycles. The author has had involvement in investigating most of these technologies in several previous EU and UK funded research projects aimed at developing lower-TRL concepts for future aero engines. These activities started with the EEFAE ANTLE project and progressed through VITAL [24], NEWAC [25], LEMCOTEC [26] and ENOVAL [27], amongst others.

Several advanced engine design concepts were researched in NEWAC by MTU and Snecma (now Safran Aircraft Engines) and by Rolls-Royce and Volvo Aero (now GKN Aerospace Sweden). The last two companies together with Oxford, Loughborough and Chalmers Universities, researched intercooled engine cycles having high overall pressure ratio (OPR) [28]. An overall assessment of the advanced cycles in NEWAC concluded that the best combinations of technologies could achieve a significant reduction in fuel burn and CO_2

emissions in a long-range aircraft, but would achieve less than the original target of a 6% reduction [29]. The biggest improvement came from combining intercooling with the geared fan architecture and active control of compressor tip clearances. Optimisation of the intercooled engine concept was reported in more detail in [30]. High OPR intercooled engines were found to be heavier than conventional engines and to have increased nacelle drag. These factors, combined with reduced efficiency in their smaller core components, accounted for their fuel burn benefits not living up to the original expectations.

Figure 5 shows the original intercooled engine concept from NEWAC.

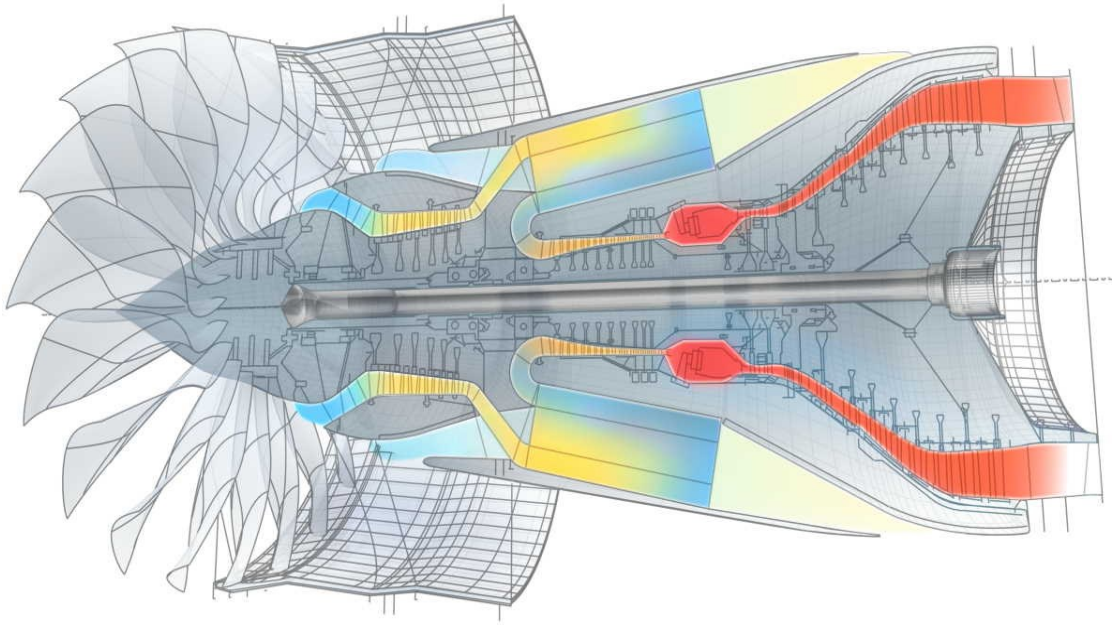

Figure 5 – Schematic Diagram of an Intercooled Engine with a low-speed LP turbine and a direct-drive fan [29]

The intercooler uses part of the fan bypass air flow to cool the IP compressor delivery air before it enters the HP compressor, and it reduces compression work by reducing the inlet air temperature for the HP compressor and the volume flow rate of the air passing through it. This saves some core turbomachinery weight by reducing annulus cross-section areas, but the intercooler itself adds weight and increases drag, offsetting much of the potential fuel burn benefit [29].

Intercooling alone was shown to give relatively modest fuel-burn benefits. Applied early in the compression system intercooling is always beneficial, but the intercooler's pressure losses need to be offset, so intercooling generally has to be combined with increased OPR to show a SFC benefit. Thus intercooling improves performance mostly by permitting increased OPR without exceeding realistic T3 limits.

Later NEWAC studies proposed a geared fan driven by a high-speed LP turbine that also drove a high-speed booster or IP compressor. The smaller-diameter and lower-torque LP shaft enabled a faster-running and smaller-diameter HP system with lower rotor hub/tip radius ratios[2]. This reduced the blade and stage counts and increased blade heights, significantly improving the HP compressor efficiency [30] and SFC.

For a fuel-burn benefit, weight and nacelle drag must also be taken into account. The weight increase from the heat exchangers is somewhat offset by the increase in core specific power, which reduces core turbomachinery weight. This saving is greater in engines with geared fans and high-speed LP turbines, since these engines are unlikely to need to add extra turbine stages when the core mass flow is reduced. Given the probable net weight and drag increases from intercooling, the technology by itself only offers modest fuel-burn reduction in turbofans, and little or no fuel-burn benefit for smaller open rotor engines in short-range aircraft. However, NEWAC also showed that intercooling could reduce NOx emissions relative to a conventional cycle in high-OPR engines. The reduction is most noticeable with conventional RQL combustors, where higher inlet temperatures result in higher stoichiometric flame temperatures. NOx emissions are also reduced with lean-burn combustors, but the benefit is not so large because their flame temperatures are less sensitive to combustor inlet temperature.

[2] In an axial-flow compressor or turbine, the hub/tip ratio is the ratio of the radius of the inner gas-path annulus line to the radius of the outer gas-path annulus line. The difference between these radii is the span or 'height' of the blading plus the radial clearance. Hub/tip ratios are commonly quoted at entry and exit to a component.

Intercooling also benefits compound cycle engines. An intercooler positioned after a compressor and before a piston engine is often called an aftercooler. Aftercooling is widely used in modern turbocharged diesel engines. Historically both intercooling and aftercooling have been used in those piston aero engines having two-stages of turbo-compression. The benefits included reduced inlet temperatures for piston engines having high levels of turbo-boost. This enabled higher compression ratio, peak cycle pressure and core specific power, without reducing component life. Another benefit was increased inlet air density, which reduced the required cylinder capacity, helping to increase power/weight ratio.

Intercooling allows increased OPR and/or a bigger combustor temperature rise and smaller core mass flow for a given TET and combustor heat input. This reduces core mass flow, which is beneficial in that it reduces the entropy generated by losses in core, but it also results in disproportionately smaller core turbomachines especially when OPR is increased. This tends to reduce core component efficiencies. Scaling-down the engine thrust requirements also reduces core component efficiencies.

The alternative Intercooled and Recuperated Aero Engine (IRA) concept has been developed by MTU and its research partners, and they rig-tested a recuperator module downstream of a gas-turbine core-engine In the EEFAE CLEAN project [31] [32]. The IRA concept was further developed in NEWAC, LEMCOTEC and ULTIMATE, with MTU partner AUTH working on improved recuperator installations to reduce the associated pressure losses [33].

In a recuperated gas turbine, heat is extracted from the core exhaust and used to preheat the air entering the combustor. The recuperator is a heat exchanger with two physically separated fluid flows, but small gas turbines have often substituted rotary regenerators, where the two flows pass alternately through the same matrix passages. Use of recuperation or regeneration is particularly beneficial for small gas turbines that cannot in practice increase OPR to improve thermal efficiency. For larger and higher pressure ratio aero engines, recuperators are preferred to regenerators. There are further benefits in

combining intercooling with recuperation, as this enables higher OPR designs to be used, while still maintaining a good margin between the turbine exhaust gas temperature (TEGT) and the HP compressor exit temperature (T3). This ensures a useful amount of heat can be transferred. Recuperation can greatly increase the thermal efficiency of small gas-turbine engines that are inherently limited on overall pressure ratio (OPR). It offers relatively smaller improvements to larger engines having higher OPR, unless they should burn a lot of fuel at low-power operation. This does not apply to most civil aero engine applications. Recuperation also increases engine weight, though research in LEMCOTEC and ULTIMATE has shown potential to minimize recuperator weight penalties.

Figure 6 shows the IRA concept from the NEWAC programme [29].

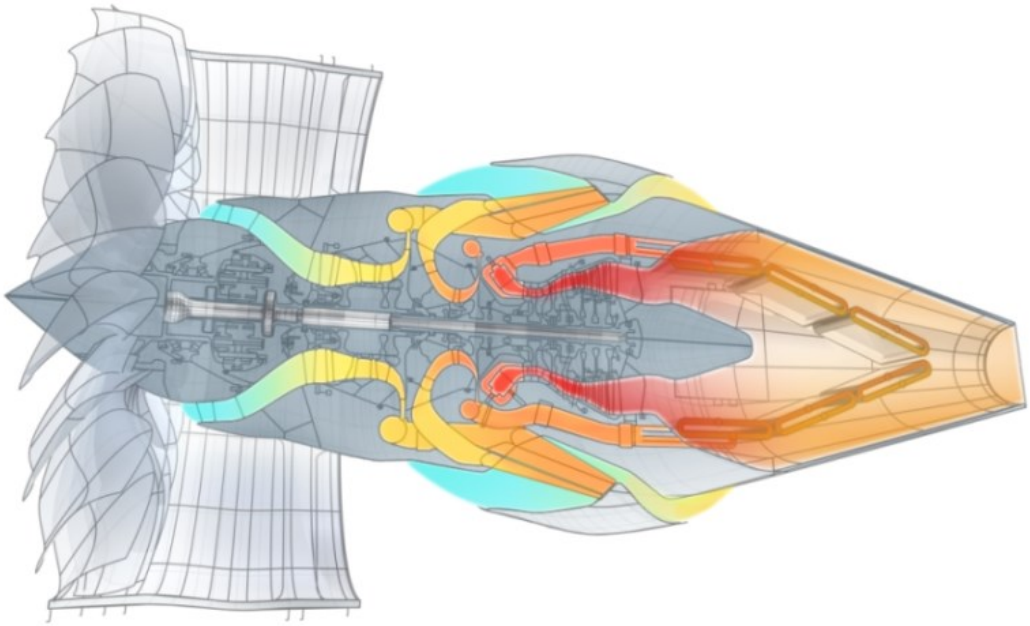

Figure 6 – Schematic Diagram of an Intercooled and Recuperated Engine (IRA) with a geared fan [29]

Intercooled and recuperated engines can have better SFC than the high-OPR intercooled engines, particularly in the case of smaller engines that would suffer larger efficiency penalties from the scaling-down of their turbomachinery.

Following-on from NEWAC, the LEMCOTEC and ULTIMATE programmes have researched improved heat-exchanger designs to increase effectiveness and

reduce weight, pressure loss and installation penalties. Significant benefits have been demonstrated from reconfiguring the gas-to-air primary-surface ‘profiled tube’ or ‘lancette’ type of recuperator [34] [8].

Separately from the NEWAC project, high OPR intercooled, and intercooled and recuperated engine cycles have been studied at other institutions. A contrary conclusion from Lebre and Brójo [35] was that recuperation or regeneration could improve SFC, but that intercooling and intercooling and recuperation offered no benefits relative to a conventional turbofan engine cycle. However, the intercooled cruise OPR figures assumed in that study were in the range 25-29 whereas higher OPR is needed to see a benefit from intercooling without recuperation. This is because the saving in compressor work needs to be sufficient to compensate for the heat exchanger pressure losses.

To reduce the pressure losses, consideration has been given to using existing compressor aerofoils as heat exchange surfaces [36], but the surface areas are too small to transfer a significant amount of heat, so the SFC improvement is limited. These and other studies often overlooked the benefits to be obtained by re-matching the heat-exchanger cycles off-design. Intercooled and recuperated cycles benefit from variable-area turbines that can reduce the OPR and raise the TET at cruise, maximising the heat transferred from the exhaust to the combustor through the recuperator. High-OPR intercooled cycles also benefit from reducing intercooler cooling-air flows at cruise, reducing pressure losses and enabling the engine to run hotter. Bypassing part of the core flow around the intercooler at cruise may also provide an additional 0.5% SFC benefit [37].

A reverse-flow-core intercooled engine was studied at Cranfield University in the LEMCOTEC project, starting with a parametric performance assessment [38]. The chief advantage of this engine arrangement, relative to a straight-through core, is that the LP shaft does not pass through the HP spool and so does not compromise the core compressor and turbine efficiencies by imposing low rotational-speeds and high hub/tip ratios. Reverse-flow-core engines also benefit from having a mixed-exhaust arrangement which helps transfer energy

to the bypass stream, and from having more freedom in the positioning of the intercooler modules to minimise bypass duct blockage and nacelle drag.

The selected engine design was described in [39] and then a more detailed study and assessment of the intercooler and LP turbine exhaust ducting pressure losses and exhaust mixer arrangements was undertaken [18]. At the end of these studies it was concluded that the reverse-flow-core arrangement did improve cruise SFC and fuel burn, but only by about one per cent relative to the geared-fan straight-through core arrangement. A schematic diagram, Figure 7, shows the proposed reverse-flow-core engine arrangement.

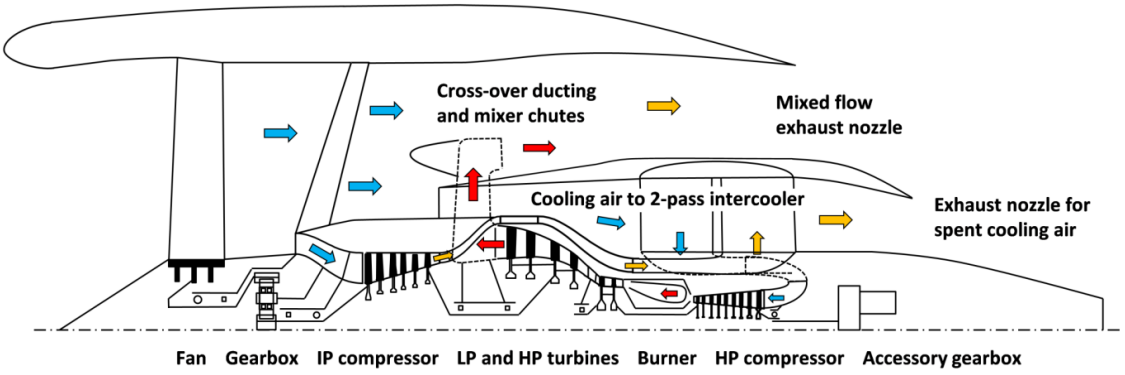

Figure 7 – Reverse-flow-core Intercooled Turbofan Schematic Diagram from the LEMCOTEC programme [40]

A 2015 paper by Jorge Sieber [41] from MTU provided a good overview of the advanced technologies developed in major EU programmes over the previous 15 years and looked ahead to see what further improvements would be possible by 2035. It concluded that 'All European technology programs combined are expected to reduce CO_2 emissions by more than 25% as compared with the year-2000 engine.' This compared with the SRIA CO_2 reduction targets of 20% at TRL 6 in 2020 and 30% in 2035, attributable to engine technologies as shown in Table 2. The paper also predicted NOx emission reductions in line with ACARE Vision 2020 targets, whereas the noise reduction targets would not quite be met. The 25% reduction in CO_2 still falls a long way short of the projected target of 43% by 2050. Most of the new technologies specific to

ULTIMATE are not included in these assessments, but ULTIMATE technologies have needed to build on the earlier research to address longer-term targets.

Contemporary research efforts have also considered distributed propulsion with boundary layer ingestion and hybrid-electric propulsion. These technologies and energy-storage are combined in turbo-electric distributed propulsion (TeDP) concept studies. The author has previously reviewed the potential benefits of such systems [6] [42]. These concepts are relevant to this study to the extent that they may affect the power requirements demanded of future engine cores at cruise, climb and take-off. A recent paper from Rolls-Royce [43] assesses the benefits of supplementing the power of a turbofan engine with stored energy at take-off, climb and descent. It predicts in-flight fuel burn reductions of over 8% on a typical short-range mission if the batteries are recharged on the ground. Alternatively the batteries could be recharged during cruise and still reduce fuel burn because the engines would still have smaller cores and operate at higher power with improved thermal efficiency during cruise. The Cycle-Integrated Parallel-Hybrid engine concept has also been studied at BHL together with the Composite Cycle Engine (CCE) concept [44]. Electrical technologies could clearly benefit advanced cycle engines by improving their operability, and hybrid-electric systems might also be used help to reduce the impact of NOx emissions at take-off, and of contrails at altitude.

2.4 Advanced Engine Study from NASA

NASA has published details of a future reference study engine, which makes an interesting comparison with year-2025 and year-2050 study engines developed in European research projects including the ULTIMATE programme.

The Advanced Air Transport Technology (AATT) ‘N+3 Technology Reference Propulsion System’ (TRPS) is a future turbofan with CFM56 thrust levels and a geared fan. It has very low specific-thrust. Paper NASA/TM-2017-219501 by Scott Jones et al. [45] provides details of its projected climb, cruise and take-off performance, tabulating data from a detailed NPSS performance model.

N+3 technology originally implied achieving TRL4-6 by 2025, roughly equivalent to EIS by 2030. Key design parameters are given in Table 5 and a performance summary is given in Table 6 for top of climb (TOC), cruise and end-of-runway (EOR) take-off cases. Note the quoted cruise thrust at 90% of the top of climb thrust is unrealistically high and flatters the engine's cruise SFC figure.

The TRPS engine has a 3-stage high-speed booster driven by a 3-stage LP turbine, an 8-stage all-axial HP compressor (HPC) and a 2-stage HP turbine (HPT). The fan is driven via a 3.1 reduction gear ratio.

Table 5 – NASA N+3 Technology Reference Propulsion System (TRPS)

Parameter	Units	Value
Fan diameter	in (m)	100 (2.54)
Nacelle diameter	in (m)	121 (3.07)
Engine length	in (m)	135 (3.43)
HP compressor last-stage blade-height	in (mm)	0.42 (10.7)
Total engine weight	lb (kg)	9300-9350 (4218-4241)
Secondary air flows	–	15%

To enable the selected cycle's very low specific thrust, it is assumed significant nacelle drag reductions can be achieved and an advanced short intake design and variable-area cold nozzle will address the operability issues associated with cross-wind take-off etc.

Note these are some of the design challenges that have been investigated by ISAE in the ULTIMATE project.

The fan bypass-stage polytropic efficiency of 97% seems optimistic and in the author's opinion this engine has unrealistically-low specific thrust to be optimal for 2030 EIS, unless perhaps it would have to meet a very stringent noise target. In other respects the engine performance seems generally credible.

Table 6 – NASA N+3 TRPS Key Performance Data

Parameter	Units	TOC	Cruise	EOR Take-off
Altitude	ft (m)	35000 (10668)	35000 (10668)	0
Mach number	–	0.80	0.80	0.25
Deviation from ISA	K	0	0	+15
True Air Speed	kn (m/s)	461.3 (237.1)	461.3 (237.1)	169.6 (87.2)
Inlet Mass Flow	lb/s(kg/s)	813.5 (369.0)	795.6 (360.9)	1903.7 (863.5)
Thrust	lbf (kN)	6073 (27.0)	5466 (24.3)	22800 (101.4)
Specific Thrust	m/s	73.2	67.4	117.5
OPR[1]	–	55.0	51.5	42.9
BPR[2]	–	23.99	24.55	25.77
Fan Pressure Ratio	–	1.300	1.276	1.218
HPC Pressure Ratio	–	14.10	13.51	13.22
T3[3]	R (K)	1531 (851)	1489 (827)	1722 (957)
T4[4]	R (K)	3150 (1750)	3035 (1686)	3400 (1889)
SFC	lb/hr/lbf (g/kN.s)	0.4636 (13.13)	0.4644 (13.15)	0.2891 (8.19)
Overall Efficiency[5]	–	42.18%	42.11%	24.87%

1. Overall Pressure Ratio
2. Bypass Ratio
3. HPC delivery temperature
4. Combustor exit temperature
5. Assuming the specification minimum fuel lower heating value (FHV) of 42797 kJ/kg

2.5 Ducted Fans v. Open Rotors

Turboprop engines remain popular for regional or ‘commuter’ aircraft and deliver significantly better fuel economy than comparable turbofan powered aircraft. However, turboprop aircraft operate at significantly lower cruise speeds than turbofan aircraft, reducing their productivity and limiting their operation to relatively-short routes. When fuel costs rose in the 1970s there was interest in developing higher-speed ‘Propfan’ engines, now commonly referred to more generically as ‘open rotors’. Research into open rotor engines as alternatives to turbofans has continued for over 40 years, but open rotors have yet to be put

into production for commercial aircraft. In the meantime higher-cruise-speed turboprop aircraft were investigated and the 50-passenger SAAB 2000 [46], was manufactured, powered by a pair of AE2100 engines with Dowty Aerospace 6-bladed propellers. However, only 63 of these aircraft were sold. At a cruise speed of 665 km/hr, it was about 80% as fast as a 0.78 Mach number turbofan-powered aircraft like the Boeing 737. To make open rotors more competitive with turbofans, the ULTIMATE project has targeted 0.75 Mach number.

Open rotor powerplants can have either tractor or pusher configuration. A second contra-rotating blade row straightens out the swirl from the first rotor, increasing the overall efficiency. This also enables quieter, lower-tip-speed propellers to be used. Low noise is essential if open rotor powerplants are to be adopted on future medium-sized commercial aircraft. For these aircraft, the pusher arrangement, with engines mounted on pylons either side of the aft fuselage, is now generally preferred in order to reduce cabin noise. Provided the core exhaust is ducted around the rotor hubs, to avoid it impinging on the propeller blades, and blades are clipped, certification noise limits should be met.

A further advantage of the pusher arrangement is that the propulsor drive-shafts do not need to run through the core of the engine and so do not compromise its mechanical and aerodynamic design. Nevertheless the tractor arrangement may still be preferred for wing mounted engines on lower speed aircraft. In this case a reverse flow core arrangement, like that of the Pratt & Whitney PT6 turboprop, should help to avoid compromising the turbomachinery design.

Contra-rotating open rotors offer significant fuel burn reductions from increased propulsive efficiency and reduced nacelle drag, but they are less attractive for larger aircraft wanting higher cruise speeds for longer flights. This is because higher power levels would be needed to fly faster and the cost and weight of the open rotor engines would increase disproportionately in relation to turbofan engines. Therefore open rotor engines have not been modelled by the author. However, the effects of scaling-down the thrust requirements for a turbofan to

levels where the core mass-flow would be more appropriate for an open rotor have been considered and are described in sections 7.3.1 and 7.3.2.

2.6 Topping Cycles

One means of reducing performance-sensitivity to loss of turbomachinery efficiency from low non-dimensional mass flows in engine cores is to replace the core turbomachinery with positive-displacement topping-cycle machinery that also generates additional power. Alternatively, a topping cycle can just be a pressure-rise combustion system.

The following core arrangements are possible:

- Valve-less, resonant, pressure-rise combustion systems
- Pulse detonation combustor (PDC) systems having inlet valves
- Wave rotors with inlet and outlet valves
- Conventional piston engines
- Rotary or nutating disc machines
- Free-piston engines

The first three options produce a pressure rise without shaft power output. The fourth and fifth options generate shaft power and may or may not also produce a pressure rise. Free-piston engines traditionally just produced a pressure rise, but they are now being developed with linear electromagnetic generators to produce electrical power output for hybrid-electric automotive applications.

2.6.1 Pressure-rise Combustion

The three pressure-gain arrangements can be categorised at top level by the number and location of the valves used to regulate their intermittent flow. For example, ‘valveless’ pulse-pressure-rise designs providing an increase of over 5% in total pressure have been run at Cambridge University [47] [48]. These combustors have fluidic inlet valves and resonance is set-up by tuning the inlet and exhaust diffuser geometries. Pressure-rise can be enhanced by modulating the fuel injection. Combustion is deflagrative rather than detonative.

Conversely, wave rotor designs have valves both at inlet and exit. A wave-rotor pressure-rise combustion rig has been run at Purdue University [49]. Wave rotors can be designed for detonation, but deflagration is considered likely to be more practical and can still provide a significant pressure rise. Notwithstanding the design challenges relating to their inlet and outlet valves, fuel injection, ignition, and cooling systems, the author considers that wave-rotor designs may have the best long-term prospects as pure-pressure-rise combustion systems.

Pressure-rise combustion systems generally feature intermittent or unsteady combustion, but an exception is the rotating-wave pulse-detonation combustor. Here the supersonic detonation wave continuously circles around within an annular combustion chamber. While the combustion is continuous the pressure-rise delivered still fluctuates spatially and temporally in the static frame of reference, particularly where the incoming fuel-air mixture and combustion products cross the instantaneous wave-front. The frequency of the pressure pulses is much higher than that typically generated in pulse-detonation tubes.

The mechanical design of rotating-detonation-wave combustors is challenging on account of their high heat transfer rates and severe wall-cooling requirements. Test-runs have typically been extremely short. Anecdotally they were also extremely noisy. One possible pulse-detonation combustion system researched in ULTIMATE is described in section 2.9.1.

2.6.2 Piston-engine Cores

Another class of topping-cycle machines extracts power during or immediately after intermittent combustion. These operate on the Otto or Diesel cycle or on a combination of the two. The historical development of piston engines for aircraft propulsion has been described in section 2.2, but for commercial aircraft these developments largely ceased in the 1950s. Since then the development of piston engines for automotive and marine use has made significant advances, particularly in the areas of fuel injection and control of exhaust emissions, and these advances could read across to aero engines.

Historic turbo-compound engines derived most of their power from the pistons and supplemented this with turbine power, but it seems a reasonable assumption that a larger proportion of the overall power would come from the turbomachinery in future CCE engine designs, not least because this will improve power/weight ratios.

The BHL CCE concept is one approach seeking to reanimate the earlier turbocompound engines of the 20th century, while benefiting from more recent piston engine developments.

2.6.3 Rotary Engine Cores and Nutating Discs

Possible alternatives to piston engines in a composite cycle include Wankel rotary and nutating-disc engines. Replacing the HP spool of a three-shaft turbofan with a large Wankel engine has been investigated by John Whurr [50]. In this concept the IP compressor was driven by the Wankel engine core. However, a follow-on study by Ricardo showed that the proposed high rotational speed of the Wankel core was not achievable with the technology then available. Scaling-up the core and running it slower was not an attractive option.

Nutating disc machines have been used as pumps and motors at least since the 19th century, but more-recent interest in nutating-disc engine concepts followed from the 1993 patent by Leonard Meyer [51], papers by Theodosius Korakianitis et al. [52] [53] and [54], and a NASA funded research project.

At Cranfield University, nutating-disc aero engine designs have been investigated by Rakeshh Mohanarangan [55], Jeremy Cochereau [56] and most recently by Joshua Sebastiampillai [57] as part of the ULTIMATE programme. The last of these studies applied nutating-disc modules to an advanced open rotor engine with contra-rotating pusher propellers. A schematic diagram of the proposed engine arrangement is shown in Figure 8. Four to six nutating disc modules are substituted for the HP spool in the reference open-rotor engine and help drive the LP compressor. Several variant designs were also studied.

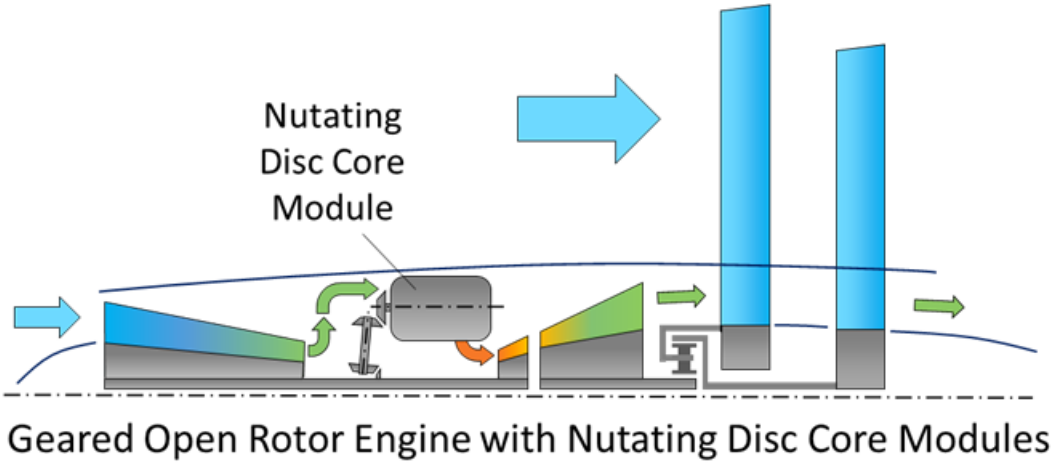

Figure 8 – Concept for an Open Rotor with a Topping Cycle
(colour-coding is indicative of cycle temperatures, with red being hottest)

Figure 9, from Meyer's patent [51], shows a nutating-disc engine with a single bi-conical disc mounted on a 'Z-shaft'. The bottom-half of the engine performs air compression and the top-half sees combustion and expansion of the gasses.

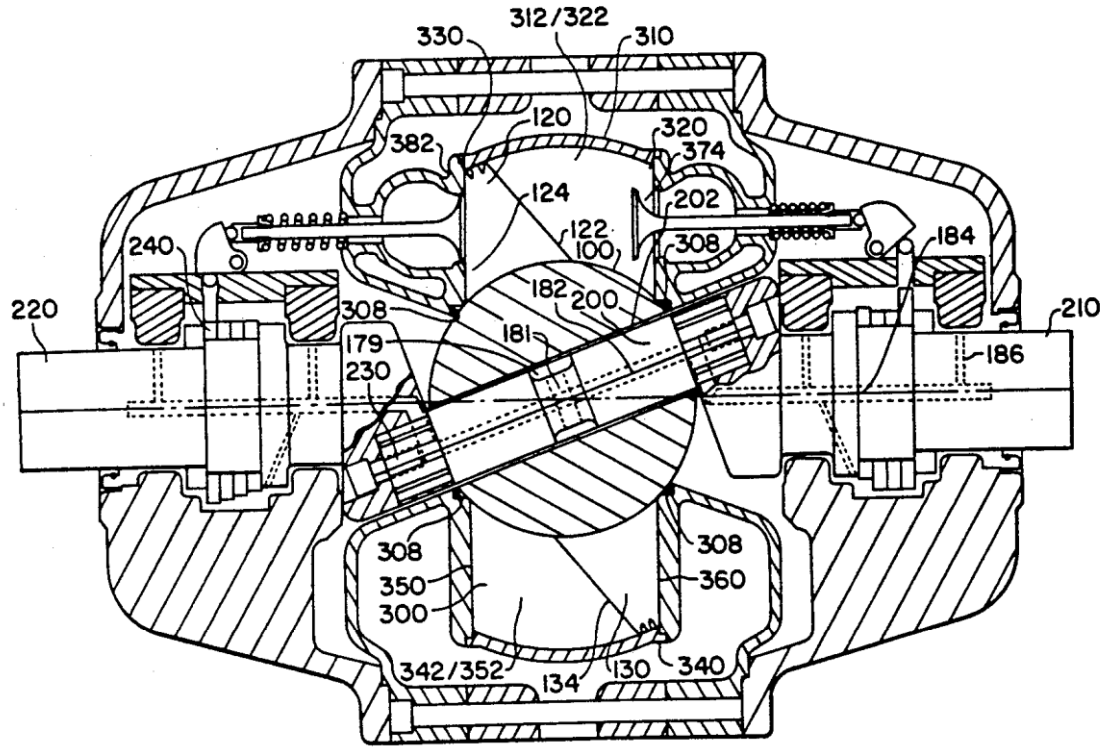

Figure 9 – Cross-section of a Nutating-disc Engine from Meyer's Patent [51]

The nutating disc is prevented from rotating with the rotating shaft, so it is forced to wobble in the manner described as ‘nutation’. This motion is similar to that of a coin spinning on a table-top just before it falls flat onto the table. In operation, the gas pressures acting on the discs make the Z-shaft rotate.

Having two separate discs for compression and expansion, as investigated by Korakianitis [52], is the preferred arrangement for higher-power engines. Two discs double the mass flow and power output and balance-out each-other’s nutating motion if they are the same size and mass and aligned in mirror image to each other. A single disc, however, will force its unbalanced wobbling motion on to the engine mountings. Furthermore, any single-disc engine will have a hot hemisphere and a cold hemisphere, introducing asymmetric thermal distortions.

Some kinds of topping-cycle machinery can provide relatively more power together and a small pressure rise to the downstream turbines, or alternatively offer a larger pressure rise and less power. Nutating-disc engines have this flexibility, which could be an advantage relative to conventional two-stroke piston engines, since those can only run with an overall pressure drop that is needed for scavenging. Positive-displacement topping-cycle machines should make best use of their available swept volumes.

A hypothetical four-stroke piston engine that just delivered a pressure rise would seem to be non-optimal, since its exhaust gasses would exit at very high temperatures, presenting challenging design problems for the exhaust valves and ducting. A small piston engine that drives a separate turbo-compressor or a larger-volume and lower-pressure piston compressor, as proposed by BHL [58], is likely to provide a lighter and more efficient design than a piston engine with over-sized pistons.

One way of providing extra compression volume is to have a stepped free-piston with the larger diameter section providing separate pre-compression. This was proposed by Herman Klingels [17] and is illustrated in Figure 10

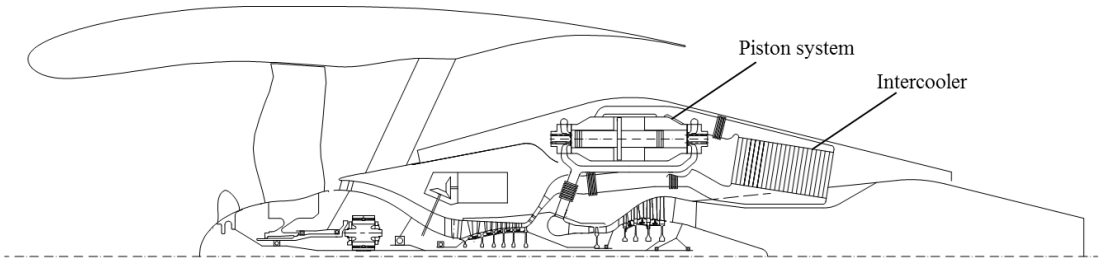

Figure 10 – Alternative Intercooled CCE Concept from MTU and BHL [58]

Nutating-disc machines, and some novel piston engine designs with separate chambers for compression and expansion, could use a larger compression chamber with a higher compression ratio to balance power requirements. However, considering cooling requirements, it seems preferable for topping-cycle machines to be designed to generate shaft-power or electrical-power output rather than a big pressure rise, not least because it will reduce the outlet temperature. The extra power could either be used to drive additional pre-compression machinery, or exported for use elsewhere in the engine. Alternatively the extra power could be used more remotely on the aircraft, e.g. to realize distributed propulsion.

Note the design and assessment of nutating-disc topping-cycle modules is addressed in more detail in Chapter 5.

2.7 Bottoming Cycles

A bottoming cycle is a Rankine, or similar, cycle that extracts additional work from an engine's exhaust heat. It is separate from the main engine cycle and commonly uses a different working fluid [16]. This is unlike most topping cycles, which are usually fully-integrated into the main performance cycle and use the same working fluids: air and the products of combustion. Though they can improve overall efficiency, the stand-alone thermal efficiency of most bottoming cycles is low because the incoming turbine exhaust gas temperature is relatively low, giving a low temperature ratio across the cycle. Bottoming cycles benefit emissions only by improving overall efficiency and reducing fuel flow.

For example, in a stationary gas turbine the extra pressure loss in a heat-recovery steam-generator will tend to reduce the pressure ratio across the main power turbine, slightly reducing its power output and partly offsetting the power increase from the steam turbine in the combined cycle. In an aero engine, there is a further negative effect because some of the thrust comes from the hot exhaust jet. Reducing its temperature reduces the jet velocity unless the nozzle pressure ratio is increased, but that also reduces the power from the turbines.

Secondary combustion can be used to raise downstream turbine exhaust gas temperatures to boost bottoming cycle efficiency. By increasing the final fuel/air ratio (FAR) this also reduces the main core mass flow and should save weight.

2.7.1 Closed-Circuit Bottoming Cycles

A closed-circuit bottoming cycle requires a pre-cooler or condenser, which will be air-cooled in an aero engine [16] [9]. If this heat exchanger uses bypass air in a matrix-type heat exchanger, then the pressure loss will reduce the amount of thrust that can be recovered from the spent cooling air. However, the warming of this air flow will tend to increase the potential thrust-recovery from the spent cooling air, and as in the case of an air-cooled intercooler, these effects will tend to cancel out. Alternatively, if a nacelle-surface heat exchanger is used, as was suggested in one of the ENOVAL project studies [59], heating the boundary layer should reduce the nacelle drag [60].

Organic Rankine Cycles (ORC) were previously considered as bottoming cycles for aircraft power generation [61], though supercritical CO_2 (S-CO_2) was later identified as the preferred closed-circuit bottoming cycle working fluid because it offered higher power density and greater thermal stability at higher operating temperatures. Also, most organic fluids are highly flammable, but CO_2 is not. Supercritical CO_2 can be compressed more efficiently than an ideal gas when close to its critical point, and its critical temperature of 304 K is appropriate. In ULTIMATE, Florian Jacob modelled a turbofan engine with a supercritical-CO_2 bottoming cycle and predicted up to 3% fuel-burn improvement relative to the reference turbofan [9] [62]. Figure 11 shows the proposed layout of the engine.

It needed large heat exchangers and Jacob concluded that space requirements for the pre-cooler would conflict with those for a possible air-cooled intercooler, so combining these two technologies would be problematic. Therefore that combination was not investigated in any detail. Conversely, the CO_2 turbomachinery was extremely small. If the latter had been drawn to scale in Figure 11, the compressor and turbine would have been barely visible.

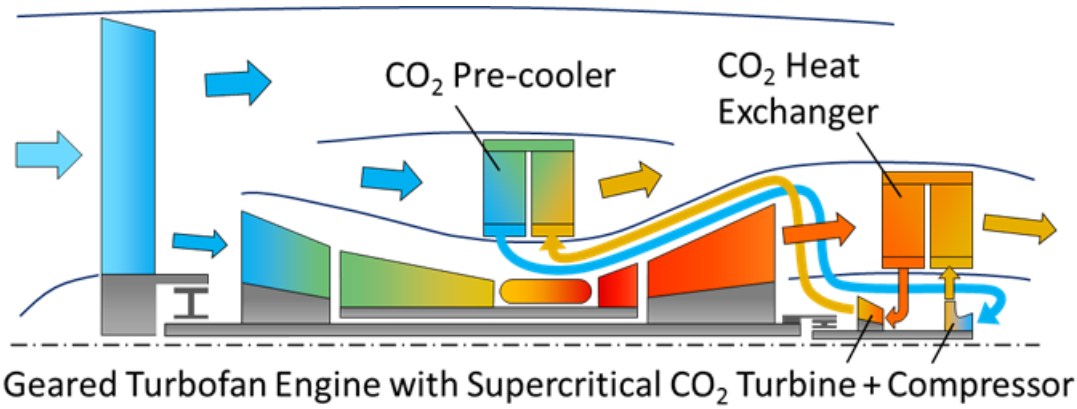

Figure 11 – Schematic of a Turbofan with a CO_2 Bottoming Cycle [62]
(colour-coding is indicative of cycle temperatures, with red being hottest)

In a fully worked-up engine installation, integration of the heat exchangers into the engine powerplant would need careful consideration to avoid conflicts with engine accessories and core dressings. Thus the closed-circuit system might be more attractive as part of a hybrid-electric propulsion system where the core-engines would have a buried or partly-buried installation, which would free-up conventional-nacelle space-constraints on the heat exchanger locations and enable the potential synergies with intercooling and secondary combustion to be realized. In such installations the CO_2 spool might simply drive an electrical generator to feed power into an airframe-wide distributed electrical system.

Another possibility is the combination of a closed-circuit bottoming cycle with cryogenic fuels. Using cryo-fuels alone in the pre-cooler will not enable very much power to be generated, but if the cryofuel is used for the last stage of cooling after an air-cooled pre-cooler, then it would enable a smaller, lower-drag air-cooled pre-cooler to be used and it might enable the CO_2 to be cooled closer

to its critical point on hotter days: at take-off for example. Mikel Beretens Izquierdo has modelled a possible cryogenic-hydrogen pre-cooler design [63].

The technologies needed for supercritical-CO_2 turbomachinery are already being actively researched and developed for power-generation and marine propulsion. Supercritical-CO_2 also seems the best choice for the closed-circuit bottoming-cycle working fluid for aero engines. While the fuel-burn benefit of the supercritical-CO_2 bottoming cycle modelled by Jacob [9] was only assessed as around 3%, the use of supercritical-CO_2 seems worth further research effort, because such a system could be added to a conventional large turbofan engine with relatively low risk and no adverse effects on noise or emissions.

The technology has the potential to be introduced well in advance of year 2050. However, the weight and drag of the air-cooled pre-cooler may mean the alternative of an open-circuit bottoming cycle using air is more attractive.

2.7.2 Open-Circuit Bottoming Cycles

An open-circuit Air Bottoming Cycle (ABC), that uses air as its working fluid, would simplify maintenance and avoid the cost, weight and drag of a pre-cooler. The ABC may be partially integrated with the main gas turbine cycle, with shared compression, and possibly also expansion, with parallel flows through parts of the compressor and turbine systems. On the other hand, the open-circuit bottoming cycles will tend to be less efficient because they cannot benefit from using a selected closed-circuit working fluid that undergoes compression close to its critical point, where much less work is required.

A study of bottoming cycles for aero engines was made in ‘EVÅF’, part of NFFP (the Swedish Aeronautical Research Programme). The initial findings report by Anders Lundbladh [10] proposed an open air-cycle where a medium pressure turbofan bypass flow is heated by the LP turbine exhaust and recycled through the LP turbine. Herman Klingels also included an ABC design in his Wärmekraftmaschine für Freikolbenverdichter patent application [17]. However, there is a need for more research on ABC cycles and components.

The author's assessment of the potential benefits of an ABC as part of his proposed advanced turbofan engine cycle #06 is given in section 6.3.

2.8 NEWAC Study Engines and Combustor Designs

The NEWAC project studied four advanced-core engine concepts. These were:

- The Intercooled and Recuperated Aero engine (IRA),
- The high OPR Intercooled Core engine (IC),
- The Active Core engine (AC)
- The Flow Controlled Core engine (FCC)

The last two concepts had more-conventional Brayton cycles, but additional technologies for tip clearance control and aspirated compression systems. The NEWAC study engines and their combustor options are shown schematically in Figure 12 [29].

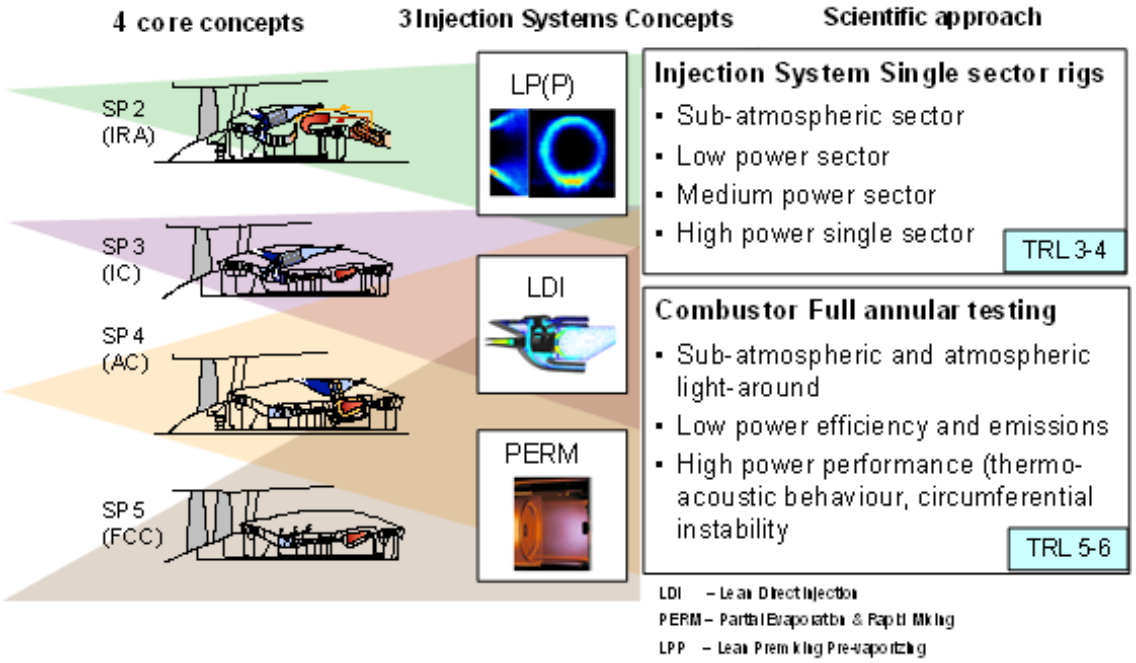

Figure 12 – Combustor Designs and Tests for NEWAC Advanced Cycle Engine Concepts

Figure 13 shows NOx emissions predictions for both the long-range (LR) and short-range (SR) turbofan concepts studied in the NEWAC programme [29]. The LDI combustor predictions were backed-up by Full-Annular (FANN) tests.

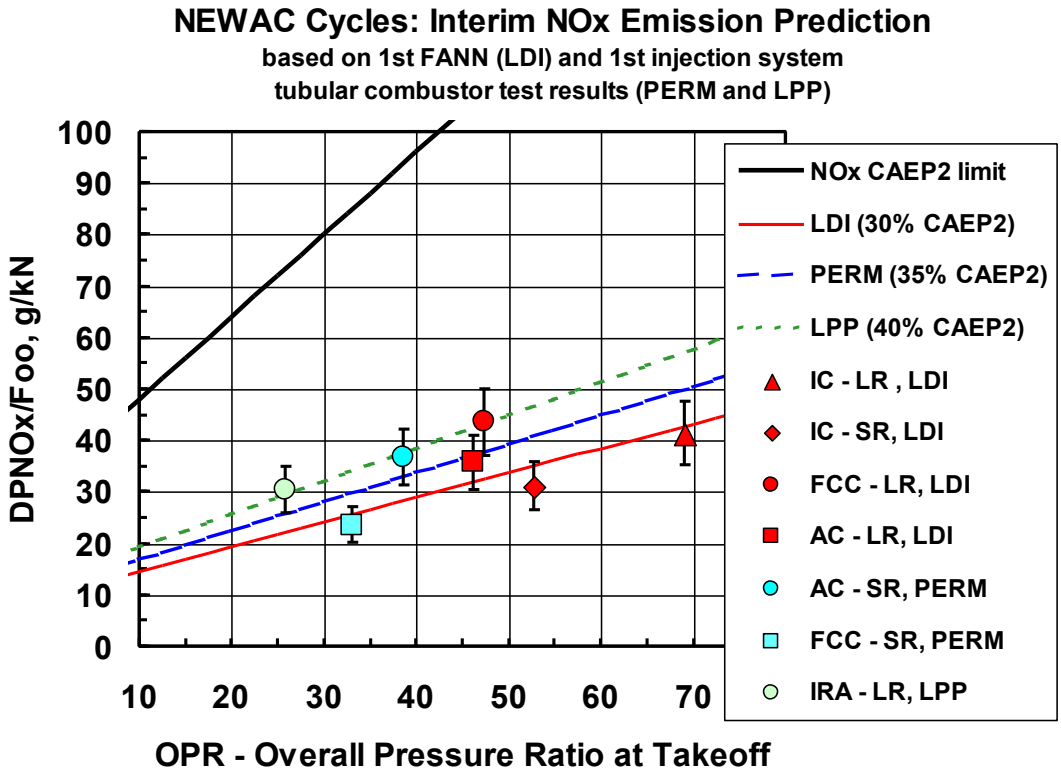

Figure 13 – NEWAC Lean-burn Combustor NOx Emissions Predictions [29]

[for the programme's advanced cycle engines in long-range (LR) and short-range (SR) aircraft applications]

MTU researched pre-mixed pre-vaporised (LPP) combustors for the proposed IRA configuration. This was possible because the optimum OPR was reduced by recuperation, and because the combustor entry temperatures, even after recuperation, were relatively low [29]. However, a more-recent trend towards raising combustor entry temperatures and OPR in intercooled and recuperated cycles makes pre-mixed combustor designs increasingly challenging, risking problems with premature ignition and flash-back. The Partial Evaporation and Rapid Mixing (PERM) combustors, or the LDI combustors researched by Rolls-

Royce, might therefore now be considered more-appropriate choices for any advanced engine not having a topping cycle. That includes the primary combustors in cycles that also incorporate inter-turbine reheat. In the subsequent LEMCOTEC programme more testing was conducted on the LDI combustor and Rolls-Royce predicted a further reduction in NOx would be achievable, taking combustion efficiency and other emissions into account.

2.9 Other ULTIMATE Engine Studies

The EU Horizon 2020 ULTIMATE project ran from 2015 to 2018 and funded the author's research. Results from five partners including Cranfield University were presented at the 2018 Farnborough International Air Show. Details are given on the ULTIMATE project website: http://www.ultimate.aero/

The main focus of ULTIMATE was the investigation of technologies that by year 2050 would have the potential to significantly improve thermal efficiency and reduce NOx emissions. The project also investigated technologies with the potential for improvements in propulsor efficiency and noise reduction. The latter research included the 'Box Prop' open rotor concept from GKN Aerospace Sweden and Chalmers University, and the variable-pitch fan and variable-geometry intake researched at Chalmers University and ISAE. However, the ULTIMATE core technology research is more relevant to this thesis.

To quantify the benefits of advanced-cycle technologies, the ULTIMATE project developed year-2050 reference long-range (intercontinental) and short-range (intra-European) engine models. For a long-range turbofan, four different engine models were produced for different purposes. The first was generated at Rolls-Royce and leading performance parameters were tabulated in ULTIMATE deliverable D1.1 [64]. Based on this tabulation a GESTPAN (GEneral Stationary and Transient Propulsion ANalsysis) model was produced at Chalmers University, a PROOSIS model was generated at Cranfield University by Florian Jacob, and a simpler Excel spreadsheet model was produced by the author.

2.9.1 Intercooled and Aftercooled Pulse Pressure Gain Combustion

As part of the ULTIMATE project, the author corresponded with Carlos Xisto at Chalmers University, who researched the combination of pulse-detonation combustion with an intercooled and/or aftercooled core compression system. Both long-range and short-range aircraft applications were considered, with the technologies applied to geared turbofan and open rotor engine configurations respectively.

Overall engine performance and pulse detonation were modelled, with particular attention given to prediction of NOx formation and the effects of the unsteady combustor exit flow on the downstream turbine. Incorporating intercooling allows higher OPR cycles without pre-ignition and increases power density while maintaining high temperature and pressure ratios across the detonation wave. Aftercooling further increases the power density, but was shown to be quite detrimental to SFC [65]. This was not surprising given the low average pressure ratios achieved in the pulse pressure gain combustor.

The engine concept is a possible realization of cycle#04 in Figure 24. By reducing the inlet temperature to the combustion system a larger pressure rise is achieved and peak cycle temperatures are reduced to help minimise NOx generation and combustor and combustor inlet valve cooling challenges.

The combustor concept has some similarities with existing wave rotor concepts, but it is not obvious that it offers benefits relative to these. One area of mutual concern is the effect that inlet valve closures will have on pressure fluctuations at exit from the HP compressor. The presence of a plenum chamber here may help alleviate the problem, but much will depend on the details of the valve arrangement and operation. A typical wave-rotor-combustor inlet valve may be superior in this respect, because it flows more continuously. However an intercooled pulse pressure gain combustion engine with detonation may be preferred because, as proposed, it would operate without a combustor exit valve, which is one of the more thermo-mechanically challenging parts of a wave rotor machine.

The pulse pressure gain combustion cycle with intercooling seems to improve SFC by about 3–4% relative to purely intercooled cycles.

Significant challenges in realizing the pulse-detonation core concept remain and even with intercooling, or aftercooling, the predicted NOx emissions were higher than originally anticipated [66]. Modelling of the combustion system did not include the ignition process, the inlet valves, or the fuel injection system needed to pre-mix and stratify the fuel-air mixtures in the detonation tubes. Achieving transition to detonation in lean kerosene-air mixtures also remains problematic and was not modelled.

2.9.2 Alternative Nutating Disc Core Designs

Normally-aspirated nutating-disc aero-engine designs have been proposed previously for propeller-driven unmanned aerial vehicle (UAV) propulsion, but at Cranfield University, in the ULTIMATE project in particular, novel highly-turbocharged nutating-disc engine configurations have been studied as possible alternatives to topping-cycle engines using pistons. Nutating-disc designs have some potential benefits relative to piston engines, but they also present big challenges. Sebastiampillai made a detailed study of open rotor engines incorporating nutating-disc topping-cycle modules [67] and [62]. The author then studied nutating-disc topping-cycle machines for larger turbofan engines, as described in Chapter 5. Different detail designs were investigated for the nutating-discs, making the studies complementary, but both researchers agreed that the nutating-disc modules should have separate discs for compression and expansion (i.e. dual discs) and that spark ignition would be needed in the pre-combustors.

Bottoming cycles also were investigated in the ULTIMATE project. Jacob made detailed studies of closed-circuit supercritical CO_2 (S-CO_2) systems [9], while the author investigated alternative open-circuit designs using air as the working fluid. The Air Bottoming Cycle (ABC) is described in section 6.3.

Chapters 5 and 6 contain more discussion of the pros and cons of technologies selected by the author for more-detailed assessment and incorporation in the advanced-cycle engine downselected as described in Chapter 4.

2.10 Combustion Systems for Engines with Novel Cycles

Beyond the year-2050 reference engine cycles, more-advanced cycles can take advantage of combinations of technologies with the potential to deliver both improved thermal efficiency and reduced emissions. The LDI combustor is well suited to the Brayton cycle engines with turbofan or open-rotor architectures, but some of the new cycles need very different combustion system designs.

Detail modelling of combustors for unconventional cycles was beyond the scope of this study, but the author did propose designs for secondary combustors located downstream of nutating-disc topping-cycle modules. These were modelled by two Cranfield MSc students and they are reviewed in section 6.2.2.

2.10.1 Combustion in Engines Incorporating Intercooling

For a given peak pressure after compression and a limiting peak cycle temperature, intercooling enables combustion with a higher FAR. This enables increased core specific power and a reduction in the volume of any topping cycle machinery and its associated cost, weight and drag. Intercooling can have a very powerful effect in reducing NOx emissions, particularly at take-off and particularly with RQL combustors. It is generally also beneficial in combination with the other ULTIMATE advanced-core-cycle technologies. An exception is the combination with a bottoming cycle, because intercooled engines generally want to have higher OPR, resulting in lower turbine exhaust gas temperatures (TEGT). However, if intercooling and bottoming cycles are also combined with secondary combustion, or if the bottoming-cycle main heat exchanger is moved upstream in the turbine suite, then the SFC and fuel-burn benefits of intercooling are still likely to be realized.

LDI primary-combustor designs, similar to those of the year-2050 reference engines, can be used for intercooled engines that do not have topping cycles.

2.10.2 Combustion in Engines with Topping Cycles

Improvements in high-speed diesel engine design, materials, fuel-injection, and turbocharging have helped to raise diesel engine efficiency and reduce emissions at source. After-treatment has further reduced their emissions. To limit peak cycle temperatures and NOx production, diesels can run lean, but this reduces their specific power. Intercooling increases specific power and should also improve emissions.

Piston-engine cores have been researched at BHL [68]. BHL has proposed piston-based topping cycles with intercooling and with secondary combustion ahead of the turbines. BHL could propose a four-stroke piston-engine design because secondary combustion significantly improved power/weight ratio.

At Chalmers University Carlos Xisto has modelled a Pulse Detonation Combustor (PDC) concept and its effects on a downstream turbine [69] [65]. However, like some other topping cycles this required a proportion of the compressor delivery air to be used for purging and cooling and this contributes to relatively high NOx emissions, despite incorporating intercooling. Topping cycles that minimise purging flows and cooling-air offtakes are to be preferred.

It was anticipated that a parallel study in the ULTIMATE research programme would provide a methodology for assessing the emissions from topping-cycle ‘pressure rise’ combustion systems and particularly those from nutating-disc systems. But the methodology did not materialise, so it has not been possible to make credible *quantitative* emissions estimates for the final study engines that incorporate the topping cycles. Nevertheless, consideration was given to restricting NOx emissions when setting the performance-cycle operating limits, and some qualitative emissions comparisons are discussed in section 8.6 for alternative advanced-cycle engine options. Determination of topping-cycle engine emissions should have high priority in follow-on studies as discussed in section 10.3.

2.10.3 Combustion in Engines Incorporating Bottoming Cycles

Bottoming cycles have little impact on primary combustor design, but there is a synergy between bottoming cycle technology and secondary combustion, since for a given heat content in the engine exhaust, the bottoming cycles can extract more energy from a smaller mass flow at a higher temperature.

2.10.4 Inter-Turbine and Other Secondary-Combustion Systems

Inter-turbine combustion was introduced by Alstom in the GT24/26 industrial gas turbines and has been subject to ongoing development to increase fuel flexibility and reduce emissions [70]. Between the 2006 and 2011 models a reduction of over 75% in NOx emissions was achieved by its improved 'Sequential EnVironmental' (SEV) burner [71]. The developed GE Alstom engine is now also known as the Ansaldo GT26 after Ansaldo Energia acquired the aftermarket business. These are the only in-service gas turbines known to the author to use secondary combustion between turbine blade rows.

Secondary combustion or inter-turbine 'burning' or 'reheat' could be used in an aero engine to boost the power output, particularly for take-off and climb. By raising the mean temperature of heat addition it may also increase thermal efficiency, and by enabling a reduction in the peak temperature of a primary combustor it may also help to reduce NOx emissions. [72].

Inter-turbine combustion can reduce fuel burn in two ways. A second combustor enables extra fuel to be burned at a higher overall fuel/air ratio, particularly at take-off and climb conditions, so that less core mass flow is needed. The smaller core will then give higher OPR and thermal efficiency at cruise, provided all, or almost all, the fuel is directed to the primary combustor at this condition. The smaller and higher specific-power core results in a lighter engine, further improving fuel burn.

There is a trade-off in the optimum positioning of the second combustor. For the best SFC when both combustors are fully-fuelled, the second combustor needs to follow closely behind the first, preferably after only one turbine stage, as in

the GT24/26 industrial gas turbines. Conversely, for maximum specific power, the second combustor could be placed further downstream, perhaps after two turbine stages. To improve part-power SFC it is beneficial to redistribute the fuel, if possible, so that a larger proportion goes to the primary combustor.

Combining inter-turbine combustion with high OPR is desirable, as then even after one or two turbine stages there will still be a substantial turbine expansion ratio remaining, from which the extra work can be extracted. To obtain high OPR there is a further synergy with intercooling. On the other hand, reducing core size and HP compressor exit non-dimensional flow will disproportionately reduce HP compressor efficiency in smaller engines where added complexity is harder to justify economically. To minimise the loss of component efficiency with smaller cores, an axi-centrifugal HP compressor could be used. In a front-fan turbofan or a tractor open-rotor powerplant, a reverse-flow core should also minimise these efficiency penalties [38] [39] [18].

Inter-turbine combustion has also been proposed to increase the thrust of combat aircraft engines, avoiding the large volume and poor fuel-economy of more-conventional reheat systems, but it is difficult to achieve high combustion efficiency in a very-compact and durable burner design. Cavity-based trapped-vortex combustors (TVC) have been proposed [73] but to the author's knowledge no such inter-turbine combustion systems have been implemented.

The use of inter-turbine combustion to improve civil aero engine performance has also been studied in the AHEAD project (Advanced Hybrid Engines for Aircraft Development) at the University of Delft and at Technion. These secondary combustor (SC) designs were based on the 'flameless' inter-turbine combustor concept [74] [75]. However, in practice these combustors had characteristics more like RQL designs.

In topping-cycle engines a secondary combustor can be located immediately after the topping cycle and ahead of the turbines, instead of between turbine stages. This is an attractive option as it avoids many of the engineering difficulties associated with inter-turbine combustion. The Napier Nomad I aero

engine incorporated a secondary combustor to raise the temperature of the piston engine's exhaust ahead of its turbine to give extra power when needed.

Victor Martinez Bueno at Cranfield University made initial CFD studies of a novel 'oxy-poor-flame' (OPF) secondary combustor design, as reported in his MSc thesis [76]. The design was proposed for the engine concept described in ULTIMATE deliverable D1.3 as #1.3.3 [67], in ULTIMATE deliverable D4.3 as #4.3.3 [62], and in this thesis and in [77] as cycle#06. The main conclusion was that increased combustor volume was needed to improve combustion efficiency and reduce pressure losses. An enlarged secondary combustor design was then modelled by Mirko Romanelli at Cranfield, as reported in his MSc thesis [78]. This design was anticipated to reduce overall CO and NOx emissions. It did have better mixing, better combustion efficiency and a flatter exit temperature profile, but because of the longer residence time the predicted NOx emissions got worse. Further details are given in section 6.2.2. These large-scale-trapped-vortex combustor designs still seem less than satisfactory, so there is an opportunity to propose better secondary combustor design concepts.

2.11 Emissions Legislation

This section describes the engine emissions legislation based on ICAO Committee on Aviation Environmental Protection (CAEP) standards and the associated Landing and Take-off (LTO) cycle.

Instead of directly assessing environmental impacts, emissions legislation has been drafted around fuel venting and the measured mass of gasses and particulate matter and aerosols in engine exhaust streams.

Legislation restricting aircraft emissions has evolved since aircraft related pollution was first recognised as a significant problem in the 1960s. The CAEP/1 standard was introduced by ICAO for engines in production in 1986 and increasingly stringent limits have been applied to NO_x emissions since then. The main purpose of the legislation has been to improve air quality around, and downwind of, airports. All large aero engines are now required to undergo

certification testing for NO_x, carbon monoxide, 'unburned' or 'total' hydrocarbons (UHC, THC or HC) and smoke/soot. However, small aero engines (those below 26.7 kN thrust) are exempted from these requirements and some alleviation is also available for engines below 89 kN take-off thrust [79].

The masses of pollutants emitted by an aircraft engine are related to the rated sea-level static take-off thrust of the engine (F_{oo}) and are assessed over a representative Landing and Take-off Cycle, known as the LTO cycle. This covers engine operation from sea level to 3,000 ft. For subsonic aircraft, the rate of emission of each species, measured at four different thrust levels, is multiplied by an assumed time spent at each condition, as shown in Table 7, and is summed to give a total mass for each pollutant (D_p) over the full LTO cycle. The legislated limits are ratios of D_p/F_{oo}. However, the times listed in Table 7, that are assumed to be spent at each condition, may not be very representative of actual aircraft operations below 3,000 ft., so some studies try to make more realistic estimates for total emissions at specific airports.

Table 7 – Landing and Take-off Cycle Specification

Static	**Rating**	**Time in mode** (min)
100%	Take-off	0.7
85%	Climb-out	2.2
30%	Approach	4.0
7%	Idle	26.0

Emissions legislation applies to turbojet and turbofan engines, but, 'In recognition to their low pollutant emission levels, turboprop aircraft are not covered by the ICAO Annex 16 Volume 2 on emissions at the moment' [80]. This exemption applies even where the thrust exceeds 26.7 kN, but it is unlikely to continue to apply to future large open rotor engines, should these enter service. (Section 2.3.4 reviews current and future emissions limits and targets.)

2.11.1 Emissions Testing

For certification, engine emissions are measured on ground-level test beds, usually close to sea level. The uninstalled thrust is calculated and the engine is run to the percentage static thrust levels given in Table 7. Measurements are made of CO, NO_x, UHC and smoke number (SN). Corrections are then made to the emissions measurements to allow for day temperature and for pressure deviations from sea-level static ISA-day conditions, and for the effects of humidity.

To allow for engine-to-engine scatter and to allow for measurement errors, a margin is added to the test measurements to give 'characteristic' levels of emissions. When more than one test is conducted and/or more than one engine has been tested, then smaller margins can be applied to the emissions measurements when calculating characteristic values. This practice accounts for the resulting reduced uncertainty in the assessment of the average-engine emissions [81].

2.11.2 The ICAO Emissions Database

The International Civil Aviation Organisation (ICAO) database, hosted by the European Aviation Safety Agency (EASA), records the results from certification tests carried out on aero engines [82].

Selected figures were extracted from the database in order to assess LTO cycle engine emissions for two representative in-service engines in the year 2000.

The use of the ground-level emissions measurements to estimate mission-level NO_x emissions is discussed in [83] and [84]. The methodology is described in section 3.8.5.

2.11.3 Current and future emissions targets

Current ICAO emissions limits for CO, HC and smoke are unchanged from CAEP/2 as defined in ICAO Annex 16 Volume 2 [85]. For CO the limit for Dp/Foo is 118 g/kN and

for HC the limit for Dp/Foo is 19.6 g/kN. The smoke number (SN) is defined as the lesser of 50 or the figure given by Equation 1.

$$SN = 83.6.Foo^{-0.274} \quad \text{Equation 1}$$

The Dp/Foo limits for NO_x are more complicated, as alleviation is given for higher OPR engines in recognition that, while higher OPR increases NO_x, it also tends to improve thermal efficiency and reduce CO_2 emissions. For engines over 89 kN sea-level static (SLS) thrust, the CAEP/2 limit for Dp/Foo in g/kN is given by Equation 2 where π_{oo} is the OPR at the SLS max thrust condition [85].

$$Dp/Foo\ (NO_x) = 32 + 1.6.\pi_{oo} \quad \text{Equation 2}$$

For existing engines, the CAEP/8 rule for NO_x is now more stringent. Equation 3 applies to engines with OPR less than 30, while for engines with OPR from 30 to 104.7, Equation 4 applies. Above OPR 104.7, Equation 2 still applies [85]. CAEP/4 and CAEP/6 specify intermediate NO_x emissions limits.

$$Dp/Foo\ (NO_x) = 7.88 + 1.408.\pi_{oo} \quad \text{Equation 3}$$

$$Dp/Foo\ (NO_x) = -9.88 + 2.0.\pi_{oo} \quad \text{Equation 4}$$

New emissions targets have been set for engine certification in 2025, and Flightpath 2050 sets longer-term targets for 2050, but the actual certification requirements for 2050 are unknown. The ‘minus 75%’ CO_2 and ‘minus 90%’ on-route NO_x reduction targets, relative to year 2000 in-service aircraft, are on an available seat kilometre (ASK) basis and further include benefits for ATC and other operational improvements, but the LTO NO_x reduction targets are usually quoted relative to the CAEP/2 legislated limits in force in the year 2000.

However, the actual reduction in LTO emissions per LTO cycle for a given aircraft mission will be different for several reasons. Firstly, most engines in service in year 2000 already had significant margins relative to CAEP/2, so the potential savings are reduced. However the actual mission-level reductions should be greater, because the year-2050 aircraft will be lighter and more

aerodynamically efficient, therefore needing lower thrusts and burning less fuel. Operational improvements like reduced taxiing times give further reductions.

2.12 Combustor Research

There is a general consensus that lean-burn combustion systems are essential for the achievement of substantial long-term and step-change reductions in aero-engine NO_x and particulate emissions. However, the required technologies for effective lean-burn combustion systems are still being developed and most aero engines still have combustors in which all the fuel is injected into a primary zone that runs rich at all high-power operating conditions.

The general principles governing the design of the current RQL combustion systems, like Rolls-Royce Phase-5 and Pratt & Whitney TALON-X combustors, are well established and discussed in textbooks such as [86] and [87], so their design principles will not be elaborated here. Engine manufacturers continue to develop this type of combustor while working on lean-burn combustor technology in parallel research programmes.

There are many reasons for the reluctance to totally commit to lean-burn designs, and several of these are evident from a recent presentation on Combustion Technology at Rolls-Royce [88]. This presentation describes the development of the in-service Phase-5 rich-burn and the yet-to-be-flight-tested lean-burn combustion systems. It highlights the very considerable investments made in combustor research by the industry and various partners including the European Commission and the UK and German governments. It notes that incremental improvements to the Phase-5 design can continue to meet medium-term requirements for corporate and regional aircraft engines, but recognises that lean-burn combustor designs will be needed, sooner rather than later, for higher OPR large civil engines. Lean-burn combustion systems are more complex and more difficult to scale-down to small engines (and it will be remembered that small engines still enjoy some alleviation from emissions regulations). Nevertheless, in the longer term, it is anticipated that all engine

types will need to use lean-burn combustors and the following discussion focuses on such systems.

2.12.1 Development of Brayton-Cycle Lean Combustion Systems

Several types of lean-burn combustion system have been proposed, researched and developed, but only a few have been developed as far as TRL 6 and subsequently entered service. To maintain combustion stability and to avoid the risk of lean blow-out, aero engines with lean-burn combustors generally need to have pilot burner zones that still run rich, or very close to stoichiometric conditions, throughout the flight envelope. The remaining main combustion zones can then run lean, though these lean modules are more at-risk from thermoacoustic instabilities. The pilot zones may be supplied by separate fuel injectors, offset from the main injectors either axially or radially as in a 'Double Annular' Combustor (DAC), or by integrating pilot and main fuel nozzles into larger fuel injectors. A broad review of low-emissions combustion technologies has been conducted recently at Cranfield University [89].

A common feature of lean combustors is that most of the air flow enters the combustor liner from the front through swirlers, with only a small proportion admitted later or used for liner-wall cooling. This is unlike RQL combustors where much of the air enters radially through their quenching and dilution holes.

General Electric and CFM led the way with DAC designs in the 1990s. In the CFM56 engine the DAC was offered as a lower-NO_x combustion option that was taken-up by Swissair, but it did not find favour with other airlines because it was more expensive than the standard combustor that was still compliant with the contemporaneous emissions limits.

2.12.2 NASA Research on Lean Combustors

One design approach is to have a larger number of simpler, smaller, LDI fuel injector nozzles arranged in an array, with some of the more central ones running relatively rich and providing pilot flames, with the others running lean. A

simplex swirl-venturi (SV) injector design and its associated 9-injector array originating from the 1990s US High Speed Research (HSR) programme are shown Figure 14.

Such Multipoint Lean Direct Injection (MLDI) combustor arrangements were tested in single-sector rigs in various NASA funded programmes [90] [91] [92]. Later arrays developed in collaboration with Woodward Combustion Systems had 13 injectors including some ‘airblast’ main injectors and an enlarged airblast central pilot injector for improved operability [93] [94]. In the airblast injectors the fuel is ejected between inner and outer swirlers (that may variously have either co-swirl or counter-swirl).

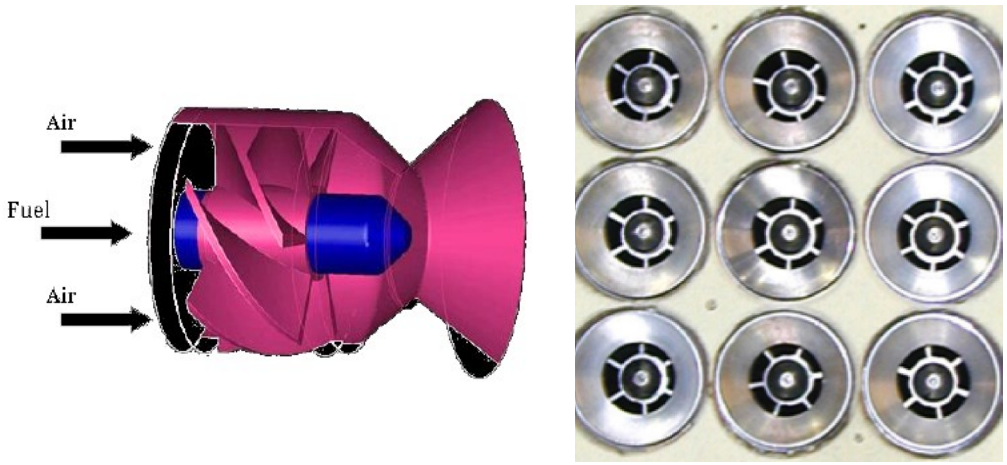

Figure 14 – NASA LDI Swirl-Venturi Combustor Swirler cut-away diagram and 9-point array [93] [91]

However, there are potential problems with these burner designs. It seems very challenging to connect a cluster of individual nozzles into one fuel injector assembly and arranging the internal fuel flows such that the fuel lines to the last non-flowing nozzles at part-power remain cool enough to avoid gumming and coking. Also, each integrated fuel injector is likely to need a large access hole through the combustor outer casing, leaving little casing material in-between to withstand the casing’s pressure loads, axial loads and bending moments. This is already a design challenge for the relatively more compact concentric LDI fuel spray nozzles that have larger ‘burner heads’ than existing RQL fuel injectors.

The most recent NASA LDI combustor research and resulting correlations are discussed further in Appendix B.

2.12.3 European Research on Lean Combustors

Research into improved LDI combustors with air-spray fuel injectors has been ongoing in various EU, national and industry funded research programmes over the last two decades. Rolls-Royce has been the lead industry partner. Results from the EU funded programmes ANTLE, NEWAC, LEMCOTEC, Clean Sky and ALECSYS show advances in the underlying technology, which should lead to lower NO_x emissions for the eventual production LDI combustor designs. Additional research at RR and RRD has been supported by UK and German National (and Regional) Government funding in programmes such as ATAP10, EFE, Samulet, SILOET 1 & 2, Lufo IV & V and AG Turbo 2020. However, in this period, study engines for the year 2020 and beyond have considered higher overall pressure ratios, which tend to increase NO_x emissions on account of higher flame temperatures and faster reaction rates.

Some early research focussed on DAC designs with two axially-offset rows of fuel injectors, but these designs, like the reverse-flow combustors used in small engines, presented larger combustor-liner surface areas that required cooling, increasing the required wall-cooling flows and reducing the amount of air available for lean combustion. The DAC designs also tended to have more-variable outlet radial temperature distributions than single-annular designs. Thus recent research by Rolls-Royce and others has focussed on single-annular designs with larger air-spray fuel injectors that have central pilot-zone fuel nozzles surrounded by concentric annular main-zone fuel nozzles that run lean. To reduce the risk of problems with thermoacoustic instability, Rolls-Royce is developing Lean Direct Injection (LDI) technology as shown in Figure 15 [88].

Fuel flow is staged to the different nozzles, with only the pilot-zone nozzles fed at low power conditions, but with all nozzles fed at high-power conditions. At intermediate power, only half of the fuel injectors may have their main-zone

nozzles fed with fuel. This more-complex fuel management ensures operability and low emissions are maintained over the full range of engine thrusts.

Significant advances in LDI combustor design have been made in the NEWAC and LEMCOTEC programmes, as was confirmed by a series of single-segment and full-annular (FANN) tests on combustor rigs in the UK and Germany. These combustors use air-spray-assisted injectors. The testing has been accompanied by detailed CFD studies using the Rolls-Royce in-house CFD code PRECISE-UNS [95]. For example, CFD studies showed how the flow distribution around the combustor liner could be modified to optimize the liner's wall cooling and showed how combustion efficiency could be improved at cruise conditions [96].

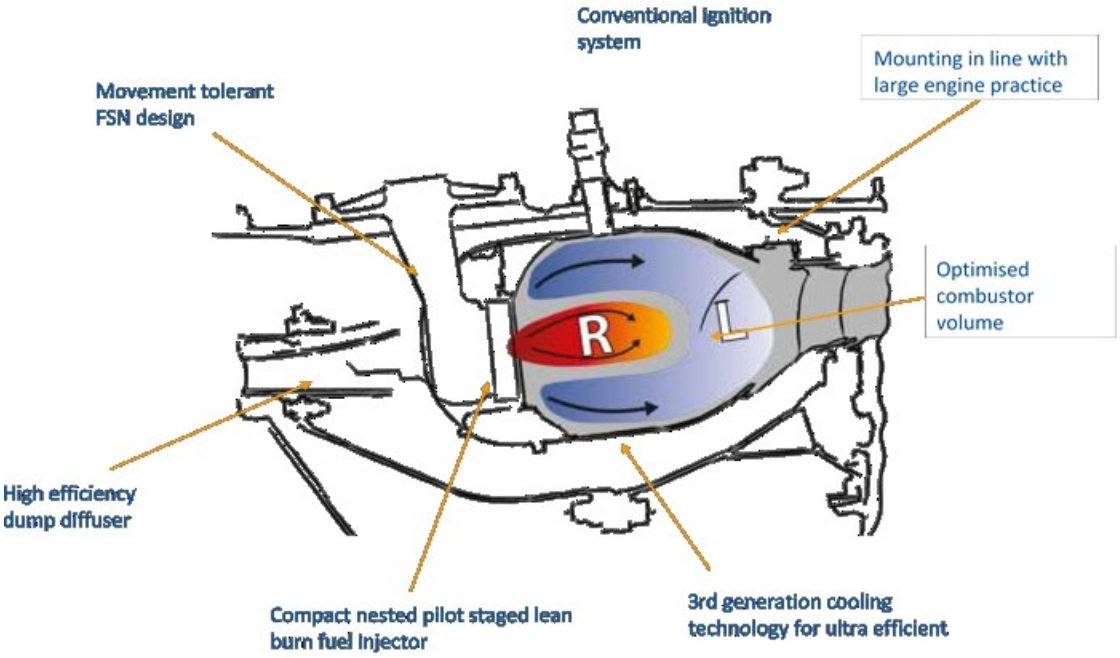

Figure 15 – Rolls-Royce LDI Combustor Concept [88]

R = rich, L = lean.

The Rolls-Royce LDI combustor technology is now approaching TRL 6. Some further details of the Rolls-Royce LDI combustor aerodynamics are shown in Figure 16 together with a comparison between the LDI fuel injector and a fuel injector for an existing Phase-5 RQL combustor. The larger air-inlet area needed for lean combustion is evident.

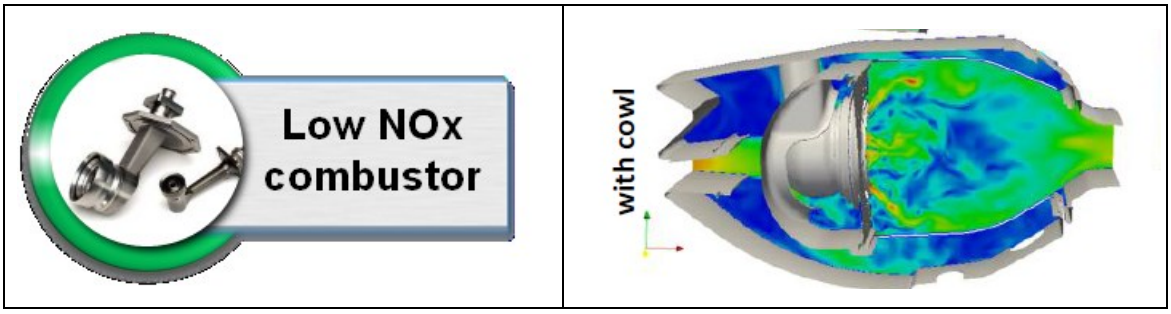

Figure 16 – Rolls-Royce LDI Combustor Technology

LDI fuel injector vs Phase-5 fuel injector and a typical velocity distribution [96]

Results presented from the LEMCOTEC programme in 2016 included a 66% reduction in Dp/Foo for NOx relative to CAEP/2 for the LEMCOTEC regional turbofan (RTF) and large turbofan (LTF) study engines as shown in Table 8. The LTF study engine for 2025+ has high OPR, similar to the TF2050 study engine in ULTIMATE, but the TF2050 is assumed to use ceramic matrix composite (CMC) materials in its combustor and not to need so much wall-cooling air. Therefore it is expected to run leaner at high power conditions, produce less NOx for a given COT at take-off, and have slightly lower Dp/Foo figures. It should also benefit from the extra years of combustor development.

Table 8 – LDI NOx Emissions for ANTLE and LEMCOTEC Study Engines

Emissions	Units	ANTLE+LDI	RTF+LDI	LTF+LDI
OPR at SLS ISA	–	40	38.8	58.5
Dp/Foo (NOx)	g/kN	38.6	21.6	42.6
CAEP/2 NOx limit	g/kN	96.0	94.1	125.6
NOx re. CAEP/2	–	-60%	-77%	-66%

Table 8 and table 9, presented at the LEMCOTEC Public Workshop in Potsdam in December 2016 [96], show how the development of Rolls-Royce LDI combustor technology has reduced predicted future LTO-cycle NOx emissions. The recent full-annular rig-test results show an improvement from the earlier ANTLE demonstrator figure when applied to the LEMCOTEC RTF and LTF engines.

Table 9 – Rolls-Royce LDI Combustor: LEMCOTEC Emissions Estimates

LTO-cycle Emissions	RTF	LTF
NO_x (re. CAEP/2)	-77%	-66%
CO (re. CAEP/2)	-79%	-77%
UHC (re. CAEP/2)	-87%	-79%
Smoke (re. CAEP/2)	-85%	-75%

Figure 17 shows that the characteristic (Ch'ic) levels declared in the ICAO emissions database for the in-service engines are significantly higher than their measured single-test or test-average (Av.) emissions. For ANTLE and the LEMCOTEC study engines it is assumed that average figures have been quoted. The relatively higher NOx emission for the LTF reflects the steeper slope of the CAEP/8 limit and confirms the ongoing difficulty in maintaining low NOx emissions in higher OPR engines. Any new correlations for LDI combustors should reproduce this trend.

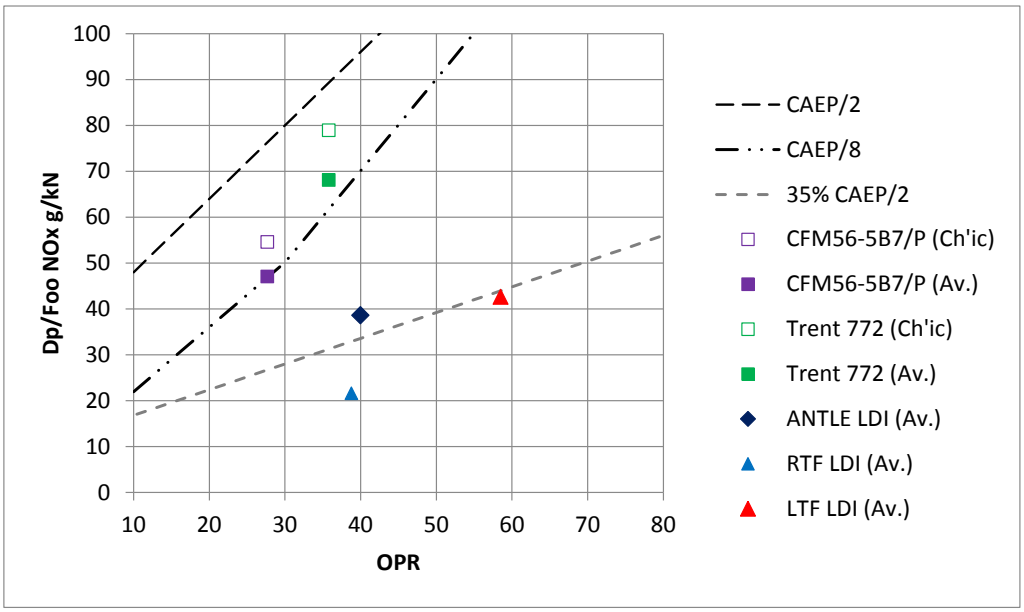

Figure 17 – Progress in Combustor Design reducing LTO NOx Emissions

There is scope to minimise the emissions of both NOx and smoke by optimizing the staging of the fuel between the various lean modules and the pilot burners,

but there remains a trade-off between minimising NOx and minimising smoke. Thus the long-term achievable levels of emissions for these two species may depend on the relative priorities given to minimising each of them.

It is anticipated that the demonstrated LDI combustor technology potential for NOx reduction will be further improved by the incorporation of advanced CMC materials for combustor liners. These will need less cooling and enable a greater proportion of the incoming air to the combustor to be provided to the lean modules, thereby reducing flame temperatures at a combustor outlet temperature (COT).

3 METHODS

The author's studies have aimed to quantify the potential performance benefits of engines with different combinations of advanced core engine technologies. The overall methodology has been summarised in Figure 1.

BHL modelled two representative year-2050 aircraft for the ULTIMATE project. Exchange rates derived from these models have been used to make fuel-burn assessments

Most of the methods and modelling tools developed by the author have been implemented as Microsoft Excel spreadsheets. The four main spreadsheet tools are described in the following sections and were developed for modelling:

- Whole-engine performance
- Nutating-disc-module compression and expansion processes
- Open-circuit bottoming-cycle stand-alone performance
- Future scenarios for air-traffic growth and CO_2 emissions

The nutating-disc and bottoming cycle models were created to avoid making the whole-engine performance model over-complicated. They were used in the component-level design studies described in Chapters 5 and 6 where more details are given on how the models were developed.

This chapter closes with a general review of emissions assessment methods. Established methods were used for emissions assessments of the year-2000 baseline study engines, and a single NASA correlation (Equation 21) was selected for NOx emissions estimates for future engines with lean combustors. The correlation was chosen following an extensive review of existing and potential new NOx emissions correlations as described in Appendix B.

3.1 Whole-Engine Performance Model and Assumptions

The design and off-design performance model was developed initially for the year-2050 reference turbofan and then used to study scale effects on the reference engine and high-OPR intercooled engines [97]. These studies also

considered the effects of varying OPR and TET. The tool was then developed to model engines with secondary combustion and topping and bottoming cycles. Finally the ULTIMATE-project exchange rates, provided by BHL [12] and [14], were used together with engine weight estimates to calculate fuel burn for the scaled engines installed on the year-2050 long-range aircraft.

In the wider ULTIMATE project, engine performance was also modelled by other researchers using different tools. Following initial modelling at Safran and Rolls-Royce [64], models were also made at Chalmers University [65] using GESTPAN [98] and at Cranfield University using the object-oriented engine performance code PROOSIS [13]. These helped to validate the author's results.

The Excel performance spreadsheet was generated from scratch by the author for maximum flexibility in modelling novel cycles. Performance equations were taken from Walsh and Fletcher [99] with thermodynamic properties as specified on pp. 113-119. Advantages of developing this modelling capability were that:

- The author understood exactly how the calculations were performed
- The inputs and outputs were friendly to the user and easily modified
- Additional functionality and new technologies were easily introduced
- Use could be made of Excel functions for tracing errors
- The progress of iteration to a converged solution was clearly visible and the user could intervene if and where necessary
- There was no need to export data to other programmes to post-process and plot the results.

Performance calculations are self-contained on one sheet which models the performance at one design point and two off-design conditions, typically mid-cruise, top of climb, and EOR take-off. An index provides ready access to each model in the workbook. Additional sheets collate and plot the results from each parametric study.

Having one design point and two off-design points was generally sufficient to characterise a cycle's performance potential, but additional off-design points

could be generated by copying a first sheet and editing the inputs for the off-design cases. This was done to estimate an altitude SFC loop for the reference turbofan. Initially the design point was a mid-cruise case, but in later models the top of climb case was used instead, since this was generally the sizing case for the core turbomachinery and most other components.

Engine performance was initially modelled at conditions consistent with the engine operating conditions and streamtube thrusts listed in Table 1. To focus on core thermal efficiency, the initial year-2050 study engines were all designed for the same low mid-cruise specific thrust, equivalent to 72 m/s, a figure originally recommended by industry partners in the ULTIMATE project [64].

Consistent rules were applied for estimating the component efficiencies, temperature limits and secondary air flows in modelling alternative cycles. These included the use of cooled cooling air (CCA) for HP turbine cooling. No customer bleed air was extracted, but in the initial studies 260 kW of aircraft accessory power was taken from the HP spool. It was assumed that engines in 2050 would still run on kerosene or drop-in-replacement bio-fuels. (The use of different fuels, water injection and hybrid-electric systems may well affect future engine designs, but these options were beyond the scope of the studies.)

Component efficiencies were user-specified at each condition with typical component efficiency deltas applied between the cruise, climb and take-off points. The HPC and HPT polytropic efficiencies were then corrected according to a correlation with HPC-exit blade-height. However, no such corrections were applied to engines modelled with nutating-disc topping-cycle modules.

The HPT cooling air flow, as a proportion of core inlet flow, was adjusted according to the HPT mass flow at design point and the rotor-inlet relative gas temperature.

The models were simplified by not using component maps for off-design performance. Appropriate component efficiencies were user-specified for each case. Nacelle drags and afterbody drags were not modelled.

Since only high power conditions were modelled, it was assumed all turbines except for the last one would operate between choked nozzles. Nozzle areas were set at the design point, though their effective areas could be altered off-design by varying nozzle discharge coefficients. Fan bypass and core exhaust systems were modelled as ideal convergent-divergent nozzles when choked. This simplification gave negligible errors relative to modelling convergent primary and secondary nozzles, since their exhaust Mach numbers were always relatively low. Additional exhaust nozzles were modelled to provide thrust recovery from the spent cooling air from the intercooler and cooled-cooling-air heat exchanger. Although mixed exhaust arrangements were proposed for the more complex cycles, these were actually modelled as separate-jets engines, with variable-area exhaust nozzles for the ABC cycles that, like mixed-jets engines, wanted relatively lower fan bypass-section pressure ratios at cruise for improved performance.

Each design or off-design case has its own block of station data listing the total and key static stations throughout the engine. Additional blocks provide data for secondary air systems, the fan and its gearing, and each compressor, turbine, combustor and nozzle. There is provision for six internal and two external bleeds, in addition to the cooled-cooling-air cooling air (CCACA) and intercooler cooling air offtakes. For simplicity the fan root section and the booster compressor were modelled as a single LP compressor (LPC) since they were assumed geared-together in all of the turbofan engine models. Appendix C illustrates typical parts of the spreadsheet.

Converged solutions for the design point and off-design points were obtained by iteration. A macro could have been used, but manually copying values from the previous iteration into the column of new guesses (until the specified iteration tolerances were met) allowed user intervention if the model was not converging. The cases could be iterated together or separately, but the off-design cases were properly modelled only after the design point had a converged solution. The iteration scheme proved to be very reliable provided the fan did not take all of the energy out of the core in the off-design cases. That problem was avoided

by reducing the initial guesses for the fan pressure ratio. Originally 34 values were input as guesses at the design point and 37 were used for each off-design case. Further matching quantities were added for more complex cycles and then some formulas had to be modified to avoid potential zero-divide errors.

The model uses both imperial and SI units. Imperial units are still widely used in the industry and are retained for much of the input and output. The author's familiarity with those units meant that any unusual or erroneous input or output values would more-easily be identified, but all key performance parameters are also tabulated in SI units, using clearly-displayed standard conversion factors.

Because the fan bypass section and the LP compressor are driven by the same turbine or turbines, the geared turbofan (GTF) has a potential variable-cycle capability. In a real engine this would be exploited using a variable-pitch fan and/or variable stators on the high-speed booster to change the work-split between the bypass section of the fan and the LP compressor. This can trade-off OPR against TET as described in section 7.2. But since the Excel models do not use component maps or schedules for variables, the user must provide an additional input for each off-design case to specify the work-split. There are several ways of doing this. In some more-recent models the off-design thrust and TET can be specified and the off-design OPR is found using in-built iteration. Alternatively the off-design OPR and TET can be set by the user and the off-design thrust calculated. Optionally the OPR can be scaled relative to the cruise, climb and take-off OPR of another (reference) engine by applying a common index to each value. This last method has been used to provide proportionate off-design scaling of compressor work and HP compressor delivery temperatures in some of the parametric studies.

For most of the parametric studies, the climb, cruise and take-off thrusts were fixed for a given engine scale, together with the design-point specific thrust and fan pressure ratio. Thus the design-point fan mass flow was known and the core mass flow and bypass ratio (BPR) could be determined by iteration.

When more advanced cycles are modelled there are more degrees of freedom and additional off-design variables that need to be specified. These include the intercooler and air bottoming cycle heat exchanger (ABCHX) mass flows and effectiveness levels.

The internal consistency of the Excel performance calculations is assured by checking conservation of mass and energy through the cycle. Mass is always conserved. Near-perfect energy balance is also obtained for most of the cycles, as shown in the example in Figure 96 in Appendix C. Where cooled-cooling-air cooling-air (CCACA) calculations are included some small errors are observed. These are quite negligible, but larger discrepancies of over 300 kW at take-off have been seen in models where air bottoming cycle (ABC) calculations were included. These errors are still under investigation to see how they can be minimised, but currently the results of the off-design take-off performance calculations for engines with ABC cycles could be up to 0.6% in error.

To help validate the Excel models, results from the spreadsheet have been compared with results from PROOSIS models also developed in the ULTIMATE project [13] [1]. Only very small discrepancies were found in the compression system, but for calculations in the combustor and turbines had discrepancies of up to about ten degrees in the calculated temperatures. These discrepancies were initially attributed to different physical properties assumed for air and combustion products by the different codes. It seemed that the thermodynamic properties used in PROOSIS and the polynomial functions from Walsh and Fletcher had diverged at higher temperatures, but [100] seems to contradict this assumption, so the reason for the discrepancy remains unclear. It does not seem large enough to invalidate use of the spreadsheet for the scoping studies on alternative cycles, but it does mean that detailed results from the PROOSIS models and the spreadsheet models cannot be directly read-across from one to the other. Neither the Excel model nor the PROOSIS model accounts for dissociation effects, but these should be relatively minor in the high-OPR performance cycles studied here. It is also not obvious how such corrections

should be applied, since the residence times are too short for equilibrium gas compositions to be achieved.

For the initial modelling of the reference and intercooled engine cycles the mid-cruise condition was taken as the design point, since mid-cruise performance data for the original reference engine was available in [64]. However, for the later studies the TOC (max climb) condition was taken as the design point. This is because TOC is the sizing case for most of the engine components. For the advanced engine cycles the cruise performance was to be determined, but the TOC and take-off cases were where component performance limits and design constraints needed to be observed. Swapping the design and off-design cases around made no noticeable difference to their performance predictions.

3.1.1 Estimating Off-Design Component Efficiencies

Component designs are expected to be optimised for the mid-cruise condition, so the fan bypass stage, LP compressor (comprising the fan root and the IP compressor) and the LP turbine have been assumed to be sub-optimal at top of climb and at take-off. Base-level polytropic component efficiencies are specified at three flight conditions. Table 10 shows the component polytropic efficiency penalties originally applied at max climb and max take-off. The HP turbine efficiency is assumed to remain constant for these relatively high power cases.

Table 10 – Reference Off-design Component Polytropic Efficiency Variations

Component	Mid-Cruise	Max Climb	Max Take-off
Fan bypass stage	datum	-2.2%	-0.7%
LP compressor (fan root + IP)	datum	-1.0%	-0.4%
HP compressor (reference cycle only)	datum	-3.8%	-1.7%
LP turbine	datum	-2.0%	-1.0%

The significant reduction in HP compressor efficiency at the max climb condition was based on the assumption that max climb would be a corner-of-the-envelope case, where the pressure ratio and non-dimensional flow would be

significantly higher than at cruise. This seemed to be valid for the reference engine, but might not apply to all the advanced cycle engines. In these cases the HP compressor efficiency variation, relative to the peak efficiency, must be assessed on a case by case basis. (In practice the take-off efficiency could be higher than the cruise efficiency on account of the higher Reynolds numbers at sea-level, but for consistency with previous studies, it was not proposed to take credit for this.)

3.1.2 Estimating Scale Effects on Component Efficiency

For the HP compressor and HP turbine only, a further scale correction is applied to account for efficiency changes from tip-clearance effects on stages with small blade heights. The base-level HP turbine polytropic efficiency is assumed to be constant, but the HP turbine and HP compressor efficiencies are corrected when these core components are scaled. For most of the parametric studies the thrust requirements are kept constant, but the HP blading is still scaled when core specific power or OPR is varied.

The most significant factor affecting the SFC of the scaled engines is the HPC scale correction factor which is taken from Kyprianidis and Rolt [30]. The HP compressor has the smallest blades and is the turbo-machine subject to the biggest changes in efficiency when it is scaled. The models assuming all-axial compression systems have corrected the polytropic efficiency δ according to the last-stage blade-height λ mm as specified by Equation 5. The last-stage blade-height is calculated at design point assuming an exit axial Mach number of 0.254 at mid-cruise and an exit hub/tip radius ratio of 0.925.

$$\delta = 0.0532 - 0.5547\left(\frac{1}{\lambda}\right) - 1.7724\left(\frac{1}{\lambda^2}\right) \qquad \text{Equation 5}$$

This efficiency correction curve in [30] and [101] (GT2014-26064) was plotted by Kyprianidis based on the methodology of Lakshminarayana [102], but the above Equation 5 to fit the curve was derived by the author. It was taken to be representative for all of the high-pressure-ratio HP compressors in the study of scale effects. However, the magnitude of this correction is dependent on

several assumptions regarding how the HP compressors would be scaled in practice. The assumption that all HP compressors would have the same exit hub/tip radius ratio is questionable and perhaps dependent on having the reverse-flow-core arrangement. In this respect the corrections may sometimes be under-estimated. The efficiency correction would ideally be recalculated for any changes in HP compressor design pressure ratio, hub/tip radius ratio etc., but Equation 5 is assumed to be representative for all of the high-pressure-ratio all-axial HP compressors in the reported performance studies.

In cycle studies where an axi-centrifugal compressor might be substituted for an all-axial compressor, a different scale-correction calculation is appropriate. The proposed method is to estimate the last-stage blade-height for an equivalent all-axial compressor and then use Equation 6 instead to estimate the efficiency correction for the axi-centrifugal or centrifugal compressor. This equation has half the rate of change of efficiency with the virtual blade-height, and 1% lower efficiency at a virtual blade-height of 13 mm. Once again the corrections would only be applied to the final core compressor.

$$\delta = 0.0166 - 0.27735\left(\frac{1}{\lambda}\right) - 0.8862\left(\frac{1}{\lambda^2}\right) \qquad \text{Equation 6}$$

Figure 18 compares the two efficiency correction curves from the above equations for the all-axial and axi-centrifugal (or just centrifugal) compressors.

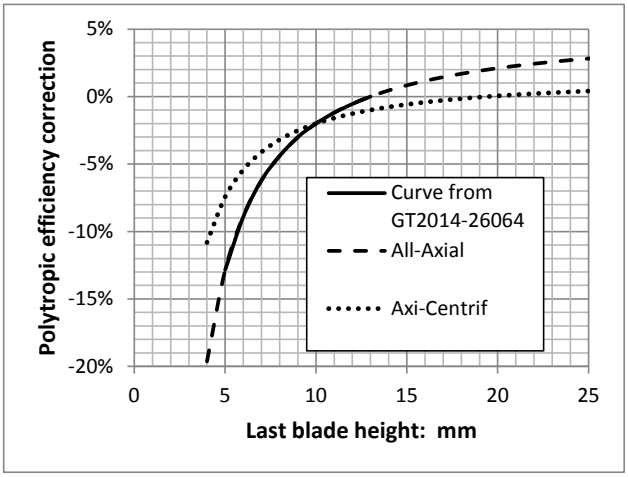

Figure 18 – Core Compressor Corrections to Polytropic Efficiency

Note the last-stage blade-height for a centrifugal compressor would be an equivalent or ‘virtual’ all-axial compressor blade-height and not an actual dimension in a centrifugal or axi-centrifugal compressor.

However, as none of the final study engines was predicted to have less than 9 mm last-stage blade-height, Equation 6 has not been used.

Ideally the scale corrections should account not only for over-tip leakage losses, but also for other secondary flows, blade thickness/chord ratios and Reynolds number effects. On the other hand, better control of tip-clearances may be achieved by 2050. There remains considerable uncertainty over the appropriate magnitude of the scale corrections, so a further investigation was made.

Some of the alternative methods have correlated efficiency loss with non-dimensional flow, either to exit flow corrected to sea level static ISA conditions for the whole compressor or to inlet corrected flow on a stage by stage basis. For example, the less-steep HP compressor efficiency correction used by Kaiser in [44] is based on the stage-wise efficiency corrections assumed by Glassman [103]. It was concluded that while the scaling penalties assumed by the author in [97] were more severe than those that had been assumed by several other researchers, they were not unrealistically high when the multiple factors tending to reduce the efficiency of small axial-flow compressors were taken into account, so they have continued to be used. None of the scale-correction methods is totally satisfactory. More research is desirable in order to find means of mitigating the loss of efficiency in smaller-sized core components.

For simplicity the efficiency correction for the two-stage HP turbine is taken to be half that of the actual or equivalent all-axial compressor efficiency correction.

No scale-corrections for efficiency are applied to the LP turbomachinery components, because they are expected to show much smaller variations with scaling. Such changes would mostly affect transfer efficiency and have little effect on the core thermal efficiency that is of greater interest in these studies.

3.1.3 Estimating Turbine Cooling Requirements

The 2050 reference turbofan has higher T_3 and TET than existing engines, so it uses cooled cooling air (CCA) to cool the HP system and to reduce the amount of cooling air required. The CCA system is designed such that sufficient cooled cooling air cooling air (CCACA) is taken from the bypass duct through a heat exchanger to bring the CCA temperature (T_c) down to 900 K when T_3 is hotter than this. Pre-swirling the air ahead of the first HP turbine rotor is assumed to compensate for heat pick-up prior to blade cooling. Both the CCA heat exchanger and the intercooler eject their spent cooling air overboard through dedicated variable-area exhaust nozzles that help to recover thrust.

Cooling the CCA is generally unnecessary at cruise, so there the CCACA flow can be zero. The intercooled engines still benefit from CCA at take-off, but the system is hardly needed for the lowest T_3 cycle options. For each engine design, the off-design CCA mass flow, whether it is pre-cooled or not, remains a fixed percentage of core mass flow to maintain a positive disc-rim sealing flow.

It is recognised that scaling-down the HP core components makes cooling them more difficult. Thus all design-point HP CCA mass flows are scaled from the 6% of core flow assumed for the reference turbofan. Scaling accounts for two factors:

- Changes in HP turbine design point mass flow
- Temperature differences between the HP turbine first blade row relative inlet gas temperature (T_{grel}) and the blade cooling air temperature (T_c)

The estimation of turbine cooling and sealing air mass-flows assumes that the temperature of the CCA is regulated to be no hotter than 900 K at all flight conditions. The top-of-climb design-point CCA mass flow is therefore estimated according to Equation 7 which accounts for two different factors and is a simplified version of the equation proposed in [97].

$$W_c = \frac{W_{cref}(T_{grel} - 900)(W_4/W_{4ref})^{0.65}}{(T_{gref} - 900)} \qquad \text{Equation 7}$$

Note the design-point CCA flow W_c for the design point T_3 and TET, is assumed to vary with the ratio of core mass flow raised to the power of 0.65. This figure is a compromise between an index of 0.8, obtained by assuming the convective heat transfer coefficients are limiting, and an index of 0.5, which would apply if the heat flux were proportional to thermal gradients in geometrically scaled components. In practice thermal barrier coating thicknesses etc. will not exactly scale. Smaller engines will also tend to have lower aspect ratio blading, so engine length and diameter will scale at different rates.

The HP turbine first-stage relative gas temperature is calculated as 25% of the temperature drop through a two-stage turbine, assuming 50% reaction blading and equal stage-temperature-drops, or 50% through a single stage (e.g. where there is intra-turbine combustion) or the equivalent temperature drop in the first stage if there are other stage numbers. The cooling air mass flow scaling rule is only applied to the first turbine blade row after a combustor and subsequent blade rows are assumed to be uncooled except in the case of inter-turbine combustion as discussed in section 3.1.5. Equation 7 has been formulated to avoid needing to specify blade metal temperatures and cooling effectiveness levels and is considered representative enough for studies where all the cycles operate with similar turbine temperatures. However it is only valid for the range of first-stage blade relative inlet gas temperatures where blade mean cooling effectiveness is around 50% and about half of the CCA is used in the first-stage blades and most of the rest is used for disc-rim sealing.

In later models, the cooling flows for the heat exchanger that cools the HP cooling air were automatically calculated for given limiting cold-side temperature effectiveness levels.

Except in the case of secondary combustion, the subsequent turbine cooling and sealing air flows are assumed just to total around 2% of core mass flow on account of improved materials and sealing technologies anticipated by 2050.

3.1.4 Integrating Intercooling

Engines with intercooling are assumed to recover thrust from the spent cooling air via separate variable-area exhaust nozzles, rather than by mixing the air back into the bypass duct. However, the off-design benefits from intercooling are increased if the amount of cooling air for the intercooler can be minimized. This raises core cycle temperatures to improve thermal efficiency and reduces cold-side pressure losses in the intercooler. Thus cruise SFC is reduced at the cost of increased TET and a small increase in cruise NOx emissions because of higher combustor flame temperatures. Conversely, the cooling flow is increased at take-off to limit TET and LTO NOx emissions. The performance modelling needs to take account of these intercooler cooling flow variations.

SFC is minimised by locating the intercooler fairly early in the overall compression system, typically between a low pressure ratio IP compressor and a high-pressure-ratio HP compressor. However, the compressor work-split is not too critical and can be varied somewhat to help optimise the overall engine arrangement. It is unlikely that the extra complexity of having two stages of cooling (intercooling and aftercooling) will be justified, so the performance models do not include this option, even for the engines with topping cycles.

Intercooling enables engines to have increased OPR and core specific power relative to the reference turbofan cycle, but without having the very high compressor delivery temperatures that challenge mechanical design and NOx emissions. Increasing OPR and TET generally gives higher thermal efficiency, but because the HP compressor last-stage blade-height and efficiency reduce as design-point OPR increases, there is an optimum OPR for best SFC and there are diminishing returns for increasing TET. Increases in max climb OPR of up to 120 are considered. It is assumed that component efficiencies are not limited by the engine architecture, but scale-corrections on efficiency are applied to the compressors and turbines operating at the highest pressures in each cycle.

3.1.5 Integrating Secondary or Inter-turbine Combustion

The Excel performance spreadsheet has the capability to model a second combustor between a first HP turbine stage and a second one. By modelling all the work in the first of those stages, the secondary combustor can also be modelled as downstream of the HP turbine. Locating it between two stages of an HP turbine (as in the GE ALSTOM GT24/26 gas turbines) or between the HP and LP turbines, is appropriate where a conventional primary combustor is followed by an intra-turbine secondary combustor. Locating it between HP stages is also appropriate if the secondary combustor immediately follows a nutating disc or piston based topping cycle geared to the HP spool, as the topping-cycle power output is then assigned to the first HP turbine stage. (However, simpler pressure-rise combustion systems without power generation can be modelled by changing the combustor pressure loss to a pressure gain.)

To model engine cycles with an ‘intra-turbine’ combustor between the first and second HP turbine stages, the stages were modelled separately and a work-split between the two parts of the HP turbine was specified. The CCA was then modelled as being returned between the first and second stages, rather than at second stage exit. This changed the performance accounting for the secondary air flows and the calculation of HP turbine efficiency. To compensate for the increase in mass-flow accounted as doing work in the second stage, the polytropic efficiency was reduced so that, without any intra-turbine combustion, the overall turbine performance and the original LP turbine design-point inlet pressures and temperatures would be maintained.

It was assumed that by 2050 uncooled ceramic materials would be used for the second combustor and for the HP turbine second-stage nozzle guide vanes, so no additional cooling air is needed for these components. However some additional non-cooled cooling air must be provided for the HP turbine second stage when it sees a higher relative inlet gas temperature because of the inter-turbine combustion.

3.1.6 Integrating the Air Bottoming Cycle (ABC)

To optimise the ABC configuration, a separate stand-alone model of this part of the overall cycle was made as described in section 3.4.

In all the engine cycles that incorporate an open-circuit bottoming cycle it was assumed that the reverse-flow-core arrangement would be used. This was originally so that the main heat exchanger for the bottoming cycle could be located ahead of the LP turbine and so that the ABC turbine could run in parallel with it as shown in Figure 2. A variable-capacity LP turbine inlet nozzle guide vane would allow the LP turbine mass flow and IP compressor pressure ratio to be optimized at off-design conditions. However, if the option is taken to delete the LP turbine and drive the IP compressor in another way, then the reverse-flow-core arrangement may not be necessary. However, the engine architecture was not critical to the performance modelling, so some simplifications were made in the whole-engine performance spreadsheet.

For these ABC engine cycles, the second LP turbine was repurposed as the ABC turbine. The exit flow from the first LP turbine was bypassed around it to the LP turbine OGV inlet, where the second turbine exit flow was added in at the same total pressure. Thus the pressure ratios of both turbines were determined by the same iteration process and matched by automatically varying the work-split between the two turbines, which jointly powered the fan and IP compressor.

3.1.7 Integrating Topping Cycles

Topping cycles were integrated in the whole-engine Excel performance model by modifying the inputs for the original HP system components. Combustion efficiency was modelled as 100%. Fuel and air mass flows, pressures and temperatures continued to be inputs, and mass flow, pressure, temperature, and power were outputs. The first HP turbine was used to model the expander disc. This provided the power to drive the compressor disc and also exported power to add to the LP turbine and ABC turbine if present. Power transfer from

the HP system to the LP system was user-specified and used to match the overall expansion in the nutating disc module to the assumed outlet pressure and temperature appropriate to the cycle and the size of the nutating discs..

In principle, volumetric efficiency or imperfect scavenging could be accounted by a percentage of recirculating flow, and part of the inlet air could be assumed to purge the topping cycle, or to bypass it to provide some cooling before being mixed back into the main core flow before exiting the topping cycle part of the model. However, since the only topping cycles modelled assume nutating-disc modules, scavenging was not an issue because 100% of the compressed air passed through the accumulator to the precombustors and the expanders. These flows were modelled as continuous in the whole-engine performance spreadsheet, so the accumulator did not need to be modelled. Also, since advanced materials that would need minimal cooling were assumed, it was also assumed that all the cooling rejected heat to the engine oil system and to overboard via an oil cooler or another closed-circuit cooling system. The oil cooler was assumed to have a separate air intake and to produce zero net thrust after the exhaust flow was heated. For simplicity this heat loss was modelled by a power offtake from the HP system which was transferred to the LP system to be added to the gearbox power loss which was also treated as heat lost to overboard.

The efficiency of a topping cycle was determined by how much power it produces, how much heat it rejects and how much pressure it delivers to the downstream components. At the concept-design stage considerable uncertainty remains regarding suitable target values for year 2050.

Since the topping cycle assumed nutating-disc modules, their performance characteristics were investigated using the time-marching models described in section 5.3. Time-averaged performance was assumed for the whole-engine model, with a combustion pressure-rise relative to the nutating-disc compressor delivery pressure.

The topping cycle outlet fuel/air ratio was constrained at design point to provide lean combustion to limit peak cycle temperatures. Rapid combustion and short residence times in the topping cycle should then have kept NOx production well below the would-be equilibrium levels at the pressure and temperature at the flame front. Therefore higher peak cycle temperatures could be used than in a lean-burn 'constant-pressure' gas turbine combustor. An appropriate time-averaged upper temperature limit for the topping cycles was taken to be 2100 K in order to avoid high rates of production of thermal NOx.

3.1.8 Estimating Heat Exchanger Performance

Heat exchanger effectiveness is limited by the trade-offs between higher effectiveness and lower pressure losses on the one hand, and higher cost, weight and nacelle drag on the other hand. Table 11 shows how the heat exchanger temperature effectiveness levels and pressure losses were set in the original models.

These figures were based on the author's prior experience in the NEWAC and LEMCOTEC programmes and anticipated some improvements in heat exchanger performance by 2050. The pressure losses are additional to duct losses in the reference turbofan model, and 'temperature effectiveness' figures are quoted throughout. Temperature effectiveness is defined as the difference between the inlet and outlet temperatures on the side of interest, divided by the difference between the overall maximum and minimum air temperatures entering and exiting the heat exchanger.

For the intercooler and the ABC heat exchangers, the cooling-air mass-flow ratio is the ratio of cold-side mass flow to hot-side mass flow.

Note the intercooler cooling-air mass flow is reduced at cruise to reduce heat loss from the core and to minimize pressure losses and improve SFC, but the mass-flow ratio is increased at take-off to limit T_3 and TET. The off-design cooling air flow is adjusted using the variable-area exhaust nozzles that recover thrust from the spent cooling air. By varying the spent-cooling-air exhaust-

nozzle area at cruise, the operating point for the intercooler can be varied to trade improved SFC against reduced compressor and turbine temperatures. Therefore Table 11 quotes a range of intercooler cooling air mass-flows for mid-cruise, with corresponding ranges of effectiveness and cold-side pressure loss.

Table 11 – Initial Heat Exchanger Performance Assumptions

Parameter	Mid-Cruise	Max Climb	Max Take-off
Intercooler:			
Max effectiveness (hot side)	50–69%	75%	70%
Hot-side pressure loss	5%	6%	5%
Cold-side pressure loss	3–6%	7%	10%
Cooling air mass flow ratio	0.8–1.1	1.2	1.5
CCA cooler:			
Max effectiveness (cold side)	-	75%	70%
Hot-side pressure loss	1%	1%	1%
Cold-side pressure loss	-	5%	20%
ABC heat exchanger:			
Max effectiveness (cold side)	75%	70%	65%
Hot-side pressure loss	5%	5%	5%
Cold-side pressure loss	5%	5%	5%
Cooling air mass flow ratio	0.7	0.7	0.7

To maintain the constant maximum 900 K CCA temperature the mass flow of cooled-cooling-air cooling-air (CCACA) is adjusted using variable-area exhaust nozzles that help to recover thrust from the spent cooling air. The mass-flow ratio of CCACA to CCA is adjusted at each condition to ensure there is sufficient CCACA mass flow to limit the cold side of the heat exchanger to 75% effectiveness at climb and to 70% effectiveness at take-off. This will minimise the size of the heat exchanger and limit the temperature of the spent CCACA.

Note the hot-side pressure loss in the CCA heat exchanger is low because the air has relatively high density and it already has low velocity, having been diffused after the HP compressor. (The same argument could be applied to a recuperator, but in that case space constraints are expected to drive the design towards higher pressure losses.)

3.1.9 General Year-2050 Cycle Temperature Limits

To make a fair comparison between the more complex cycles and the reference engine, the latter's hot-day take-off T_3 and TET values are taken as limiting and HP compressors are generally limited to a maximum pressure ratio of 26 to minimise the compromises associated with inlet and outlet hub/tip radius ratios, inlet blade-tip relative Mach number, compressor length and flexibility.

In modelling the scaled and intercooled cycles some trade-offs between the mid-cruise and max-climb TET and T_3 are allowed, relative to the original reference engine cycle. When scaling the engine core, the OPR for a given T_3 varies because the HP compressor efficiency changes. The temperature limits assumed for cruise, max climb and max take-off are given in Table 12.

The cycle temperatures and pressure ratios are hardly more aggressive than those targeted for 2025-2030 EIS by previous EU research programmes, but there are important differences in the core engine designs, materials and cooling arrangements assumed within the ULTIMATE programme for year 2050. Cycle temperatures have been set to help limit NOx emissions. However, higher peak cycle temperatures are allowed in cycles with topping-cycle machinery as discussed in section 3.1.4.

Table 12 – General Year-2050 Cycle Temperature Limits

	Mid-Cruise	**Max Climb**	**Max Take-off**
TET (K)	1730	1890	1950
T_3 (K)	913	993	1063
Deviation from ISA (K)	0	+10	+15

The larger engines benefit from working up to the maximum T_3 and TET. The smaller engines also generally benefit from this, but see relatively smaller penalties for reducing OPR and T_3. Reducing OPR should save weight. Reducing OPR, T_3 or TET will also tend to reduce cost and NOx emissions.

3.2 Aircraft modelling and Fuel-burn Exchange Rates

Aircraft modelling at BHL in the ULTIMATE project [12] generated year-2050 fuel-burn exchange-rates. Linear and non-linear exchange rates were derived: the latter for more accurate assessment of the effects of large changes in engine weight or performance. However, for simplicity, and to avoid the need for iteration, the linear exchange rates have been used. The application of the exchange rates for the long-range or intercontinental aircraft is described in [13] and [14]. For reference, the linear exchange rates are listed in Table 13.

Table 13 – Year-2050 Intercontinental Aircraft Fuel-burn Exchange Rates

Parameter	Mission FB variation
+1% $SFC_{weighted}$	+1.51% FB
+500 kg total engine weight	+1.03% FB
+1% fan diameter	+0.16% FB

The change in the weighted SFC ($SFC_{weighted}$) figure for the whole mission is calculated according to Equation 8 where SF_{CR}, SFC_{TOC} and SFC_{EOR} are the SFC figures for mid-cruise, TOC and EOR take-off respectively.

$$\frac{\Delta SFC}{SFC_{ref}}(\%)_{weighted} = 92.9\left(\frac{SFC_{CR}}{12.71} - 1\right) + 6.1\left(\frac{SFC_{TOC}}{13.39} - 1\right) + 1.0\left(\frac{SFC_{EOR}}{8.29} - 1\right) \quad \text{Equation 8}$$

The proportionate change in the fuel burn (ΔFB) is calculated (as a percentage) according to Equation 9. Equation 8 and **Equation 9** are rearranged from [14]. They are specifically for a 7000 NM mission by the aircraft that set the final thrust requirements for the engines modelled in this study.

$$\Delta FB(\%) = 151(\Delta SFC_{weighted}) + 1.03\left(\frac{W_{tot,eng} - 5528}{500}\right) + 16\left(\frac{d_{fan}}{2.835} - 1\right)$$

Equation 9

3.3 TERA Models

A suite of tools for Techno-economic and Environmental Risk Assessment (TERA) has been developed for aero engine modelling by Cranfield University and its research partners over several EU programmes including VITAL, NEWAC and DREAM. TERA tools have also been used by partners in the ULTIMATE programme, together with the object-oriented performance modelling software 'PROOSIS' developed in conjunction with Empresarios Agrupados (EA). Isight software was also used to manage interfaces between different TERA tools and to conduct optimisation studies.

The author has not made direct use of these tools in the reported studies, but some results generated by other researchers using TERA tools have been read-across. ULTIMATE project deliverable D2.5 [104] describes TERA tools used by Cranfield University and by some other project participants.

3.3.1 Engine Weight Assessment

In the ULTIMATE project, WeiCo, a Chalmers University TERA tool, was used by other researchers to provide weight estimates for the conventional turbofan engine components and heat exchangers. However, new methods were needed to assess the weights of the new components in the advanced cycles. Some models for the new components are described in Chapters 5 and 6.

The author's engine weight assessments took the WeiCo weight assessment for the final TF2050 reference engine as their starting point. The TF2050 model was taken to have the same weight and weight breakdown as the author's cycle#01 year-2050 reference engine model. The weight quoted for the TF2050

engine was 5161 kg including the nacelle [13]. The weight breakdown for the penultimate iteration leading to this weight was presented by Jacob as figure 5.3-8 in [62], giving the percentage figures listed here in Table 14.

Table 14 – Relative Component Weight Breakdown for the TF2050

Components	Weight
Fan	29.6%
IP Compressor	7.9%
HP Compressor	3.0%
Combustor	2.4%
HP Turbine	2.4%
LP Turbine	7.9%
Hot Nozzle	1.9%
Cold Nozzle	2.1%
Engine Shafts	1.1%
Main Bearings	1.3%
Reduction Gearbox	4.2%
Accessories	5.0%
Nacelle	31.1%

The weight breakdown for the year-2050 reference engine (cycle#01), provided a benchmark for weight assessments for the alternative cycles. Component weights for the alternative cycles have been scaled according to the component sizes implied by the performance models. TOC design point figures were used for sizing the turbomachinery components, but for intercoolers and other heat exchangers, take-off performance figures were used because the components would be sized to meet cooling requirements at take-off.

The weights of geometrically-scaled engine components might be expected to increase by their diameters cubed, or by their non-dimensional flows raised to

the power 1.5, but in practice they are often more-nearly just proportional to non-dimensional flow, or to diameter squared, for the following reasons:

- Wall thickness and aerofoil thickness rarely scale proportionately with the overall component dimensions
- It is often possible to make larger components hollow, or with more hollowness when compared to smaller versions that would typically be solid.
- Modular designs enable the number of modules to be increased in larger engines, rather than making the modules themselves larger.
- Larger turbomachines can have more higher-aspect-ratio blades, rather than increasing blade chords, so their lengths may not scale with their diameters.

In the author's industrial experience, most component weights scale as their diameters raised to a power between 2.3 and 2.5, while their mass-flows scale with the square of diameter. For simplicity therefore, most turbomachinery weights have been scaled by their non-dimensional mass-flows raised to the power of 1.2, but with additional corrections applied for major design changes.

Weight derivations for the novel components are discussed in Chapter 6.

3.4 The Air Bottoming Cycle (ABC) Stand-alone Model

A simple stand-alone spreadsheet model for open-circuit ABC systems has been developed using Excel. The open-circuit ABC system increases core thermal efficiency by making better use of heat in the turbine exhaust, but this potentially large benefit is reduced by several practical engineering constraints.

The ABC thermal efficiency clearly benefits synergistically from the raised first turbine inlet temperature provided by the secondary combustor in the cycle#06 engine concept, so this was the first cycle to be modelled. The originally proposed arrangement was as shown in Figure 2. In this arrangement, air for the ABC is taken as a bleed from IP compressor delivery, prior to the intercooler, and diverted to the air bottoming cycle heat exchanger (ABCHX) where it is heated by the exhaust gasses from a first turbine downstream of the

secondary combustor. The heated air then expands through a dedicated ABC turbine before being mixed with the first turbine exhaust and expanded through a further common turbine to generate more shaft power before being mixed with bypass duct air to provide additional thrust. This arrangement differs from that previously proposed by Lundbladh et al. [10]. It also differs from the arrangement finally modelled in the whole-engine performance model, which omitted the common turbine stage and computed the extra thrust by expanding the spent ABC turbine air to ambient via a separate thrust nozzle. This simplified arrangement was adopted following studies made with the stand-alone model.

Considered in isolation, the thermal efficiency of the bottoming cycle is fundamentally limited by the ratio between its ABC-turbine inlet air temperature and the inlet temperature of the air to its compressor. It is further reduced by the inefficiencies in the compression and expansion processes, and by the other pressure losses, not-least those in the heat exchanger. The ABC-turbine inlet air temperature depends on the first-turbine exhaust gas temperature and the effectiveness of the ABCHX. For reference, the temperature-effectiveness for the cold (air) side of the ABCHX is defined by Equation 10, and the hot (gas) side temperature-effectiveness is defined by Equation 11.

$$\xi = \frac{\mathrm{T}_{out,\mathrm{cold}} - \mathrm{T}_{in,\mathrm{cold}}}{\mathrm{T}_{in,\mathrm{hot}} - \mathrm{T}_{in,\mathrm{cold}}} \qquad \text{Equation 10}$$

$$\xi = \frac{\mathrm{T}_{in,\mathrm{hot}} - \mathrm{T}_{out,\mathrm{hot}}}{\mathrm{T}_{in,\mathrm{hot}} - \mathrm{T}_{in,\mathrm{cold}}} \qquad \text{Equation 11}$$

The ABC stand-alone Excel spreadsheet model was created to explore the above sensitivities including the best pressure ratios and performance for a range of inlet conditions and the best arrangement to be modelled in the whole-engine performance spreadsheet.

As in the case of a supercritical CO_2 (S-CO_2) bottoming cycle, just maximising the thermal efficiency of the bottoming cycle in isolation will not tend to give the

best overall cycle efficiency or fuel burn. Taking heat away from the inlet to any core turbine downstream of the ABCHX will reduce its power output and a lower exhaust gas temperature will also reduce the thrust from the core exhaust nozzle, unless its pressure ratio is increased by reducing the turbine expansion ratio, which will further reduce the turbine power. Thus the optimum location for the ABCHX within the core expansion systems needs to be determined with respect to core turbine expansion ratios, and so both flows must be modelled.

In the stand-alone model, the ABC air is first compressed from ambient (1) to the inlet of the cold side of the ABCHX (2). After being heated the air passes from the heat exchanger exit (3) through the ABC turbine to its exit (4) and then through an exhaust nozzle to generate thrust by expanding to ambient (5). Meanwhile the main core flow (6) enters the HP turbine and expands to the ABC heat exchanger hot-side inlet (7). On exiting the heat exchanger (8) the gas expands through the LP turbine to its exit (9) and then through the hot exhaust nozzle to generate thrust by expanding to ambient (10). The system is shown schematically in Figure 19.

The total power generated by the three turbines, less the power needed to provide the air compression, provides the net power output from the system[3]. It also provides a figure of merit for the given combination of input parameters.

By running the model with zero or negligible ABC air flow and zero pressure losses in the heat exchanger, a baseline level of net power can be calculated.

[3] In practice the turbines would not be expanding to ambient pressure, but would be followed by exhaust systems that provided their contributions to jet thrust. However, this would just be using the available energy in the air and gas streams in another useful way. The efficiency of the transfer of this energy into thrust through the exhaust nozzles should be slightly higher than the efficiency for power generation in the ABC and LP turbines, but the discrepancy is a minor factor when comparing the overall efficiencies of variant systems. The overall compression and expansion polytropic efficiencies were set to 90% for most of the studies.

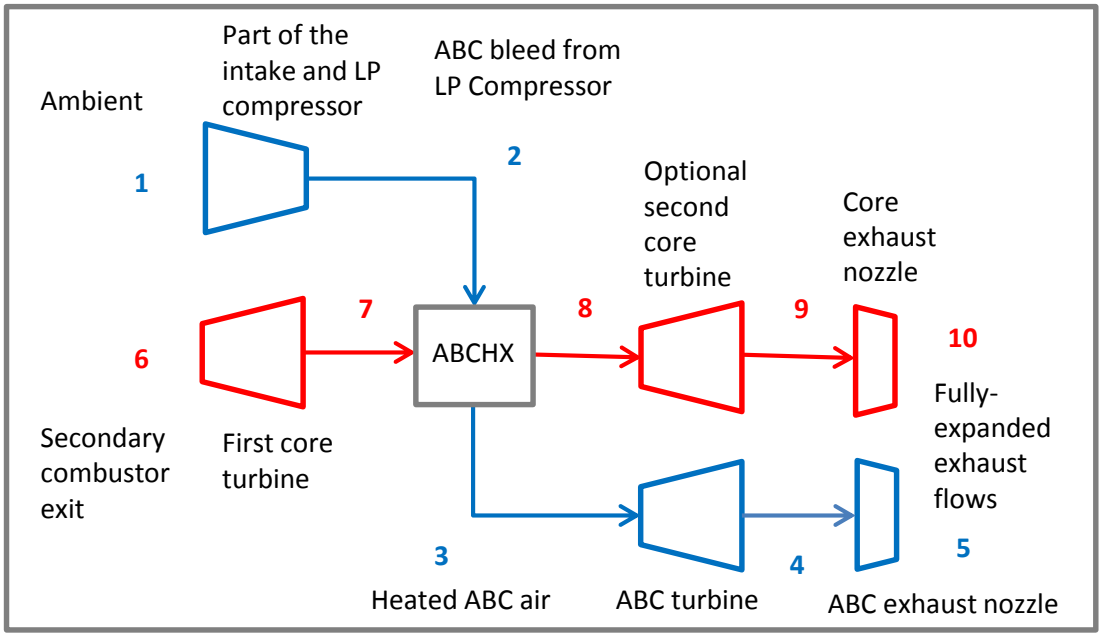

Figure 19 – Simple Schematic of an ABC System

(Air flows are shown as blue and combustion products as red)

Some iteration is required to provide converged solutions, so the Excel 'Goal Seek' function is used to find the heat exchanger exit temperature that corresponds to the limiting (hot-side or cold-side) temperature effectiveness in each case.

Modifications made to the original model are described in section 6.3 where results obtained from the ABC parametric studies are discussed.

3.5 Time-Marching Models for Nutating Discs

Excel spreadsheet models were generated for the compression and expansion processes which occur in separate chambers within the nutating-disc module. The model cannot be adequately described without first explaining how the nutating-discs operate, so description of the models is deferred to Chapter 5 where the nutating-disc modules are described and the results obtained with the models are discussed.

3.6 Models for Civil Aviation Scenario Studies

Another Excel spreadsheet was created by the author to assess the potential benefits of the advanced-cycle technologies on total CO_2 emissions up to and beyond the year 2050. The spreadsheet also enabled analysis of the potential economic impact of changes in the cost of jet fuel and the possible introduction of taxation on CO_2 emissions. The development of this spreadsheet and the results from the initial scenario studies were originally reported in ULTIMATE deliverable D5.5 [105]. A summary of the results is given in Chapter 9.

The scenarios were originally proposed by John Whurr from Rolls-Royce as recorded in ULTIMATE deliverable D5.2 [106].

3.6.1 Estimating Fleet Fuel Burn and CO_2 Emissions

The ULTIMATE year-2050 reference aircraft and engines had been estimated to provide fuel-burn reductions of between 45% and 59% relative to baseline year-2000 aircraft and engines. However, to assess the overall fleet performance of commercial aircraft, the proportion of fuel burn that should be attributed to shorter-range and longer-range aircraft types needed to be assessed. It seems likely that the proportion of flights on long-range aircraft, and the average flight distances, will tend to increase up until 2050, since short-range aircraft will face increasing competition from high-speed rail services. However, for simplicity, it was assumed the overall fuel burn per passenger kilometre actually flown was the average of the short-range and long-range fuel-burn figures, equivalent to the whole fleet being characterised by 54% of the 'available seat kilometres' (ASK) provided by the short-range aircraft and 46% by the long-range aircraft. This means that over the period of 50 years from 2000 to 2050, the average reduction in fuel burn per passenger kilometre for new aircraft is predicted to be 52.1%, corresponding to a compounded annual fuel-burn reduction rate of about 1.461%, or 13.7% per decade.

The SRIA targets for Air Traffic Control (ATC) and operations improvements from year 2000 onwards, as quoted in Table 2, would require fleet-wide

improvements of 0.362% per annum in the first two decades and 0.368% per annum over the next 15 years, or 0.365% per annum over 35 years. The target figures imply that no further ATC improvements are expected after 2035. Further assumptions are listed in Table 15.

Table 15 – Assumptions for a Baseline Scenario for CO_2 Emissions

Baseline air traffic growth rate	4.5% RPK p.a. until 2030, then reducing by 0.3% and another 0.3% every five years until 2065 and then by 0.2% and another 0.2% every five years, down to 1% RPK p.a. in 2100.
Passenger load factor	80% constant (PLF=RPK/ASK)
Fuel savings from ATC and operations	0.365% p.a. to 2035 and zero thereafter (as per SRIA targets).
Aircraft and engine fuel savings without ULTIMATE advanced technologies	For the latest equipment: 1.461% p.a. to 2050; then reduced to 1.2% and then reduced by another 0.3% every five years, until zero after 2070.
Roll-over of technologies through the whole fleet	Fleet average fuel burn per ASK trails new aircraft by ten years.
Fleet-wide penetration of ULTIMATE advanced technologies	Uniformly from after 2050 up to a maximum of 90% by 2075, for airliners and also for the total civil aircraft fleet including cargo aircraft and business jets.
Price of crude oil	$75 per barrel in 2020, increasing by $5 per barrel per decade.
Price of jet fuel	$0.71025 per kg in 2020, increasing by $0.04735 per kg per decade.

Most of the following scenarios showing the effects of introducing ULTIMATE technologies assumed they would meet the 15% fuel burn reduction target set at the outset of the project. It has also generally been assumed that the fuel-burn benefits would only be applicable to 90% of the commercial fleet (comprising airliners and regional aircraft) or to 90% of the overall civil aircraft fleet including other aircraft types. The same percentage was applied in both cases assuming advanced-cycle technologies would be equally applicable to airliners and to larger business jet aircraft, for example.

The overall rates of performance improvement and total CO_2 emissions are assessed across the whole of the civil aircraft fleet. To allow for older and less fuel-efficient aircraft and engines in the fleet, it was assumed that fleet-average fuel-economy lags behind that of the latest new equipment by a constant ten years. This allows for growth in the overall market and the retirement of older equipment, and it also allows for the fact that it takes a few years for production of new models to fully ramp-up and for production of older models to be phased-out. The typical active service-life of individual aircraft is assumed to be about 25 years (though older aircraft may be kept in reserve and used to provide some extra flights at times of peak demand.)

As noted above, the latest figure for new engine and aircraft compound annual fuel savings up to the year 2050 is 1.461% p.a. This is an aggregate figure for the whole fleet, calculated supposing 54% of the total ASK is provided by intra-European (short-range, single-aisle or narrowbody) aircraft and 46% is provided by intercontinental (long-range, twin-aisle or widebody) aircraft. The percentage figures are assumed to remain constant, at least up to 2050, but the average number of seats per aircraft and average aircraft design range are expected to increase steadily from year 2000 to year 2050, as reflected in Table 1.

There are large uncertainties regarding historic air-traffic statistics, the projected rates of increase in air-traffic growth, in the rates of improvement in aircraft and engine technologies, and not least in the future cost of fuel to the airlines and inflation rates. Figures for future fuel costs are taken as proposed in [106]. The price of jet fuel per US barrel is assumed to be 1.2 times that of Brent crude, and one barrel of jet fuel weighs about 126.7 kg based on a density of 797 kg/m^3 [106]. Thus the price of jet fuel per kg is roughly 1.2/126.7 times the cost per barrel of crude oil or 0.947 US cents per USD per barrel of crude oil. Fuel costs in the study make no allowance for any premium added for the substitution of bio-fuels for fossil-fuel kerosene. Some airlines, such as Scandinavian Airlines (aka SAS) are now proposing to pass that extra cost directly onto those passengers who are voluntarily willing to pay something

extra towards making the substitution. It is unclear whether or not that could prove to be a viable long-term solution to covering the higher cost of bio-fuels.

Inconsistencies in reporting make current and historic global passenger figures somewhat uncertain, but the most-recent figure of 7.7 trillion RPK reported in 2017 by www.statistic.com has been taken as a benchmark and equated to 9.625 trillion ASK in that year, assuming a typical PLF is 80%, based on data in [24]. Allowing for 4.5% annual air-traffic growth, this gives about 11 trillion ASK in 2020. The figures for 2020 are relevant because of the ATAG target to cap total CO_2 emissions from the aviation sector at the 2020 level, and then to halve this figure by 2050. Given the assumption of constant 4.5% p.a. average growth up to 2030, there would have been 4.55 trillion ASK in year 2000. This figure may be a 10% over-estimate, but as the new benchmark for CO_2 emissions from aviation will be based on year-2020 emissions, the year-2000 ASK figure is less important.

Converting relative values of fuel burn to actual total fuel burn and mission-level CO_2 emissions requires further assumptions to be made. A significant factor is the difference between the scheduled kilometres flown and the actual distances flown through the air in revenue operation. This is largely attributable to the efficiency of ATC routing and the timing of arrivals at busy airports. This air traffic management (ATM) is assumed to be improving in the timeframe from year 2000 to year 2035. However, even at the end of this period, aircraft routing will not be perfect and planes will still need to make approach and departure manoeuvres. Therefore, in this study it is assumed that a 15% fuel saving from ATM and airline operations is theoretically possible, but that the actual improvement will never be better than a 12% reduction relative to year 2000, as implied by the SRIA targets. For year 2000 this is equivalent to burning 17.65% more fuel than just flying the ideal point-to-point distances at the given fuel burn per kilometre. In practice one would expect longer flights to be routed relatively more efficiently than shorter ones, but for simplicity the same factor is applied to intra-European and intercontinental aircraft missions and to overall operations.

Relatively more freight is flown in passenger aircraft on long-haul routes than on short-haul routes, but again for simplicity the different aircraft types will be treated equally. To account for passenger aircraft that carry freight, it will be assumed that the typical fuel burn for 80% PLF plus freight is equivalent to the design-mission fuel burn for 100% PLF.

For the overall civil aircraft fleet, an extra margin is added to the total fuel consumption of the passenger fleet in revenue passenger operations, to allow for operations by dedicated freighter aircraft, private business aircraft, charter flights, non-revenue positioning or training flights, and other miscellaneous aircraft operations. Figure 12 in ULTIMATE deliverable D5.2 [106] indicated that airliners and regional aircraft in 2050 would account for 87.4% of civil aviation energy use. However the airliners figure also includes dedicated cargo aircraft, so fuel use by commercial passenger aircraft will be a slightly smaller proportion. While the author expected fuel consumption from APU use to reduce, growth in cargo operations was expected to increase faster than growth in passenger travel. Thus over the next few decades it was assumed the rise and fall in these individual factors would more or less balance out. To account for the additional fuel burned on non-revenue flights, by other aircraft types and by APUs etc., these factors were estimated to add 20% extra to the overall fuel burn in the baseline case. However, Boeing's latest 2018 World Air Cargo Forecast [107] predicted only 4.2% growth in revenue tonne kilometres (RTK) over the next 20 years, slightly less than the author's baseline scenario for passenger growth. More recently air cargo growth has been hit by the US trade war with China, so the faster cargo growth assumption may be incorrect.

Taking the typical chemical formula for kerosene as $C_{12.5}H_{24.4}$ then one kilogram contains 0.85925 kg of carbon and will produce 3.148 kg of CO_2 on complete combustion.

3.6.2 Airline DOC Model

To put the future cost of jet fuel into context it is necessary to consider how other airline costs are likely to evolve in the 21st century. A simple 'top-down'

model[4] of airline fleet-average operating costs is based on the 'MAJORS, NATIONALS & LARGE REGIONALS System' US airline financial data for year-2017 from the Bureau of Transportation Statistics. Its figures are summarised in Table 16. Note 'Flying Operations' includes the cost of fuel and oil together with flight crew expenses and air navigation charges etc.

Table 16 – US Airline-system Financial Data for the Year 2017

Category	Cost: USD billions	Cost re. total DOC
Flying Operations	15.78	30.6%
Maintenance	5.26	10.2%
Passenger Service	3.38	6.6%
Aircraft and Traffic Servicing	7.10	13.8%
Promotions and Sales	2.41	4.7%
General and Administrative	4.52	8.8%
Depreciation and Amortization	2.77	5.4%
Transport Related	10.31	20.0%
Total Operating Expenses	51.53	100.0%

The cost breakdown is taken to be representative of the future global fleet. For 2017 the fuel cost is assumed to have been about 18.75% of DOC at a time when the average cost of oil was about $55/barrel [106]. These figures provide a benchmark for the simple DOC model described in section 9.5. The Cost per Available Seat Kilometre (CASK) in 2017 comes out at about 6 US cents, which is broadly consistent with figures from the ICAO for early years of the 21st century: IATA Airline Cost Performance (IATA Economics Briefing No. 5). See: https://www.iata.org/whatwedo/Documents/economics/airline_cost_performance.pdf

For comparison, US network airlines had costs approaching 7 US cents/ASK, whereas the low-cost operators had costs from 4 to 5 US cents/ASK. The

[4] A top-down model takes the anticipated end-result or overall figure and breaks it down into subcomponents, whereas a bottom-up model calculates the end-result based on subcomponent figures or model inputs.

aggregate DOC figures are therefore only indicative of average airline costs, but nevertheless interesting trends have emerged as discussed in Chapter 9.

3.7 Emissions Assessments

Improved thermal efficiency cannot justify increased noxious exhaust emissions and future aero engines will need to meet stricter emissions constraints. Various different tools were considered for modelling combustion and emissions, but for quantitative assessment of NOx emissions from future LDI combustors it was eventually concluded that a simple correlation would be more appropriate.

A detailed study of potential emissions assessment methodologies for the year 2050 reference engines was made and reported in the confidential ULTIMATE project deliverable D2.3 [108]. The study had the limited objective of providing a methodology for assessing the emissions from the 'constant pressure' primary combustors in the year-2050 reference engines and for some of the advanced-cycle aero engines that retained LDI primary combustors while incorporating additional technologies. The following sections provide a summary of the study and more details are given in Appendix B.

3.7.1 Reference Engines for Combustor Emissions Assessments

Whilst the two different Advanced Tube and Wing (ATW) aircraft designs were being worked-up by BHL, representative thrust requirements for the reference engine studies were taken from previous EU projects that had investigated engines for both long-range and short-range missions. These original thrust requirements were also used in the ULTIMATE project deliverable D1.1 [64] for initial modelling of the geared fan and geared open rotor powerplants that would become the year-2050 reference engines. However, by the time the updated reference engine cycles were reported in ULTIMATE deliverable D2.6 [13], iteration with the ULTIMATE aircraft modelling task had significantly reduced the engine thrust requirements. Further refinements to the ULTIMATE reference engine models were then made and the latest performance results were used for the emissions assessments.

3.7.2 Methods for Combustor Performance and Sizing

Across the operating envelope, engine performance models should specify combustion efficiency and pressure loss in addition to the inlet fuel/air ratio, mass-flow, pressure and temperature. Combustion efficiency determines the actual heat release in the combustor, but low combustion efficiency is also indicative of high levels of carbon monoxide (CO), unburned hydrocarbons (UHC) and/or smoke. The combustor volume and geometry are determined by the design philosophy, by adjacent component dimensions, and by overall performance requirements including altitude relight capability.

For primary combustors burning kerosene (Jet-A, Jet-A1 or similar fuels), altitude relight is a key requirement that sets a minimum combustor volume to give an adequate residence time to achieve a respectable combustion efficiency and temperature-rise when an engine is cold and just 'windmilling'. This enables the engine to 'pull-away' to higher power operation. A windmill relight envelope usually extends up to 25–30,000 ft. and covers a specified range of airspeeds. If the aircraft is flying too slowly, the windmilling turbomachinery will also be turning very slowly and with very poor efficiency, so that the engine may fail to 'pull-away'. Conversely, if the aircraft is flying too fast, then the flames in the combustor can be continually 'blown-out' by the relatively high velocity of the air passing through it. In this case the flames may fail to 'light-around' the whole of the combustor and again the engine may fail to accelerate.

To expand the relight envelope, an increased combustor volume will increase combustion efficiency and turbine entry temperature by increasing the residence time of the air and fuel in the combustor. Optimized fuel scheduling and igniter design and positioning can also improve relight and pull-away. However, the combustor is likely to be designed with the smallest volume that meets the altitude relight requirements. This will save weight and minimize thermal NOx production, as the latter processes are relatively slow in comparison with hydrocarbon fuel combustion. On the other hand, combustors

with lower residence times are likely to have higher CO, smoke and UHC emissions, particularly at low power conditions.

3.7.3 Stirred-Reactor Combustion Models

The first tool to be considered for combustor and emissions modelling was a stirred-reactor model. This should be capable of modelling the LDI style of combustor anticipated for the reference engine and secondary combustors also.

Perfectly-stirred and partially-stirred reactor models and various series of stirred reactors have been used to model the major zones within gas turbine combustors, at a less detailed level than CFD modelling. Alternative terminology refers to well-stirred reactor (WSR) and plug-flow reactor (PFR) models, the latter representing regions of very low turbulence, as in some pre-mixed combustors and combustion rigs. Cranfield University has developed such in-house models as part of the suite of computer programs designated 'Hephaestus' [109], a sub-set of the TERA suite of tools. These models can fairly quickly scope-out different design options and provide initial combustor dimensions for follow-on CFD work. Studies have shown that the performance and emissions of combustors modelled using Hephaestus methods can be closely correlated to the LTO combustor emissions for existing engines in the ICAO database [110] [82] [109].

Consideration was given to the use of Hephaestus models linked by 'Isight' software to engine-performance and dimensional-model programs. This could have extended the TERA suite of software and permitted exploration of design trade-offs from changes in the proportions of LDI combustors and alternative combustor designs, and from changes in the scheduling of fuel flow through the fuel injectors. However, the creation of Hephaestus models is not automated. Setting them up would have required a considerable number of inputs that are not readily generated by performance models like PROOSIS, or by WeiCo (that estimates preliminary engine dimensions, major component weights and costs). While the user might be prompted to provide a file of additional combustor dimensional and fuel distribution inputs, these values would be highly

speculative in the absence of worked-up aerodynamic and mechanical designs for a particular combustor. If several different people were to model LDI combustors for a range of different engine performance cycles, the results would most likely also be highly variable, unless a rigidly-defined set of design rules could be imposed. The author judged that there was too-much uncertainty in the geometries likely to be used in the year-2050 designs to make effective use of this tool.

It was therefore concluded that a simpler algorithm or set of algorithms would provide more consistent emissions estimates over the range of different combustor sizes and operating conditions of interest. These algorithms or correlations should only need the performance data obtained from regular performance codes and models. Their use would therefore provide a more consistent methodology and guarantee consistent assessments for the LTO emissions of different engines and of their total NO_x emissions over the flight envelope. The derivation of these simpler and more appropriate methodologies, based on existing LDI combustor emissions measurements and correlations, is described in the section 3.7.5.

The use of Hephaestus models in follow-on studies to estimate the emissions of more novel or radical combustor designs, such as secondary or inter-turbine combustors is still worth considering. In such cases, correlations based on one standard combustor design will not suit all the different possible combustor configurations, so each novel design would need to be assessed on its own merits.

3.7.4 Higher Fidelity Combustor Modelling Options

The detail design, modelling, analysis, testing and subsequent optimization of combustors, their fuel injectors and fuel delivery systems, is a major engine development activity. Sophisticated Large Eddy Simulation (LES) CFD models like PRECISE-UNS are created that follow the vaporisation of fuel droplets and the sequential formation of numerous intermediate and end-of-combustion products. These are amongst the most computationally intensive models used

in the industry, as they not only need to model turbulent flows in detail, but also the complex chemical reactions following hundreds of species and thousands of different reactions, leading to the non-equilibrium mixture of combustion products. Modelling the formation of oxides of nitrogen from hydrocarbon fuel combustion is particularly challenging, so much so that many kinetic-mechanism schemes simply ignore them. For example, 'Complete Low and High Temperature' kinetic schemes from the 'CRECK Modeling Group' at Polytechnic University of Milan [111] come with 451 chemical species and 17848 different reactions excluding NOx, or with 484 species and 19341 reactions if NOx is included. Even the reduced high-temperature scheme for simpler kerosene surrogates has 121 species and 2613 reactions.

One system of combustor modelling tools used to manage geometry and create boundary conditions for CFD studies is called Prometheus. This is being developed at Rolls-Royce and in parts of its University Technology Centre network that include Loughborough and Southampton Universities. Various aspects of the system have been described in recent papers [112] [113].

Such methods are well beyond the scope of the author's concept design studies. Elsewhere, within the ULTIMATE project, CFD methods have been used to provide insight into several novel combustor designs, such as pulse pressure gain combustors [65], and secondary combustion systems [76]. However, no new CFD models for more conventional RQL or LDI combustors have been created, since a large body of literature exists from previous research programmes and the detail design of a specific LDI combustor for a year-2050 EIS engine would be highly speculative. Furthermore, past studies have shown the emissions predictions from simpler CFD models can be highly variable, depending on the modelling techniques and assumptions. LES combustor models have been demonstrated to give greatly superior results to Reynolds Averaged Navier-Stokes predictions [114], but they are more computationally expensive.

3.7.5 Alternative Emissions Assessment Methods

It was thought that some automotive engine modelling tools might have been used to assess the emissions for engines incorporating diesel cycles, but attempts by a colleague to adapt such tools for the nutating-disc modules' emissions assessment proved unsatisfactory, so the author was only able to provide qualitative emissions assessments for the engines with nutating-disc topping cycle modules.

Cranfield MSc students Victor Martinez Bueno and Mirko Romanelli used CFD models to assess emissions from the secondary combustor proposed for the preferred advanced engine cycle. Their studies are described in section 6.2.2.

3.8 Emissions Correlations

Correlations provide simple and widely-used methods of estimating engine exhaust emissions. Reviews of the different families of correlations were made by Pervier [109] and by Chandrasekaran and Guha [115]. Methodologies exist for constructing correlations to predict the off-design performance of existing combustors throughout the flight envelope, based on their emissions at the ICAO LTO-cycle ground-level (GL) test conditions. Other correlations are based on combustor rig-test measurements, and some correlations estimate a generic emissions capability for a particular combustor technology given multiple inputs.

For NOx emissions anticipated from fully developed year-2050 LDI combustors, existing predictions and correlations are reviewed, and in Appendix B, potential new correlations are discussed. However, as reported in [108], the author had insufficient data to validate the proposed new correlations, so they cannot be recommended over existing correlations for lean combustor configurations.

3.8.1 ICAO Database-based Correlations

To estimate baseline emissions throughout the flight envelope for year-2000 in-service engine technology, correlations can be constructed based on Trent 700 and CFM56 figures taken from the ICAO emissions database [82]. The availability of these data enables representative correlations to be produced.

Several methods are known for generating correlations to predict emissions throughout the flight envelope based on the ICAO database figures. These include the Boeing Fuel Flow methods, the Advanced Emission Model, the DLR method, and the 'P3T3' method. These methods can be applied to CO, NOx and UHC emissions. Most methods for NOx emissions also include corrections for atmospheric humidity [116].

3.8.2 The Boeing Fuel Flow Method 2

This method, variously referred to as BM2, BFF2 or BFFM2, uses a five-step process to estimate emission indices based on ICAO database figures. It takes the ambient pressure, temperature and humidity, and engine fuel flow and flight Mach number as inputs [117].

Humidity particularly affects NOx emissions and it increases $EINO_x$ by e^H where H is the humidity correction factor which is calculated according to Equation 12, where $\boldsymbol{\omega}$ is the specific humidity.

$$H = -19(\omega - 0.006344) \qquad \text{Equation 12}$$

The humidity correction is not applied to other pollutant species. The figure of 0.006344 corresponds to the specific humidity $\boldsymbol{\omega}$, or h, on an ISA day at sea-level and having 60% relative humidity (RH, or Φ, which is not to be confused with equivalence ratio). This humidity could be typical for ground-level emissions testing. If the actual RH is 60% then H is zero the factor e^H is unity. For completely dry air e^H is 1.127, and for saturated air on an ISA day at sea-level, e^H is about 0.923. Thus the effects of humidity can be quite significant, with higher specific humidity reducing NO_x emissions.

Figure 20 shows how the humidity correction factor H can vary with altitude and typically increases predicted NOx emissions at high altitudes by about 12.5% relative to typical sea-level test results. At typical cruise altitudes, the variation of H with humidity levels is quite small, so there are almost negligible errors in estimated cruise and top-of-climb NOx emissions, whether the air at altitude is considered to be totally dry, or to have 60% RH, or to be saturated.

The reduction in NOx emissions is primarily due to the reduction in flame temperature resulting from the higher water vapour content and specific heat, so it is inappropriate to apply the humidity correction to any method that would model engine performance correctly with humidity and then use those lower combustion temperatures in the NOx correlations. Preliminary aero engine performance is generally modelled assuming totally dry air.

The effect of ambient humidity on NOx emissions is similar to the effect of water or steam injection, since these also affect the proportion of water vapour in the final combustion products and reduce flame temperatures.

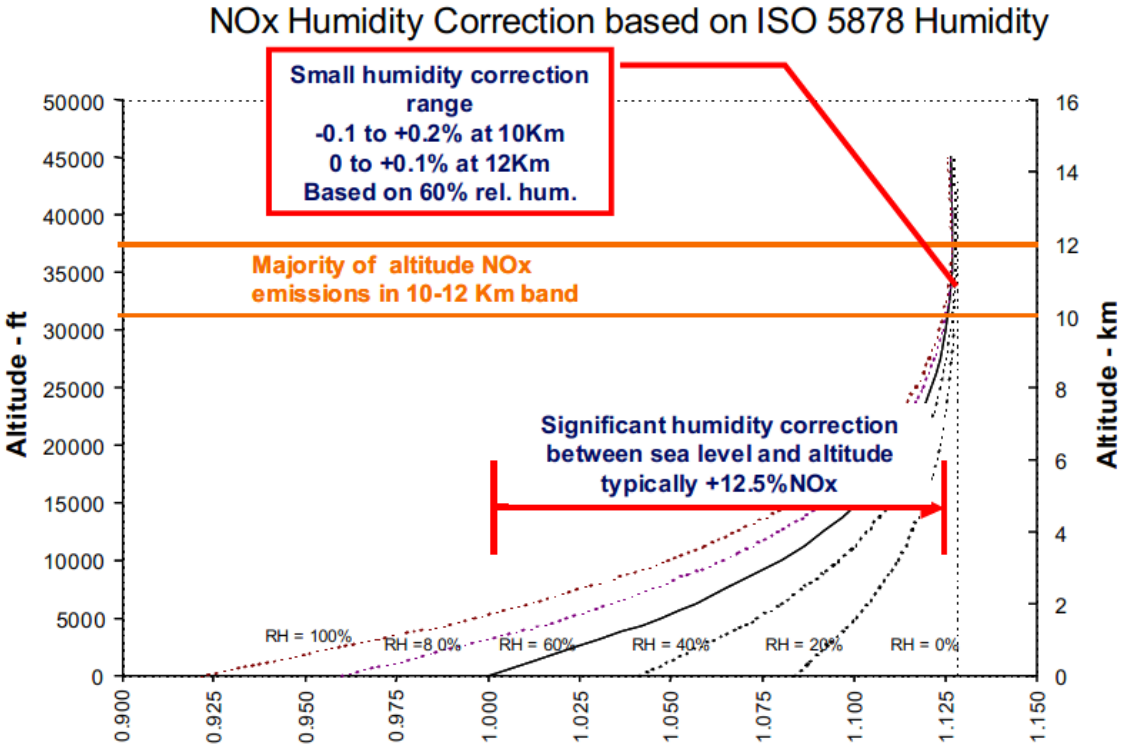

Figure 20 – Humidity Correction Factor *H* for NOx at altitude [83]

It appears that the humidity correction formulation originates from testing on automobile engines carried-out in the USA around 1970, but different corrections are now applied to different types of combustion engines (e.g. spark ignition vs compression ignition engines), so it is not obvious that Equation 12 should be applicable to all gas turbines using different types of fuel. However, it is worth noting that, at a given flame temperature, increasing the hydrogen to

carbon ratio in a hydrocarbon fuel is not effective in reducing NOx and generally has the opposite effect.

3.8.3 The Advanced Emission Model (AEM3)

The AEM3 method (version 1.5), based on the BM2 method, is from the Eurocontrol Experimental Centre at Brétigny-sur-Orge in France [116]. The AEM3 methodology makes a correction to the calculation of the humidity correction factor used in the original BM2 specific humidity calculation. The correct formula for ω as a function of ambient pressure P_{amb} and the actual water vapour pressure P_a is given by Equation 13, in which e is the ratio of the molecular weights of water vapour and air. Equation 13 gives specific humidity defined as kg of water vapour per kg of moist air, whereas Equation 12 gives specific humidity defined as kg of water vapour per kg of dry air. In practice the difference between these two differently defined humidity figures is almost negligible.

$$\omega = eP_a \,/\, P_{amb}((1-e)P_a) \quad \text{where } e = 0.62198 \qquad \text{Equation 13}$$

P_a is the product of the relative humidity Φ and the saturation vapour pressure P_v which may be taken to be equal to the partial vapour pressure over liquid water (e_L). A simple correlation for e_L as a function of ambient temperature is given by Equation 14.

$$e_L(T) = 100 * 6.112 * e\text{^}\left[\frac{17.62 * (T - 273.15)}{243.12 + (T - 273.15)}\right] \qquad \text{Equation 14}$$

This is the Commission for Instruments and Methods of Observation (CIMO) formulation with pressures in Pa and temperatures in K [118]. An alternative formulation for P_v, given by Jelinek et al. [116] gives saturation pressures 1.3% to 2% higher over the typical range of atmospheric temperatures. Note the copy of the formulation in [109] is misprinted.

The AEM3 method follows five steps:

- Access the ICAO data and correct the ICAO fuel flows at the four certification cases to allow for engine installation effects, since the ICAO data are provided only for uninstalled engines. Table 17 lists the standard fuel flow correction factors inherited from the BM2 method.

Table 17 – Recommended Correction Factors for the AEM3 Method [116]

Take off	Climb out	Approach	Taxi/ground idle
1.010	1.013	1.020	1.100

- Curve-fit the ICAO data for each species, by plotting the four tabulated emission indices against the corrected fuel flows.
- Calculate the ambient pressure and temperature correction factors, δ_{amb} and θ_{amb}, respectively, for the desired flight conditions and apply these factors in the appropriate equations to give the modified fuel flow W_{ff} from the actual fuel flow W_f.
- Read the reference emissions index values from the curves generated in the second step, reading-in with the W_{ff} figure to give *REICO*, *REIHC* and $REINO_x$ values for CO, UHC and NOx respectively.
- Calculate the emissions indices: *EICO*, *EIHC* and $EINO_x$ from the *REICO*, *REIHC* and $REINO_x$ values, and apply any humidity corrections.

The last three steps can be repeated for each point on a flight mission and the total emissions can then be obtained by summing the products of the durations, fuel flows and emission indices obtained for each flight condition. These calculations could be performed using Excel or MATLAB, but since they can be automated without any iteration, in principle a simple set of formulas (or even one long formula) is all that is needed for each flight case for each species.

The BM2 and AEM3 methods specify using log-log plots for the data. Linear trendlines may be fitted to the data using a 'linear least squares' fit and taking the fuel flow as the independent (x-axis) variable. Since there are just four data points for each species, the slope of the trendline and its intersection with the y-

axis can be solved relatively simply. However, a straight line may not always provide a good fit to the data, particularly not for the CO and UHC emissions. An alternative approach is to plot straight lines between adjacent points, but then the equation for the correct line needs to be selected, e.g. by using 'IF' statements in Excel code, for example, adding additional complexity.

Alternatively, a third-order polynomial curve can pass exactly through all four LTO cycle data points for each species, but such curves tend to deviate further from lower order curve fits, or straight-line ruling between the points (Runge's phenomenon), so historically the use of a third order polynomial curve fit has not been recommended. In practice though, for NOx emissions calculations, the differences seem negligible, (given all the other uncertainties in emissions estimation) and exact-fit third order 'Lagrange' polynomial coefficients are more simply computed than those for a second order least squares curve-fit. A cubic spline curve fit to the data might be another option, and is a known means of addressing Runge's phenomenon, but it seems not to have been adopted hitherto for use in emissions calculations.

3.8.4 The DLR Method

The DLR method [119] is similar to the BM2 and AEM3 methods, but it does not use log-log plots for the data. It just applies a second-order polynomial least-squares curve fit to the data. The DLR method also deviates from the previous methods in the way that it calculates the fuel-flow-correction factor and calculates the NOx emission index at altitude. Schaefer gives more details of the DLR method [120].

The DLR method and the preceding methods all make certain assumptions about the way the engine is installed and how the combustor is operated. For typical year-2000 in-service engines, these assumptions may be reasonable, but they are likely to be inappropriate for 'zero-bleed' engines, engines with variable cycles and engines having staged fuel-flows to their combustor fuel injectors. Where more detailed engine performance models and cycle data are

available, the P3T3 method should give better results for NOx emissions than the methods described hitherto.

3.8.5 The P3T3 Method for NOx Prediction

This method is a further development of the ICAO database methods. It should be able to overcome some of their limitations for NOx emissions estimates that are particularly sensitive to combustion temperatures because it takes combustor performance parameters into account [109]. It requires an engine performance model to predict combustor inlet temperature T_{31}, inlet pressure P_{31} and overall fuel/air ratio FAR_{31} at ground level, for calibration against the ICAO database emissions indices, and to generate the equivalent performance data at altitude for on-route emissions predictions. Such data were in-scope for the ULTIMATE project, but there remained the common difficulty in modelling low-power idle and descent performance using preliminary design performance models, so scaling or extrapolation of the performance model data to lower thrusts was needed for some of the ULTIMATE study engines, in order to cover the low-power conditions [108].

A further complication relates to the use of combustor inlet conditions for pressure, temperature and air mass flow P_{31}, T_{31} and W_{31}, rather than the HP compressor exit conditions that are more commonly quoted from preliminary performance models. There is usually no difference in the temperatures, unless the HP compressor rear drive cone is cooled by air that flows radially outwards into the annulus (though this may well be a design feature of future advanced engines with cooled-cooling-air systems). P_{31} should account for the HP compressor exit diffuser pressure loss and W_{31} for secondary air flows that bypass the combustor. W_{31} is used to calculate the FAR in the combustor FAR_{31}. However, provided P_3 and W_3 are consistently substituted for P_{31} and W_{31} in the P3T3 method, then this should only give very small errors. Therefore this simplification has been made in the reported studies.

In the P3T3 method the $EINO_x$ figures $\boldsymbol{EINO}_{x_{GL}}$ (g/kg) from the four ICAO LTO-cycle points are plotted against the combustor inlet temperatures $\boldsymbol{T}_{\mathbf{31}_{GL}}$ (K) from

the performance model and a second order polynomial curve fit is obtained. Combustor inlet pressure $\boldsymbol{P_{3_{GL}}}$ and the overall fuel/air ratio FAR_{GL} are then plotted against $\boldsymbol{T_{31_{GL}}}$. Further second order polynomial curve fits are obtained. To obtain the NO_x emission index for an altitude condition: $\boldsymbol{EINO_{x_{GL}}}$ is calculated first, using the altitude temperature T_{31}. This figure is then corrected for the pressure $\boldsymbol{P_{31_{ALT}}}$ and fuel/air ratio FAR_{ALT}, and for humidity, using Equation 15 and the humidity correction factor H from Equation 14 as described in [109]. The overall P3T3 methodology for altitude NOx prediction is shown in Figure 21 [83].

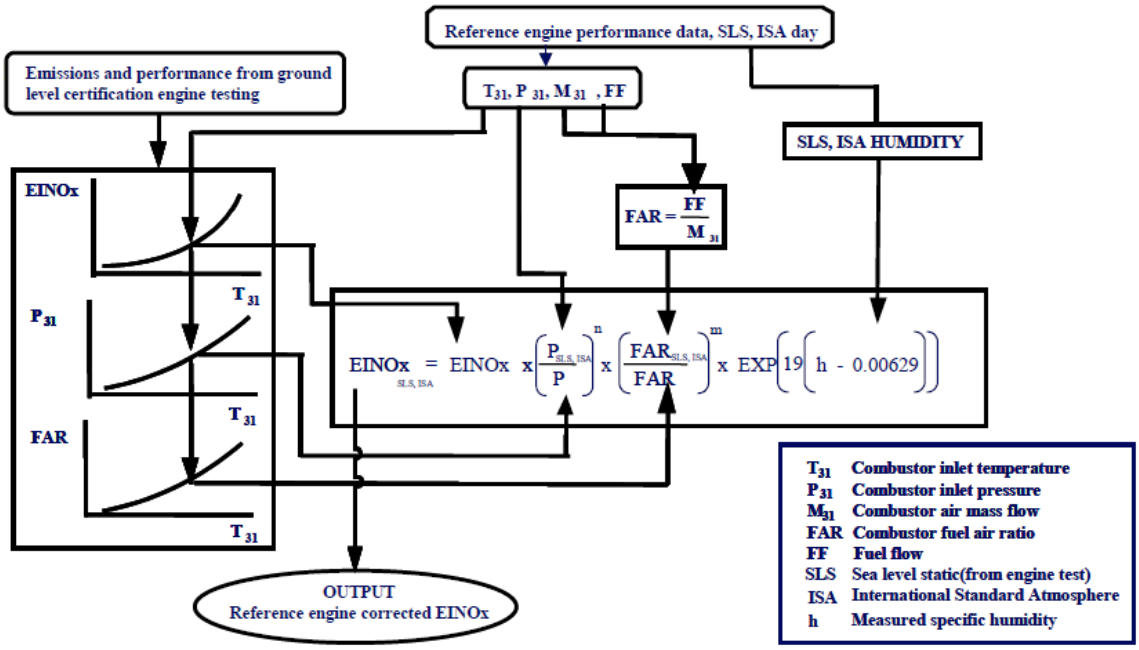

Figure 21 – NOx Emissions Correction Scheme from ICAO Annex 16 Volume II

$$EINO_{x_{ALT}} = EINO_{x_{GL}} \, (P_{ALT}/P_{GL})^n \, (FAR_{ALT}/FAR_{GL})^m \, e^H \qquad \text{Equation 15}$$

Whereas 'NOx formation theory' is supposed to give the pressure exponent n the value of 0.5, a range of experimentally determined pressure exponents empirically derived from rig and engine tests are tabulated in [83].

Madden and Park [84] and Pervier [109] suggest the exponent *n* be taken as 0.4 if no engine-specific value has been determined, and also that the exponent *m* be set to zero (so the FAR term in Equation 15 could be omitted). These practices have been followed in the current studies.

Even without the humidity correction, the P3T3 method is inappropriate for application to pollutant species other than NOx, as each species should have its own pressure dependency.

3.8.6 Direct Correlations for NOx Emissions

To estimate NOx emissions for new combustors from first principles, without reference to the ICAO engine emissions database, correlations based on multiple engine or rig test results can be constructed with reference to simple combustor design and engine performance parameters.

Numerous correlations for conventional combustors are found in the literature. For example, as quoted in [86], Lefebvre has provided Equation 16 for historic NOx emissions from conventional gas turbine combustors.

$$EINO_x = 9 \times 10^{-8} P^{1.25} V_C e^{0.01T_{st}} / \dot{m}_A T_{pz} \qquad \text{Equation 16}$$

In this case $EINO_x$ is in g/kg of fuel, V_C is the combustor volume (m^3), *P* is the combustor pressure (Pa), $\dot{m}_A$ is the air mass flow (kg/s) and T_{st} and T_{pz} are the stoichiometric and primary zone temperatures, respectively (K). For a given pressure and temperature, the ratio $V_C/\dot{m}_A$ is proportional to residence time.

Odgers and Kretschmer [121] list ten possible correlations for NOx emissions. They proposed Equation 17 after considering the nine previously proposed formulations, and they derived the constants from 59 experimental points, though some potential inputs were selectively discarded. This equation uses the combustion temperature T_c (K) and the NOx formation time τ (s) together with the pressure *P* (Pa).

$$EINO_x = 29e^{(-21670/T_c)} P^{0.66} \times (1 - e^{(-250\tau)}) \qquad \text{Equation 17}$$

For diffusion flames T_c is taken to be 'the maximum equilibrium temperature possible corresponding to the inlet conditions', which may generally be taken to be equivalent to the stoichiometric combustion temperature. However, for lean premixed combustors T_c is taken to be 'the dissociated flame temperature corresponding to the equivalence ratio and the inlet conditions'. As the residence time increases, the emission index should approach the equilibrium value according to the $(1 - e^{(-250\tau)})$ term, but it does not seem that equilibrium values were used to derive the constants in the remainder of the equation. The term $(1 - e^{(-250\tau)})$ implies a reaction-rate towards equilibrium that would only be valid for particular combinations of pressure and temperature.

Determining the NOx formation time τ also presents difficulties. Factors to be considered include the time-delay in vaporising the liquid-fuel droplets and in mixing the fuel vapour with the air. In a RQL combustor, where all the fuel is injected into a rich primary zone, the initial fuel-rich combustion does not generate NOx at the highest rate. That occurs during the short period of time while the fuel-rich gas mixes with the dilution air and completes its combustion while close to the stoichiometric temperature. The formation time is not the total residence time in such combustors and neither time is a constant for a given design, since hotter gasses will pass through the combustor more quickly.

Odgers and Kretschmer suggest that a typical NOx formation time for a combustor with so-called airblast or air-spray atomisers is 0.8 ms. For short formation times, the thermal NOx generated in accordance with Equation 17 is roughly proportional to the formation time, and a time of 0.8 ms implies that only 18.1% of the equilibrium level of NOx is formed, as shown in Figure 22. However, in lean-burn combustors the effective NOx formation times might be up to 10 ms.

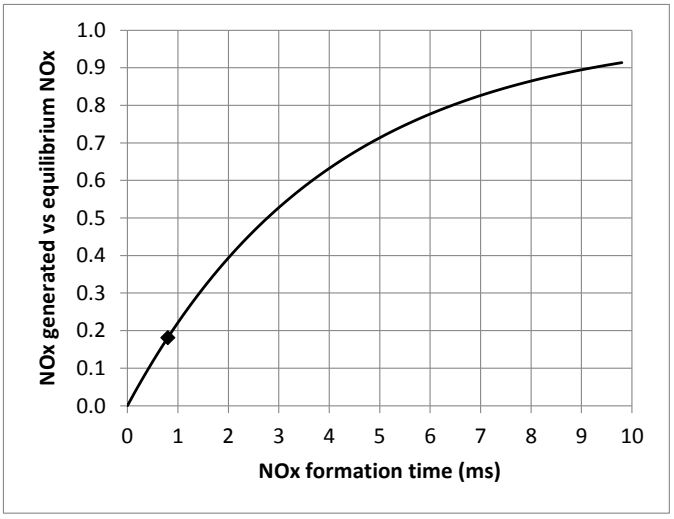

Figure 22 – Proportion of Equilibrium NOx generated using Equation 17

Equation 18, from Rizk and Mongia [122], takes fuel evaporation into account. It also includes the stoichiometric combustion temperature T_{st} (K), pressure P (Pa), pressure loss ΔP (Pa) and the residence time t_r (s) less the droplet evaporation time t_e (s).

$$EINO_x = 15 \times 10^{14} \, (t_r - t_e)^{0.5} \, e^{\left(-\frac{71100}{T_{st}}\right)} \, P^{-0.05} \, (\Delta P/P)^{0.5} \qquad \text{Equation 18}$$

However, the fuel droplet evaporation times are not known for the study engines, and use of the $\Delta P/P$ term implies that the equation is specific to a particular combustor geometry.

More recently, Kyprianidis, Nalianda and Dahlquist [123] have reviewed existing methods for the assessment of modern RQL combustor NOx emissions and proposed the new formulation in Equation 19 for existing and advanced RQL combustor designs for future engine cycles having high OPR and high HP TET.

$$EINO_x = \left(a + b \, e^{(c.T_3)}\right) \left(\frac{P_3}{P_{3,ref}}\right)^d \, e^{f\,(h_{SL} - h)} \, \left(\frac{\Delta T_c}{\Delta T_{c,ref}}\right)^{TF} \qquad \text{Equation 19}$$

For the modern RQL combustors, Kyprianidis et al. propose the constants and exponents in Table 18, based on in-house engine performance data and ICAO emissions databank data [82]. The inclusion of the humidity correction term in

Equation 19 is an improvement on earlier correlations. Humidity effects should definitely be taken into account for any on-route NOx emissions assessments. However, this correlation needs estimates of the primary zone temperatures at each operating point, and some other parameters that are not provided by simple engine performance models and would require more detailed combustor design studies. Nevertheless, the equation might have been used (together with appropriate additional assumptions) to estimate NOx emissions for year-2000 baseline engines. Rather than making such assumptions, the P3T3 calculation method of section 3.8.5, was considered preferable for year-2000 in-service engines, since representative ICAO-database figures were available.

Table 18 – Proposed Constants and Exponents in Equation 19 Equation 17 for modern RQL combustors, adapted from [123]

Parameter	Units	Proposed Value
a	–	8.4
b	–	0.0209
c	–	0.0082
d	–	0.4
f	–	19
TF (Technology Factor)	–	0
$P_{3,ref}$	Pa	3000000
$\Delta T_{c,ref}$	K	300
h	kg H_2O / kg dry air	0.006344

LDI technology that provides pilot injector zones and lean modules, fuel staging and airspray fuel-atomisation, seems the most promising approach for the combustors for year-2050 Brayton-cycle engines, assuming they will still run on kerosene or ‘drop-in’ replacement fuel. The above correlations are inappropriate for these future combustion systems, so emissions assessment methods more specific to lean combustors were used, as described in the following section.

3.8.7 NASA Correlations for Lean Combustors

In a NASA study reported in 1978, Roffe and Venkataramani [124] produced a simple correlation for lean premixed combustion based on flametube experiments with propane. Reformatted as Equation 20, the correlation is based on the flame temperature T (K) and the residence time τ (ms).

$$EINO_x = \tau . e^{(2.8T^{0.5} - 0.0263T - 72.28)} \qquad \text{Equation 20}$$

This equation assumes $EINO_x$ is proportional to τ (at least up to 2 ms) and independent of pressure (in the range 5–30 atmospheres) as indicated by the experimental results. It has the merit of simplicity, but seems inappropriate for use in aero engines, not least because propane has higher hydrogen to carbon ratio than kerosene.

A further correlation for advanced combustor NOx emissions from the NASA Advanced Subsonic Technology Project (AST) was attributed to S. Jones at NASA by Antoine and Kroo [125], but the same correlation was previously attributed by Lukachko and Waitz [126] to Bill Haller at NASA and the NASA-Industry Advanced Subsonic Engine (ASE) study. It was one of several correlations used by Alexiou et al. in the NEWAC project [127] and has been described as applicable to dual-annular staged combustors. Nevertheless it has also been applied to studies of lean premixed prevaporized (LPP) combustors. It is reproduced here as Equation 21 with the units converted so that the compressor delivery temperature T_3 and combustor exit temperature T_4 are K and the pressure P_3 is kPa.

$$EINO_x = 0.007549 T_4 \, (P_3 / 3027)^{0.37} \, e^{(1.8T_3 - 1471)/345} \qquad \text{Equation 21}$$

3.8.8 Recommended Correlation for Year-2050 LDI Combustors

Equation 21 is now also recommended for future LDI designs having staged combustion, including those for the year-2050 ULTIMATE reference engines. Its use was demonstrated in ULTIMATE deliverable D2.5 [128] and it is recommended by the author as the preferred option for all year-2050 study

engines that are without topping cycle combustors. The decision to use Equation 21 in these studies was only taken after an extensive review of alternative correlations including more-recent ones developed at NASA for specific LDI combustor configurations and some potential new correlations that would take more account of the underlying physics and chemistry. Appendix B reviews the alternative correlations considered.

It might seem that some more-recent correlations for LDI designs with staged combustion should be preferred, but they all presented difficulties because they were either very specific to particular designs or to narrow ranges of test conditions. Equation 21 remains more generic and straightforward to apply.

However, because Equation 21 provides a continuous function, it cannot be expected to be very accurate where fuel staging switches different injector nozzles on and off. It may also tend to underestimate NOx emissions at idle, where only the pilot nozzles are operating, though combustor operations at idle make relatively little contribution to overall NOx emissions.

The results presented in section 8.6 were obtained using Equation 21, which was recommended by the author for use by other ULTIMATE project partners.

An extended review and assessment of potential alternative NOx emissions correlations is provided in Appendix B, based on the work reported in [108].

.

4 INITIAL CONCEPT SELECTION

In this chapter a rationale is established for qualitatively selecting combinations of advanced core-engine technologies with potential to help meet ACARE 'Flightpath 2050' targets for CO_2, noise and emissions [4]. The systematic assessment and down-selection of a preferred cycle is then described. This part of the author's study was originally reported at ISABE in 2017 in [77].

By 2050 new short-range commercial aircraft may use open-rotor engines with contra-rotating propellers, but longer-range aircraft, cruising slightly faster, are more likely to be powered by high bypass ratio geared turbofan engines [2]. For improved fan and propulsive efficiencies these engines could have variable-pitch fan blades or variable-area exhaust nozzles. However, these engines will not meet the industry's ambitious mid-century fuel-burn targets without also making improvements to core thermal efficiency. This requires fundamental changes to the engine cycle, because further increases to OPR and TET applied to the currently used open-circuit Brayton performance cycle can only give diminishing returns. Combustor entry and exit temperatures will also need to be restricted to limit NOx emissions.

Technology combinations are considered for both long-range and short-range aircraft applications, but long-range aircraft have more to gain from performance improvements because fuel constitutes a larger proportion of their take-off weight. Synergies between novel technologies can increase thermal efficiency and reduce fuel burn. Particular technologies considered include intercooling, recuperation, inter-turbine or other secondary combustion, and topping and bottoming cycles.

For short-range aircraft a larger proportion of the performance improvement may come from reduced cruise speeds and open rotors improving propulsive efficiency. But in terms of meeting the ACARE SRIA targets, the short-range aircraft also benefits from the relatively lower thermal efficiencies of the baseline engines in service in year-2000 and against which they are benchmarked.

4.1 Selection of Advanced Cycles for More Detailed Study

Here a qualitative assessment of different technology combinations is made, leading to the down-selection of a preferred cycle and engine architecture. This study was made in parallel with the study assessing scaled and intercooled engines, as reported in [97] and in section 7.3. Preliminary results from Excel models for those performance cycles and some alternative cycles, combined with results from ULTIMATE project partners at BHL, highlighted the potential of combining topping cycles with both intercooling and secondary combustion. Intercooling and secondary combustion are beneficial in increasing core specific power by enabling a higher fuel air ratio by the exit of the second combustor, while avoiding the very high flame temperatures that would produce excessive NOx emissions. Minimising the core mass flow reduces the losses associated with core compression and expansion, and minimises the cost and weight of core components.

Novel core components potentially include heat exchangers for intercooling and recuperation, and for cooled cooling air to permit higher compressor delivery temperatures. However, secondary combustion tends to result in higher turbine exhaust temperatures. Use of this still relatively high-grade exhaust heat can then be made in a recuperator or in a bottoming cycle, but it is not easy to combine recuperation with the pressure-rise combustion in a topping cycle, hence the interest in integrating a bottoming cycle with the topping cycle, intercooling and secondary combustion technologies.

4.2 Candidate Engine Technologies

The advanced technologies studied and their individual potential benefits are discussed in the following sub-sections.

4.2.1 Turbofan Engine Architecture

The overall engine layout for the year-2050 reference turbofan is similar to the Rolls-Royce UltraFan® engine concept shown in Figure 23 [40].

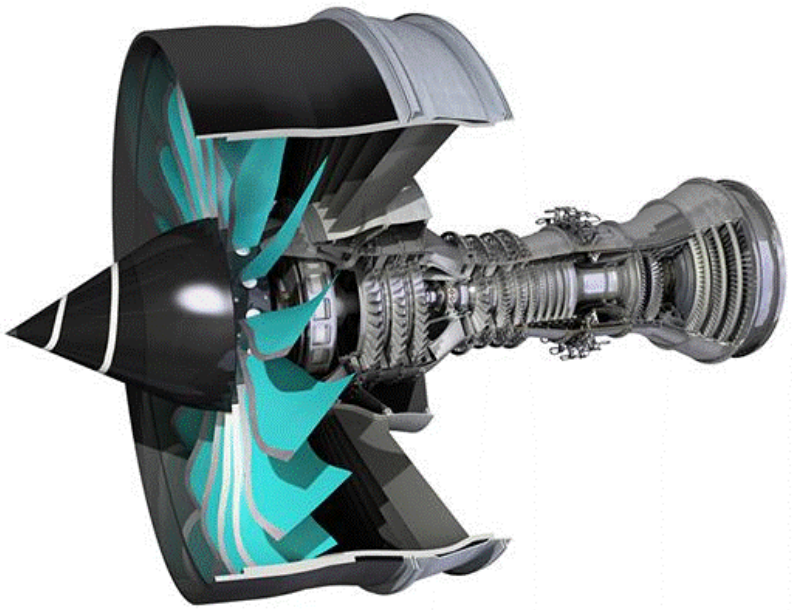

Figure 23 – Rolls-Royce Variable-pitch-geared-fan UltraFan® Engine

The HP compressor is driven by a two-stage HP turbine and a second high-speed turbine drives the IP compressor directly and also drives the fan via a reduction gearbox. The IP and HP compressors have variable inlet guide vanes. The variable-pitch fan illustrated, or alternatively a variable-area exhaust nozzle, would improve operability and allow further design trade-offs to improve fan efficiency or to improve propulsive efficiency. However, neither technology may be essential, particularly if higher levels of specific thrust and fan pressure ratio would be accepted. Thus the merits of alternative core-engine cycles might be assessed without modelling variable-area nozzles or variable-pitch fans.

However, very different engine architectures could be preferred for the more advanced turbofan engine designs that feature combinations of intercooling, recuperation, topping and bottoming cycles etc. The geared single-rotation front fan and the high-speed IP compressor, or booster, are likely to be retained, but the other components may be rearranged. Reverse-flow-core arrangements, similar to the ATF3-6 turbofan [129], were investigated for an intercooled engine in LEMCOTEC [38], [39]. One such arrangement can be seen in Figure 7.

By placing the fan, IP compressor and turbines in front of the HP compressor, the HP system no longer had other shafts passing through it and was better isolated from thrust loads that cause casing distortions. The HP compressor efficiency was improved and the optimum OPR was increased, though in the LEMCOTEC study the final SFC and fuel-burn improvements relative to a more conventional geared-fan intercooled engine arrangement were assessed to be relatively small [18].

4.2.2 Intercooling

Previous studies had shown that intercooling could improve large turbofan engine cruise SFC by around 3% in higher-OPR engines, though in smaller engines the benefit would be somewhat less [28] [97] [40]. Intercooling has been discussed in section 2.3 and the original intercooled engine concept from NEWAC has been shown in Figure 5.

High-OPR intercooled engines are particularly sensitive to the loss of core component efficiency due to the relatively small size of their turbomachinery.

An investigation of the sensitivity of engine performance to HP compressor and HP turbine scale effects is reported in section 7.3, which describes the modelling of a reference high bypass ratio turbofan engine with a conventional cycle and component technology levels projected to year 2050. The reference-engine year-2050 technologies include improved materials and cooled cooling air (CCA) for cooling the HP turbine. The study considers the effects of scaling-down the engine's thrust requirements and/or adding an intercooler between the all-axial HP and IP compressors. Key performance parameters for the initial reference engine and the intercooled variant with the best SFC are listed in Table 19. Thrust levels are the same as those specified for the study engines in the EU Framework 6 NEWAC programme [29]. The full-scale engines provide 260 kW of aircraft accessory power at all conditions, but no customer bleed air. Take-off performance is quoted for a hot-day end-of-runway case, so the static thrust would be higher. Refer to section 8.4 for fuel burn assessments of several different advanced-cycle engines including a higher OPR intercooled engine.

As both engines in Table 19 have the same specific thrust, the SFC differences reflect changes in the core thermal and transfer efficiencies, rather than changes in propulsive efficiency.

Table 19 – Performance of the Original Reference and Intercooled Engines

Parameter	Brayton Cycle	Intercooled Cycle
Take-off at sea level, 0.25 M, ISA+15 K		
Net thrust (kN)	253	253
TET (K)	1950	1950
Mid-cruise at 10,668 m, 0.82 M, ISA		
Thrust (kN)	49	49
Specific thrust (m/s)	72	72
Fan pressure ratio	1.33	1.33
OPR	64.4	91.9
Bypass ratio	20.7	27.6
SFC (mg/N.s)	12.88	12.51
Relative SFC	datum	-2.9%
Max climb at 10,668 m, 0.82 M, ISA+10 K		
Net thrust (kN)	67	67
OPR	75	120
SFC (mg/N.s)	13.91	13.38
Relative SFC	datum	-3.8%

4.2.3 Recuperation

In a recuperated gas turbine, heat is extracted from the core exhaust and used to preheat the air entering the combustor. Previous recuperated engine concepts have been described in section 2.3 and Figure 6 showed the IRA concept from the NEWAC programme [29].

Rather than taking heat from LP turbine exit, the overall cycle efficiency could be improved by extracting more heat from an earlier inter-turbine location. This would enable an increase in the combustor inlet temperature, reducing the required fuel flow for a given recuperator effectiveness. However, moving the

recuperator too-far upstream is counter-productive because it reduces the power generated by the downstream turbine stages. Another option with similar effect would be to boost the inlet temperature to the recuperator by adding inter-turbine reheat. Either option would tend to increase NOx emissions and is likely to make the LPP combustor design more problematic because higher inlet temperatures make auto-ignition and flash-back more likely. A different type of lean combustor might need to be adopted.

The original IRA design for the CLEAN programme, and later for NEWAC and LEMCOTEC, particularly targeted reducing 'Landing and Take-Off' (LTO) cycle NOx emissions. These engines claimed 9–13% cruise SFC improvements relative to conventional-cycle reference engines [8]. Even though the actual benefit strongly depends on the technology level of the reference engines assumed, ongoing studies indicated that, relative to projected year 2050 conventional cycle reference engines, significant improvements were still achievable by incorporating more advanced recuperation systems [7].

4.2.4 Secondary Combustion

A second combustor can be an inter-turbine combustor, or in a compound-cycle engine it can be a combustor positioned between the topping-cycle core machinery and the downstream turbines. Preferably these combustors would be of the 'flameless' variety, made possible by the high inlet temperature. Unlike the primary combustors, the secondary combustors would not need to be capable of altitude relight, since they would only be fuelled at high-power conditions. Secondary combustors for aero engines were researched in the project AHEAD (Advanced Hybrid Engines for Aircraft Development) by Technion [75]. Section 6.2.2 gives details of secondary combustor studies.

In a simple-cycle gas turbine it is theoretically more efficient to maximize the HP turbine entry temperature by burning all the fuel in a primary combustor, rather than diverting some of the fuel to a secondary combustor, but in practice there is a limit to the TET that can be used because of the temperature capabilities of the materials, turbine cooling requirements and the increased NOx generation

at high combustor temperatures. In a high OPR engine it can therefore be beneficial to have a second combustor to reheat the core flow after some initial expansion in the first one or two turbine stages. Thermodynamic efficiency can be improved by raising the mean temperature of heat addition and by increasing the core specific power so that the losses in compression and expansion only apply to a smaller core mass flow. To compensate for the reduced core mass flow, the LP turbine may need a higher pressure ratio and an extra stage, but with a high-speed LP turbine and a geared fan, the smaller core mass flow should still tend to reduce overall engine weight.

Adjusting the fuel-flow-split between primary and secondary combustors provides an additional off-design variable-cycle capability with a potential benefit from reducing the secondary combustor fuel flow preferentially at part-power conditions. The engine would then run with higher OPR and primary combustor fuel/air ratio. However, this will only improve SFC if high component efficiencies are maintained when the cycle rematches.

SFC improvements from secondary combustion alone may be modest, but the potential weight reduction could make a significant contribution to reducing fuel burn. However, since secondary combustion tends to raise TEGT, it is expected to confer greater SFC benefits to recuperated engines and engines with bottoming cycles.

4.2.5 Variable Geometry

Low specific thrust engines with low fan pressure ratios have un-choked bypass exhaust nozzles at take-off. This means fan mass flow is relatively reduced at low flight Mach numbers, risking either fan surge or flutter during take-off, or compromising fan efficiency at cruise and top of climb. These problems can be avoided with a variable-area cold-flow exhaust nozzle, or by having variable-pitch fan rotor-blades. For the low specific thrust turbofan engines originally anticipated for 2050, one or possibly both of these solutions is likely to be needed. The variable-pitch fan also holds out the prospect of providing reverse thrust without a conventional thrust reverser, though an auxiliary intake may be

needed to provide reliable thrust-reversal at higher forward speeds. Avoiding the extra weight and extra nacelle drag associated with conventional thrust reversers means that optimised engine designs can benefit from lower specific thrust and higher propulsive efficiency.

In this study it has been assumed that the year-2050 turbofan could have a variable-pitch geared fan with the capability to provide reverse thrust if needed. The IP and HP compressors would also have Variable Inlet Guide Vanes (VIGV). Having variable-pitch fan blades and/or IP compressor VIGVs enables the fan bypass-section pressure ratio and mass flow, as well as the fan root-section and IP-compressor pressure ratios and mass flows, to be varied relative to their rotational speeds. Because the geared fan and IP compressor are driven in a fixed-speed relationship by the same turbine, this means the work-split between the fan bypass section and the fan root and IP compressor can be varied by actuating these variables. This capability can be used to optimize the engine's off-design performance.

Part of the benefit from intercooling, or from intercooling and recuperation, also comes from creating variable-cycle engines. In intercooled engines, maximizing intercooling at take-off reduces combustor and turbine temperatures and enables reduced core size and lower NOx emissions. At climb and cruise conditions the amount of cooling air for the intercooler can be reduced, raising core cycle temperatures to improve thermal efficiency while also reducing pressure losses on the cold side of the heat exchanger. It may also be possible to reduce hot-side pressure losses at cruise conditions by allowing part of the core flow to bypass the intercooler, as proposed in [130], though no benefit has been claimed for this in the author's performance modelling.

The intercoolers and CCA heat exchangers use bypass duct air for cooling with the spent cooling air flows either mixed back into the main bypass duct, or ejected through separate exhaust nozzles to generate thrust directly. The amount of cooling in these heat exchangers is controlled by varying the cold-side air flows by means of variable-area mixers or variable-area exhaust

nozzles. In principle, mixing these heated air flows back into the bypass stream should be the more efficient option, thanks to the 'mixing gain' effect, but in practice it makes little difference because the temperature of the spent cooling air is not very much higher than that of the bypass stream air. For simplicity in performance modelling, it has been assumed that the spent cooling air flows are ejected through separate variable-area exhaust nozzles.

Variable-area nozzles might also be added to the core and main bypass exhaust systems to improve jet-velocity matching and fan bypass-section efficiency and operability, as discussed in [97] and [40]. However, if the fan already has variable-pitch, then having variable-area exhaust nozzles as well should be unnecessary from the operability point of view, unless extremely-low fan pressure ratios would be adopted, which was not the case in these studies.

There is also the option of adding a variable-area turbine inlet Nozzle Guide Vane (NGV) to vary the expansion ratios of the upstream and immediately downstream turbine stages. Engines using recuperation, including the IRA design and the in-service WR21 marine gas turbine, use variable-capacity LP turbines to rematch the engine cycles off-design [31]. At lower-power conditions, such as at cruise, partially-closing the LP turbine NGV will reduce core mass flow and OPR, while increasing TET and TEGT. This results in more heat being transferred to the combustor inlet via the recuperator, reducing the fuel demand and significantly improving part-power SFC.

A variable-area IP turbine was investigated in the ANTLE research programme, as an alternative means of controlling the off-design IP compressor working line [131], but the high pressure and temperature environment of the IP turbine NGV made this a much more challenging mechanical design than a variable-area LP turbine. Variable-cycle capability introduces extra degrees of freedom in the optimisation of engine performance and can improve operability, so this needs to be considered when comparing different advanced engine-cycle options.

4.2.6 Topping Cycles

The term ‘topping cycle’ can be taken to mean several different things. For example: it can mean the gas turbine in a combined-cycle powerplant where the gas turbine exhaust passes through a heat recovery steam generator (HRSG) to power a steam turbine (or other bottoming cycle). It has also been applied to the solid oxide fuel cell (SOFC) in a hybrid SOFC/gas turbine power generation system. In this study the topping cycle is taken to refer to the part of the overall engine cycle coming after the last turbo-compressor’s diffuser and before the first turbine stage, but only if the intervening components raise the maximum cycle pressure and/or generate shaft power. A conventional gas turbine core’s ‘constant pressure’ combustion system does not qualify as a topping cycle.

The simpler topping cycles provide pressure-rise combustion without additional shaft power output. They can for example use valve-less resonant pressure-rise combustors [47], pulse-detonation combustors with inlet valves [65], ‘wave rotors’ with rotary inlet and outlet valves [49] or ‘free-piston’ engines [17] [58]. Combustion is intermittent in these designs, but there is also the possibility of developing a rotating detonation wave combustor, where a detonation wave runs continuously around an annular combustion chamber [132]. Even though combustion would be continuous, the exiting flow would still be highly unsteady, but with perturbations generated at frequencies an order of magnitude higher than typical of intermittent-pulse-detonation combustors.

Alternatively, the positive displacement topping cycles could involve more complex machinery to generate additional mechanical or electrical power. The power could be used to help drive the main propulsor, or to drive aircraft accessories, or to power a core compressor such as an IP turbo-compressor or an additional piston compressor. These are not new concepts, as several highly efficient turbo-compound aero engines were developed in the mid-20th century, though only the Wright R-3350 Duplex Cyclone turbo-compound went into airline service [133]. In that turbo-compound engine most of the power for the propeller came from the topping-cycle piston-engine, but it was supplemented

by power from turbines driven by the exhaust gasses. In the Napier E.145 Nomad II engine, a larger proportion of the power came from the gas turbine [23]. Some more recent proposals for turbo-compound engines have preferred to generate most of the propulsor's power from the turbomachinery, rather than the topping cycle, as this is expected to improve the power/weight ratio. Whurr, for example, proposed replacing the HP spool of a three-shaft turbofan with a large high-speed Wankel engine [50] that would just have driven the supercharging IP compressor, while the fan would have been driven by the turbine. Topping cycles using more conventional piston engines have been investigated in LEMCOTEC [44] and in ULTIMATE [58]. Like the Napier E.125 Nomad I [23] these engine cycles also include secondary combustion upstream of the turbines. Different levels of power output from the piston engine core were considered and in studies at BHL a preferred configuration was found to have a piston engine driving additional piston compressors in order to further supercharge the core flow following an IP compressor [44].

Various mechanical arrangements are possible for power generating topping cycles, apart from conventional piston engines, free-piston engines and the Wankel rotary engine. Nutating disc designs appeared to offer advantages [5] and so have been studied in some detail, as described in Chapter 5. They are very compact and their inlet and outlet flows are more continuous than those of most other machines, potentially providing easier integration with turbo-machinery. On the other hand they present significant design challenges, not least requiring complex rotor sealing arrangements, akin to those that have plagued development of Wankel engines and limited their applicability. The author's conclusions regarding alternative topping-cycle machinery options are given in section 10.3.

4.2.7 Bottoming Cycles

Unlike the topping cycles described above, a bottoming cycle uses a working fluid that is separate from the main core engine fluid flow. The bottoming cycle normally takes all of its heat input from the main cycle's core exhaust. For

energy applications the most common working fluid is water, as in the Rankine-cycle steam turbines normally incorporated into combined-cycle powerplants. Potential alternative working fluids include ammonia, carbon dioxide and organic compounds. Kalina cycles are claimed to be more efficient, particularly for modest temperature ratios, but they are also more complex, using two fluids, typically water and ammonia [134]. Another possibility would be to use a Stirling cycle, but none of these options is likely to provide a power/weight ratio that would make it attractive for an aero engine application.

Bottoming cycles are generally closed-circuit, but where air is the working fluid, an open-circuit cycle can be used instead. Air behaves like an ideal gas, so adiabatic compression results in a significant temperature rise and the compression process uses relatively large amounts of power. Conversely, the fluids used in closed-circuit systems are typically compressed close to or below their critical temperatures, where compression is more energy efficient and more nearly isothermal thanks to real gas properties. This means that closed-circuit cycles have the potential for higher thermal efficiency than open-circuit cycles using air.

For a closed-circuit bottoming cycle on an aero engine, supercritical carbon dioxide (S-CO_2) has been considered a preferred working fluid and its use has been studied in the ULTIMATE project [9]. S-CO_2 offers much more compact turbomachinery than steam, it has good thermal stability and it is not flammable. Keeping the CO_2 supercritical avoids potential problems with two-phase flow and minimises the size of the turbomachinery. On the other hand, closed-circuit systems need not only to extract heat from the main engine's core exhaust, but also to reject heat in an air-cooled pre-cooler or condenser ahead of the bottoming cycle compressor. A third heat exchanger, a recuperator internal to the S-CO_2 closed-circuit, may also be used to pre-heat the compressed CO_2 ahead of the main heat exchanger, while cooling the reduced pressure CO_2 ahead of the pre-cooler. This closed-circuit recuperator (not to be confused with a recuperator in a recuperated engine cycle) might further improve the thermal efficiency of the stand-alone closed-circuit cycle. When added to a simple-cycle

gas turbine, the S-CO_2 bottoming cycle was predicted to improve fuel-burn by almost 2%, with the prospect of further improvements if combined with inter-turbine combustion and intercooling [9].

While the S-CO_2 system has lightweight turbomachinery, its pre-cooler is a large heat exchanger comparable to the intercooler in a high-OPR intercooled engine or an IRA. Like an intercooler, it imposes a pressure loss on the cooling air that passes through it. With these considerations in mind, an open-circuit air-cycle bottoming cycle has been considered a realistic alternative. A recent study of a turbofan including such a bottoming cycle, described as an 'Exhaust Heated Bleed Engine' (EHB), concluded that SFC might be improved by 3-8%, but the weight penalty and potential fuel-burn benefits were not assessed [10].

It is still not obvious which type of bottoming cycle should be preferred. The two variants might well provide similar fuel-burn benefits. For simplicity, the less-complex open-circuit bottoming cycle has been modelled in this study to assess the potential benefits from bottoming cycles. It is assumed that the air it uses would be bled-off from the main core flow at a suitable point in the compression system. By analogy with cycles employing recuperation, a further benefit is expected from locating the main heat exchanger between two turbine stages a little upstream of the core exhaust nozzle. The higher gas temperature there will improve the bottoming cycle thermal efficiency and the higher gas density enables a more compact heat exchanger. Splitting a regular LP turbine into two parts, either side of the heat exchanger, generally gives an unsatisfactory engine mechanical arrangement. However, the novel reverse-flow-core engine architecture proposed in Figure 2 may offer a design solution.

4.3 Qualitative Assessment of Potential Synergies

All the individual technologies discussed in section 4.2 above, taken in isolation, were assessed as likely to improve fuel burn, particularly in long-range aircraft. Even the relatively heavy option of recuperation alone might well improve fuel burn, given recent advances in heat exchanger technology.

Other potential technologies, such as using alternative fuels or water injection were ruled out-of-scope for this study. These technologies have considerable potential for application to engines by 2050, but they should not affect the basic cycle selection. The same argument applies to hybrid-electric and distributed-propulsion arrangements. While these technologies may also find applications on aircraft in the 2050 timeframe, they are not expected to influence selection of the top-level core-engine cycles and configurations. It is contended that the best cycles will be needed irrespective of propulsor arrangements in hybrid systems.

To investigate the potential benefits of combining multiple technologies into a single powerplant, a matrix was drawn up to identify all possible combinations of five core engine technologies. Including intercooling, recuperation, secondary combustion and a bottoming cycle provides 16 possible combinations. These options were then permed with conventional combustion, topping cycles that can deliver pressure-rise combustion, or topping cycles that provide extra power output. This provided 48 possible options as shown in Figure 24.

Based on anticipated synergies between the generic technologies, an initial qualitative down-selection of potential cycles was made from the 48 top-level technology combinations. The cycles selected as credible candidates to reduce SFC and fuel burn in long-range and short-range aircraft applications are indicated by green cells in Figure 24. Some good technology combinations, such as intercooling and recuperation, are well known. Others may be less obvious. The initial selection excluded technology combinations considered unlikely to offer an overall benefit relative to simpler combinations.

Figure 24 includes some brief notes on the logic behind selecting the different combinations of technologies, but further details are given below.

The first numbered option, cycle#01, gives a conventional Brayton cycle with no added technologies. It is applicable to turbofans like the reference turbofan in Table 19, but also to open rotor engines. (Note some cycle numbers are now out of sequence because the previous cycle notation in references [62] and [77] has been retained to avoid potential confusion.)

	Major cycle variants			Bottoming cycles		Remarks
	Primary Combustion	Inter-cooled	Second Combustor	None	Included	
No Recuperator	Constant pressure	No	No	Reference Cycle #01	Cycle #16	High TEGT with second combustor
			Yes		Cycle #17	will benefit bottoming cycles
		Yes	No	Cycle #02		Intercooling reduces TEGT unless
			Yes	Cycle #18	Cycle #03	a second combustor is added
	Pressure-rise combustion	No	No			Pressure rise is beneficial, but
			Yes			NOx limits peak temperatures
		Yes	No	Cycle #04		Intercooling reduces TEGT unless
			Yes			a second combustor is added
	Pressure-rise topping cycle with power offtake	No	No			Topping cycles generating power
			Yes		Cycle #14	can raise peak temperatures and
		Yes	No	Cycle #19	Cycle #15	OPR at a limiting TEGT, raising
			Yes	Cycle #05	Cycle #06	overall thermal efficiency
Recuperated cycles	Constant pressure	No	No			Some benefits, but recuperation
			Yes			is better still with intercooling
		Yes	No	Cycle #07		High TEGT with second combustor
			Yes	Cycle #08	Cycle #09	will benefit bottoming cycles
	Pressure-rise combustion	No	No			Some benefits, but recuperation
			Yes			is better still with intercooling
		Yes	No	Cycle #10		High TEGT with second combustor
			Yes	Cycle #11	Cycle #12	will benefit bottoming cycles
	Pressure rise topping cycle with power offtake	No	No			Recuperation reduces pressure
			Yes			rise in topping cycles, so it is only
		Yes	No			attractive if applied to a core flow
			Yes		Cycle #13	bypassing the topping cycle

	Potential for significant improvement		Little or no advantage re. simpler or reference cycles

Figure 24 – Qualitative Assessment of Potential Synergies between various advanced cycle technologies

The cycles numbered #02 to #12 were identified in [77] as being of particular interest. Cycle#13 was the most-complex, combining five different advanced technologies. It was not originally considered by the author to be an attractive option, but Herman Klingels noted that the core flow could be split, with part passing through a topping cycle and part going through a recuperator to the secondary combustor [17]. Therefore this combination is also of interest.

Cycle numbers #14 to #19 have been added to Figure 24 since [77]. Cycle#14 and cycle#15 are simpler alternatives to cycle#06. Cycle#16 and cycle#17 are simpler alternatives to cycle#03 as investigated by Florian Jacob. Cycle#18 was an intermediate step to modelling cycle#03, and cycle#19 was a simpler alternative to cycle#05 studied by Joshua Sebastiampillai [62]. (Subsequently it was shown that cycle#18 offered no benefits over the simpler cycle#02.)

Each of the top-level technologies in Figure 24 could be delivered in several different ways, so in principle a much larger matrix of design options could be constructed. Each of the individual technologies alone was considered likely to improve SFC and fuel burn, particularly in long-range aircraft. Even the relatively-heavy option of recuperation alone might improve fuel burn in a large engine, given advances in heat exchanger technology expected by 2050.

Cycle#02 is a high-OPR intercooled engine. Intercooling is generally synergistic with other technologies, but the combination with a bottoming cycle is a poor one, because a high OPR intercooled engine has relatively low TEGT, severely limiting the potential efficiency of any bottoming cycle. However, if an inter-turbine combustor is also added, then the TEGT would be increased and the bottoming cycle should give a useful benefit. This combination, cycle#03, was researched by Florian Jacob in ULTIMATE with the S-CO_2 bottoming cycle option [9]. Increasing the TEGT gave scope for a more efficient bottoming cycle, but made the main cycle less efficient, so an overall cycle assessment was necessary to quantify the benefit.

The combination of intercooling with pressure-rise combustion also displays synergy because it enables a significant combustor pressure rise to be obtained even with a high pressure ratio in the upstream turbomachinery. By varying the amount of intercooling and/or aftercooling, the combustor inlet temperature and kinetics can be held fairly constant over a wide range of off-design conditions.

Another study in ULTIMATE has considered combining pulse detonation with intercooling and aftercooling [65]. This concept uses cycle#04 in Figure 24. SFC improvements of around 8% seem achievable relative to a reference 2050 high-bypass ratio geared turbofan engine. These results confirmed the increase in core specific power and the potential to reduce turbomachinery weight, which could compensate for the weight penalties of a heavier combustion system. It was concluded that using aftercooling in cruise gave SFC penalties that would outweigh any possible benefit from a further increase in combustor pressure rise, but aftercooling could still be beneficial during higher-power operation, in

order to reduce HP compressor delivery temperature to decrease the risk of pre-ignition and reduce NOx emissions.

More ambitious topping cycles combine well with intercooling and also with secondary combustion to enable boosted power for take-off and climb without generating excessive NOx emissions. This three-way combination is cycle#05 on Figure 24, and adding a bottoming cycle as well gives cycle#06. Both these cycles have been investigated in ULTIMATE. The former was studied by Joshua Sebastiampillai for an open rotor powerplant [62] [14] and the latter has been studied by the author for a turbofan engine, as described in section 7.5.2.

Combining recuperation with intercooling, as in the IRA, gives cycle#07 and adding inter-turbine combustion gives cycle#08. A bottoming-cycle main heat exchanger would be competing with the recuperator for the engine core's exhaust heat, so it probably only makes sense to add a bottoming cycle to a recuperated engine if that engine also has an inter-turbine combustor to raise its TEGT. This gives cycle#09. In this last case the two heat exchangers could be placed in series after the turbines, with the recuperator the first in line.

An intercooled and recuperated engine could have a pressure-rise combustion system giving cycle#10, but a more complex power-generating topping cycle seems unlikely to be beneficial in this case. This is because these cycles will generally want lower topping-cycle inlet temperatures to permit higher pressure ratios, ease cooling and help to limit NOx production. As in the previous examples, the options of adding an inter-turbine combustor after the pressure-rise primary combustor, or of adding a bottoming cycle, could be attractive. These options give cycle#11 and cycle#12 respectively.

These preliminary qualitative assessments assumed that the added intercooler, recuperator, topping cycle and/or secondary combustor would act in series on the same core mass flow. However, there might also be merit in a split cycle where the core flow is divided-up so that different combinations of technologies can be applied to parallel core streams. For example, some core flow might bypass the topping cycle and be heated by a recuperator before being added to

a secondary combustor as proposed by Klingels [17]. In this way there might be a case for combining all five different technologies, as in cycle #13, but such added complexity was considered beyond the scope of the current studies.

4.4 Further Engine Cycle Down-selection

Initial studies exploring the potential benefits of intercooling and of combining multiple technologies in one powerplant were reported in ULTIMATE deliverable D1.3 [67]. Details of the studies were subsequently disseminated in [40] [77] and [97]. The initial studies provided the rationale for down-selecting engine cycles and architectures to be studied in more detail.

A major objective was to integrate a topping cycle with the gas-turbine in order to attack the 'combustor' losses in a regular Brayton-cycle gas turbine. Current combustion chambers have a total pressure drop that contributes to combustor losses and reduces thermal efficiency, but the entropy generation within the combustor is even worse, because the potential for the heat addition to raise the gas pressure is not exploited. The solution is to introduce technologies that provide a pressure rise during constant-volume combustion (the Otto cycle) or extract work during the combustion process at constant pressure (the Diesel cycle) or some combination of the two. Technology enablers for pressure-rise combustion include pulse detonation tubes, wave rotors with or without pulse detonation, various piston engine configurations and rotary engines including the Wankel engine and nutating-disc engines. Each of these concepts has its pros and cons when implemented in a composite cycle engine.

The second major objective was to investigate the addition of a bottoming cycle to make better use of exhaust heat from the core engine. While a hot exhaust jet converts some of this available energy into additional thrust, this thermodynamic conversion process is relatively inefficient in low specific-thrust subsonic aero engines because of low total to static temperature ratios across the exhaust nozzles. In most cases a bottoming cycle makes better use of residual exhaust heat than a thrust nozzle.

There seemed little benefit in combining recuperation with topping or bottoming cycles, and because recuperation was being addressed in other ULTIMATE research projects, recuperation was deselected. This reduced the matrix of top-level cycle combinations to that shown in Figure 25.

	Major cycle variants			Bottoming cycles	
	Primary Combustion	Inter-cooled	Second Combustor	None	Included
No Recuperator	Constant pressure	No	No	Cycle #01 (reference cycle)	
			Yes		
		Yes	No		
			Yes		Cycle #03 (no topping cycle)
	Pressure-rise combustion	No	No		
			Yes		
		Yes	No		
			Yes		
	Pressure-rise topping cycle with power offtake	No	No		
			Yes		Cycle #14 (no intercooling)
		Yes	No		Cycle #15 (no second combustor)
			Yes	Cycle #05 (no bottoming cycle)	Cycle #06 (selected cycle)

Figure 25 – Variants on Cycle#06 to quantify Technology Benefits

The author chose to investigate in more detail a turbofan with an open-circuit bottoming cycle, a topping cycle, intercooling and secondary combustion. Such an engine having the cycle#06 combines all the major technologies except recuperation. The performance modelling of this turbofan is described in section 7.5, demonstrating its potential SFC benefit relative to the year 2050 reference turbofan, cycle#01. The cycle modelling was followed by multi-disciplinary assessment of the engines with design optimization and trade-studies for minimum fuel burn and emissions, as reported in Chapter 8.

To quantify the contribution of each of the four new technologies to the overall engine performance, it was proposed to model four further variants, each omitting one of the four down-selected technologies: the air-cycle bottoming cycle, the power-generating nutating-disc topping cycle, intercooling, or secondary combustion. The four variants on cycle#06 are noted on Figure 25. They are: cycle#03 omitting the topping cycle, cycle#05 omitting the bottoming cycle, cycle#14 omitting intercooling and cycle#15 omitting the secondary

combustion. However, in the time available to the author, of these four further cycles, only cycle#03 has been modelled.

4.5 Component Technology Down-Selection

A further activity was the selection of specific technologies for detail study. For example, various options existed regarding topping and bottoming cycles.

The only topping-cycle technology addressed by the author in any detail has been the nutating-disc arrangement. The double-disc nutating-disc engine is a fairly-recent pressure-rise combustion concept for the topping cycle, which it was thought might be competitive with more established topping-cycle technologies. Relative to conventional piston engines, the nutating disc-engine has several pros and cons, as investigated in Chapter 5. That assessment has highlighted challenges in the nutating-disc detail design, materials and bearings, particularly when developing the technology for the higher-OPR engines. Considering the severity of these challenges, it now seems likely that the development of alternative pressure-rise combustion systems would be more attractive alternatives. Nevertheless the performance cycles developed for use with nutating discs are also relevant to other pressure-rise-combustor designs with similar performance characteristics.

Bottoming cycles can be open-circuit or closed-circuit systems. It is not obvious which would be preferable for an aero engine application so both options were addressed at Cranfield in the ULTIMATE project. A closed-circuit arrangement offers very compact turbomachinery and higher thermal efficiency than an open-circuit cycle running on air. Air tends to make less-efficient bottoming cycles because it does not benefit from the reduced work required to compress a working fluid like CO_2 that is used closer to its critical point. However, an open-circuit air bottoming cycle (ABC) might have better power/weight and lower drag, because it avoids the need for a pre-cooler or condenser and the associated cost, weight and installation drag. The ABC may also be partially integrated with the main gas turbine cycle, with parallel flows through certain elements of the compressor and turbine systems.

A major factor determining the attractiveness of a bottoming cycle is the level of TEGT inherited from the main cycle. A high TEGT gives scope for a more efficient bottoming cycle, but it may also result from a less-efficient core-engine cycle. Section 6.3 investigates increasing the efficiency of the ABC by locating the heat exchanger between turbine stages, rather than downstream of the last turbine stage. In the former case the ABC heat exchanger hot-side inlet temperature would be higher than the TEGT.

Intercooling technology was investigated at Chalmers University in ENOVAL and ULTIMATE, following earlier studies in NEWAC and LEMCOTEC. The preferred intercooler configuration typically had two-pass cross-flow with the hotter air contained in elliptical-section tubes in order to maximise the 'area goodness' of the design and minimise pressure losses. Alternative designs were reviewed in [59].

Secondary combustion can take place after a topping cycle and before the turbines, or between turbine stages, where it may be referred to as inter-turbine reheat (ITR) or inter-turbine burning (ITB). Design studies on possible secondary combustors for the cycle#06 turbofan are reported in section 6.2.2.

4.6 Advanced Engine Architecture

Cycle#06 combines four major technologies that between them will significantly reduce the core mass flow relative to the reference cycle turbofan. This confirms that the turbofan will need a geared fan on account of its high bypass ratio. It also makes the reverse-flow-core arrangement quite attractive as the small high pressure spool will not then need to have another shaft running through it. Reverse flow core arrangements have previously been investigated in the LEMCOTEC project [38] [39] [18].

The reverse-flow arrangement means that the intercooler can be moved to the aft end of the engine. Placing the topping cycle modules around the engine core is a fairly obvious choice and is consistent with the arrangements proposed by Kaiser [44] [58]. The secondary combustor is proposed as a fully annular design

discharging into the downstream HP turbine. The proposed arrangement is shown in Figure 26, which was included in the poster [19] presented by the author at Cranfield University in 2017.

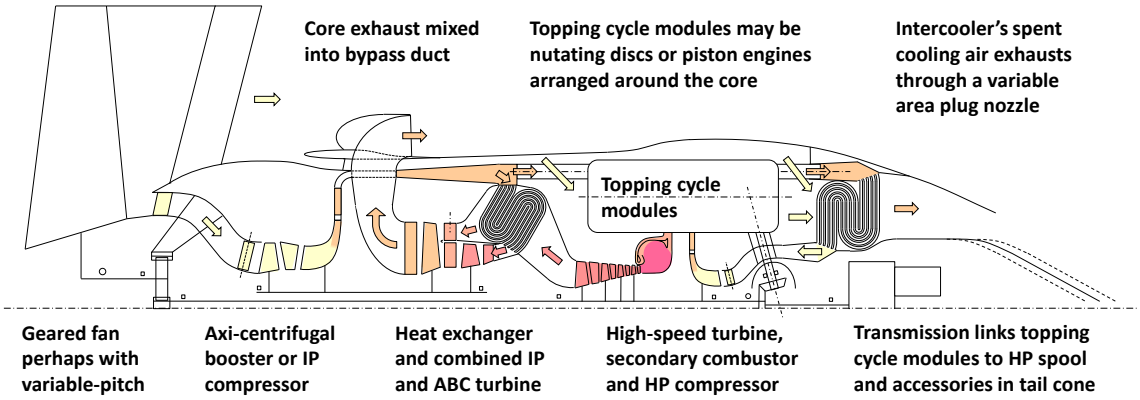

Figure 26 – A Possible Schematic Arrangement for Turbofan Cycle#06

The turbines do not have the high overall expansion ratios of the reference and high-OPR intercooled engine cycles (as in Table 19) because much of the overall expansion occurs in the topping-cycle machinery instead. The main purpose of the turbines is to drive the fan through the reduction gearbox and to do this a multi-stage turbine design is needed, typically three or four stages.

Optionally the HP turbine may also drive a small HP compressor to further turbocharge the topping cycle modules after the intercooler. This is shown in Figure 26. It should enable a lower compression ratio to be used in the topping cycle, thereby saving weight, but the studies reported in Chapter 7 initially suggested that it would be unnecessary, so it was not included in the whole-engine performance model for cycle#06. The overall pressure ratio can be made up by having a higher pressure ratio in the nutating-disc compressor (NDC) or in the IP compressor. However further investigation showed that if the pressure ratio in the NDC would be increased to the desired extent then the inlet non-dimensional flow would exceed the expander non-dimensional outlet flow that would otherwise be taken to size the discs. A larger-diameter NDC would be required, but this would be undesirable not only because of adding weight, but also because of installation drag penalties. The alternative of having

a much higher pressure ratio IP compressor before the intercooler would be detrimental to performance, so most probably the centrifugal compressor would be retained in a fully optimised design.

In the illustrated arrangement, power output from the topping cycle modules is added to the HP turbine shaft via bevel gears. However, a variable ratio transmission is likely to be needed, as it was in the case of the Napier Nomad II engine [23]. Figure 26 shows the IP compressor driven by the LP turbine (as in the Garratt ATF3 engine, which has a reverse-flow core). The IP compressor provides the core airflow going into the intercooler and also the working air for the open-circuit bottoming cycle. This air goes to the ABC heat exchanger (ABCHX), after which it runs through a two-stage turbine. It was originally proposed to integrate the second stage of this ABC turbine with the single-stage core-exhaust LP turbine, so that both flows could drive the IP compressor, but alternative turbine arrangements have now been modelled where the LP turbine is omitted and power from the ABC is added to power from the HP turbine and nutating disc to drive the fan and the IP compressor. Transmission designs are discussed in section 6.4.

The reverse-flow core arrangement may not be the best arrangement for all of the advanced cycles identified in Figure 25, but it still seems an attractive option for cycles including intercooling.

5 NUTATING-DISC DESIGN STUDIES

There are many options for topping cycle machines to be added to gas turbines to improve thermal efficiency, but this study focuses on nutating-disc machines that have the potential to generate additional power for propulsion, rather than just providing a pressure rise. Nutating discs (ND) offer some advantages over conventional piston or Wankel rotary engines, but they also present significant design challenges, particularly when highly turbocharged. It had been intended to compare nutating-disc modules with alternative designs, but with limited time it was decided to make a more detailed examination of the pros and cons of the nutating-disc options. Some of the work described in this section was previously reported in ULTIMATE deliverable D4.3 [62].

5.1 Thermodynamic Cycle

The thermodynamic cycle that best describes a nutating-disc engine is part Otto Cycle and part Diesel Cycle, as described by Korakianitis et al. [52]. Figure 27 from Joshua Sebastiampillai [62] shows a Pressure–Volume (P-V) diagram that represents the thermodynamic processes within a nutating disc engine. It also includes a top-down view of a single-nutating-disc engine configuration to show where the thermodynamic processes occur. These processes are the same whether it has one disc or multiple compression and expander discs [54], and is only slightly modified by variant porting and valve arrangements.

The processes as described in [62] with reference to Figure 27 are as follows:

- Process 01-02: adiabatic isentropic compression of the working fluid.
- Processes 02-04: adiabatic expansion of the fluid from the end of the compression process through the accumulator and finally to the combustion chamber.
- Processes 04-06: constant volume combustion and constant pressure combustion (either spark or compression ignited)
- Process 06-07: the adiabatic expansion of the combustion products through to the exhaust ports.

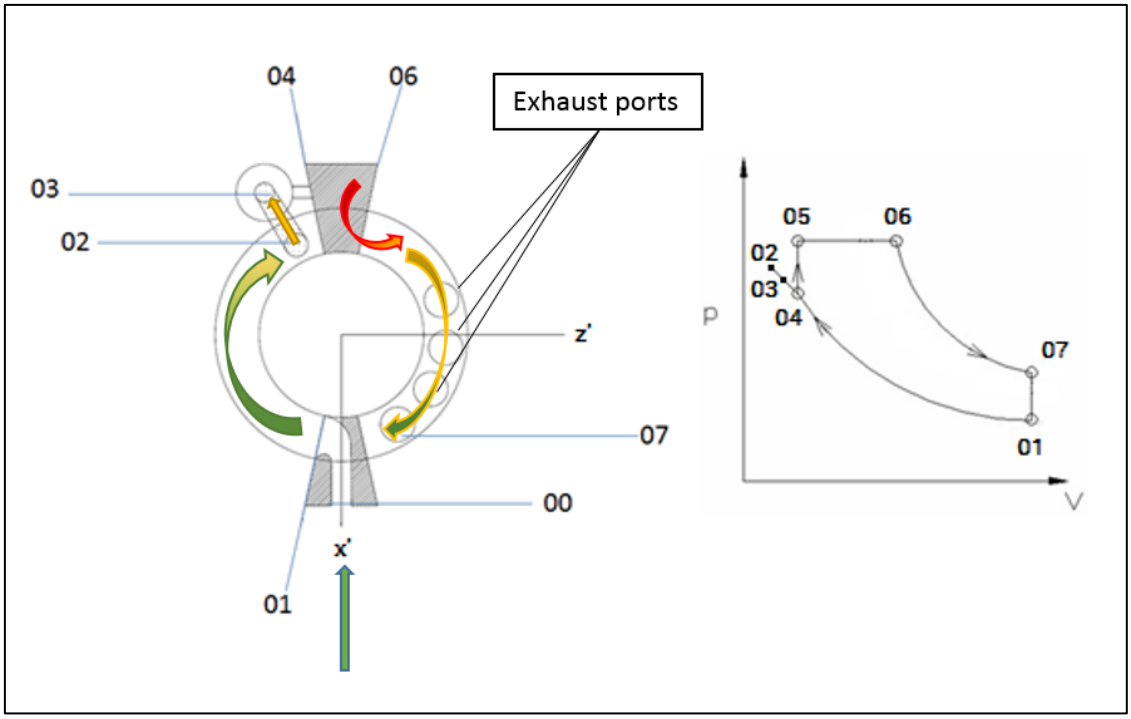

Figure 27 – Thermodynamic Cycle and Stations in a Single-disc Engine [62]

These processes occur on both sides of the disc, with compression and expansion thermodynamic processes on one side of the disc lasting for about 270° of shaft rotation and overlapping each other by about 90°. This means the engine achieves two complete cycles per shaft revolution, as opposed to 2-stroke and 4-stroke internal combustion engines, where a full shaft-rotation only provides one, or half of, a complete cycle, respectively [53].

The methodology proposed by Korakianitis et al. describes the performance of a naturally-aspirated nutating-disc engine. The performance of the ND engine core is determined by a set of independent variables. A few of the independent variables that are needed to determine the steady-state performance of the ND engine core are: the isentropic compression efficiency, the expansion efficiency and the heat loss factor through the combustion chamber. In all, there are eighteen independent variables that affect the performance of the ND engine, according to the steady state performance model in [52].

Although Mohanarangan [55] and Sebastiampillai [67] [62] have generated performance models for nutating discs, the author chose to create new Excel models to simulate the dynamic performance of the compressor and expander discs and to apply a simple steady-state approximation to the results from these models in the overall engine performance spreadsheet described in section 3.1. A mechanical design concept for the corresponding double-disc module was developed in parallel and is described in the following section.

Note: in order to calculate the typical size of a nutating disc module, preliminary whole-engine performance data for cycle#06 was used, specifically the exit flow at secondary combustor inlet, which is defined in Table 20 in Chapter 6.

5.2 Nutating-disc Topping-cycle-module Design Concept

Having two separate discs is preferred for a high-power engine. Two discs will double the mass flow and power output and balance-out each-other's nutating motion if they are the same size and mass and aligned in mirror image to each other. A single disc, however, will force its unbalanced wobbling motion on to the engine mountings. Furthermore, any single-disc engine will have a hot hemisphere and a cold hemisphere introducing asymmetric thermal distortions.

In double-disc arrangements each disc has '*D2h'* cyclic symmetry (like a traditionally-patterned basketball) so the same processes occur simultaneously in diametrically opposed volumes. The separate compression and expansion nutating discs may have different shapes or sizes, though for simplicity both discs are initially assumed to have the same geometry. Figure 3, repeated here as Figure 28, shows the main features of the proposed topping-cycle module.

The 3-D computer model was produced by Francesco Mastropierro, based on the author's drawings and intermediate 3-D models from Eleni Chatzidimitriou. Half of the module is cut-away and the model is simplified by omitting the sealing features and details of the systems for fuel injection, oil cooling, ignition etc. This design was then realized as a display model for the ULTIMATE Project Stand at the 2018 Farnborough International Air Show, as shown in Figure 29.

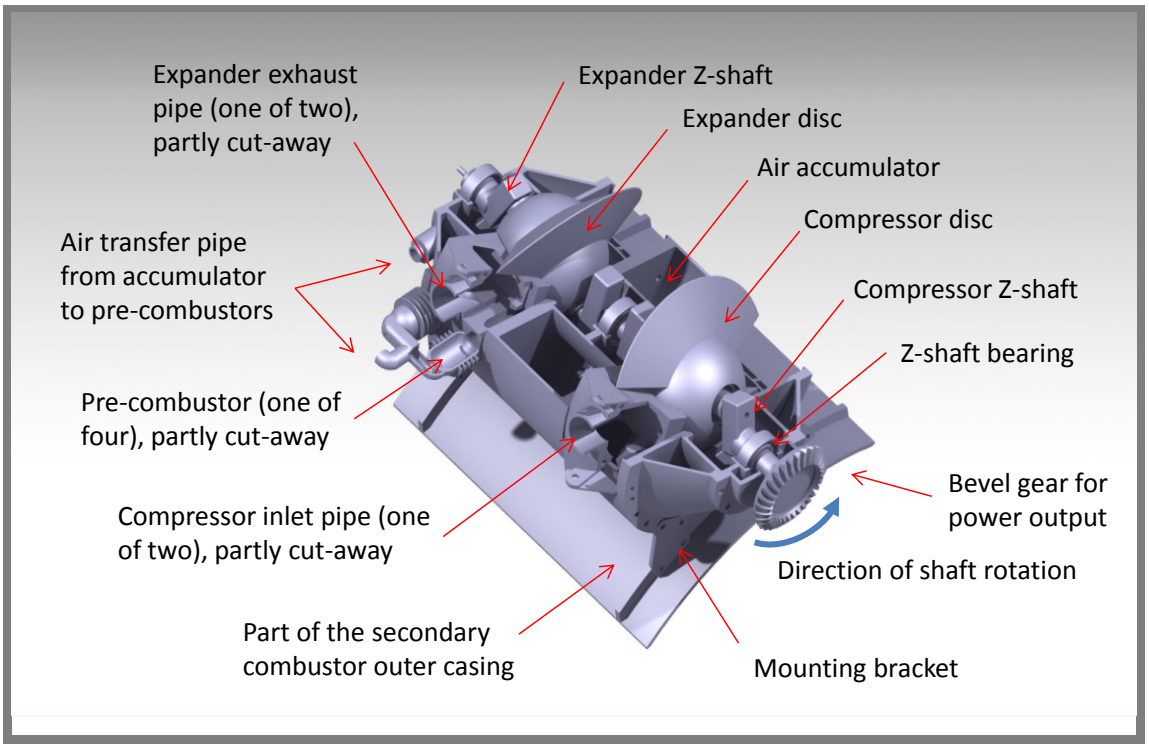

Figure 28 – Concept for a Nutating-disc Topping-cycle Module
(3-D solid model courtesy of Francesco Mastropierro)

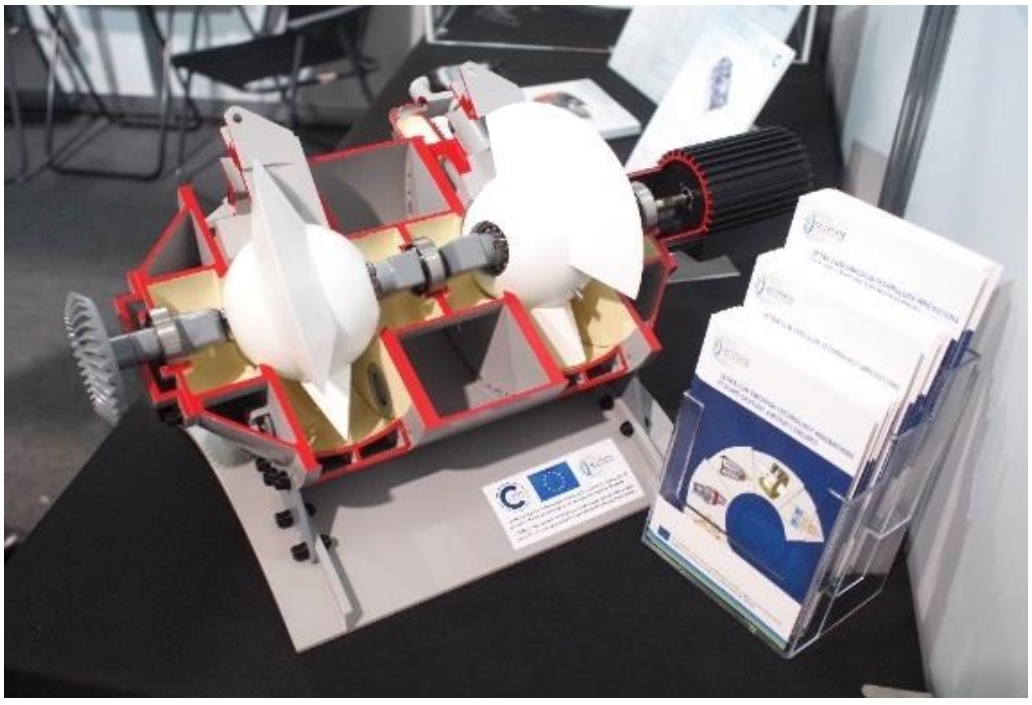

Figure 29 – Model of a Nutating-disc Module displayed at Farnborough

The model was also displayed at the ULTIMATE project Final Review Meeting in Brussels. It was assembled by the author from components manufactured by Malcolm Nicholls Limited and Eleni Chatzidimitriou. In this model, the two nutating discs are rotably-mounted on roller bearings on the Z-shafts as shown schematically in Figure 30.

Rotation of the Z-shafts causes the discs to nutate, or ‘wobble’, because the discs are prevented from rotating with the shaft. They only rotate relative to the shaft. In this two-disc machine, the expander disc provides the power to drive the compressor disc and be exported to the rest of the engine via the bevel-gear drive shown on the end of the compressor Z-shaft. Note the expander disc is on the left and the compressor disc is on the right in Figure 30.

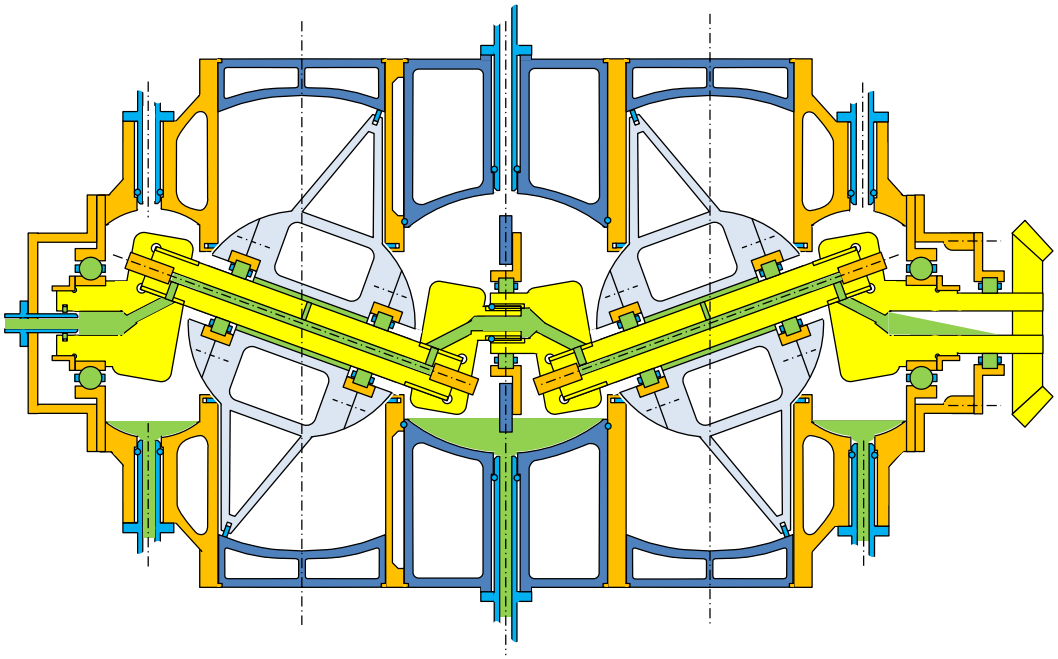

Figure 30 – Vertical Section through a Nutating-disc Module showing the main casings (blue and orange), the rotating shaft (yellow), the nutating discs (grey) and oil or oily components (green)

Figure 30 also shows a concept for the oil feed, vent and scavenging arrangements for a real module, assuming that it would be installed with its main axis horizontal. The Z-shafts are provided with a central oil-feed from a

muff at the expander-end of the module and the oil is then distributed to the three bearing chambers. Excess oil passes to a gearbox at the compressor end.

Each disc has a basic ‘flying-saucer’ shape, but with the disc rim cut-away in two places down to the spherical hub as seen in Figure 29. Each disc is centred in its ‘cheese-shaped’ or ‘doubly-truncated spherical’ chamber. Static wedges are inserted where the disc rims have been cut away. For the compressor disc, both wedges contain the inlet ports. For the expander disc each contains an exhaust port and connects two pre-combustors to the expander disc chamber as shown in Figure 31. The wedges also house the anti-rotation mechanisms. In the model, rotation of the discs is prevented by pins projecting from the disc hubs and slide in axial slots in the wedges. Assuming no clearance in the slots, the resulting true motion of a disc is similar to that in Figure 97 in Appendix D.

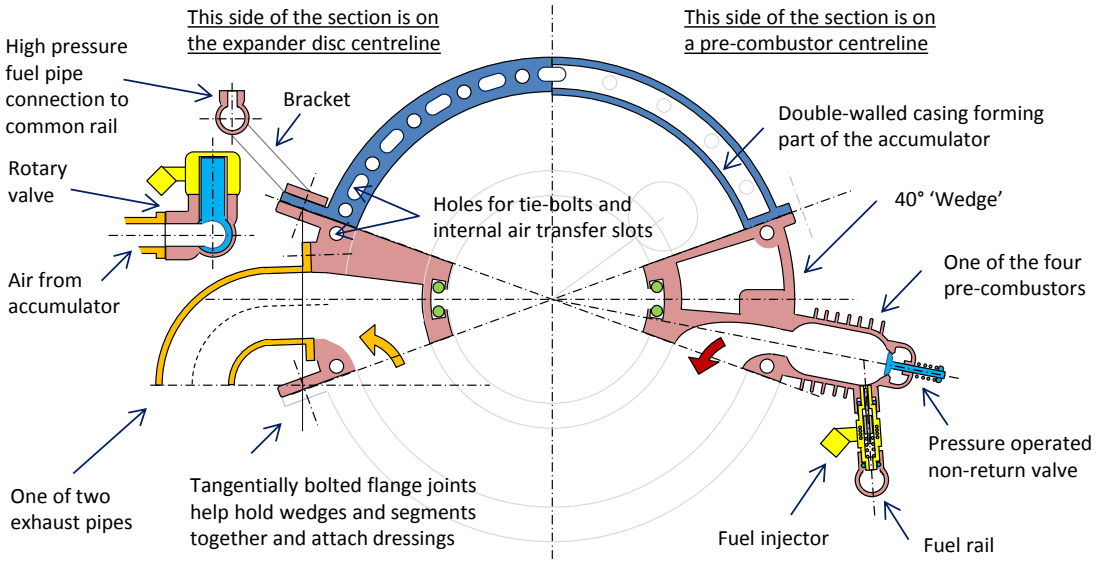

Figure 31 – Composite Cross-section through an Expander-disc Chamber showing the wedges, an exhaust port and a pre-combustor

For each disc, as the shaft rotates, two pairs of diametrically-opposed virtual lines-of-contact precess around the disc-chamber side-walls as the conical faces of the disc ‘roll-around’ against them. However, the disc rims and the sidewalls are not continuous, being interrupted by the wedges where the core flow enters and exits the compressor and expander chambers.

In practice there is no direct physical contact between the discs and the sidewalls because the sealing is provided by ‘radial’ sealing elements. These elements must accommodate a little sliding contact, since the relative motion of the conical faces of each disc against the two side-walls is not pure rolling. Rolling contact with either side would require the disc to precess and this is prevented by the anti-rotation features.

The sealing for nutating disc machines is complex and somewhat similar to that of Wankel engines. Figure 30 shows oil seals around the hubs of the discs and sealing strips at the rims of the nutating discs, but further vital sealing elements not shown in this cross-section. Detail design of the seals was out-of-scope for this study, but the seals proposed for an earlier design are shown in Figure 32.

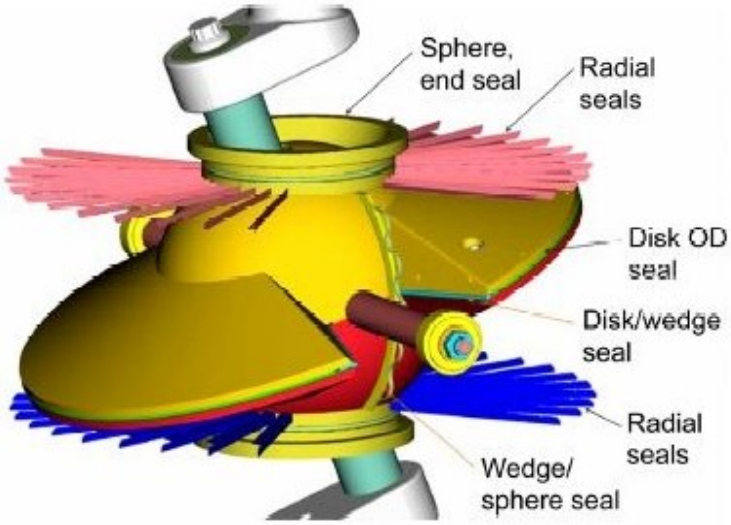

Figure 32 – Possible Nutating Disc Sealing Arrangements [135]

At any instant the seals isolate either four or six separate volumes within the cheese-shaped casing and between the wedges. The number depends on the rotational position of the Z-shaft and the angle of the disc relative to the wedges. As the shaft rotates, these volumes serially expand and contract, with the air or gas inside them clocking-around in the same direction as the shaft rotates until squeezed-up against a wedge. The air or gas enters or exits each moving volume via exposed ports in the wedges or via valves in the side-walls.

The air that is compressed by the compressor disc passes through non-return valves into the accumulator. This includes the spaces between the inner and outer walls of the casings, shown as blue in Figure 30. The double-walled compressor and expander casings, the end casings and the accumulator casing in the middle are all interconnected. Thus the compressed air can pass from the cooler compressor-end to the hotter expander end of the module, where it cools the expander casing and the sidewalls for the expander chamber. The air then passes through transfer pipes and valves to the pre-combustors, where the fuel is injected and ignition occurs before the hot gasses expand and do work within the expander chamber. The pressure of the gases in this chamber causes the expander-disc to nutate and drives the rotation of the Z-shafts. This provides more than enough torque to make the compressor disc nutate. The remaining power is then exported via a bevel-gear drive to be added to the turbine shaft driving the geared fan, as shown schematically in Figure 2.

The proposed new ND module design shares some novel features with the designs proposed by Joshua Sebastiampillai in [67] and [62], but in detail it differs significantly from these and earlier ND engine proposals. The discs were provisionally sized at 360 mm diameter for the cycle#06 engine as explained in section 5.4. The display model has 240 mm diameter discs and so is nominally two-thirds-scale. These discs are larger than most of the designs from Meyer, Korakianitis and Cochereau, but consistent with accommodating the cycle#06 turbofan engine core mass flow in six modules. However, the larger disc diameter creates dynamic stresses that are an order of magnitude higher than the earlier 101.6 mm diameter designs if they would be run at the same speed. Shaft speeds of around 6000 rpm were envisaged.

Figure 4 showed the proposed arrangement of six modules equally spaced around a secondary combustor. The secondary-combustor in this scale drawing was sized as it was for the second CFD study described in section 6.2.2. The outer diameters of the nutating-disc casings are 420 mm, consistent with 360 mm diameter discs. However, an improved installation design (with lower bypass duct loss or nacelle drag) would be possible if the discs could be

reduced to 300 mm diameter and the casings reduced to 350 mm diameter. These figures cover the range of sizes originally anticipated for the final scaled engine design with six modules.

It is not necessary that the compressor and expander discs should have the same size and geometry, and for Sebastiampillai's open rotor engine study, the compressor and expander discs were individually sized. However, from the mechanical design point of view there are advantages in making their diameters the same, or very similar. It means the casings can be assembled using a single set of long 'through-bolts' to hold them together, as indicated in Figure 33. Having equally-sized discs does however place some constraints on the performance cycles that can be selected.

The new design integrates the accumulator volume within the mainly-cylindrical outer casings, so that the compressor and expander disc chambers are jacketed by compressor delivery air. This means that most of the heat lost through cooling the expander disc casings is fed back into the air going to the pre-combustors. The design is therefore referred to as the Recuperated Nutating-Disc Module (RNDM), though the pre-combustors themselves are anticipated to need extra cooling, which is why they are shown with cooling fins, similar to air-cooled piston engines. All the casings are expected to run hot, which provides tribological challenges for the seals. Seal deterioration could be the Achilles heel of the RNDM, but it is anticipated that new materials could be developed by 2050 to address this problem.

A key feature of any nutating-disc engine design is the constraint provided to the discs to stop them rotating with the Z-shafts. Without dedicated anti-rotation devices there would be excessively-high contact forces and high wear-rates on the disc-to-wedge sealing elements. Various anti-rotation arrangements are possible and their detail design determines the exact motion of the discs. For the display-model the anti-rotation features are just steel pins projecting from the hubs of the discs and running in slots in the plastic 'wedge' components, but more sophisticated low-friction designs were studied for a real engine.

It is assumed that the expander disc and its sealing elements will be fabricated from advanced ceramic-composite materials and will run hot, so its gas-washed surfaces will not be cooled. The internal bearing-chambers would be insulated by thermal barrier coatings to reduce the heat transferred to the oil, but high oil-flows will likely still be needed to maintain acceptable temperatures for the Z-shafts and bearings.

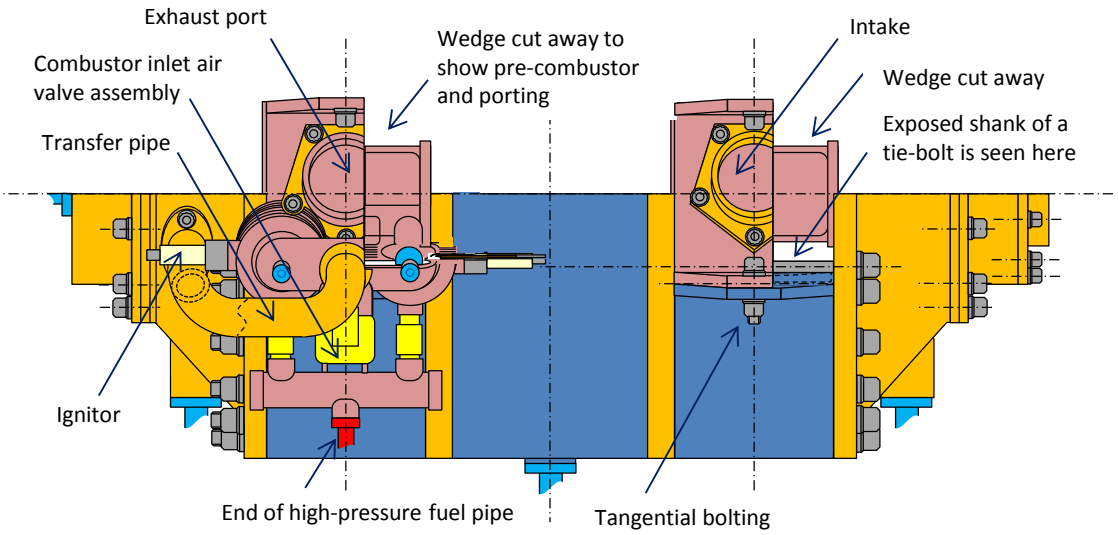

Figure 33 – Cut-away View on ND Module showing Combustion System

Figure 33 also shows some details of the pre-combustors and their compressed air supply, fuel injectors and ignitors. The two adjacent pre-combustors are fired alternately. Compression ignition was briefly considered, but judged to be impractical in this engine configuration. However, with electronic control of the air inlet valve and fuel injectors it should be possible to stratify the charge in the pre-combustor and run lean to minimise NOx emissions. Fuel can continue to be injected into the pre-combustor after ignition, but the increase in pressure with constant volume combustion will tend to shut-off the air supply. (A non-return valve, shown as light blue in Figure 33, is included to prevent back-flow of air towards the accumulator.) This implies three possible ways of operating the engine:

1. Introduce all the air at once and aim to maximise the pressure rise through near-constant-volume combustion.

2. Add the air and fuel gradually and aim for constant pressure (diesel-cycle) combustion.
3. Interrupt the supply of air during an initial pressure spike following ignition and resume air (and fuel) injection for a limited period after the pressure has fallen below the pressure in the accumulator.

Each approach has its pros and cons, and different approaches might be followed at different engine power-levels and in different flight regimes. Further options are opened-up by the ability to vary the compression ratio and the amount of intercooling. A fixed-ratio transmission would link the Z-shaft rotational speed to the fan (though there is also the possibility to have a variable-pitch fan and/or a variable ratio transmission, as was employed in the Napier Nomad CCE [23].)

The precombustors in the nutating-disc model have not been definitively sized in relation to the volume swept by the discs. As illustrated in Figure 31 and in other figures in this section, the pre-combustors are relatively larger than in previous designs or shown in Meyer's patent for example [51]. While no sizing calculations were made, it was argued that a highly turbocharged ND machine would normally operate at lower compression ratio than a normally aspirated design. It would therefore expect to have relatively-larger volumes of air being injected into the pre-combustor, relative to the overall capacity of the expander.

Earlier studies have investigated varying the ratio of constant volume to constant pressure combustion in nutating disc engines. This will depend on the way in which the engine is operated. To avoid overcomplicating the initial performance studies with different options, the performance has been modelled using option 2 above, i.e. assuming diesel-cycle operation.

Intercooling the upstream compression system enables the ND modules to run with higher core inlet pressures, but without excessive inlet temperatures. It has the potential to increase efficiency and reduced NOx emissions. By increasing the inlet air density, this reduces the compression work and results in module designs that are more compact, but the higher operating pressures also

increase mechanical loads on bearings etc. Most previously proposed nutating-disc engine designs have been ‘normally aspirated’, i.e. without supercharging or turbocharging, so they have not needed to address the same problems.

5.3 Nutating-disc Compressor Time-marching Model

In comparison with a gas turbine the compression, combustion and expansion processes in the nutating-disc modules are discontinuous, though not so discontinuous as those in a single-piston engine. To better understand these processes, time-marching models were created in Excel. Since the proposed topping-cycle modules have compressor and expander discs operating in separate chambers, the compressor and expander performance can be analysed independently.

The compressor model was created first and is simpler. It assumes the inlet pressure and exit pressure are constant and that all the compression occurs within the nutating disc chamber. In reality the accumulator volume will be finite so its pressure (and temperature) will not be constant, but these are second-order effects that can be ignored provided the accumulator volume is relatively large. It is also assumed that the sealing of the discs is perfect with zero seal clearance, compression is adiabatic, the ports and valves open instantaneously and there are no pressure losses through them, which will tend to give optimistic performance predictions at high rotational speeds. However some irreversibility is allowed for by taking the polytropic compression efficiency to be 95%, which is not atypical for positive displacement machines. (Gamma is fixed at 1.4.) In the proposed design, some heat will seep into the compressor from the accumulator, though this should be limited by the use of thermal barrier coatings and some is heat also removed by oil cooling of the bearing chambers.

To a first approximation the heat ingress may be accounted for by the assumed compression efficiency. As great accuracy is not demanded, the nutating disc is conveniently divided into coarse ten-degree segments, or cells, as shown in Figure 34, and each time-step is taken to correspond to a 10° clocking of the Z-shaft. Small-angle approximations are made. Supposing the shaft axis is

vertical, the space above each 10° disc segment and below the casing is treated like a column that has a sinusoidal variation in its height and volume.

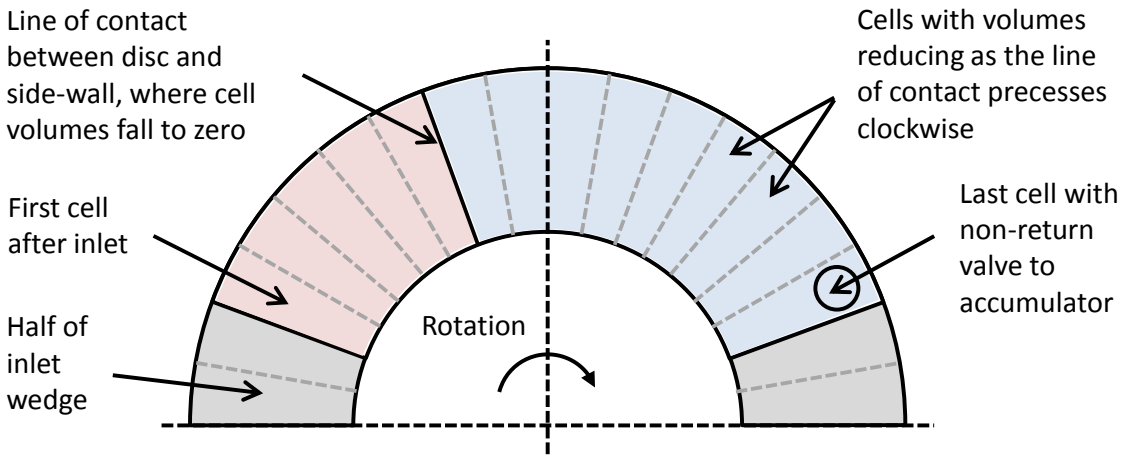

Figure 34 – Schematic Diagram showing how Cells are modelled

Given the symmetry of the disc, chamber and wedges, it is only necessary to model what happens in one quadrant: i.e. in the top half, and in one 140° space between two wedges, as shown in Figure 34 and Figure 35. However, it is necessary to consider a full 360° shaft rotation to model the full cycle of operation. The Excel model keeps track of what happens in each cell.

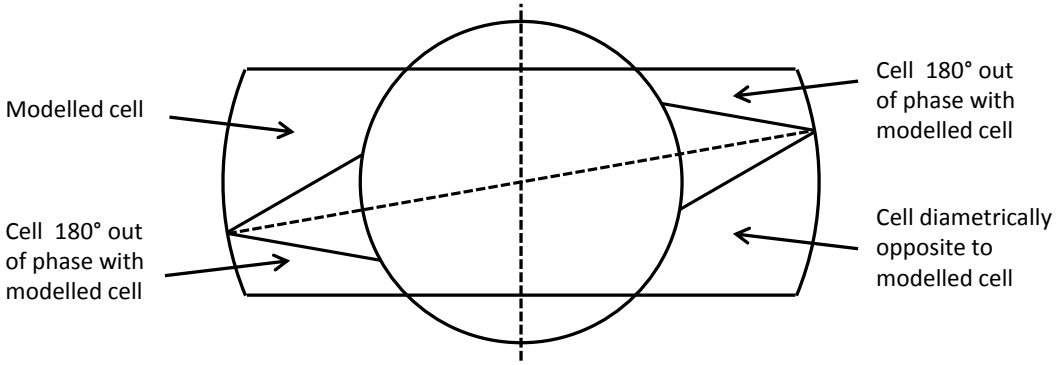

Figure 35 – Schematic Cross-section showing Cells in Different Quadrants as modelled in the Excel spreadsheet

All cells that are in direct contact with each other have the same pressure and temperature at any one time. When the inlet port is open, the pressure in the connected cells is the inlet pressure. When the non-return valve (in the last

segment before the wedge) is open, the pressure in the connected cells matches the accumulator pressure and the compression work is finished. This is not strictly correct if the accumulator is being charged-up, as then more work must be done. However, in quasi-steady-state operation, as much air will be leaving the accumulator as entering it, so on average no extra work will be required to transfer the air into the accumulator. Also, because of the discrete time-steps, there can be an overshoot in pressure before the non-return valve opens (unless the valve is set to open at the modelled pressure). Thus the model is more accurate when the accumulator pressure is set to match the trapped air's pressure at a particular time-step. In the proposed design the accumulator pressure is determined by the operation of valves admitting the air into the pre-combustors. This means that the accumulator pressure, once it has been built-up, can be regulated, so that the compressor can be operated at variable pressure ratios. However, assuming the inlet porting geometry is fixed, the inlet volume flow rate and the mass flow for a given inlet air density will tend to be proportional to the Z-shaft rotational speed. In practice however the mass flow will tend to be smaller than calculated in the model, due to seal leakage at low rotational speeds and due to increased intake pressure losses at high rotational speeds. There may also be a small amount of back-flow from the accumulator if the non-return valve does not close promptly.

Figure 36 shows a part of the spreadsheet listing the volume of each cell in one quadrant. The cell contents are colour-coded to show the cells in contact with each other. For the induction stroke the cells are coloured blue and for the compression stroke the cells are coloured red. Each new row in the spreadsheet represents a later time step. Each time-step adds or subtracts one cell from each group, such that the combined volumes wax and wane as the Z-shaft rotates and as the line of contact between the disc's upper conical flank and the flat (top) side-wall clocks-around, one cell at a time. The inlet wedge is on the right-hand side of the matrix and the air flow is predominantly from right to left, though there can be some temporary flow-reversal at the inlet. (Note this is opposite to the direction of flow indicated in Figure 34.)

Volumes of segments cc Red cells are reducing volumes in compression Blue cells are increasing volumes during induction

Segment		5°	15°	25°	35°	45°	55°	65°	75°	85°	95°	105°	115°	125°	135°	145°	155°	165°	175°	Anti-	Occupied volumes		
Phase/Angle		0.09	0.26	0.44	0.61	0.79	0.96	1.13	1.31	1.48	1.66	1.83	2.01	2.18	2.36	2.53	2.71	2.88	3.05	Phase	Total	Red	Blue
0	0.00	0	0	55	41	28	17	9	3	0	0	3	9	17	28	41	55	0	0	180	308	154	154
10	0.17	0	0	41	28	17	9	3	0	0	3	9	17	28	41	55	71	0	0	190	324	99	225
20	0.35	0	0	28	17	9	3	0	0	3	9	17	28	41	55	71	87	0	0	200	370	58	312
30	0.52	0	0	17	9	3	0	0	3	9	17	28	41	55	71	87	104	0	0	210	446	30	417
40	0.70	0	0	9	3	0	0	3	9	17	28	41	55	71	87	104	121	0	0	220	550	13	537
50	0.87	0	0	3	0	0	3	9	17	28	41	55	71	87	104	121	136	0	0	230	677	4	673
60	1.05	0	0	0	0	3	9	17	28	41	55	71	87	104	121	136	151	0	0	240	824	0	824
70	1.22	0	0	0	3	9	17	28	41	55	71	87	104	121	136	151	163	0	0	250	987		987
80	1.40	0	0	3	9	17	28	41	55	71	87	104	121	136	151	163	174	0	0	260	1161		1161
90	1.57	0	0	9	17	28	41	55	71	87	104	121	136	151	163	174	183	0	0	270	1340		1340
100	1.75	0	0	17	28	41	55	71	87	104	121	136	151	163	174	183	188	0	0	280	1520		1520
110	1.92	0	0	28	41	55	71	87	104	121	136	151	163	174	183	188	191	0	0	290	1694		1694
120	2.09	0	0	41	55	71	87	104	121	136	151	163	174	183	188	191	191	0	0	300	1857	191	1666
130	2.27	0	0	55	71	87	104	121	136	151	163	174	183	188	191	191	188	0	0	310	2004	379	1625
140	2.44	0	0	71	87	104	121	136	151	163	174	183	188	191	191	188	183	0	0	320	2131	562	1569
150	2.62	0	0	87	104	121	136	151	163	174	183	188	191	191	188	183	174	0	0	330	2235	736	1498
160	2.79	0	0	104	121	136	151	163	174	183	188	191	191	188	183	174	163	0	0	340	2311	900	1411
170	2.97	0	0	121	136	151	163	174	183	188	191	191	188	183	174	163	151	0	0	350	2357	1050	1307
180	3.14	0	0	136	151	163	174	183	188	191	191	188	183	174	163	151	136	0	0	0	2373	1186	1186
190	3.32	0	0	151	163	174	183	188	191	191	188	183	174	163	151	136	121	0	0	10	2357	1307	1050
200	3.49	0	0	163	174	183	188	191	191	188	183	174	163	151	136	121	104	0	0	20	2311	1411	900
210	3.67	0	0	174	183	188	191	191	188	183	174	163	151	136	121	104	87	0	0	30	2235	1498	736
220	3.84	0	0	183	188	191	191	188	183	174	163	151	136	121	104	87	71	0	0	40	2131	1569	562
230	4.01	0	0	188	191	191	188	183	174	163	151	136	121	104	87	71	55	0	0	50	2004	1625	379
240	4.19	0	0	191	191	188	183	174	163	151	136	121	104	87	71	55	41	0	0	60	1857	1666	191
250	4.36	0	0	191	188	183	174	163	151	136	121	104	87	71	55	41	28	0	0	70	1694	1694	
260	4.54	0	0	188	183	174	163	151	136	121	104	87	71	55	41	28	17	0	0	80	1520	1520	
270	4.71	0	0	183	174	163	151	136	121	104	87	71	55	41	28	17	9	0	0	90	1340	1340	
280	4.89	0	0	174	163	151	136	121	104	87	71	55	41	28	17	9	3	0	0	100	1161	1161	
290	5.06	0	0	163	151	136	121	104	87	71	55	41	28	17	9	3	0	0	0	110	987	987	
300	5.24	0	0	151	136	121	104	87	71	55	41	28	17	9	3	0	0	0	0	120	824	824	0
310	5.41	0	0	136	121	104	87	71	55	41	28	17	9	3	0	0	3	0	0	130	677	673	4
320	5.59	0	0	121	104	87	71	55	41	28	17	9	3	0	0	3	9	0	0	140	550	537	13
330	5.76	0	0	104	87	71	55	41	28	17	9	3	0	0	3	9	17	0	0	150	446	417	30
340	5.93	0	0	87	71	55	41	28	17	9	3	0	0	3	9	17	28	0	0	160	370	312	58
350	6.11	0	0	71	55	41	28	17	9	3	0	0	3	9	17	28	41	0	0	170	324	225	99
360	6.28	0	0	55	41	28	17	9	3	0	0	3	9	17	28	41	55	0	0	180	308	154	154

Figure 36 – Part of the Excel Time-marching Model for the ND Compressor

Subsequent blocks or matrices of data list the computed mass, pressure and temperature of the air in each cell, and in each colour-coded group of cells. The total inlet and outlet mass flows over a full shaft-rotation are also compared. Since only one side of one half of the disc is modelled, only a quarter of the overall mass-flow through the compressor is accounted, so the overall mass-flow in one nutating-disc module is four-times the modelled flow. The work done is calculated and various parameters are plotted.

While cells are in contact with the inlet wedge, their pressures and temperatures are the same as the inlet pressure and temperature, but once the connected cells are closed-off from the inlet, the connected volume is reducing and the pressures and temperatures in all of the connected cells increase together until the pressure matches the pressure set for the non-return valve to open.

Although no back-flow is modelled through the non-return valve, the same is not true of the inlet port. This is because the connected volume starts to reduce before it is closed-off from the inlet. The phase angle at which the inlet closes can be set by the user. This could simply be when the line of contact between the disc and the side-wall reaches the first cell after the inlet wedge, but by engineering a narrower transfer port from the inlet wedge to the first cell, it is possible to make the port close earlier and so trap more air.

In the current studies it is assumed that the inlet port on the modelled side of the disc is closed-off for 110° out of the 360° of shaft rotation. However, when there is no inlet flow (or some back-flow) on one-side of the disc, there is always incoming flow on the other 180° out-of-phase side, so the combined flow into the shared inlet-port is always uni-directional.

Knowing the pressures in each cell, it is possible to calculate the forces and bending moments imposed by the gas loads on to the Z-shafts. The gas bending moments that are perpendicular to the plane of the Z-shaft apply a torque to the shaft, which varies according to the phase-angle or time-step. The shaft-torque driving the compressor peaks just as the non-return valve opens and the peak value depends on the accumulator pressure, though it is not directly proportional to it. The loads on the bearings between the Z-shaft and the disc are also computed, taking account of the forces both parallel and perpendicular to the plane of the Z-shaft. The forces due to the gas loads vary with the phase angle, but the total loads on the bearings include inertial loads that are continuous and proportional to the square of the rotational speed.

User-inputs enable the disc diameter, disc-rim thickness, disc hub/tip ratio and angle of nutation to be varied. Based on design studies assuming six modules, and matching the ND expander outlet capacity to the preliminary performance from Table 20, the disc diameter was set to be 360 mm, with hub/tip ratio of 53% and an angle of nutation of 20°. The hub/tip ratio was increased from 50% to 53% to make more space for the bearings between the Z-shaft and the disc.

The angle of nutation was limited to 20° in order to accommodate oil seals around the hub of the nutating disc.

The following example outputs are for a case where the inlet pressure is 5.6 bar, the inlet temperature is 120° C and the shaft speed is 6900 rpm. The accumulator air pressure is set at 70 bar and the compressor outlet air temperature is 840 K. Figure 37 shows how the total pressures at the non-return valve vary with the Z-shaft phase angle, both for the modelled cells and for those cells that are 180° out of phase with them.

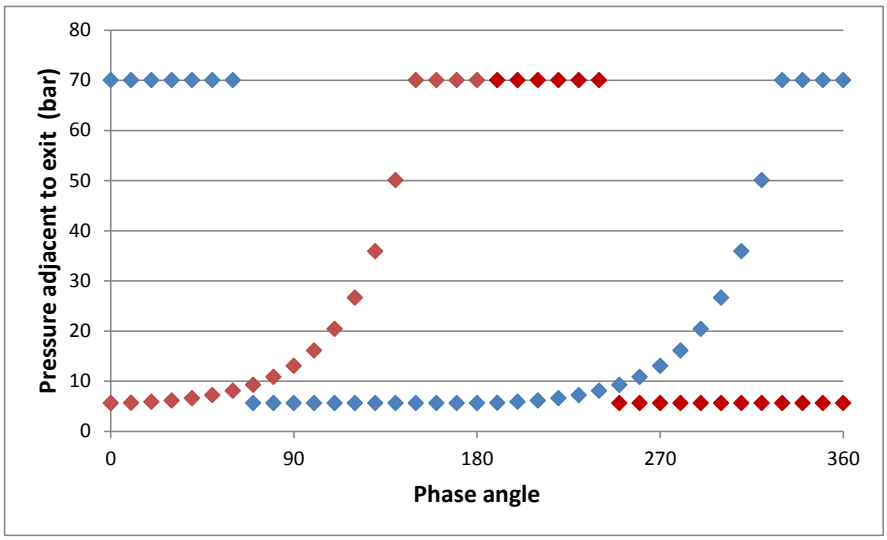

Figure 37 – Example of Pressures adjacent to the Non-return Valves

The differential pressure acting across the centre of each modelled segment of the disc, as a function of the phase angle, is shown in Figure 38. These differential pressures generate the bending moments that react the Z-shaft torque that drives the compressor, as shown in Figure 39. The mass of the orbiting bearings and the inertia of the discs also add to these bending moments. For the proposed bearings, bearing locations and masses of the bearings and disc, the total bending moments are as shown in Figure 40. These figures are calculated assuming the Z-shaft is rigid, runs at constant speed and is not subject to any torsional vibration or resonance. The resulting journal loads acting on each of the pair of bearings between the disc and the Z-shaft are shown in Figure 41.

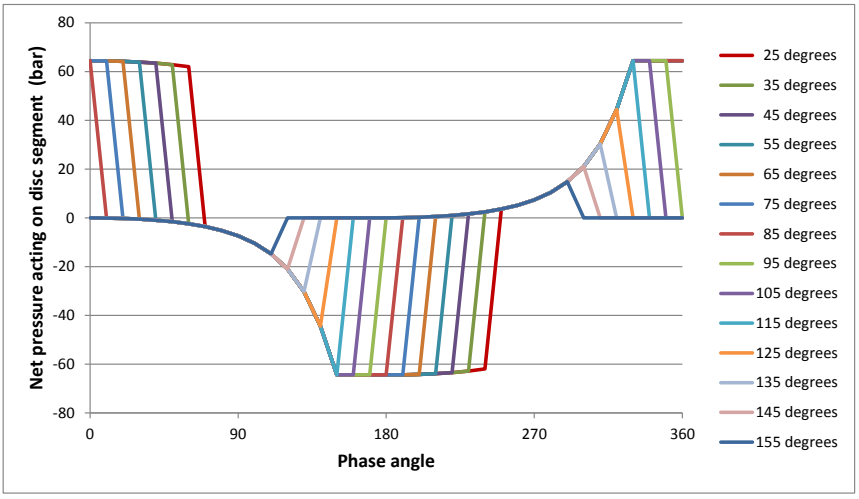

Figure 38 – Differential Pressures acting across Each 10° Disc Segment

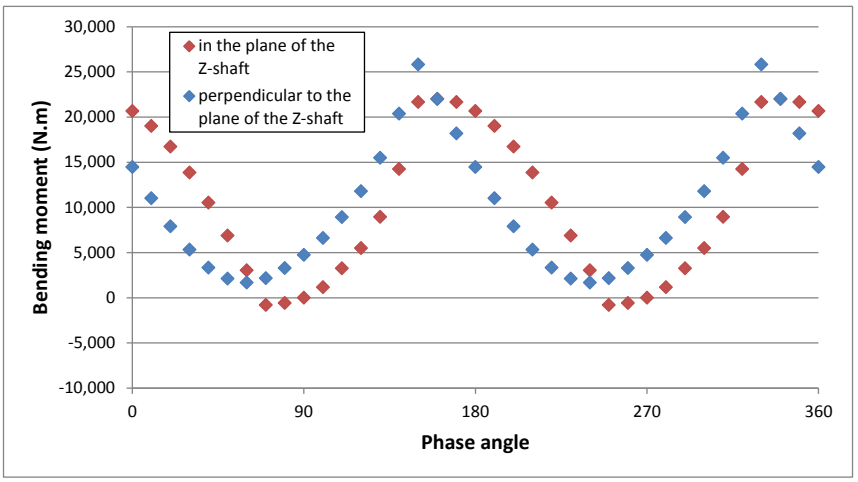

Figure 39 – Resolved Gas-load Bending Moments acting on the Z-shaft

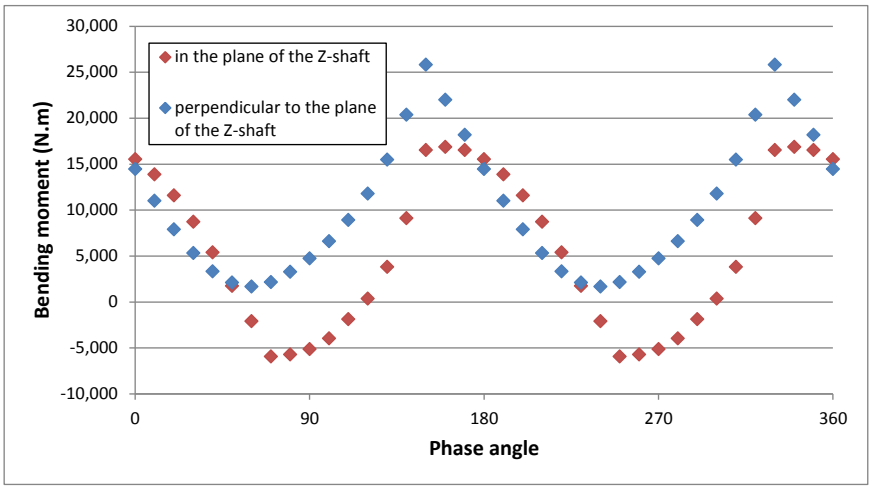

Figure 40 – Resolved Total Bending Moments acting on the Z-shaft

To put these loads into context, it should be appreciated that there are proposed to be 12 such compressor disc bearings in the engine, and each one sees a peak journal load significantly higher than the engine's gross take-off thrust. Furthermore, the compressor delivery pressure has been limited to 70 bar in this example, whereas the delivery pressure would ideally be in excess of 100 bar at take-off for better performance.

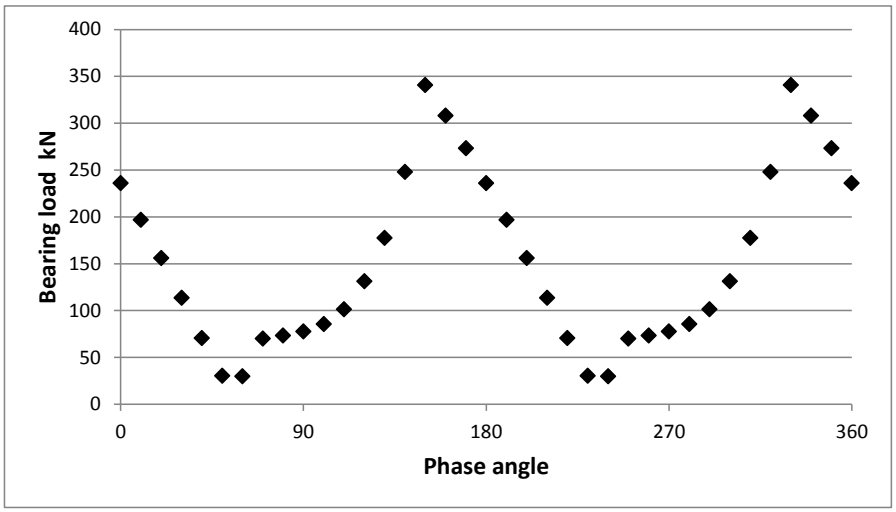

Figure 41 – Journal Loads on a Compressor Disc Bearing

The calculated bearing loads are also up to twice the quoted dynamic-load limit for a commercial roller bearing such as 'SKF NU 2310 ECP', and an order of magnitude higher than the fatigue limits quoted for this bearing with oil-jet lubrication, as assessed using the SKF on-line bearing calculation tool [136].

Custom aerospace-standard roller or taper-roller bearings, supplied with finely-filtered lubricating oil, should withstand higher fatigue loadings than commercial bearings, but it is clear that the highly-turbocharged nutating-disc machines will stretch existing rolling-element bearing technology. It should also be noted that the expander discs' bearings will experience even higher loads than those of the compressor discs on account of the sustained higher operating pressures and driving torques following diesel-cycle combustion.

It is highly desirable to use rolling-element bearings in aero engines because they are tolerant to short interruptions in the oil supply, whereas plain bearings

are not. However, it seems that the proposed roller bearings will be grossly overloaded at the operating pressures desired for the advanced cycle engines. Even with the best aerospace-standard bearings, lubrication and oil filtration quality, the fatigue lives are likely to be limiting. Aerospace-quality roller bearings would probably give adequate life in a normally aspirated nutating-disc engine delivering air to an accumulator at 20 bar, but in the absence of significant improvements in bearing technology by year 2050, it is likely that plain bearings with high-pressure oil-feed would need to be substituted. No calculations have been made for such bearings.

Making the bearings larger would not help much, because it would increase the inertial loads. Furthermore, the space envelope available for the bearings has already been fully utilised for the proposed 53% hub/tip ratio disc design.

Note the bearings supporting and axially locating the Z-shaft are not so highly loaded, are not subject to orbital motion. They also have space-envelopes that are less constrained, so they are not limiting the overall design.

5.4 Nutating-disc Expander Time-marching Model

This model was developed from the compressor model, initially just by running the compressor model in reverse. However the expansion process is more complicated than the compression process because it includes fuel injection, ignition and combustion and higher levels of heat transfer. Because of the higher temperatures and cooling requirements, these effects cannot be ignored. Nevertheless, even in its primitive state the basic model was useful in sizing the expander disc. This is because it could model the exit flow corresponding to the preliminary performance specified in Table 20, even when the peak cycle pressures and temperatures were uncertain.

It has been assumed that the ignition occurs inside the pre-combustor just as it opens to the expander chamber. The gasses would then be admitted to the expansion chamber, where additional combustion and heat-release occurs. On completion of combustion adiabatic expansion follows until the pressure drops

to the exhaust back-pressure. To simplify the calculations, they were performed in reverse, starting with the known exit pressure, gamma was assumed to be constant at 1.333 and the polytropic expansion efficiency was taken as 95.24%.

Thus it was concluded that with six ND modules for cycle#06, each disc should be 360 mm diameter and the Z-shaft should rotate at about 6900 rpm at take-off. The disc diameter and number of modules were then fed into the whole-engine mechanical design study.

5.5 Nutating-disc Mass-flow Continuity

One advantage of nutating-disc core modules is that they have continuous compressor inlet and expander outlet flows, though these flows are not entirely steady. This continuity makes integration with upstream and downstream turbomachinery easier and with less loss of efficiency than most other types of topping cycle, though wave rotors are similar in this respect.

The time-dependencies of mass flows into and out of the ND compressor are shown in Figure 42. This shows the total flow through both intake wedges and for both sides of the disc (i.e. for all four quadrants). Note the outlet flow is at a maximum when two of the four non-return valves have just opened.

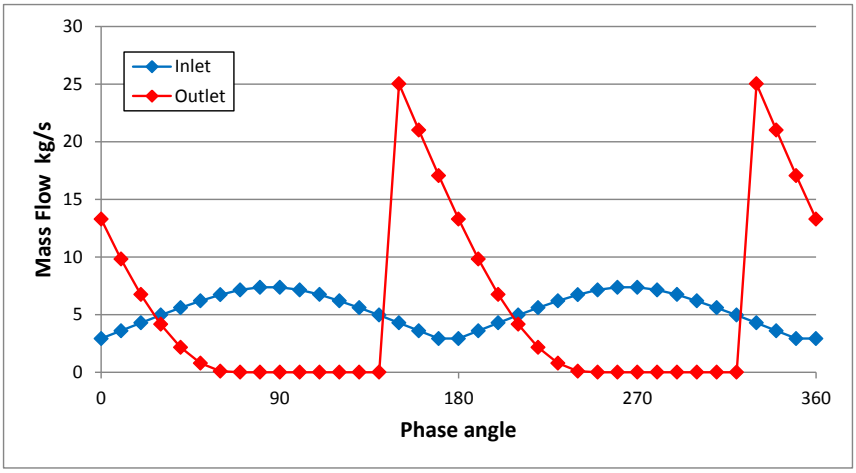

Figure 42 – Total Flows in and out of a single ND Compressor

The unsteadiness in inlet flow would still be a concern for the upstream compressor, except that in the proposed engine the flow will be distributed

between the six modules. With each module running 60° out of phase with the next one, then the overall mass-flow is much steadier. Furthermore, the proposed engine design has an intercooler upstream of the ND modules and this will act like a plenum chamber between the turbomachinery and the ND modules and help damp-out the residual mass flow and pressure fluctuations.

Considering the exhaust flows exiting the nutating disc modules, the outlet pressure and temperature were set to 21 bar and 1453 K respectively in order to match the take-off performance targeted in Table 20. The inlet pressure and temperature, when the transfer port from the pre-combustor first opens, were originally estimated as 138 bar and 2277 K. However that assumed all the fuel would be injected before ignition. In practice it seems preferable to have a more diesel-like cycle with the fuel introduced progressively. This will reduce the peak cycle pressure and temperature and tend to reduce NOx emissions.

By arranging the six nutating disc modules to be 60° out of phase with each other, steadier expander outlet flows are generated, as shown in Figure 43.

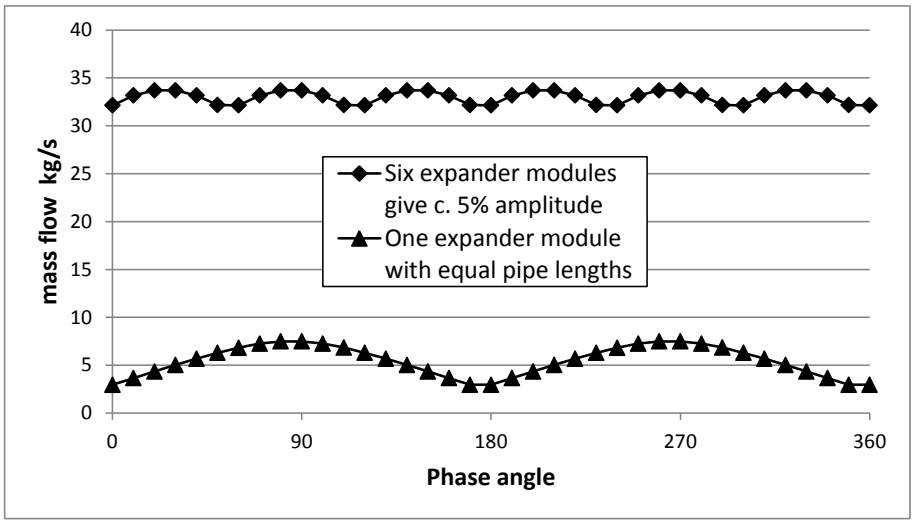

Figure 43 – Total Flows out of ND Expanders with Equal Pipe Lengths

However, a further reduction in mass flow variation is possible, taking advantage of the fact that half of the exhaust pipes are longer than the others in the installation shown in Figure 4. By tuning the different exhaust pipe lengths,

the ripple in the overall exit mass flow rate from the six modules can be reduced to less than 1% as shown in Figure 44. After passing through the secondary combustor the pressure-fluctuations should be negligible, eliminating any adverse effects on downstream turbines.

These plots assume the exit pressure is constant. In practice the pressure will also vary, depending on the intervening volume between the ND modules and the turbine nozzle guide vanes. The pressure variations will be small if the volume of the secondary combustor is, as proposed, relatively large.

Results from these time-marching Excel models and other component-level studies were used to refine the steady-state performance assumptions made in the main Excel whole-engine performance models.

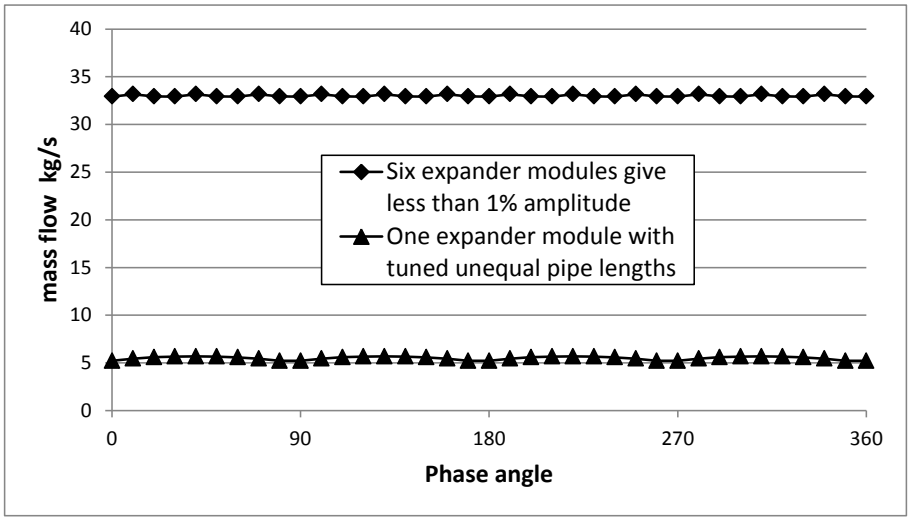

Figure 44 – Total Flows out of ND Expanders with Unequal Pipe Lengths

5.6 Nutating-disc State-of-the-Art

Studies by the author and by Joshua Sebastiampillai regarding the double-nutating-disc topping-cycle core-engine modules have revealed the strengths and weaknesses of the concept. On the positive side it offers a compact and potentially light-weight design with relatively steady inlet and outlet flows making it fairly easy to integrate with upstream and downstream turbomachinery. It may for the most part be recuperatively air-cooled, assuming it will benefit from the

development of advanced ceramic-matrix composite materials. However, the design concept still relies on poppet valves and complex sealing systems. The latter are likely to need significant R&D efforts to demonstrate the necessary reliability and durability for a commercial aircraft engine. Also, while the bearing loads may be acceptable in a normally-aspirated nutating-disc machine, the use of rolling-element bearings may not be possible when operating at the high peak pressures and shaft rotational speeds targeted for highly-turbocharged engine cycles. Current bearing technology is only expected to deliver very limited life. Other problems include the likely need for spark ignition and the probability of high oil-consumption resulting in increased particulate emissions.

The efficient nutating-disc core-engine design concepts are therefore highly dependent on further enabling technology developments in the following areas:

- Ceramic matrix composite materials
- Materials for high-temperature oil-free sealing elements
- Improved bearing materials and lubrication

While significant advances in these areas are anticipated by 2045 to support TRL6 for 2050, the pace of progress is uncertain. The current level of nutating-disc technology is about TRL3 and only TRL2 for the design described above.

It is the opinion of the author that an alternative topping-cycle design using opposed-piston and/or free-piston technology is likely to prove more attractive than nutating discs, and therefore research into those technologies should be given higher priority.

6 OTHER NOVEL COMPONENT DESIGN STUDIES

To make realistic ‘bottom-up’ performance assessments for the advanced-cycle engines it was first necessary to create models for their novel components.

These component models enabled the viability of the novel component designs to be assessed and weight estimates to be produced. However, in order to produce these models it was necessary to put the designs in a whole-engine context. Thus a preliminary ‘top-down’ estimate of the performance of an engine with the full cycle#06 combination of novel technologies was generated. As shown in Table 20 it targeted an ambitious 20% reduction in SFC relative to the reference turbofan engine. These preliminary performance figures were used for designing the nutating-disc modules and the secondary combustor.

Table 20 – Preliminary Performance for Cycle#06 Component Design

Engine Parameters	**Units**	**Top of Climb**	**Mid-Cruise**	**EOR Take-off**
Altitude	ft (m)	35000 (10668)	37000 (11278)	0
Mach Number	–	0.82	0.80	0.20
Deviation from ISA	K	+10	0	+15
Net Thrust	kN	50	33	183
Fuel Flow	kg/s	0.545	0.334	1.245
SFC	g/kN.s	10.9	10.1	6.8
TF2050 SFC for reference	g/kN.s	13.7	12.6	8.3
Re. Reference TF2050	–	-20%	-20%	-18%
Fan Mass Flow	kg/s	450	390	1020
Secondary Combustor Design Parameters (after topping cycle)				
Inlet Pressure	bar	9.04	6.03	21.0
Outlet Pressure	bar	8.61	5.74	20.0
Inlet Mass Flow	kg/s	14.1	10.1	32.9
Inlet Temperature	K	1404	1265	1453
Inlet FAR	–	0.031	0.027	0.031
Outlet FAR	–	0.039	0.034	0.039
Outlet Temperature	K	1637	1481	1671

6.1 Heat Exchangers

6.1.1 Intercooler Design

Research into aero engine intercooling systems in NEWAC and LEMCOTEC has been described in section 2.3. In the ULTIMATE project the Milestone M1.1 document [69] included a 'technology simulator' for a generic two-pass cross-flow air-cooled intercooler. Its formulas are based on the intercooler design developed at Chalmers University in LEMCOTEC. While the arrangement of the inlet and outlet ducts may be varied depending on the engine installation, the methodology to assess the heat transfer, pressure loss, size and weight of the matrix is relevant to all the intercoolers in the current study engines.

However, in the design of any heat exchanger there are always trade-offs to be made between effectiveness, pressure loss, size, cost and weight. In scoping-out the potential of the various different advanced cycles with intercooling, it was not appropriate to make detail trade-off studies to optimally size the intercoolers for each application. Thus design-point intercooler effectiveness levels and pressure losses were set based on past experience from the more-detailed studies in NEWAC and LEMCOTEC, as described in section 3.1.4. The methodology of [69] was only considered for weight estimation.

The smaller core components in intercooled engines are lighter, but previous studies have shown high-OPR intercooled engines to be heavier (and more expensive) than conventional engines. The weight increase comes not only from the weight of the heat exchanger, but also from the support structure and ducting. The author's estimate presented at the NEWAC final project review in Brussels in 2011 for the large high-OPR intercooled engine was a 15.3% weight increase. A later study at Cranfield, which optimised both conventional and intercooled engines for minimum fuel burn, predicted engine weight increases of between 16.5% and 22.3% [101]. However, ongoing improvements in heat exchanger design should reduce the weight penalty for intercooling by year-2050. Secondary combustion also reduces core mass flow and weight. Weight estimates for the current intercooled study engines are given in section 8.2.

6.1.2 Recuperator Design

Recuperators tend to be large, heavy and often mechanically-unreliable heat exchangers, so considerable efforts have been made to develop more compact, lower-pressure-loss designs with higher effectiveness. For future aero engine application, considerable research has been conducted by MTU and AUTH in the EU research programmes CLEAN, NEWAC, LEMCOTEC and ULTIMATE.

The original MTU recuperator module design using profiled tubes was proposed for a recuperated turboshaft engine for the Abrams battle tank, but this engine bid was unsuccessful. Whereas the installation of a single module in the gas turbine exhaust stream would have been satisfactory in that application, the relatively-large frontal area of the heat exchanger was a problem for the IRA turbofan engine installation. Scaling-up the module would also have added disproportionately to its weight. Therefore MTU proposed splitting-up the recuperator into eight smaller heat exchangers and arranging them at an angle to the core exhaust as shown in Figure 6. A model of a quarter of the proposed recuperator installation was built and aerodynamically tested at AUTH. The design was refined in the NEWAC programme to minimise the pressure losses associated with this installation. Subsequent research in LEMCOTEC proposed alternative designs to minimise both hot-side pressure losses and weight. In ULTIMATE a radically different arrangement was studied using a liquid sodium and potassium mix to transfer heat from the core exhaust to combustor inlet.

Since recuperated aero engines and novel recuperator designs were being researched by other partners in the ULTIMATE project, the author chose to focus on other technologies and combinations of technologies that did not include recuperation. To extract power from the ‘waste’ heat in an engine’s core exhaust, an alternative to recuperation is to add a bottoming cycle, so the less-researched potential of bottoming cycles was investigated instead. However the author’s original Excel performance model was constructed with the capability to model recuperated engine cycles.

The patent application from Klingels at MTU [17] envisaged adding recuperation to a composite cycle engine that already includes intercooling, secondary combustion and an air bottoming cycle in addition to a free-piston topping cycle. This would correspond to cycle#13, the most-complex engine cycle considered in Figure 24, except that in his case recuperation was only shown as being used to preheat some air that had bypassed the topping cycle on its way to the secondary combustor. There is no obvious merit in taking some of the exhaust heat for recuperation and some to power a bottoming cycle, though it is possible that a bottoming cycle might make use of the low-grade heat still remaining downstream of a recuperator.

6.1.3 State-of-the-Art for Heat Exchangers

Recent studies in LEMCOTEC and ULTIMATE demonstrate that significant improvements in heat exchanger design and installation are still possible [8] [34]. For light-weight, low-loss, high-effectiveness heat exchangers, reducing approach velocities and increasing inlet areas will also help. This is generally in conflict with aero engine design requirements to minimise frontal area and drag, but those problems are reduced when core flows are reduced in more advanced engine cycles. The conflict might also be resolved if the heat exchangers could be mounted outside of the nacelle and buried inside the airframe.

6.2 Combustion Systems

6.2.1 Primary Combustion Systems

Lean Direct Injection (LDI) combustion technology is preferred for the year-2050 reference aircraft engines and for all other advanced-cycle engines without pressure-rise combustion systems. However, the design of future LDI combustors cannot be predicted with certainty as very different burner arrangements are being research by NASA and in EU programmes.

Combustion arrangements in topping cycle machines vary widely, so each case must be considered on its merits. For the nutating-disc core modules, separate precombustors are proposed as described in Chapter 5.

6.2.2 Secondary Combustion Systems

For study engines without topping cycles, the secondary combustors are inter-turbine designs located between upstream and downstream turbine stages. These turbine stages may be on the same shaft system or on separate shafts not mechanically linked to each other. In the former case the combustors may more accurately be described as ‘intra-turbine’ designs, though ‘inter-turbine’ combustion is generally used to refer to either configuration. The distinction may seem academic, but it has a significant effect on the operability of the engine.

If the upstream and downstream turbines are on separate shaft systems, then when the amount of fuel provided to the inter-turbine combustor is varied, the work-split between the turbines and shaft systems will vary. For example, if the inter-turbine combustor is lit-up, the temperature and also the pressure at inlet to the downstream turbine will increase. The back-pressure on the upstream turbine will then reduce its expansion ratio and power output. Conversely, if the inter-turbine combustion would be extinguished, the expansion ratio and power output of the upstream turbine could suddenly increase. This has the potential to drive a compressor attached to the upstream turbine into surge.

This potential problem is largely eliminated if the upstream and downstream turbines are on the same shaft system or are otherwise mechanically linked. Changes in the fuel flow to the inter-turbine combustor will still change the work-split between the upstream and downstream stages, but overall the effects will largely cancel out. It will be noted that the GT24/26 industrial gas turbine has this latter intra-turbine combustor arrangement.

Florian Jacob at Cranfield University investigated inter-turbine combustion in combination with a closed-circuit S-CO_2 bottoming cycle [9]. This cycle corresponds to cycle#17 on Figure 24. There is a synergy between inter-turbine combustion and a bottoming cycle because the second combustor increases core specific power at the same time as raising the exhaust gas temperature. This improves the thermal efficiency and power output of the bottoming cycle. However, for an overall improvement in SFC, the inter-turbine combustor needs

to be located quite close to the primary combustor; preferably just a single turbine stage behind it. Thus the downstream turbines and exhaust nozzle will still have a large expansion ratio to extract useful work from the extra heat input.

The design of inter-turbine combustors has not been investigated in detail. The GT24/26 secondary combustor usually runs on natural gas and is not seen as appropriate for an aero engine. More recently the AHEAD project researched an inter-turbine combustor for an aero engine, as described in section 4.2.4.

Where the primary combustion occurs in a topping cycle, the secondary combustor may be located between the topping cycle machinery and the downstream turbines. This is the arrangement assumed for the secondary combustor in the author's engine design studies based on cycle#06.

Two Cranfield University MSc students have worked on candidate secondary combustor designs proposed by the author for the cycle#06 engine. The first study was performed by Victor Martinez Bueno and reported in his thesis [76]. Unfortunately an error resulting in the combustor being undersized was not noticed until the end of this study. His CFD models showed high exit Mach numbers and high pressure losses and predicted poor combustion efficiency. Nevertheless lessons were learned from this study and a revised design was proposed, modelled by Mirko Romanelli and reported in his thesis [78]. This second study used the performance data from Table 20 and the dimensions proposed by the author for the revised combustor shown in Figure 45. This assumes 12 exhaust pipes from the six nutating disc modules would enter the combustor axially, upstream of a forced mixer that entrains flow into the main annular vortex where it circulates before passing on to the downstream turbine.

In the absence of better weight estimates for the inter-turbine combustors in cycle#03 and cycle#18, these are assumed to have the same weight as the primary combustors in those engines.

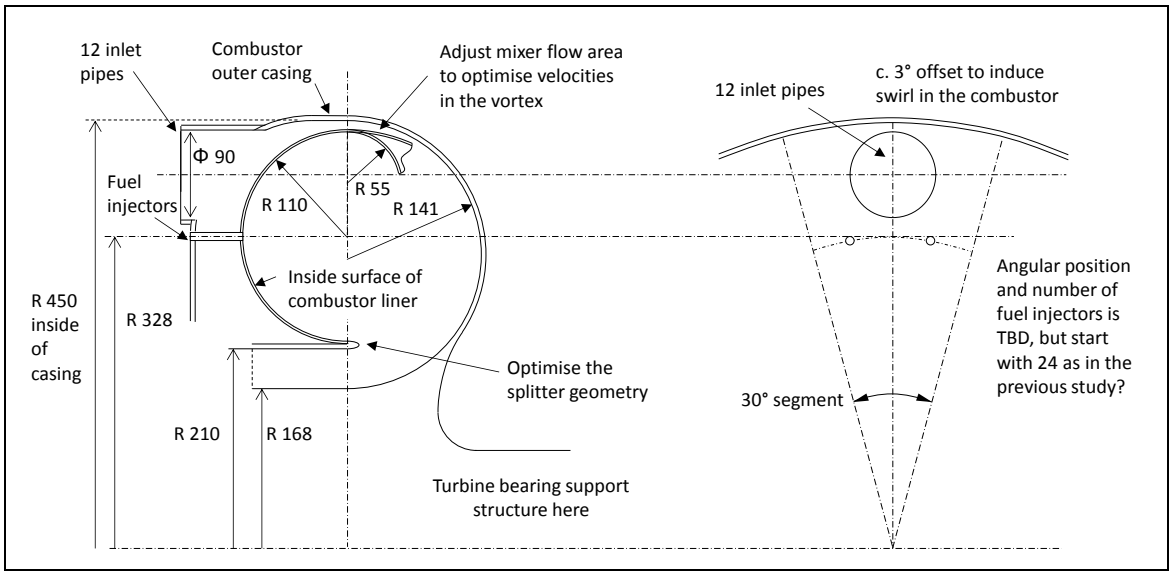

Figure 45 – Secondary Combustor Geometry
(as proposed by the author in February 2018)

The secondary combustion occurs immediately downstream of the mixer and in the main vortex, in the wake of the fuel injectors. The concept of 'oxy-poor' or so-called 'flameless' combustion was similar to that researched by Technion in the AHEAD project [75]. The basic design of Figure 45 was later modified by Mirko Romanelli to add swirl to the incoming flow and to inject some of the incoming flow into the main vortex in-between the fuel injectors and the mixer.

The front end of the secondary combustor now acts as a plenum chamber to help to smooth-out the flow through the mixer, through the combustor and into the downstream turbines. The incoming pipes would swirl the flow such that flow entering the main vortex would follow helical flow paths to enhance mixing.

Figure 46 shows some predicted temperatures for Romanelli's final design [78]. The final design reduced pressure loss in the secondary combustor, increased combustion efficiency by virtue of better mixing and a longer mixing length, and reduced the tip-bias in the outlet radial temperature profile that enters the turbine. However, the predicted NOx emissions increased on account of the longer residence time for the gasses in this larger combustor.

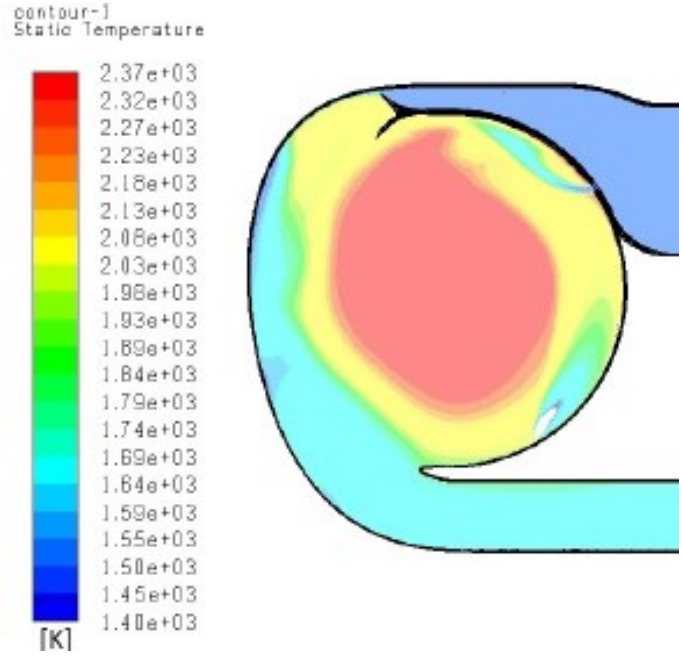

Figure 46 – Secondary Combustor Temperature Contours [78]

The basic concept of oxy-poor combustion is to minimise net NOx formation by recirculating the flow within the combustor to give a very uniform fuel-air mixture that is close to stoichiometric conditions. This means that the CO molecules will have plenty of time preferentially to scavenge oxygen from the NO molecules in order to form more CO_2. (Exhaust gas recirculation in diesel engines has a similar effect.) The combustor should then combine high combustion efficiency with low NOx emissions. This can work well in large-volume industrial furnaces giving so-called ‘green flame’ combustion, but the conditions required to make this work successfully in an aero engine are more difficult to achieve. Instead of having an average of six to ten recirculations in the main vortex, the incoming flow is limited to one or two recirculations by the smaller volume of the aero engine combustor. This results in less-perfect mixing and larger variations in fuel-air ratio in the main vortex. Aero engine combustors must also operate over a wide range of conditions with varying overall fuel-air ratios and combustion pressures and temperatures.

By adding new inlet slots, Romanelli’s final design did succeed in entraining more of the incoming gas from the topping cycle into the vortex. Therefore more

of the combustion occurred in the vortex, rather than downstream of the mixer, but this meant that much of the combustion in the vortex was occurring closer to stoichiometric conditions and with higher flame temperatures, resulting in increased production of thermal NOx, aggravated by relatively long residence times. This is in contrast to Victor Martínez Bueno's smaller-volume combustor design, where the temperatures in the vortex were generally lower and N_2O-intermediated NO generation was believed to be more significant.

So far the proposed secondary combustors have not met the original objective of 'oxy-poor' combustion, but have operated instead more like RQL combustor designs. It remains to be seen whether some further innovations, perhaps including variable geometry, might be able to get closer to the original design intent. In the meantime it cannot be claimed that the proposed secondary combustor will reduce NOx emissions. Radically different designs may need to be investigated.

The conclusion to be drawn from these observations is that the strategy of minimising NOx formation by providing a very-oxy-poor environment in the secondary combustor does not seem practical in this aero engine. Therefore the alternative philosophy of RQL combustion may need to be developed instead to deliver lower NOx emissions and enable a more compact combustor design.

6.2.2.1 State-of-the-Art for Secondary Combustion

Taken in isolation, this technology does not offer much benefit in terms of SFC. However, in combination with intercooling, recuperation or bottoming cycles, it is capable of improving overall thermal efficiency. It also has the potential to reduce NOx emissions, though that has not been properly demonstrated in these studies.

The 'oxy-poor' low-NOx combustion design philosophy does not really seem to work in the ULTIMATE aero-engine designs, so it is recommended that future design studies target RQL (rich-burn and quick-quench to lean) combustion instead to minimise NOx. Another factor that needs further research is how best

to schedule fuel-flows between the primary and secondary combustors at off-design conditions.

6.3 Open-circuit Air Bottoming Cycle (ABC)

Given the significant design and performance-modelling challenges of closed-circuit bottoming cycles, the author has only modelled open-circuit ABC designs. Anders Lundbladh [10] and Herman Klingels [17] have previously proposed ABC designs. The former proposal integrated the ABC turbine with the LP turbine and the latter proposal had a separate ABC turbine geared to the HP turbine shaft. In Figure 7 a new arrangement was proposed for integrating the ABC turbine with the LP turbine, but on subsequent investigation, it seemed that it might not be the best arrangement.

The simple stand-alone ABC system spreadsheet model has been described in Section 3.4. It was used to explore optimum pressure ratios and performance for a range of inlet conditions.

The power output and efficiency of the ABC cycle modelled in isolation, can be significantly improved by placing the ABCHX further upstream in the main-engine gas-path, between HP and LP turbine stages, rather than downstream of the last turbine stage. This has the secondary benefit of increasing the hot-side gas pressure and density in the heat exchanger, making it easier to produce a compact low-loss ABCHX design for a given level of temperature-effectiveness. A high air-side temperature-effectiveness is required to maximise the inlet air temperature to the ABC turbine, but the down-side is that this will tend to make the ABCHX larger and heavier and/or increase pressure losses on both sides.

Other factors to be considered are the ideal pressure for the air entering the cold side of the ABCHX, and the pressure ratio and efficiency of the associated upstream compression system, comprising part of the flow through the fan root section and the IP compressor.

To address all these ABC design issues, a series of parametric studies was performed using the stand-alone model to simplify the processes downstream

of the secondary combustor. Turbomachinery efficiencies and heat exchanger pressure losses were specified, with the latter taken to include the losses in the inlet and outlet ducting at entry and exit from the ABCHX. The pressure and temperature of the gas entering the HP turbine was also fixed for each study. Modelling on the air side started at ambient pressure and temperature. The air-compressor pressure ratio was set and ambient air was compressed before passing through the ABCHX and being expanded back through the ABC turbine to generate power. After the HP turbine exit flow had passed through the ABCHX, the gas was further modelled as expanding through the LP turbine.

For simplicity, unit HP turbine inlet mass-flow was specified and turbine cooling and sealing air flows were ignored. To further simplify the parametric studies, the thrust nozzle pressure ratios were set to unity so that the total power generated by the virtual ABC and LP turbines included the power needed to accelerate the air and gas through the thrust nozzles.

Initially fixed values were used for specific heat at constant pressure (Cp) and for gamma[5], but more-accurate values were subsequently input for each process to demonstrate that using fixed values had given negligible errors.

The net power generated in the modelled system provided a figure of merit for the given combination of input parameters.[6] By running the model with zero or negligible ABC air flow and no pressure losses in the heat exchanger, a baseline level of net power could be calculated. A net power increase of 50 kW per kg/s of core flow with the ABC corresponded to about 3 percentage points of thermal efficiency, or 6% reduction in SFC.

---

[5] The ratio of the specific heat at constant pressure to the specific heat at constant volume.

[6] In practice the turbines would not be expanding to ambient pressure, but would be followed by exhaust systems that provided their contributions to jet thrust. However, this would just be using the available energy in the air and gas streams in another useful way. The efficiency of the transfer of this energy into thrust through the exhaust nozzles should be slightly higher than the efficiency for power generation in the ABC and LP turbines, but the discrepancy was a minor factor when comparing the overall efficiencies of variant systems. The overall compression and expansion polytropic efficiencies were set to 90% for most of the studies.

Only sea-level static take-off cases were modelled, but logically the relative benefits for the same temperature ratios per unit turbine mass-flow would be almost identical if they had been modelled at altitude and with forward velocity. For initial studies the HP turbine inlet pressure and inlet temperature (after the secondary combustor) were fixed as consistent with the preliminary take-off performance shown in Table 20, though strictly those figures were for an EOR case. Different HP and LP turbine pressure-ratio splits were modelled and the pressure ratio of the compression system was varied together with the ratio of the air mass flow relative to the flow in the HP turbine.

To avoid modelling unrealistic designs, temperature-effectiveness levels on both sides of the ABCHX were monitored and limited to values no greater than 90% on the air side and 85% on the gas side. (These figures should give roughly equal design-difficulty on the two sides, on account of the combustion products having lower density.) Trade-offs for different effectiveness levels were also considered because high effectiveness also implied higher pressure losses and higher ABCHX weight. It was demonstrated that if the effectiveness levels were reduced to 80% on the air side and 70% on the gas side, the maximum pressure losses on both sides should then reduce from an estimated 8% to 5% or less. (To keep the models simple, the ABCHX percentage pressure losses on the hot and cold sides were assumed to be equal.)

Parametric studies using the stand-alone spreadsheet model generated some interesting and useful results, helping to optimise the cycle#06 whole-engine performance model. They showed that, in order to maximise the overall thermal efficiency for the secondary combustor exit conditions assumed, it was better to place the ABCHX downstream of the last core turbine, rather than further upstream in the expansion system. In other words; it was better to do all the work in the HP turbine and not have the LP turbine. This was an unexpected result, since moving the recuperator upstream in an LP turbine of a recuperated engine would normally improve overall engine performance. However, this did not necessarily mean that placing the ABCHX downstream of the last turbine stage would always give the lowest fuel burn, as this location will tend to make

the ABCHX relatively larger and heavier. Nevertheless, it strongly suggested that the LP turbine could be omitted and a simpler ABC turbine designed without integrating it with the LP turbine as originally proposed.

In the initial studies, the ABCHX pressure losses were fixed consistent with the upper limits on hot-side and cold-side temperature-effectiveness, typically 90% effectiveness on the cold side and 85% on the hot side. These effectiveness limits seemed reasonable given that the hot gas would be less dense than the cold air and have lower heat transfer coefficients at a given Mach number. Normally the cold side limited the heat transfer, but the hot side could be limiting when the air mass-flow was large with respect to the gas mass-flow.

As the cold-side mass flow was reduced, the heat transferred by the ABCHX reduced, and the mean temperature-difference between the hot and cold sides increased. The overall performance benefit from adding the ABC was shown to be maximised by increasing the ratio of ABC air-flow to HP turbine mass-flow, but only up to the point where the hot-side effectiveness of the ABCHX became limiting. This implied that air/gas mass-flow ratios around 100% would be optimal, as this was roughly where the limiting effectiveness switched between the hot and cold sides. However, for fixed heat-transfer coefficients, the required heat-transfer surface area would be roughly proportional to the heat transferred divided by the mean temperature difference, and this ratio could be proportional to the size of the matrix and to the pressure loss through the matrix. Since the ratio reduces rapidly as the air/gas mass-flow ratio reduces, a significant reduction in heat exchanger weight and matrix pressure loss could be achieved by modest reductions to the otherwise optimum air-side mass-flow.

For 90% maximum cold-side effectiveness, it was found that reducing the mass-flow ratio to 80% roughly halved the size of the heat exchanger matrix and matrix pressure loss. At fixed pressure loss this would reduce the net power benefit from adding the ABC by about a third, but because the pressure loss reduced when the mean temperature difference between the hot and cold sides was raised, the reduction in net power was much smaller. Considering the

shape of the curve of power increase v. mass-flow ratio it seemed likely that the fuel-burn optimum air/gas mass-flow ratio would be around 80-90%.

The stand-alone model was therefore modified so that the pressure losses varied automatically in proportion to the required heat transfer surface area, which was assumed to be in inverse-proportion to the mean temperature difference between the hot and cold sides, all other factors being equal. This avoided over-penalising the pressure losses when the ratio of ABC air flow to core flow was relatively low.

In a heat exchanger having the air inside tubes, the number of tubes increases as the ABC air mass flow increases, but the tubes also need to get longer as the mean temperature-difference reduces, and this accounts for the increasing pressure loss on both sides of the heat exchanger. However, the entry and exit losses give the tubes a minimum pressure loss even if they are very short.

Results from one of the parametric studies are given as an example. In this stand-alone model study the following conditions were fixed:

- Sea-level static ambient pressure with air inlet temperature 300 K,
- HP turbine inlet temperature 1671 K and inlet pressure 20 bar,
- ABC air-compressor pressure ratio 6,
- HP turbine pressure ratio 16,
- Polytropic compression and expansion efficiencies 90%,
- Heat exchanger pressure losses minimum 2% and maximum of 8%.

The high HP turbine pressure ratio implies that there would be no real LP turbine in this case. The exhaust gasses, having passed through the ABCHX would go directly to a core exhaust nozzle (or would be mixed into the bypass flow in the proposed reverse-flow core arrangement).

Figure 47 shows the net amount of extra power generated in this parametric study, as a function of the ratio of ABC air mass flow to core mass flow. However, increasing the ABC air mass flow implies a larger heat exchanger matrix with increased weight and pressure loss penalties.

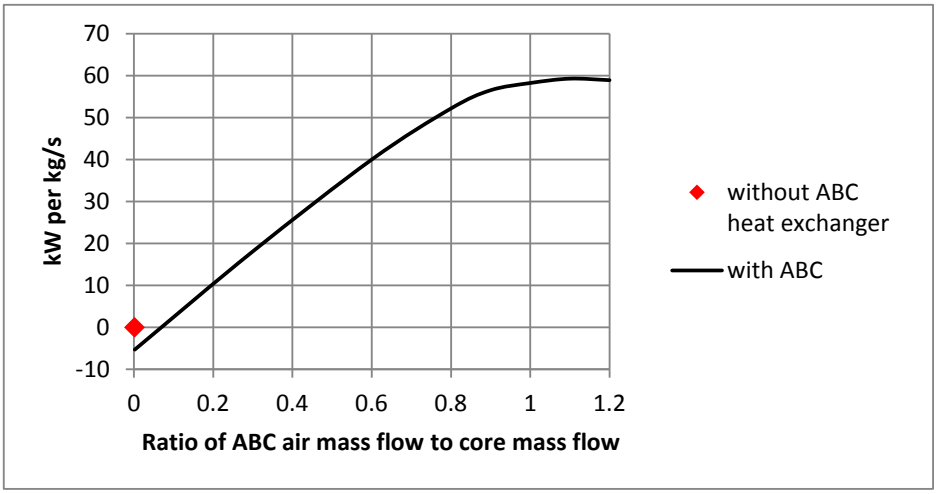

Figure 47 – Example Showing the Extra Power generated with an ABC

Figure 48 shows how the corresponding temperature effectiveness on each side of the ABC heat exchanger was assumed to vary with the mass flow ratio.

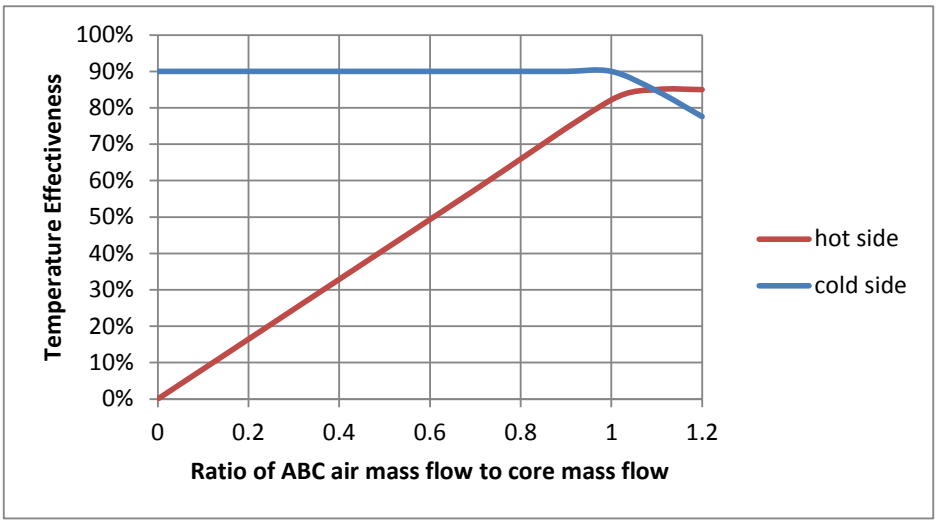

Figure 48 – Assumed ABC Heat Exchanger Temperature Effectiveness

Figure 49 shows how the hot-side and cold-side pressure losses in the ABC heat exchanger were predicted to vary in this example, which assumed the heat exchanger was sized to give maximum pressure losses of 8% when the hot and cold mass flows were equal and a minimum of 2% for entry and exit losses

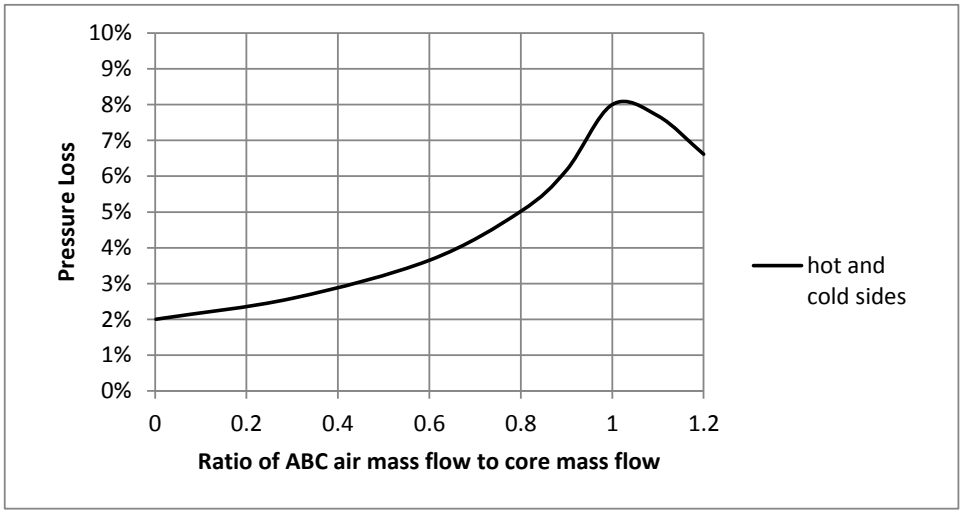

Figure 49 – Assumed ABC Heat Exchanger Pressure Losses

With very small air mass flows, the modest overall performance penalty observed in Figure 47 was to be expected, because of the small pressure losses on both sides of the heat exchanger which would not have been there if there were no heat exchanger. However, as the ABC air mass-flow was increased, the net power (the power generated by the turbines, less the power required to drive the air compressor) increased to a maximum when the air mass-flow was about 110% of the gas flow (and the thermal capacities of the hot and cold flows were roughly equal).

The overall results from these studies were informative. Given the assumptions made about how the heat exchanger pressure losses reduce with reduced heat transfer, there were diminishing returns for increasing the ABC air mass-flow much above 80% of core-mass flow. 80% was therefore taken as the initial design-point target for the air mass-flow. The extra net power obtainable from the ABC peaks at around 60 kW/kg of core mass-flow, equivalent to about 2 MW at take-off, or an improvement in SFC of 4–5%.

The simple models also showed that the results were not very sensitive to the polytropic compression and expansion efficiencies in the range 85% to 95%, though higher efficiencies did result in improved performance.

These were encouraging results, but it should be noted that the HP turbine inlet temperature was relatively high, consistent with having a secondary combustor, so it was still possible that reducing the fuel flow to the secondary combustor, or even deleting it in an engine without an ABC, might be a simpler way of improving SFC. However, the resulting reduction in core specific power would add mass-flow and weight to the core turbomachinery, so the assessment of the trade-offs can only be made using detailed engine models.

6.3.1 Conclusions from the Stand-Alone ABC Model

It had been thought that increasing the hot-side inlet temperature of the heat exchanger by shifting work from the HP turbine to the LP turbine would improve overall performance, but purely from the performance point of view it seems better to locate the ABCHX at the exit of the last turbine stage. However, this might increase the size and weight of the heat exchanger, so from the fuel-burn point of view it might still be better to locate the heat exchanger ahead of the last core-turbine stage, as shown in Figure 7. Nevertheless, based on the above observation, and also for simplicity, it was decided to model the overall performance of cycle#06 with the ABCHX located downstream of a higher-pressure-ratio HP turbine and without the LP turbine.

The results were surprisingly insensitive to compressor pressure ratios in the range 4 to 8. In the real engine the ABC air would either be bled-off from the IP compressor, or taken from IP compressor delivery upstream of the intercooler, but the latter arrangement is simpler. Based on the author's previous high-OPR intercooled engine studies, a 'fan plus IP compressor' pressure ratio of around 4 to 8 upstream of the intercooler, at high power conditions, would also be close to the optimum for intercooler placement, as indicated by figure 14 in [30].

Since the original concept was to power the IP compressor from the combined output of the ABC turbine and the LP turbine, any shortfall in the power required to drive the IP compressor would now need to be made-up by power taken from the HP turbine and/or the nutating-disc modules. Therefore the whole-engine performance models for all the cycles that included the ABC were configured to

drive the IP compressor from the last core turbine (either HP or LP) and to add the power from the ABC to the power from that turbine.

6.3.2 State-of-the-Art for Air Bottoming Cycles

The combination of an ABC and secondary combustion seems promising, offering up to 5% reduced SFC. The heat exchanger technology requirements are similar to intercoolers in terms of pressure capability and to recuperators in terms of temperature capability. Apart from the heat exchanger, no new technology is required to implement an ABC, so this is seen as a low-risk development that could be introduced well ahead of year 2050. However, to realize the full potential benefits, technology for an efficient low-NOx secondary combustor would also need to be developed, which may be more challenging.

It is worth noting that integrating a bottoming cycle in a buried core-engine installation for a distributed or hybrid-electric propulsion system may provide additional benefits.

6.4 Closed-circuit Bottoming Cycle

Closed-circuit bottoming cycles have not been modelled by the author because when comparing the author's results with Jacob's in [9], the ABC arrangement seems a simpler option that more than matches the closed-cycle performance in an aero engine. However, if future engines should switch to using a cryogenic fuel, the balance might shift in favour of a closed-circuit arrangement.

Using kerosene to cool the closed-circuit supercritical CO_2 working fluid close to its critical temperature (31.1°C) is not very practical because it has a limited heat-sink capability that is also wanted for cooling engine oil. However, with liquid hydrogen (LH2), liquefied natural gas (LNG) or pure liquid methane, the fuel would have spare capacity to help cool the CO_2. The larger temperature differential enables a relatively compact 'pre-cooler' heat exchanger to be used. This reduces the need for bulky air-cooled pre-coolers, though to maximise the overall performance it is likely that an air pre-cooler would still be used for the first stage of cooling, where the temperature gradients are more favourable.

To further improve performance of the cooling system, the author proposed an innovative arrangement to increase the cooling capability of the hydrogen while avoiding the risk of freezing CO_2 in the heat exchanger. The liquid hydrogen is first compressed to a supercritical pressure, which raises its temperature closer to the CO_2 freezing point. The hydrogen then enters the pre-cooler, but not in a counter-flow arrangement, so as not to freeze the CO_2. It is then expanded in a small turbine or positive displacement device. The power extracted may be used to drive the hydrogen compressor. The pressure of the hydrogen falls, but remains high enough to be injected into the combustion chamber. However, the temperature of the hydrogen also reduces, enabling it to be used a second time to cool more CO_2 via a further set of passages in the heat exchanger. To further protect the CO_2 from the risk of freezing, a valve enables some of the fuel to bypass the heat exchanger when a sudden increase in fuel flow is demanded.

The concept was developed by Mikel Beretens in his Cranfield University MSc study [63]. The schematic diagram in Figure 50 shows typical inlet and outlet temperatures (but the intermediate CO_2 temperature of 310 K on this diagram is incorrect).

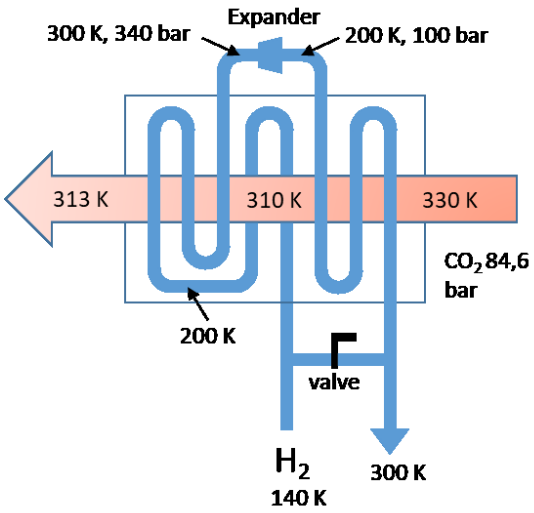

Figure 50 – Cryogenic Heat Exchanger for maximum cooling of CO_2 by H_2

Incorporating a catalyst in the hydrogen lines in the heat exchanger to convert up to 75% of low temperature parahydrogen isomer to orthohydrogen could also

significantly increase the potential to absorb heat. Nevertheless the relatively low engine fuel mass flow, even for a 100%-hydrogen-fuelled engine, still limits the overall cooling potential of the cryogenic pre-cooler.

6.5 Transmission Systems for Topping and Bottoming Cycles

Nutating disc modules can have bevel gears at their compressor ends that connect via ‘radial’ drive shafts to a bevel gear on the main turbine shaft, as shown schematically in Figure 2. However, alternative arrangements could also be considered.

An MSc project undertaken at Cranfield by Olatz Cánovas Ahedo [137] provided insights into potential transmission systems for linking a high-speed supercritical CO_2 turbine to the lower speed LP system of a geared turbofan engine. This was determined to be the most efficient means of utilising the extra power generated by a bottoming cycle. A Matlab preliminary design tool for sizing and estimating the weight and efficiency of the required reduction gearbox was produced as part of that project.

A similar arrangement might be used with the ABC turbine, particularly if it is mounted in the tail-cone of an engine with a conventional ‘straight-through’ core. In this case however, the rotational speed of the ABC turbine will be lower than the S-CO_2 turbine as it has significantly higher non-dimensional flow.

A design study of alternative ABC turbine and transmission arrangements is one of the recommendations for further work noted in section 10.3.

7 PERFORMANCE ASSESSMENT OF YEAR-2050 ENGINES

This Chapter reviews the year-2050 aircraft requirements and the whole-engine performance modelling using the spreadsheet described in section 3.1. It covers the study of scale effects on engine performance, studies of alternative cycles including the selected engine cycle (cycle#06) with intercooling, secondary combustion and topping and bottoming cycles. The sensitivity of performance results to component efficiency assumptions is also investigated to provide an indication of the uncertainties inherent in the performance analysis.

Not all of the originally proposed advanced cycles have been modelled to the latest set of thrust requirements, but section 7.6 tabulates performance for the engines identified in Figure 24 and Figure 25 as cycles #01, #02, #03, #06 and #18. The last of these, combining intercooling and inter-turbine combustion is clearly not an attractive option because its SFC is worse than the simply intercooled engine cycle#02 and it is not much lighter. However, it was an intermediate step to modelling cycle#03 that adds the ABC and shows a benefit. Cycle#06 has the best overall performance, but is also the cycle with the greatest uncertainty.

7.1 Year-2050 Aircraft and Engines

The ULTIMATE project has provided a framework for predicting credible levels of performance for aircraft and engines that could be entering service in 2050. Aircraft performance studies undertaken by BHL were disseminated in [11], based on the results in ULTIMATE deliverable D2.1 [12].

These studies included two advanced ‘tube and wing’ configured aircraft that have provided thrust requirements for more detailed engine design studies and have facilitated performance assessments over complete flight missions. The two airframes were an ‘intra-European’ aircraft with twin open rotor powerplants and an ‘intercontinental’ aircraft with two turbofan engines. However, the revised thrust requirements were not defined in time for the initial engine

studies, so the reference turbofan engine thrusts were taken from the previous Framework 6 EU research programme NEWAC [28] [29].

Factors influencing the choice of propulsor configuration include: initial cost, maintenance cost, weight, propulsive efficiency, nacelle drag, noise, installation and reverse thrust requirements.

Reverse thrust is a requirement for most commercial aircraft because it provides an effective means of stopping them on icy runways. Turboprops and open rotor engines with variable-pitch blades can provide reverse thrust at relatively little cost or weight penalty, but conventional thrust reverser designs for large turbofan engines come with significant penalties. They add cost, weight and drag, and are a disincentive to the development of engines with larger fans for increased propulsive efficiency. In this study it is assumed the year-2050 turbofan engines would have variable-pitch fans with the capability to provide reverse thrust if needed. All the engines are modelled with the same low cruise specific thrust that ULTIMATE industry partners considered likely to be feasible by 2050. Ground clearance is a possible restriction on fan diameter for under-wing mounted engines, but no constraint is applied in the author's studies because the thrust requirements for long-range aircraft in 2050 should be significantly reduced by airframe and engine weight savings and overall efficiency improvements reducing fuel load and take-off weight.

These design studies review combinations of core engine technologies to identify synergies between them. Engine performance is compared at typical mid-cruise, max climb and max take-off conditions. Consistent rules are applied for component efficiencies, temperature limits and turbine cooling flows as described in the methods section 3.1. This section compares the performance of alternative engines for 2050 EIS. It is assumed they will still run on kerosene or a drop-in replacement bio-fuel, but the use of different fuels could well affect future engine designs. The potential benefits of cryogenic fuels are discussed in section 10.3.2.

A significant observation from the ABC component design studies for the cycle#06 engine concept was that the original engine architecture proposed in Figure 2 and Figure 26 could be simplified without losing engine performance.

Unlike two-stroke diesel engines, where inlet and exhaust ports are both open at the same time, the nutating disc core modules with their non-return valves can accept a compressor inlet pressure that is lower than their expander outlet pressure. The compressor can have a higher pressure ratio even when it is only the same size as the expander. This advantageous modification allows the centrifugal HP compressor shown in Figure 2 and Figure 26 to be omitted, provided that the IP compressor delivery pressure would not be too low. It also means that more of the power generated by the nutating-disc expanders can be used to drive the nutating-disc compressors, reducing the time-averaged power left-over to be exported to the rest of the engine. This power might be transmitted by the originally proposed double-bevel-gear arrangement shown in Figure 26 or by other arrangements considered in section 6.4.

A further simplification, suggested by the ABC study in section 6.3, has been to increase the pressure ratio of the core HP turbine (which ultimately drives the fan) and eliminate the core LP turbine originally proposed to be integrated with the second-stage of the ABC turbine. In this case the HP turbine exhaust, after passing through the ABCHX, would discharge directly into the bypass duct, as would the ABC-turbine exhaust flow. This would originally have meant that the ABC turbine alone would be driving the IP compressor, but the ABC turbine cannot produce enough power to do this, given that the IP compressor air flow is more than twice as large. In the example given in section 6.3, for unit HP turbine mass flow, the ABC turbine generates 272 kW and its share of the compression system uses 193 kW. In a real engine the power to drive the fan root stage would come from the HP turbine and the nutating disc modules, rather than from the ABC turbine. The fan root contributes 10-15% of the LP compression work, so the IP compressor power requirement is about 169 kW, or 62% of the ABC turbine output. The remaining 38% (103 kW) is not enough to drive the rest of the IP compressor, which would need about 211 kW per unit

HP turbine mass flow to drive it. This was one reason why it was originally proposed to boost the ABC turbine's power output by combining its last stage with the single-stage LP turbine downstream of the ABCHX. This LP turbine could have made-up the power shortfall, which, factored-up by the HP turbine mass flow at take-off, amounts to about 3.6 MW.

However, rather than retaining the original design concept illustrated in Figure 6.2, the preferred solution now is to drive the IP compressor directly from the HP turbine and nutating-disc module, and to use shaft power transfer to add-on the power from the ABC turbine. It seems reasonable to assume that efficient power transfer between different shafts will be possible in the 2050 timeframe. Such a system would help to match off-design power demands and might be needed anyway to improve engine operability and transient performance.

7.2 Year-2050 Reference Brayton-cycle Turbofan

In this initial Excel performance model for the year-2050 reference engine the stream-tube thrusts were fixed at three key flight conditions. These thrusts were based on those used in the previous EU research programmes VITAL and NEWAC for a long-range twin-engined aircraft [29] of around 240 tonnes maximum take-off weight. The thrust requirements and installation details are shown in Table 21. Note take-off performance is quoted for a hot-day end-of-runway case, so the static take-off thrust would be higher.

Table 21 – Initial Long-range Aircraft Thrust Requirements (per engine)

Parameter	Mid-Cruise	Max Climb	Max Take-off
Altitude (ft)	35,000	35,000	0
Altitude (m)	10,668	10,668	0
Mach number	0.82	0.82	0.25
Deviation from ISA (K)	0	+10	+15
Net thrust (kN)	49	67	253
Power offtake (kW)	260	260	260
Intake pressure recovery	0.997	0.997	0.997

The reference engine configuration is a conventional Brayton cycle turbofan with its component efficiencies, materials, OPR and operating temperatures projected forwards to year 2050 entry into service as described in section 3.1.1. The specified component efficiencies create overall engine performance consistent with the recommendations of ULTIMATE industry partners in [64]. Similar to the Rolls-Royce UltraFan® engine in Figure 23, the reference turbofan has the following key features:

- A geared variable-pitch fan with a high-speed booster and LP turbine
- Fixed-area separate-jet exhaust nozzles
- An all-axial HP compressor driven by a two-stage HP turbine
- Cooled cooling air for cooling the HP system
- High OPR and very low specific thrust, giving bypass ratios of over twenty

Aircraft accessory power was assumed to be taken from the HP spool, but no compressed air was supplied to the aircraft. (For scaled engines the thrusts and power offtakes at each condition are scaled by a common thrust scale factor.)

The resulting performance that was modelled for the initial reference Brayton-cycle turbofan engine for 2050 entry into service is summarised in Table 22.

Table 22 – Original Reference Year-2050 Turbofan Performance

Parameter	Mid-Cruise	Max Climb	Max Take-off
TET (K)	1580	1890	1950
T3 (K)	880	992	1063
OPR	64.4	75.0	62.0
HP compressor ratio	20.0	25.9	23.2
Fan bypass pressure ratio	1.33	1.43	1.34
Bypass ratio	20.7	20.4	20.0
Specific thrust (m/s)	72	95	157
SFC (mg/N.s)	12.9	13.9	8.7
FHV (MJ/kg)	42.797	42.797	42.797

The design-point figures match the thrust requirements of Table 21 and the general consensus on projected technology developments provided by the ULTIMATE consortium industry partners in ULTIMATE deliverable D 1.1 [64]. Note the jet-fuel specification minimum fuel heating value (FHV) was used to calculate the SFC figures.

Base-level polytropic efficiencies were specified at the three flight conditions given in Table 21, starting with the mid-cruise case and applying the efficiency deltas given in Table 10 together with the scale corrections to HP compressor and HP turbine efficiencies to account for tip-clearance effects, as described in section 3.1.2. Since component designs are assumed optimised for the mid-cruise condition, they are sub-optimal at top of climb and at take-off. These efficiency deltas provide performance consistent with the thrusts and cycle temperatures given in Table 21 and Table 22 and with performance data quoted in [64]. The basic HP turbine efficiency was assumed not to vary with the high-power cruise, climb and take-off flight conditions, but the HP turbine and HP compressor efficiencies did change when the core was physically scaled.

The fan root section and IP compressor were modelled as a single component referred to as the LP compressor (LPC).

The off-design component efficiency penalties in the reference turbofan model make the core thermal and overall efficiency for top of climb and take-off worse than at mid-cruise. They account for the worsening SFC at the high thrust end of the altitude SFC loop as shown in Figure 51. The fan and compressor off-design efficiencies reduce at top of climb because of their high inlet Mach numbers, which are a consequence of minimising weight by under-sizing the components for this ‘corner of the envelope’ condition where relatively little fuel is burned. Between the mid-cruise and max climb points, parabolic variation in the component efficiency deltas was assumed in order to plot the ‘SFC loop’.

Fan efficiency at climb and take-off might be slightly improved by using variable-area exhaust nozzles, but they were not modelled for the reference turbofan.

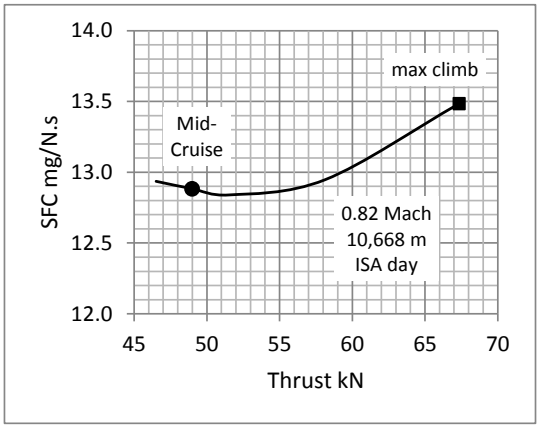

Figure 51 – SFC Loop for the Full-scale Reference Turbofan

The cycle temperatures and overall pressure ratios may appear to be only a little more aggressive than those targeted in LEMCOTEC for 2025-2030 entry into service, but there are important differences in the core engine designs. The ULTIMATE reference engine assumes ceramic matrix composite turbine stator blades and improved turbine annulus sealing that greatly reduces the required secondary air system flows. The deletion of film cooling in the HP turbine statics improves aerodynamic efficiency. Restricting increases in OPR and T_3 saves cost and weight and maintains more respectable blade heights to maximize HP compressor and turbine efficiency. Another benefit of restricting OPR and TET is that it avoids the combination of very high combustor inlet pressures and temperatures that would tend to increase flame temperatures and NOx emissions at take-off, even with advanced lean-burn combustor technology.

Before studying more advanced cycles, the reference turbofan was investigated to confirm that its cycle had been set up to give optimal performance. Figure 52 shows the effect of varying fan bypass pressure ratios, assuming nozzle areas are held constant between the cruise, climb and take-off cases. As design-point changes are being considered here, the component efficiencies were held constant at each condition. It is clear that a fan bypass pressure ratio of 1.33 at mid-cruise gives very close to the optimum SFC at all three plotted conditions.

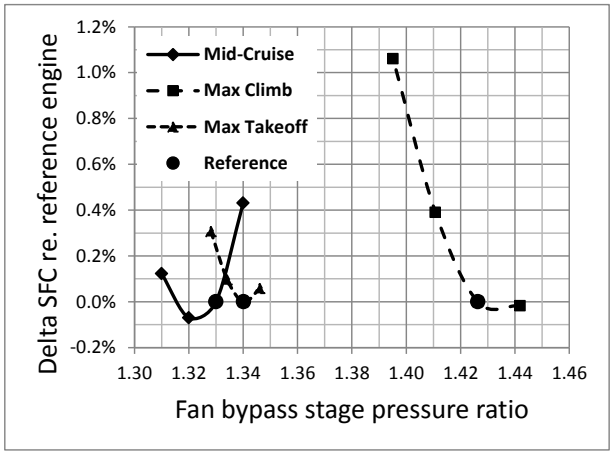

Figure 52 – Effect of Fan Pressure Ratio on SFC

Fan bypass pressure ratios at or very close to these figures were used for all the turbofan models, since they all targeted the same mid-cruise specific thrust. The optimisation study was not systematically repeated for the other cycles, but their exhaust jet velocity ratios were checked to ensure that their matching had remained close to the optimum for best cruise SFC.

Because the reference engine is assumed to have a variable-pitch fan and also variable stator vanes on its IP compressor, it should be possible to vary the work-split between the core and bypass streams. Figure 53 shows how OPR and TET at the mid-cruise design point might be traded-off against each other. Assuming the component efficiencies stay constant when compressor pressure ratios change, the mid-cruise SFC hardly varies during this trade-off, as shown in Figure 54.

Constant component efficiency may be a reasonable assumption for small changes, but it may not be a reasonable assumption over the full range of compressor pressure ratios shown in Figure 53. The IP compressor's peak efficiency and off-design variation will depend on its detail design, the number of variable stages and how the variables are operated in this variable-cycle engine.

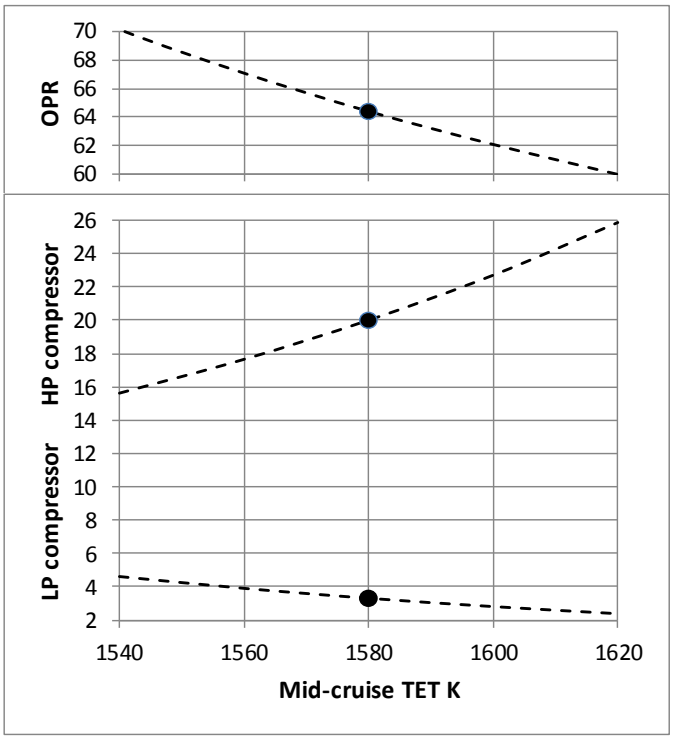

Figure 53 – Effect of Fan and LP Compressor Work-split on Compressor Pressure Ratios at Cruise assuming Constant Efficiencies

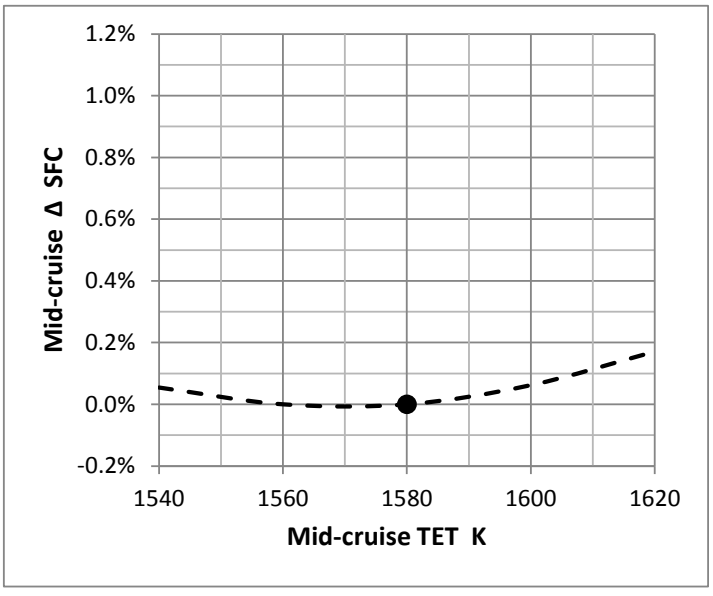

Figure 54 – Effect on Mid-cruise SFC of Varying the Work-split for the Fan and LP Compressor, at Constant Component Efficiency

Small variations in work-split could be used in practice to optimise the overall compression efficiency throughout the flight envelope. Figure 55 shows the working line for the altitude SFC loop and how the mid-cruise working point could be repositioned along the dashed line by changing the trade-off between OPR and TET. The selected matching for cruise gives performance consistent with [64] and implies a particular schedule for the IP compressor variable vanes.

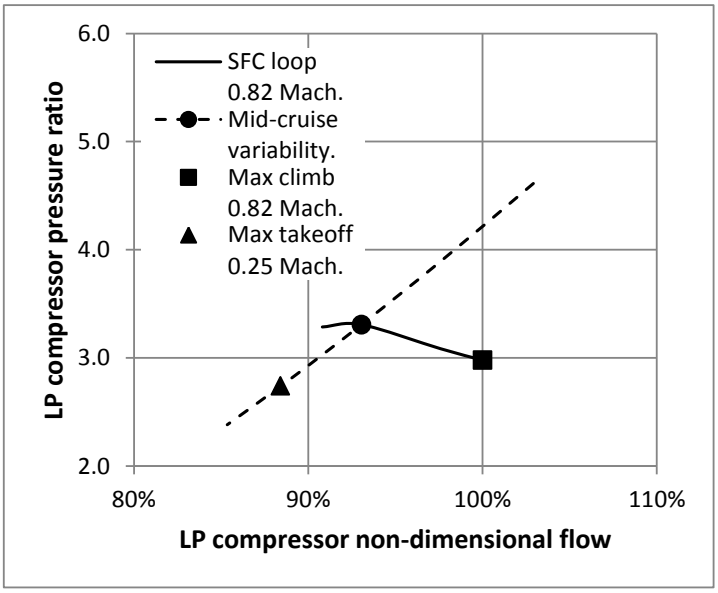

Figure 55 – Reference Turbofan LP Compressor Altitude Working Line showing the Effect of Varying the Fan and LP Compressor Work-split

Thermal efficiency in the Brayton cycle tends to be maximised by increasing OPR and TET, but higher OPR reduces HP compressor last-stage blade-height, and higher T_3 and TET require increased cooling air flows. Thus it is not obvious that maximising T_3 and TET will always give the best SFC. However, Figure 56 shows that for the component efficiency and cooling technology levels assumed for the reference turbofan, SFC is minimised by maximizing both T_3 and TET at take-off. Limiting T_3 also limits OPR, and since all the engines in this study are designed for the same cruise specific thrust, varying the core mass flow also varies the bypass ratio. Bypass ratio is increased by increasing TET, or by reducing T_3. Reducing TET or T_3 increases the HP compressor last-stage blade-height, improving HP compressor efficiency and slightly increasing OPR

for a given T_3. Figure 57 shows the effects of reducing the max take-off T_3 and TET on the reference turbofan mid-cruise OPR and bypass ratio.

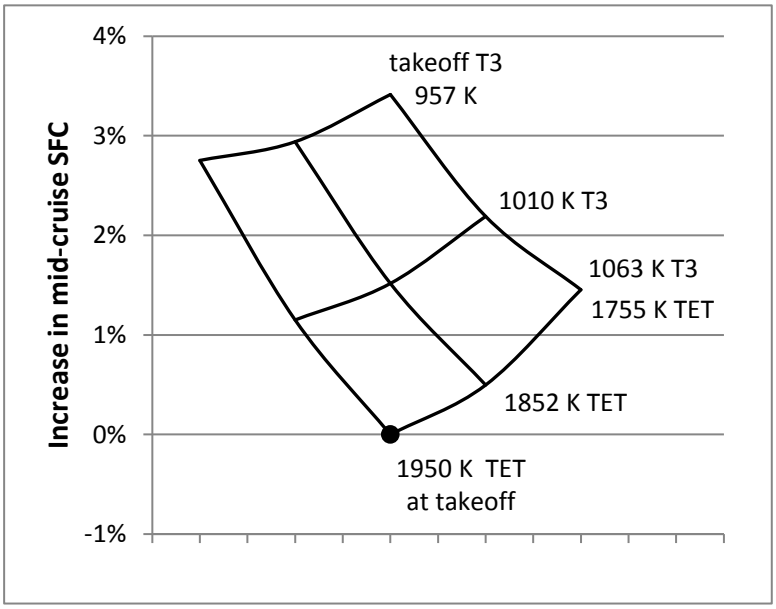

Figure 56 – Effect on SFC of reducing Hot-day Take-off TET and T_3 on the Reference Engine at Mid-cruise

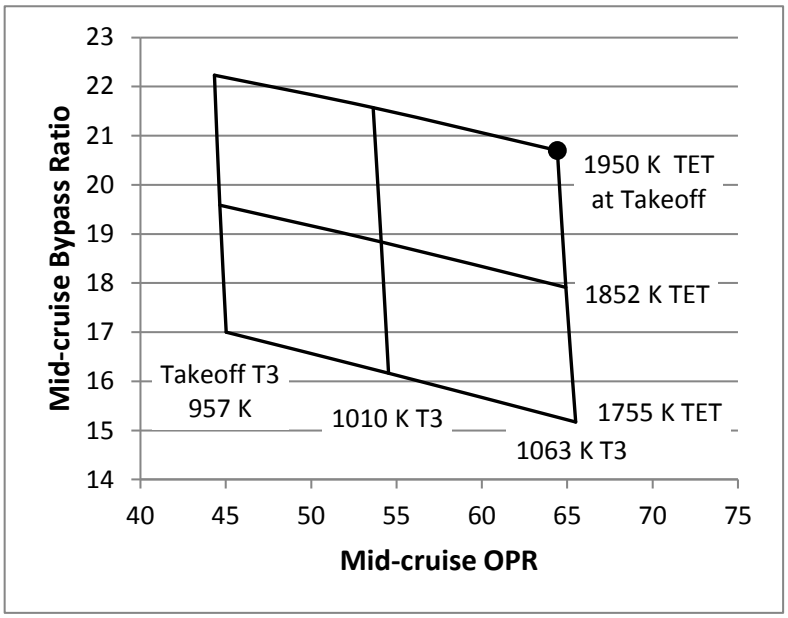

Figure 57 – Effect on OPR/BPR of reducing Hot-day Take-off TET and T_3 on the Reference Engine at Mid-cruise

Note the high-OPR engine cycles that have the highest take-off and climb T_3 temperatures need to cool the CCA at take-off and climb to 900 K, as do the intermediate OPR cycles with 1010 K T_3 at hot-day take-off, though in this case less CCACA mass flow is needed. However, the lowest OPR and T_3 cycles only need to pre-cool the CCA air at take-off conditions. These cycles do not need to use any CCACA at the ISA day mid-cruise condition because T_3 remains below 900 K. The mass flow of CCACA in the CCA heat exchanger is regulated according to the amount of pre-cooling required and the heat exchanger is sized to meet the max hot-day take-off cooling requirement.

7.3 Consequences of Reduced Thrust Requirements

In developing models for advanced cycle engines it is clear that the theoretical benefits of higher core specific power and increased overall pressure ratios must be offset by reductions in core component efficiency and by increases in secondary air flows consequent upon the scaling-down of core turbomachinery. Aircraft are also becoming aerodynamically and structurally more efficient, so for a similar numbers of passengers, design payloads and ranges, future aircraft will have lower take-off weights and lower thrust requirements, compounding these problems for aircraft-engine designers. Therefore the author's first studies addressed the effects of scaling on component and whole-engine performance.

The study of scale effects became the chief topic of the first conference paper prepared by the author for ISABE 2017 [97]. The paper compares scale effects on conventional and intercooled geared-turbofan engines. In preparing that paper the main efforts were devoted to improving the Excel performance models and their modelling assumptions. Feedback from co-authors to the paper encouraged the author to revise most of the original scaled performance by scaling the customer power offtake by the engine thrust scale factor. Originally the power offtakes were kept constant because it was assumed that the major power demand would be for the ECS and the thrust reductions would be a consequence of having more efficient and lighter-weight aircraft and engines. However, the range of thrust scaling considered, from 100% down to

25% made the power offtake from the smaller engines unrealistically high, so the parametric studies were reworked with scaled power-offtakes. While the Excel models had the capability for customer bleed-air offtake, no bleed air was extracted in these studies, assuming that by 2050 all the engines would be zero-bleed with the ECS and airframe anti-icing electrically powered.

In estimating scaled engine performance three factors were taken into account:

- Scale correction to HPC polytropic efficiency
- Scale correction to HPT polytropic efficiency
- Scale correction to HPT cooling and sealing air flows

Methods adopted to account for these effects are described in sections 3.1.2 and 3.1.3. The mass flow for the cooling air for the cooled-cooling-air system was also adjusted to limit the cooling air temperature for the HP turbine to 900 K at all conditions.

7.3.1 Scale Effects on the Year-2050 Reference Turbofan

Figure 58 shows the effect of thrust scaling on mid-cruise SFC, when cruise, climb and take-off thrusts are scaled pro rata. It also shows the effects of reducing T_3 and TET on engines having different thrust scales. Specific thrust is held constant at the mid-cruise condition, so total engine mass flow is proportional to the thrust.

The ratio of CCA mass flow to core mass flow increases as the TET increases and as core mass flow reduces, as shown in Figure 59. The ratio also increases when T_3 reduces because this also reduces the core mass flow and because T_{grel} increases when less work is demanded of the HP turbine. It is assumed that reducing T_3 at climb and take-off does not reduce T_c, but as T_3 reduces, the required CCACA mass flow reduces instead. Figure 59 also shows how the HP compressor last-stage blade-height varies as thrust is scaled. Core mass flow and HP compressor last-stage blade-height reduce as the thrust requirements reduce, and as TET increases. Conversely, the core mass-flow and the HP compressor last-stage blade-height increase when T_3 and OPR increase.

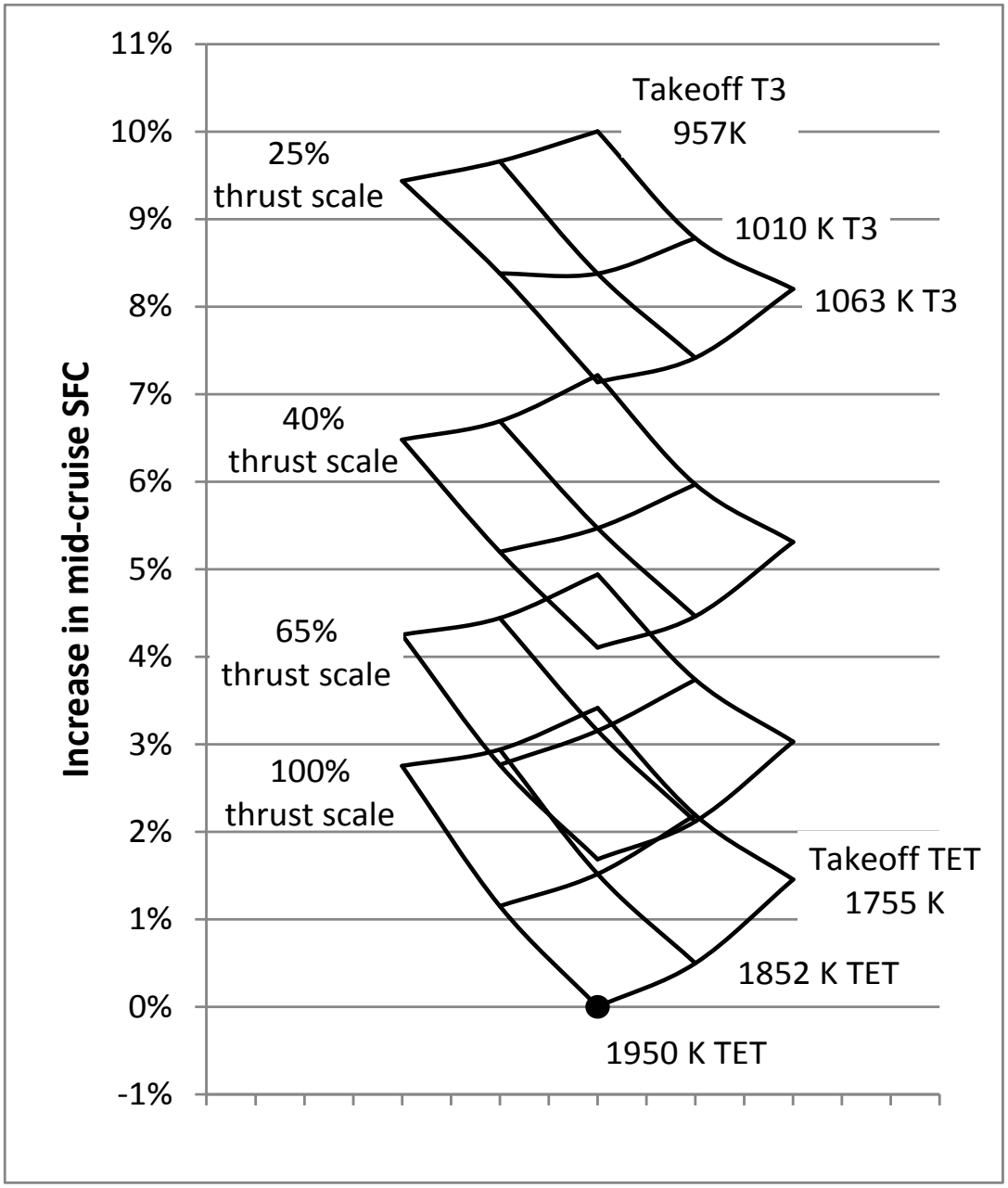

Figure 58 – Effect on Mid-cruise SFC of Scaling the Reference Engine for Various Hot-day Take-off T_3 and TET Temperature Limits

Smaller blade heights reduce compressor efficiency, reducing OPR for a given T_3 as shown in Figure 60. The combined effects of reduced HP compressor and turbine efficiency, reduced OPR and the need for more cooling air, mean that the core thermal efficiency and specific power tend to reduce as thrust reduces.

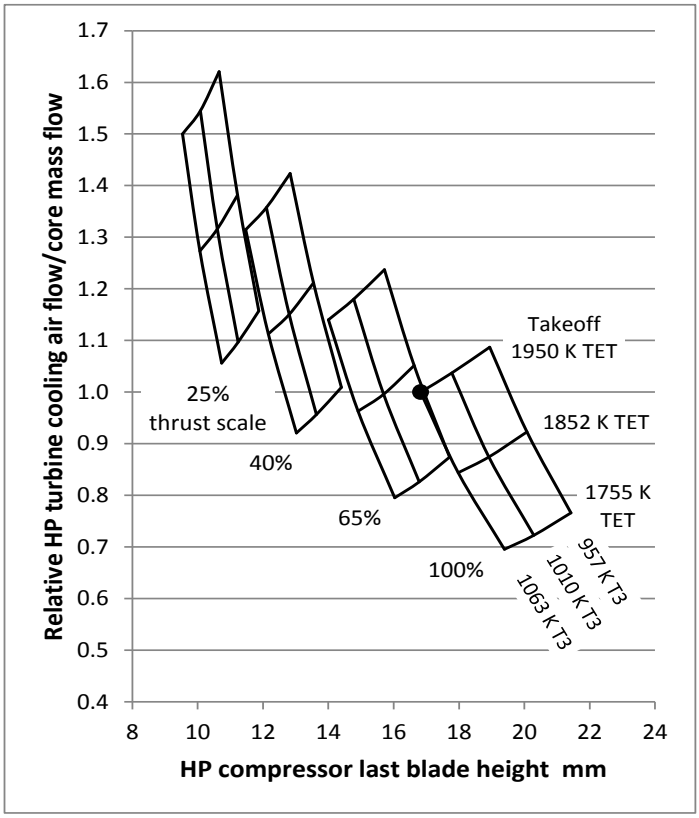

Figure 59 – Effect of Scaling on HP Cooling-flows and Blade-height for the Reference Engine, v. T_3 and TET Limits at Hot-day Take-off

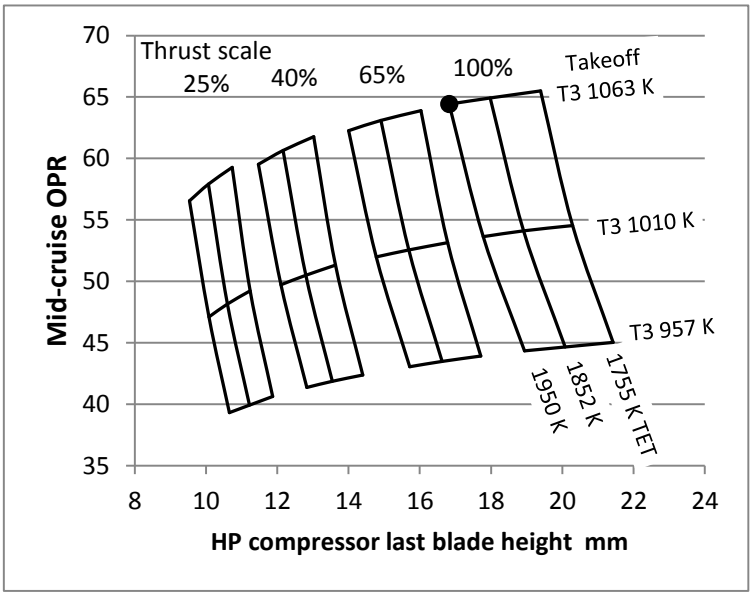

Figure 60 – Effect of Scaling on OPR and HP Compressor Blade-height v. Reference Engine Hot-day Take-off T_3 and TET

Figure 61 shows how bypass ratio varies (roughly in inverse proportion to the scaled core mass-flow at fixed thrust and fixed specific thrust).

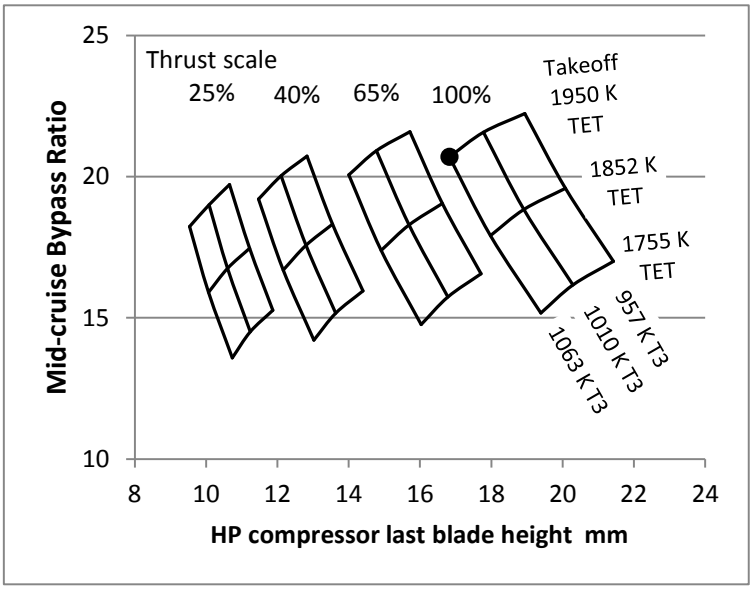

Figure 61 – Effect of Scaling on BPR and HP Compressor Blade-height v. Reference Engine Hot-day Take-off T_3 and TET

7.3.2 Scale Effects on High-OPR Intercooled Engines

In intercooled turbofan engines, part of the fan bypass air-flow is used to cool the intermediate pressure (IP) compressor delivery air before this enters the HP compressor. Intercooled engines can have the same geared fan arrangement as Figure 23, but with intercooler modules positioned as shown in Figure 5. However, in detail, these intercooler modules may instead adopt the two-pass cross-flow arrangement proposed in [130]. Their spent cooling air is assumed to be ducted to a separate variable-area exhaust nozzle, or nozzles, rather than being mixed back into the main bypass duct.

The reverse-flow core and mixed exhaust arrangement of Figure 7 has not been modelled explicitly, though it has potential to reduce noise and improve SFC and fuel burn, for both conventional and intercooled engines. The potential benefit of this architecture is instead accounted for by the higher compressor and turbine efficiencies that are expected from reduced hub/tip ratios.

The NEWAC project showed that high OPR intercooled cores, or intercooled and recuperated cores, should reduce SFC and NOx emissions. However, the required heat exchangers would add significant weight and drag to such propulsion systems, offsetting much of the potential fuel burn benefit [29]. Some rig testing has been conducted on potential intercooler geometries and installations [138] [139] [140] [141] and [142], but intercooling has not yet seen full-scale engine demonstration in gas-turbine aircraft engines.

Intercooling, like recuperation, inter-turbine combustion and added topping and bottoming cycles, has the potential to improve thermal efficiency, but these new technologies also tend to increase core specific power and reduce core mass flow, tending to give smaller and less efficient core components and lower transfer efficiency. Turbine cooling also gets more difficult as engine cores get smaller. The core-size-dependent performance penalties become increasingly significant with the development of more aerodynamically efficient and lighter-weight aircraft having lower thrust requirements. Intercooling therefore is most attractive for the large aero engines typically used on long-range aircraft.

In this study, using Excel performance models, the effects of engine thrust and core size on performance for intercooled engines are compared with those for the conventional engine cycles reported in section 7.3.1. Larger intercooled engines are shown to offer 3–4% SFC improvement relative to conventional cycle engines, while smaller engines may only realize half of this benefit. The study has provided a foundation for later investigations of more complex cycles.

Intercooling reduces compression work by reducing the inlet air temperature for the HP compressor and the volume flow rate of the air passing through it, enabling higher OPR without raising HP compressor delivery air temperatures to very high levels. It also reduces annulus cross-section areas in the HP system, saving some weight, but by reducing blade heights it also reduces core HP-component efficiencies.

Small blade height at the back of the HP compressor was a major issue for intercooled engine designs in the NEWAC programme. The original three-shaft

study engines had fans directly driven by the low-speed LP turbines via high-torque shafts. The LP and IP system shafts passed through the central bores of the HP spools, imposing minimum bore diameters and limiting HP rotational speeds. Thus the HP turbomachinery could not be scaled down very much in diameter and it needed to have higher hub/tip radius ratio blading, giving much smaller blade heights and reduced component efficiencies.

This problem was alleviated in a later NEWAC study by having a geared fan driven by a high-speed turbine. The lower torque and smaller diameter shaft also drove the IP compressor or ‘booster’, eliminating the need for a separate IP turbine and its shaft. This enabled a faster-running smaller-diameter HP system with increased blade heights, lower hub/tip radius ratios and notably improved compressor efficiency [143].

In the more recent LEMCOTEC programme a reverse-flow-core intercooled turbofan was investigated [38]. This arrangement is shown schematically in Figure 7. By placing the fan, IP compressor and turbines in front of the HP compressor, the HP system no longer needs to have other shafts passing through it [39]. HP compressor efficiency is improved and the optimum OPR is increased, but following reassessment of the exhaust mixer performance and ducting losses it was concluded that the overall improvements in SFC and fuel burn from this architecture were only about one per cent [18].

The reverse-flow-core arrangement is also an option for other novel cycles with core components that may not integrate so well into the more conventional straight-through-flow and front-fan turbofan engine layout. However, ongoing development of improved materials for discs and shafts may reduce the small performance benefit that the reverse-flow-core arrangement currently offers. Nevertheless some advantages are still seen for a mixed exhaust arrangement and mounting the intercooler at the aft end of the engine. In the reported performance studies it has been assumed that, in year-2050, in one way or another, small cores would not be penalised by large LP-shaft diameters.

Previous studies of intercooled turbofan engines have shown that positioning the intercooler relatively early in the overall compression system gives better SFC [143] [144]. Thus all the high OPR intercooled engines modelled have high-pressure-ratio HP compressors driven by two-stage HP turbines. Intercooling enables these engines to have increased OPR and core specific power relative to the reference turbofan cycle, but without the very high T_3 temperatures that challenge mechanical design and NOx emissions. Increasing OPR and TET generally gives higher thermal efficiency, but because the HP compressor last-stage blade-height and efficiency reduce as the design point OPR increases, there is an optimum OPR for best SFC and there are diminishing returns for increasing TET. In the reported study, increases in max climb OPR of up to 60% are considered; giving 120 as the limiting OPR.

In these intercooled engines most of the cycle benefit from intercooling comes from having smaller core components that increase OPR and core specific power at a thrust. Intercooling enables this to be done without exceeding any cycle temperature limits. Overcooling the core flow at cruise does not improve thermal efficiency, but reducing the intercooler cold-side cooling air mass flow at cruise and climb, relative to take-off, significantly reduces the cold-side pressure losses and so helps to improve overall cycle performance. The downside is that the engine runs hotter at cruise with potential impact on component life, but the T_3 levels are still generally much lower than for the non-intercooled engines, so this can help to compensate for the higher mid-cruise TET levels.

For the 100% thrust-scale engine, the highest permitted max-climb OPR and TET give the best climb and cruise SFC. However, the improvement in mid-cruise SFC relative to the conventional reference engine seems smaller than the improvement in max-climb SFC. In order to minimise mid-cruise SFC, a parametric study investigated the trade-off between intercooler effectiveness, TET and OPR at the mid-cruise condition. Mid-cruise intercooler effectiveness was varied between 50% and 69%. The results for two different engines with max climb design point pressure ratios of 75 and 120 are shown in Figure 62 and Figure 63.

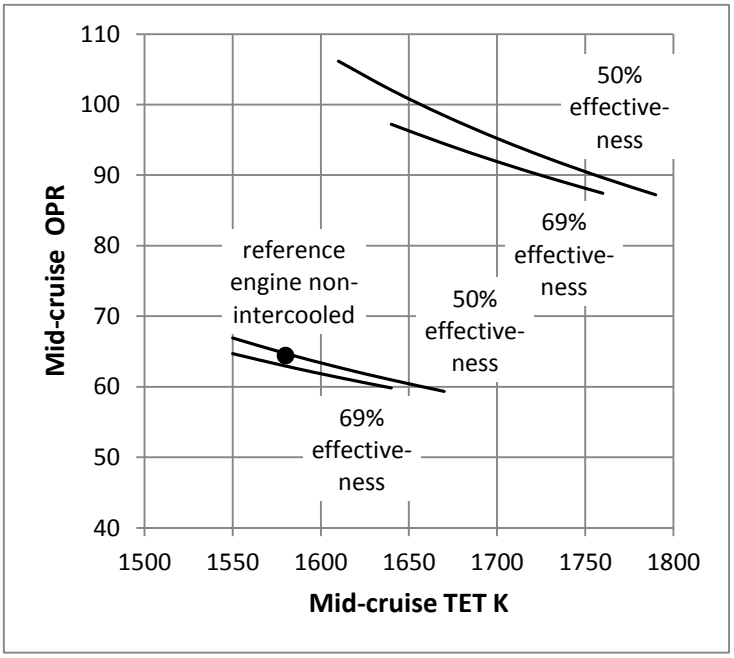

Figure 62 – Mid-cruise OPR v. TET, and Intercooler Effectiveness for two different engines with 75 and 120 OPR at the max climb design point

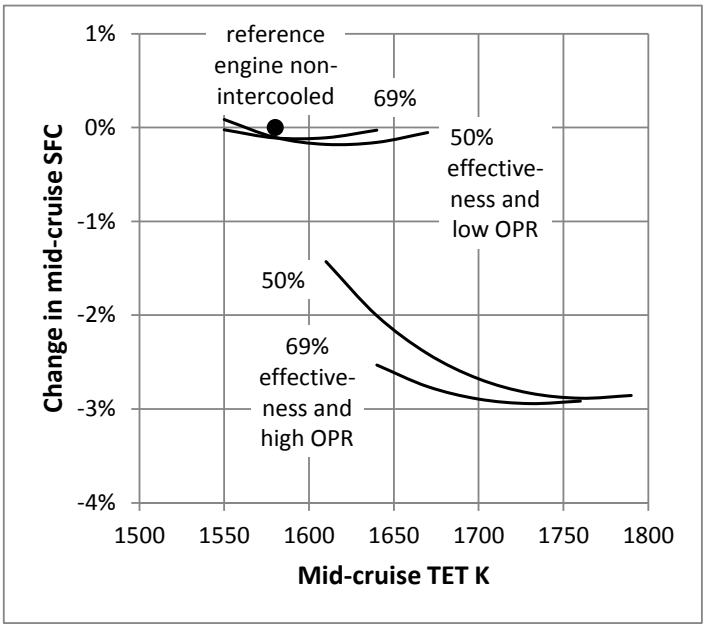

Figure 63 – Mid-cruise SFC v. TET, OPR and Intercooler Effectiveness for two different engines with 75 and 120 OPR at the max climb design point

Figure 62 shows how the mid-cruise OPR varies with intercooler effectiveness and TET, and Figure 63 shows how the SFC varies. The highest max-climb OPR cycles give the best max-climb SFC, but mid-cruise SFC for the higher OPR cycles is improved by reducing off-design OPR and optimising intercooler effectiveness and TET. This also increases the mid-cruise bypass ratio by reducing the core mass flow.

The max climb design-point cases in the scaling parametric study were run with the assumed limiting intercooler effectiveness of 75% and TET of 1890 K, but with OPR levels ranging from 75 to 120. TET is limited to 1950 K for the hot-day take-off cases by adjusting the fan bypass section to LP compressor work-split.

The HP compressor last-stage blade-height is significantly reduced in the higher OPR intercooled engine cycles. This is costing these cycles 1-2% of HP compressor efficiency and 0.5-1.0% of HP turbine efficiency relative to the reference turbofan. The SFC levels of the intercooled engines are therefore several percentage-points worse than they would have been had the component efficiencies not been reduced by the scaling-down of the core components relative to those in the non-intercooled engines.

Some intercooled cycles would seem to benefit from having HP compressor pressure ratios of 30 or more at max climb. However, the design of HP compressors with such high pressure-ratios is difficult and likely to lead to reduced component efficiency. As already noted in section 3.1.9 this is because of the need for low hub/tip radius ratio and high blade-tip inlet Mach number at inlet, and high hub/tip radius ratio and small blade-height at exit. Therefore in this study the HP compressor pressure ratios were generally limited to 26 at top of climb. However, the HP compressor pressure ratios typically fall to around 22–23 at take-off and to 18–21 at mid-cruise.

The lower cycle temperatures in the HP compressors of the intercooled engines result in more lightly-loaded two-stage HP turbines, as do the lower T_3 and higher TET variants for the conventional cycle engines. Their turbines might

merit having slightly-higher component efficiencies, but no credit has been taken for this in the author's studies.

The scaled intercooled engine cycles are run to the limiting max climb and max take-off TET specified in Table 12, but in this study the mid-cruise TET is varied in the range 1640 K to 1730 K. The intercooler mid-cruise effectiveness is varied in the range 50% to 69%, with the higher values giving better SFC in engines with higher OPR. This is in line with the trend in Figure 63. Increasing TET gives the best SFC, but for little penalty, the TET can be reduced by increasing OPR or intercooler effectiveness.

In practice it seems the optimum performance is likely to be obtained as much by optimising the cycle matching to maximise HP and LP compressor efficiencies, as by adjusting the amount of cooling air provided to the intercooler at cruise. However, such finessing is beyond the scope of these studies.

Figure 64 and Figure 65 show how max climb SFC and mid-cruise SFC vary with OPR and thrust scale. The smaller core-size intercooled engines are designed with 75, 90, 105 or 120 OPR at max climb, whereas OPR for the conventional engines is limited by T3 as shown in Figure 60.

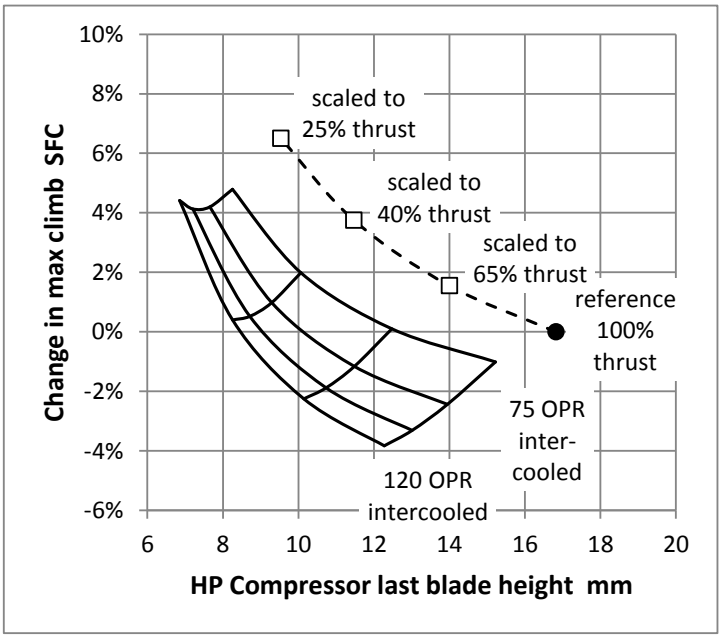

Figure 64 – Max Climb SFC for Conventional and Intercooled Engines

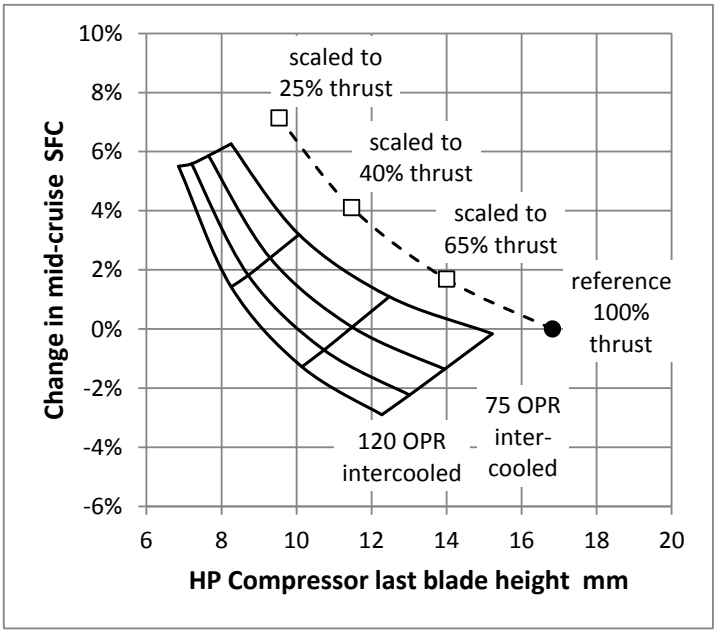

Figure 65 – Mid-Cruise SFC for Conventional and Intercooled Engines

For the scaled intercooled engines, the OPR rather than T3 has been varied. Figure 66 and Figure 67 show the max climb and max take-off T3 figures, for the intercooled cycles at max climb and at mid-cruise, are substantially lower than those for the scaled conventional reference engines that had the best SFC.

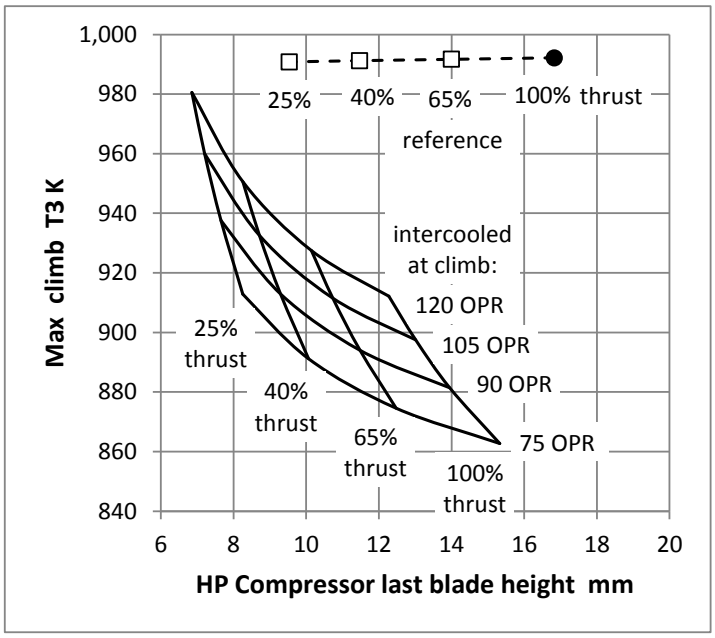

Figure 66 – Max Climb T_3 for Conventional and Intercooled Engines

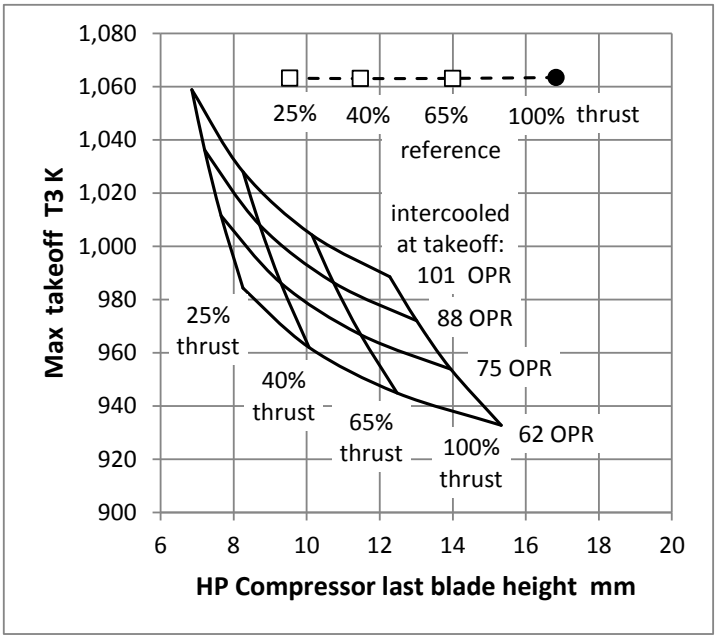

Figure 67 – Max Take-off T_3 for Conventional and Intercooled Engines

Note T3 increases significantly at an OPR as the HP systems are scaled down. For the highest OPR and 25% thrust scale cases, T3 approaches the limits set for max climb and max take-off in Table 12, but this high-OPR cycle does not give the best max climb SFC.

A summary of the results for the conventional and intercooled engine cycles found to have the best combination of max climb and mid-cruise SFC at each thrust scale is given in Table 23.

For intercooled engines there is the option to reduce T3 and TET operationally at the mid-cruise condition by increasing the intercooler effectiveness and core mass flow, but at the expense of a small increase in SFC. Potentially this might improve turbine life and reduce maintenance costs, so it is a trade-off worth considering.

Note the revised aircraft thrust requirements for optimised year-2050 long-range aircraft correspond to a thrust scale of around 75%. Performance for the reference and selected high-OPR intercooled engines, scaled to the revised thrust requirements is reported in section 7.6.

Table 23 – Performance of Selected Scaled Year-2050 Turbofans (Reference Brayton and Intercooled Cycles)

Parameter	Brayton Cycle Turbofans				Intercooled Cycle Turbofans			
Engine Geometry								
Thrust Scale:	100%	65%	40%	25%	100%	65%	40%	25%
HP compressor exit blade height (mm)	16.8	14.0	11.5	9.5	12.3	10.1	8.3	7.2
Take-off, Sea-level, 0.25 M, ISA+15 K								
Thrust (kN)	252	164	101	63	252	164	101	63
Mid-cruise Performance, 35,000 ft (10668 m), 0.82 M, ISA								
Thrust (kN)	49.0	31.8	19.6	12.2	49.0	31.8	19.6	12.2
OPR	64.4	62.3	59.5	56.5	91.9	91.9	91.9	83.5
Bypass ratio	20.7	20.0	19.2	18.2	27.6	26.4	24.8	22.1
SFC (mg/N.s)	12.88	13.10	13.41	13.80	12.51	12.72	13.07	13.60
Relative SFC	datum	+1.7%	+4.1%	+7.1%	-2.9%	-1.3%	+1.4%	+5.6%
Max Climb Performance, 35,000 ft (10668 m), 0.82 M, ISA+10 K								
Thrust (kN)	67.3	43.8	26.9	16.8	67.3	43.8	26.9	16.8
OPR	75.0	72.4	69.0	65.5	120	120	120	105
SFC (mg/N.s)	13.91	14.13	14.43	14.81	13.38	13.60	13.98	14.49
Relative SFC	datum	+1.5%	+3.8%	+6.5%	-3.8%	-2.2%	+0.5%	+4.1%

7.4 Revised Thrust Levels for Year-2050 Turbofans

As anticipated, the year-2050 reference aircraft studies at BHL in the ULTIMATE project resulted in a scaling-down of the thrust requirements for the long-range aircraft and a reduction in the specified mid-cruise flight Mach number from 0.82 to 0.80 in order to reduce fuel burn [11] and [12]. To match the new requirements Florian Jacob updated his PROOSIS engine performance model to give revised engine performance [1]. This included applying non-linear scale factors from BHL giving some further minor changes to the thrust requirements and increasing the typical mid-cruise altitude. The changing

requirements and performance assumptions for the final year-2050 reference engines (TF2050 and cycle#01 etc.) are shown in Table 24.

Table 24 – Revised Engine Requirements for Year-2050 Turbofans

Parameter	**Units**	**Original Spec.**	**Revised as** [1]	**Scale Factor**
Max Climb				
Altitude	ft (m)	35,000 (10668)	35,000 (10668)	–
Mach Number	–	0.82	0.82	–
Deviation from ISA	K	+10	+10	–
Thrust	kN	67.35	49.99	74.22%
Power Offtake	kW	260	0	–
Mid-Cruise				
Altitude	ft (m)	35,000 (10668)	37,000 (11278)	105.71%
Mach Number	–	0.82	0.80	97.56%
Deviation from ISA	K	0	0	–
Thrust	kN	49.00	32.56	66.45%
Power Offtake	kW	260	0	–
Max Take-off				
Altitude	ft (m)	0	0	–
Mach Number	–	0.25	0.20	80%
Deviation from ISA	K	+15	+15	–
Thrust	kN	252.07	183.46	72.78%
Power Offtake	kW	260	0	–

The new thrust levels are strictly only applicable to Jacob's updated reference engines, since the advanced cycle engines each have different SFC and installed weight. Re-optimising the aircraft for the advanced cycle engines should result in further new thrust requirements. However, it was not practical to keep reiterating thrust levels, so the revised thrust figures and flight conditions in Table 24 have been used for the final performance studies.

The author's Excel spreadsheet was used to scale the original year-2050 reference engine model to these revised thrusts. The results of this final scaling are presented in sections 7.6 and 8.4 where they are compared with the final

advanced-cycle engine performance and fuel-burn assessments. Note reduced thrust levels were anticipated in generating the preliminary performance estimates for cycle#06 as described in Chapter 6 and shown in Table 20.

The changes in the thrusts, offtakes, design-point altitudes and Mach numbers mean that the earlier performance results cannot be directly compared with later ones. The later models also used the more-typical FHV figure of 43.124 MJ/kg, as assumed by Jacob in [1], instead of the minimum figure of 42.797 MJ/kg used in the original reference and high OPR intercooled engine scaling studies.

7.5 Studies on Alternative Engine Cycles

The series of performance studies on more-complex cycles was also carried-out using the Excel performance spreadsheet described in section 3.1. Following the original scaling study on the year-2050 reference engine, the high-OPR intercooled engine was modelled and its sensitivity to scaling was investigated as described in section 7.3.2. The reference and selected high-OPR engines were then resized for the revised thrust requirements of Table 24 before the remaining advanced-cycle engine options were modelled to common thrust requirements. The final studies, modelling cycle#06 and some of the variants shown in Figure 25, are described hereafter.

It was not possible to fully automate execution of the Excel models, so it was not possible to complete detailed optimisation studies for all of the advanced-cycle engine options within the timeframe of the PhD project. Therefore the parametric studies that were undertaken for cycle#06 and its variants have not yet mapped-out all of the potential design-spaces for engines using the four proposed new technologies. Recommendations for further studies are included in section 10.3.

7.5.1 Intercooling, Secondary Combustion and a Bottoming Cycle

Cycle#03 was derived from cycle#02 by adding the ABC. The secondary combustor was modelled as an intra-turbine combustor between the first and second HP turbine stages. While it is assumed that the secondary combustor

would be fabricated from CMC materials that would not require significant cooling, the higher gas temperatures at inlet to the second stage of the HP turbine required an increase in the cooling air mass flow for cooling the second-stage rotor blades. Both stages are assumed to have the same TET. The second stage should be easier to cool, but the taller blades are subject to higher stress levels, so may need to be cooled to lower mean metal temperatures than the first stage blades. Ideally the second stage might be cooled by a separate CCA system taking lower-pressure bleed air from the HP compressor to maximise its efficiency, but for simplicity the cooling of the second stage has been modelled using uncooled cooling air. This lower-pressure cooling air is in any case relatively cool as it is taken from an intercooled compression system.

7.5.2 Preferred Configuration with all Four Technologies

Cycle#06 in Figure 25 was modelled after the reference engine cycle#01 and the high-OPR intercooled engine cycle#02 and after cycle#03 had added the ABC. It incorporates intercooling, topping and bottoming cycles and secondary combustion immediately after the topping cycle modules. The topping cycle is assumed to comprise the six topping-cycle modules as described in Chapter 5.

As discussed in section 4.6, cycle#06 has been modelled without the additional centrifugal compressor after the intercooler, but using it to offload the nutating-disc compressor would make little difference to the overall performance.

7.6 Comparison of Advanced-Cycle Engine Performance

The characteristics and modelled performance of the advanced-cycle engine variants down-selected for more detailed study in section 4.1 (as shown in Figure 25) are compared in the following tables. These tables also include data for Jacob's final TF2050 reference engine [1] that was sized to match BHL's fuel-burn-optimised long-range year-2050 aircraft. The engines compared in this section and in 8.4 are all resized to match the reduced thrust levels and revised flight conditions and fuel heating value etc. This was so that the (linear) fuel-burn exchange rates from BHL could be used for fuel-burn assessments.

The author's final cycle#01 scaled-down reference engine has mid-cruise performance that very closely matches Jacob's final TF2050 model, but at TOC and EOR take-off conditions cycle#01 has up to 3% worse SFC on account of its assumed greater reductions in off-design component efficiencies. As a result of the fuel-burn optimisation study, the reference and intercooled engines now have lower bypass ratios, higher specific thrusts and higher fan pressure ratios than the engines in the earlier scaling studies described in sections 7.3.1 and 7.3.2. The later engine SFC levels are penalised relative to the original full-scale engines because of efficiency penalties from scaling-down the cores and from increasing specific thrust, but they benefit from not needing to provide customer power offtake. It is assumed fuel cells would provide aircraft auxiliary power.

Table 25 provides a summary of the different technologies and architectures assumed for various cycles. The final scaled models for cycles #01, #02, #03, #06 and #18 all have the same thrusts and specific thrust at the TOC design point, a geared front fan and a high-speed IP compressor or booster.

Table 25 – Configurations for Various Advanced Cycle Engines

Engine Cycle	**TF2050 and #01**	**#02**	**#03**	**#05**	**#06**	**#14**	**#15**	**#18**
Intercooling	No	Yes	Yes	Yes	Yes	No	Yes	Yes
Topping Cycle	No	No	No	Yes	Yes	Yes	Yes	No
Bottoming Cycle	No	No	Yes	No	Yes	Yes	Yes	No
Secondary Combustion	No	No	Yes	Yes	Yes	Yes	No	Yes
Reverse-flow Architecture	No	No	Yes	Yes	Yes	Yes	Yes	Yes
HPT Cooled Cooling Air	Yes	Yes	Yes	Yes	Yes	Yes	No	No
Number of HPT Stages	2	2	2	3	3	3	2	2
Fan Diameter (m)	2.84	2.84	2.84	2.84	2.84	2.84	2.84	2.84

Table 26 compares the TOC design-point performance of the reference and high-OPR intercooled engines before and after scaling. The flight conditions are the same, but the scaled engines were modelled with a higher fuel heating value (FHV) so a more relevant comparison is made of overall efficiency. Note the 260 kW customer power offtake for the original study engines is credited in

their quoted overall efficiency figures – it adds about 0.3 percentage points to their overall efficiency, an increase of about 0.7%.

Table 26 – Final Scaling of Reference and Intercooled Engines
(Max Climb Design-Point, 10688 m, 0.82 Mach, ISA+10 K)

Engine	Original Reference	Scaled #01 Reference	Original Intercooled	Scaled #02 Intercooled
Thrust (kN)	67.35	49.99	67.35	49.99
Specific Thrust (m/s)	95.5	111.3	94.0	111.3
True Air Speed (m/s)	247.8	247.8	247.8	247.8
Fan bypass pressure ratio	1.426	1.510	1.424	1.510
Bypass Ratio (re. core flow)	20.41	16.52	23.42	18.76
OPR	75.0	75.0	120	120
HPC Exit Blade Height (mm)	16.82	14.87	12.27	10.87
T3 (K)	992.2	998.5	912.2	931.3
TET (K)	1890	1890	1890	1890
Power Offtake (kW)	260	0	260	0
FHV (MJ/kg)	42.797	43.124	42.797	43.124
SFC (g/kN.s)	13.91	14.08	13.38	13.51
Relative SFC	-1.2%	new datum	-5.0%	-4.1%
Overall Efficiency	41.92%	40.80%	43.59%	42.55%
Relative Efficiency	+2.7%	new datum	+6.8%	+4.3%

Table 27 compares performance at the top of climb flight condition for six different cycles, including the final TF2050 model from [1], [62] and [14]. Table 28 gives performance for the same engines at mid-cruise and Table 29 gives their performance at end of runway (EOR) take-off. Note the turbine cooling air (TCA) is the balance of the turbine cooling and sealing air that is tapped from the core compressors at lower pressures and temperatures than the cooled-cooling-air (CCA) and so does not pass through the CCA system. ‘NDC’ refers to the nutating-disc compressors. The ABC cycles (#03 and #06) split their core inlet flow between the intercooler and ABCHX in the ratio 5:4. Cycle#06 uses a variable-area bypass nozzle to simulate mixing and improve jet velocity ratios.

Table 27 – Summary Comparison of Advanced Cycle Engines at Max Climb (Scaled Engines, TOC design point, 10688 m, 0.82 Mach, ISA+10 K, TAS 247.8 m/s)

Parameter\Engine Cycle	TF2050	#01	#02	#03	#06	#18
Thrust (kN)	49.99	49.99	49.99	49.99	49.99	49.99
SFC (g/kN.s)	13.73	14.08	13.51	12.84	12.02	13.93
Relative SFC (%)	-2.5	datum	-4.1	-8.7	-14.6	-1.1
Overall Efficiency (%)	41.85	40.80	42.55	44.72	47.79	41.25
Inlet mass flow (kg/s)	449.1	449.1	449.1	449.1	449.1	449.1
Specific Thrust (m/s)	111.3	111.3	111.3	111.3	111.3	111.3
OPR (turbomachinery+NDC)	75.4	75.0	120.0	120.0	80.0	120.0
BPR (based on core flow)	16.08	16.52	18.76	14.23	19.10	24.35
Fan bypass pressure ratio	1.51	1.51	1.51	1.51	1.51	1.51
Jet velocity ratio bypass/core	–	0.753	0.784	0.808	0.775	0.726
Fan (bypass) efficiency (%) *is*	92	92.58	92.58	92.58	92.58	92.58
Bypass duct loss (%)	1.1	1.0	1.0	1.0	1.0	1.0
LPC pressure ratio	3.33	2.98	5.04	5.04	8.74	5.04
LPC efficiency (%) *is*	–	89.53	88.79	88.79	87.99	88.79
IP/HP and IC duct loss (%)	1.3	2.67	8.51	8.51	8.51	8.51
Intercooler effectiveness (%)	–	–	75.0	75.0	75.0	75.0
Intercooler cold-side loss (%)	–	–	6.93	7.93	7.93	7.93
Intercooler cooling flow (kg/s)	–	–	27.7	19.7	14.9	21.3
HPC/NDC pressure ratio	23.01	25.86	26.00	26.00	10.0	26.00
HPC/NDC efficiency (%) *is*	85	80.4	77.26	74.86	93.25	75.42
T3 (K)	1011	998.5	931.3	948.9	683.0	944.7
CCA air flow (% of core)	–	7.7	6.9	4.2	–	7.2
CCACA air flow (% of CCA)	–	20.1	10.0	10.0	–	10.0
First combustor loss (%)	3.0	3.0	3.0	3.0	–	3.0
HP1 turbine TET (K)	1890	1890	1890	1890	–	1890
HP2 turbine TET (K)	–	–	–	1890	1890	1890
HPT efficiency (%) *is*	91	90.6	89.6	–	–	–
Second combustor loss (%)	–	–	–	3.0	3.0	3.0
HPC last blade height (mm)	–	14.87	10.87	9.08	–	9.43
TCA air flow (% of core)	–	2.05	2.05	6.05	6.05	6.05

Table 28 – Summary Comparison of Advanced Cycle Engines at Mid-Cruise (Scaled Engines, 11277.6 m, 0.80 Mach, ISA, TAS 235.3 m/s)

Parameter\Engine Cycle	TF2050	#01	#02	#03	#06	#18
Thrust (kN)	32.56	32.56	32.56	32.57	32.59	32.56
SFC (g/kN.s)	12.62	12.63	12.24	11.60	10.76	12.61
Relative SFC (%)	-0.1	datum	-3.1	-8.2	-14.8	-0.2
Overall Efficiency (%)	43.24	43.19	44.57	47.18	50.69	43.26
Inlet mass flow (kg/s)	384.7	384.9	378.7	376.9	394.4	379.7
Specific Thrust (m/s)	84.6	84.6	86.0	86.4	82.6	85.8
OPR (turbomachinery + NDC)	62.10	64.42	89.59	88.20	60.20	89.59
BPR (based on core flow)	16.84	16.52	22.75	17.55	24.80	29.63
Fan bypass pressure ratio	1.39	1.393	1.407	1.414	1.387	1.402
Jet velocity ratio bypass/core	–	0.924	0.999	1.049	1.007	0.933
Cold nozzle area re. TOC (%)	100	100	100	100	105	100
Fan (bypass) efficiency (%) *is*	95	94.97	94.96	94.96	94.97	94.96
Bypass duct loss (%)	1.1	1.0	1.0	1.0	1.0	1.0
LPC pressure ratio	3.44	3.381	3.870	3.655	4.626	3.770
LPC efficiency (%) *is*	–	90.54	90.37	90.44	90.14	90.40
IP/HP and IC duct loss (%)	1.64	2.67	7.54	7.54	7.54	7.54
Intercooler effectiveness (%)	–	–	49.28	50.00	75.00	49.28
Intercooler cold-side loss (%)	–	–	6.94	4.86	7.93	6.94
Intercooler cooling flow (kg/s)	–	–	17.53	9.03	9.34	13.63
HPC/NDC pressure ratio	18.34	19.57	25.03	26.1	14.08	25.70
HPC/NDC efficiency (%) *is*	87	86.07	82.60	80.08	92.95	80.68
T3 (K)	860	872.7	870.7	887.2	654.1	884.8
CCA air flow (% of core)	–	7.7	6.9	6.4	–	7.2
CCACA air flow (% of CCA)	–	0.0	0.0	0.0	–	0.0
First combustor loss (%)	3.0	3.0	3.0	3.0	–	3.0
HP1 turbine TET (K)	1540	1547	1723	1730	–	1720
HP2 turbine TET (K)	–	–	–	1730	1481	1721
HPT efficiency (%) *is*	90	90.80	89.72	–	–	–
Second combustor loss (%)	–	–	–	3.0	3.0	3.0
TCA air flow (% of core)	–	2.05	2.05	6.05	6.05	6.05

Table 29 – Summary Comparison of Advanced Cycle Engines at Take-off (Sea level, 0.20 Mach, ISA+15K, TAS 69.5 m/s)

Parameter\Engine Cycle	TF2050	#01	#02	#03	#06	#18
Thrust (kN)	183.46	183.46	183.46	183.37	183.49	183.46
SFC (g/kN.s)	8.28	8.533	8.312	7.734	6.91	8.551
Relative SFC (%)	-2.9	datum	-2.6	-9.4	-19.0	+0.2
Inlet mass flow (kg/s)	1002	1005	1020	1006	1007	1017
Specific Thrust (m/s)	183.1	182.5	179.8	182.3	182.2	180.5
OPR (turbomachinery + NDC)	60.13	62.00	99.95	92.80	69.68	99.95
BPR (based on core flow)	16.14	16.00	18.50	14.97	19.41	23.90
Fan bypass pressure ratio	1.39	1.390	1.388	1.394	1.392	1.388
Fan (bypass) efficiency (%) *is*	93	94.24	94.24	94.24	94.24	94.24
Bypass duct loss (%)	1.1	1.0	1.0	1.0	1.0	1.0
LPC pressure ratio	2.92	3.097	5.913	4.225	4.626	5.950
LPC efficiency (%) *is*	–	90.19	89.34	89.78	89.66	89.33
IP/HP and IC duct loss (%)	1.64	2.67	7.54	7.54	7.54	7.54
Intercooler effectiveness (%)	–	–	52.75	75.0	75.00	52.75
Intercooler cold-side loss (%)	–	–	10.9	7.93	7.93	10.9
Intercooler cooling flow (kg/s)	–	–	78.5	45.49	35.63	61.24
HPC/NDC pressure ratio	20.92	20.57	18.28	23.76	16.29	18.17
HPC/NDC efficiency (%) *is*	86	84.15	81.44	78.41	92.88	79.65
T3 (K)	1053	1065	1037	1007	836.5	1049.6
CCA air flow (% of core)	–	7.7	6.9	4.2	–	7.2
CCACA air flow (% of CCA)	–	35.1	21.0	21.0	–	21.0
First combustor loss (%)	3.0	3.0	3.0	3.0	–	3.0
HP1 turbine TET (K)	1921	1913.5	1953.3	1950	–	1950
HP2 turbine TET (K)	–	–	–	1950	1671	1930.8
HPT efficiency (%) *is*	91	90.62	89.56	–	–	–
Second combustor loss (%)	–	–	–	3.0	3.0	3.0
TCA air flow (% of core)	–	2.05	2.05	6.05	6.05	6.05

The performance of the cycle#01 reference engine matches the TF2050 SFC at mid-cruise, but it deviates at climb and take-off, where its SFC is significantly worse. Both engine models were derived following guidelines provided by

ULTIMATE industry partners in [64] for cruise performance, but using different modelling tools and assumptions. Thus some differences were to be expected.

7.7 Uncertainty Analysis for Performance Assessments

The reference engine performance models have component efficiencies and pressure losses originally chosen by the author to reproduce the overall mid-cruise performance recommended by industry partners in [64]. When the engines were scaled, scale-corrections to efficiency were applied to the HP compressors and turbines as shown in Table 30.

Table 30 – The Effects of Reduced Component Efficiency on Cycle#01

Cycle	**Cycle#01**			**Cycle#01 -1%**		
Parameter/Case	**TOC**	**CR**	**EOR**	**TOC**	**CR**	**EOR**
Thrust (kN)	49.99	32.56	183.46	49.9	32.56	183.46
SFC (g/kN.s)	14.08	12.63	8.53	14.51	13.06	8.86
Change in SFC (%)	datum	datum	datum	+3.0	+3.4	+3.8
TET (K)	1890.0	1547.5	1913.6	1890.0	1550.9	1920.5
T3 (K)	998.5	872.7	1065.3	1011.2	883.1	1077.7
OPR	75.0	64.4	62.0	75.0	64.4	62.0
BPR	16.52	16.52	15.98	15.84	15.87	15.36
Polytropic Efficiencies (%)						
Fan bypass	93.0	95.2	94.5	92.0	94.2	93.5
LP Compressor	91.0	92.0	91.6	90.0	91.0	90.6
HP Compressor Basic	86.0	89.6	88.2	85.0	88.6	87.2
Scale-corrected	86.8	90.4	89.0	85.9	89.5	88.1
HP Turbine Basic	88.6	88.6	88.6	87.6	87.6	87.6
Scale-corrected	89.0	89.0	89.0	88.1	88.1	88.1
LP Turbine	91.2	93.2	92.2	90.2	92.2	91.2
HPC last blade ht. (mm)	14.87			15.22		

To test the sensitivity of the overall performance of the reference engine to the input assumptions, cycle#01 has been modelled again with a one per cent reduction in component polytropic efficiencies. The results with these 'design-point exchange rate' are also compared with the performance of the original model in Table 30. The cycle with lower efficiencies has been matched to the same OPR and TET at the top of climb design point. The result is a 3–4% increase in SFC a 10–14 K increase in T3 and a 2.4% increase in HP compressor last-stage blade-height, The TET at take-off increases by about 7 K, but is still within the limits set at the start of the study.

Other design point matchings are possible, but would not make much difference to the change in SFC. A similar exercise on the other study engine cycles would be expected to show similar results.

7.8 Diagrams to Compare Different Performance Cycles

Temperature–entropy (T-s) and Sankey diagrams can be used to compare different cycles. The engine performance spreadsheet plots the temperature-entropy diagrams and provides the data needed to construct Sankey diagrams in PowerPoint. For example, Figure 68 compares the take-off temperature and entropy values for the reference engine (cycle#01) with those of the high-OPR intercooled engine (cycle#02).

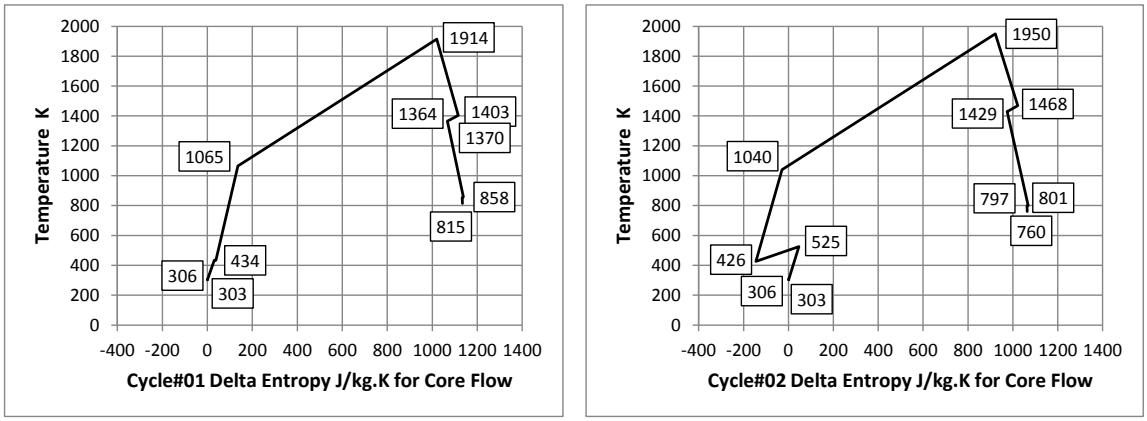

Figure 68 – Take-off Temperature–Entropy Diagrams for Cycle#01 and #02

One example of a novel Sankey diagram (Figure 69) is also presented. This shows the different types of energy flow in a high bypass ratio intercooled geared fan turbofan engine at cruise. The width of the bands is proportional to the power at that point in the cycle, normalized by 100% of the chemical power available in the fuel flowing into the combustor.

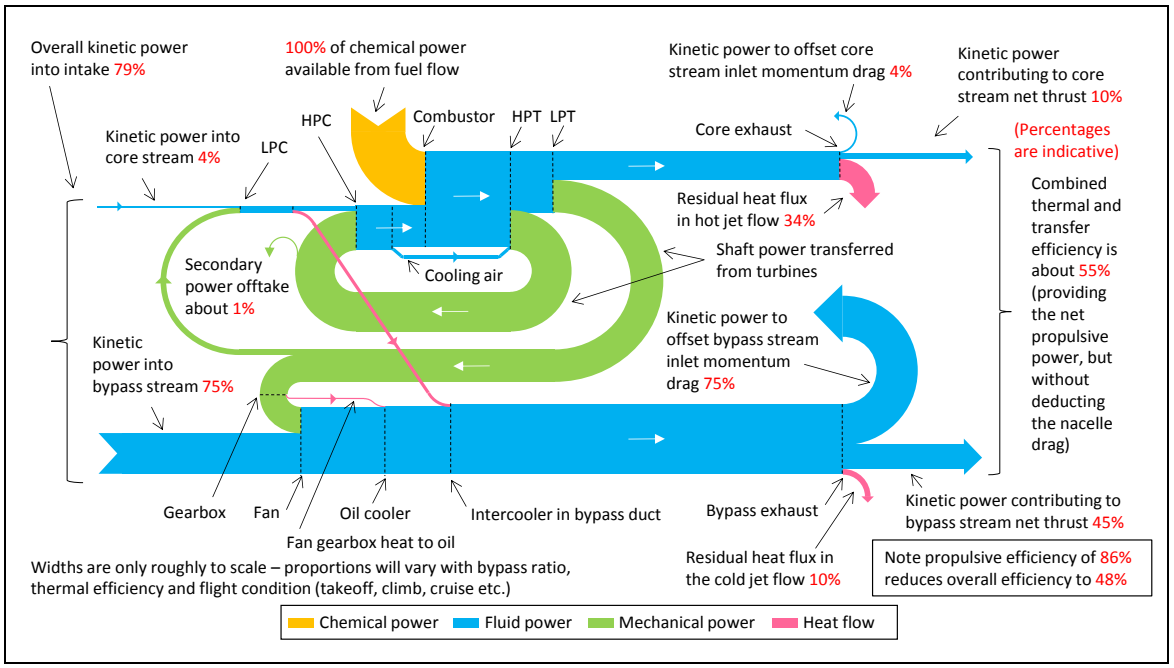

Figure 69 – Colour-coded Sankey Diagram for an Intercooled Turbofan

8 TECHNOLOGY EVALUATION OF ADVANCED CYCLES

This Chapter makes further assessments of the advanced-cycle engines that have had their performance modelled as described in Chapter 7. The cycle options are a subset of those identified in Figure 24 and Figure 25. Comparisons are made with baseline year-2000 in-service engines and other ULTIMATE project study engines. Engine weight, fuel burn and NOx emissions are estimated quantitatively and engine noise is considered qualitatively. An uncertainty analysis is included and the development potential and the risks for the different options are reviewed.

8.1 Comparison with In-service Engines in Year 2000

ACARE targets are baselined to engines in-service in year 2000. The ULTIMATE project and previous EU programmes such as NEWAC and LEMCOTEC have taken a CFM56-like engine in an Airbus A320-like aircraft as a baseline for short-haul aircraft and a Trent 700-like engine in an Airbus A330-like aircraft as a baseline for a long-haul aircraft.

8.2 Weight Assessments

As described in section 3.3.1, the engine weight assessments have taken as their starting-point the WeiCo weight assessment for the final TF2050 reference engine, equivalent to cycle#01 in Figure 24 and Figure 25.

The same percentage breakdown has been taken for the cycle#01 component weights. Component weights for the alternative cycles have been estimated as described in section 3.3.1 and Chapter 6 and scaled according to the component sizes implied by the relevant cycle performance. The resulting weights are listed in Table 31.

Table 31 – Component Weight Breakdown (kg) for Alternative Cycles

Parameter\Engine	#01	#02	#03	#06	#18
Fan	1529	1529	1529	1529	1529
Reduction Gearbox	217	219	219	222	219
IP Compressor	408	542	741	784	402
HP Compressor	155	72	49	–	53
Combustor	124	62	41	–	43
HP Turbine	124	54	38	–	42
LP Turbine	408	485	312	205	442
Hot Nozzle	98	80	89	60	71
Cold Nozzle	109	102	102	106	105
Engine Shafts	57	56	45	36	48
Main Bearings	67	66	51	40	54
Accessories	258	255	246	232	258
Intercooler	–	733	800	627	572
Nutating-disc Modules	–	–	–	666	–
Extra Transmissions	–	–	–	76	–
Secondary Combustor	–	–	82	75	87
ABC Heat Exchanger	–	–	640	502	–
ABC Turbine	–	–	125	125	–
Total Engine	3554	4254	5109	5518	3925
Relative to Cycle#01	datum	+20%	+44%	+55%	+10%
Nacelle	1607	1607	1607	1607	1607
Total Engine and Nacelle	5161	5862	6716	7125	5532
Relative to Cycle#01	datum	+14%	+30%	+38%	+7%

8.3 Nacelle and Afterbody Drags

Nacelle and afterbody drags for the different advanced cycle options have not been systematically assessed, though such assessments are candidates for further work as noted in section 10.3. Since all the engines specified in Table 25 are assumed to have the same fan diameter they will all have similar nacelle diameters and nacelle drags. There should however be some differences in

nacelle drag resulting from the different engine architectures. The high-OPR intercooled engines are expected to need slightly-fatter nacelles than the reference engines. The engines with topping cycles are also likely to need slightly-fatter nacelles, and the engines with reverse-flow cores are expected to have higher afterbody drags, but in these cases the drag increase would be offset by the benefit of having a mixed exhaust. Neither effect has been modelled, but the effects have been assumed to cancel out.

8.4 Fuel-burn Assessments

The methodology for assessing the fuel-burn benefits of alternative engines on the reference advanced year-2050 tube-and-wing aircraft has been covered in section 3.2 and is also described in [14]. The results are given in Table 32. Note the design mission fuel burn when the exchange rates were calculated was 47500 kg prior to the final scaling of the TF2050 engine.

Table 32 – Fuel-Burn Calculations for Alternative Cycles

Parameter\Engine Cycle	#01	#02	#03	#06	#18
Weighted SFC (g/kN.s)	12.71	12.28	11.60	10.80	12.65
Δ $SFC_{weighted}$ from Equation 8	-0.2%	-3.3%	-8.5%	-15.0%	-0.4%
Engine + nacelle Weight (kg)	5161	5862	6716	7125	5387
Fan Diameter (m)	2.84	2.84	2.84	2.84	2.84
Δ Fuel burn from Equation 9	-1.0%	-4.4%	-10.3%	-19.3%	-0.9%
Design mission fuel burn (kg)	47056	45472	42655	38353	47117
Fuel burn saving (kg)	datum	1584	4401	8703	-61
Fuel burn saving (%)	datum	3.4%	9.4%	18.5%	-0.1%

8.4.1 Uncertainty in the Fuel-burn Assessments

There are five major sources of uncertainty in the fuel burn assessments:

- The performance of the novel technologies
- The SFC assessments at design and off-design (see section 7.7)
- The component weight assessments
- Changes in installed nacelle drag (which have not been assessed)

- The linear fuel-burn exchange rates for the aircraft

The combination of these five factors compounds the overall uncertainty. However, the *relative* fuel burn comparison between the different engine cycles is of greatest interest, and in this respect the uncertainty is somewhat less, because consistent methods and assumptions have been adopted.

The 18.5% fuel burn reduction for cycle#06 might prove to be optimistic if more detailed study would add to the engine weight and/or nacelle drag.

8.5 Noise Assessments

The author has only made qualitative noise assessments.

The reference turbofan for year 2050 should be quieter than existing engines and has been assessed at Chalmers University in the ULTIMATE project [145], but the advanced cycle turbofans may or may not be quieter than the reference engine.

All the study engines have low-speed geared fans and lower specific thrust than existing engines, which should reduce fan noise relative to currently-in-service large engines. The associated high-speed LP turbines may generate more noise on account of slightly higher Mach numbers than current direct-drive turbines, but the higher blade-passing frequencies should mean that this noise is better attenuated.

Engines configured with intercoolers and/or bottoming-cycle heat exchangers can expect to benefit from additional attenuation of core turbomachinery and combustion noise. The ABC turbine, downstream of the ABC heat exchanger, is an additional noise source, but should be no worse than the LP turbine. In the proposed reverse-flow-core arrangement it is well buried inside the engine.

The alternative closed-circuit bottoming cycle has no direct gas-path to the atmosphere and would be expected to generate relatively high frequencies that are more-easily attenuated.

The reverse-flow core arrangement with its mixed exhaust flow should generally be quieter than a conventional separate-jets engine.

Gearbox noise is an unknown as is the noise from lean-burn primary and secondary combustors. All combustion systems have the potential to generate noise through combustion instability and acoustic resonance. The control or elimination of these noise sources, particularly troublesome in lean-burn combustion systems, is largely down to detail design. However, it seems reasonable to assume that improved simulation techniques will enable these potential problems to be averted by the year 2050.

The topping cycle machines are the main concern, though it is arguable that the dual-disc nutating-disc modules should at least have low vibration, since they are overall well-balanced, and they should be at least as quiet as conventional piston engines, given their relatively steady exhaust streams.

The author is unaware of any noise measurements having been made on actual nutating disc engines, and even if data were to exist for normally-aspirated designs, their applicability to the highly-turbocharged high-speed units proposed for the year-2050 engines would be questionable.

The operating speeds of the proposed nutating-disc modules are higher than most high-speed piston engines, so the noise they generate should also be higher-frequency, particularly noting that in each module ignition occurs twice for each shaft-revolution and as noted in section 5.5 the proposed arrangement of six modules for cycle#06 operating 60° out-of-phase with each other, raises the firing frequency by a further factor of three, feeding the secondary combustor with only small pressure fluctuations at around 41 kHz at take-off.

However, piston engines with multiple cylinders out-of-phase obviously also benefit from having raised noise frequencies.

The most fuel efficient engines should benefit a bit more from the scaling-down of the aircraft take-off weight and reduced thrust requirements, as this further iteration has not been taken into account.

Where the nutating-disc modules feed into secondary combustors or plenum chambers, these should also be quite effective in reducing the noise propagated downstream; however, the combustion systems themselves add some noise.

8.6 Emissions Assessments

Quantitative NOx emissions assessments have been made for the year-2000 baseline and for the year-2050 study engines that are assumed to incorporate advanced the LDI combustors. The latter estimates, using the author's recommended NASA correlation, Equation 21, are compared with the CAEP limits, SRIA Flightpath 2050 targets and year-2000 baseline engines.

Another ULTIMATE study was expected to develop a quantitative emissions correlation or methodology for engines with the nutating-disc core, but attempts to adapt existing diesel-engine methods proved unsatisfactory. Therefore only qualitative assessments have been made. Also, as explained in section 6.2.2, predictions have only been made for the primary combustors in other engine cycles, not for secondary combustion.

For several of the study engines the emissions would come from the same advanced lean direct injection (LDI) type of combustor assumed for the year-2050 reference engine, so assessments could be made using Equation 21.

In a more rigorous comparison, the actual emissions should be slightly lower for the advanced cycle engines on account of their improved fuel burn and potential to be further scaled-down or de-rated to match the reduced thrust requirements for the year-2050 intercontinental aircraft mission.

8.6.1 Year-2000 Baseline Engine Emissions Assessments

Declared ICAO database emissions for representative year-2000 in-service engines have been taken as the starting points for estimating the potential improvements arising from year-2050 technology. This applies not only to the LTO-cycle emissions, which for year-2000 engines can be read from the ICAO emissions database, but also to the on-route emissions of NOx at top of climb

and at mid-cruise conditions. For the year-2000 baseline engines this required the modelling of their performance at sea-level and at altitude. The baseline engine performance data were provided by Joshua Sebastiampillai and Florian Jacob from their PROOSIS performance models described in ULTIMATE deliverable D2.6 [13]. However the original PROOSIS models would not run down to low static thrusts, so some extrapolation of the available performance was made in order to get down to the 30% and 7% sea-level static thrust cases needed for the LTO-cycle emissions assessments.

The year-2000 baseline engine emissions figures were then computed by the author and reported in the ULTIMATE deliverable D2.3 [108]. All the engine performance modelling assumes dry air, so humidity effects were accounted for by applying the correction to the high altitude NOx emissions estimates as part of the P3T3 method as described in Section 3.8.5.

For long-range aircraft, the reported emissions for the Trent 772 were taken to be representative of engines in-service in 2000, and for short-range aircraft the emissions of the CFM56-5B7/P engine were taken. The selection of the Trent 772B was straightforward, but various standards of CFM56-5B logged over 140 different emissions tests [82]. The number of tests was large because the CFM56 was offered with multiple ratings and an optional lower-emissions double-annular combustor (DAC), though most CFM56 engine operators did not take-up this costlier option. Discounting the DAC combustors, very early tests and tests conducted since 2000, left a series of tests conducted in 1995 on one engine configured for a range of different thrust ratings. CAEP/2 and CAEP/4 NO_x limits were met at all ratings, but the higher rated engines would now fail CAEP/6 and all engines would now fail CAEP/8. (An improved combustor design was tested in 2006.) Therefore emissions data for the CFM56-5B7/P engine that had the single-annular combustor and an intermediate thrust rating were used in the ULTIMATE project studies, to be fairly representative of the in-service fleet in year 2000. Few details of these assessments are included in this thesis as they are not relevant to the larger turbofan engines modelled.

8.6.2 Long-range Aircraft Engine Performance

A Trent 772B-like engine in an A330-like aircraft provides the other appropriate year-2000 baseline for emissions comparisons in these studies. Such a combination was also used in previous EU Framework Programmes including VITAL, NEWAC and LEMCOTEC to provide baseline year-2000 state-of-the-art in-service engine performance, noise and emissions figures.

The Rolls-Royce Trent 772B itself was certificated with an early 'Phase-5' combustor in 1994.

The ULTIMATE deliverable D2.6 [13] describes modelling a Trent 772B-like engine, designated LRTF2000, and tabulates its TOC, CR and EOR design-point performance. Selected performance parameters for these three cases are listed in Table 33. Note the mid-cruise performance is quoted for an ISA day.

Table 33 – Selected Performance Parameters for the LRTF2000 Turbofan

Parameter	Units	TOC	CR	EOR
Mach number	-	0.82	0.82	0.25
Altitude	m	10668	10668	0
Deviation from ISA day temperature	K	10	0	15
Total net thrust (FN)	kN	73.01	52.43	250.95
SFC	g/kN.s	18.64	17.25	12.96
Engine air inlet mass flow	kg/s	381.8	358.8	939.0
Bypass ratio	-	4.7	5.2	5.1
OPR	-	46.5	36.5	39.2
Combustor Inlet Pressure (P_3)	kPa	1714	1347	4131
Combustor Inlet Temperature (T_3)	K	874	760	941
HP Turbine Entry Temperature (TET)	K	1691	1422	1757

For the purposes of emissions assessment, additional LTO-cycle performance data points were generated using the LRTF2000 model. Table 34 gives a summary of these data.

Table 34 – Selected LTO-cycle Performance Data for the LRTF2000

Parameter	Units	T/O	C/O	App	Idle
Mach number	-	0	0	0	0
Altitude	m	0	0	0	0
Deviation from ISA day temperature	K	0	0	0	0
Total net thrust (FN)	kN	316.3	268.9	94.9	22.1
Relative thrust	-	100%	85%	30%	7%
SFC	g/kN.s	9.81	9.30	8.60	12.13
Engine air inlet mass flow	kg/s	938.9	871.8	526.3	252.5
Bypass ratio	-	5.05	5.20	5.89	6.41
OPR	-	40.1	34.9	15.9	6.71
Combustor Inlet Temperature	K	897	851	682	528
Combustor Outlet Temperature (COT)	K	1681	1564	1154	1013
HP Turbine Entry Temperature (TET)	K	1603	1493	1106	972

In this case the design-point bypass ratio of the LRTF2000 is a good match to the Trent 772B, but the OPR as modelled is higher than that quoted for the engine in the ICAO database [82]. This means the LRTF2000 might be expected to have higher NOx emissions than the Trent 772B. However, in estimating the design-point NOx emissions using the P3T3 methodology, it is still possible to produce credible mission-level emissions estimates by taking the relative fuel flows and temperature differences in the combustor and datuming the LRTF2000 emissions to the Trent 772B databank figures.

The combined combustor and HP compressor exit diffuser pressure loss is modelled as a constant 4.0% dP/P in the LRTF2000 model.

The LRTF2000 NOx emissions, estimated using the P3T3 methodology, are given in Table 35. Note the OPR for calculation of the NOx limit for DP/Foo is re-datumed to 35.79 as for the Trent 772 in the ICAO database. For the emissions assessments, the LTO-cycle pollutant emissions are summed over the times specified in Table 7 for the LTO-cycle, and also quoted for one minute of operation at each of the TOC, CR and EOR conditions. Humidity corrections are applied to the NOx emissions estimates as previously described.

Table 35 – Emissions Estimates for the SRTF2000 Turbofan for 60% relative humidity

Parameter	Unit	T/O	C/O	App	Idle	TOC	CR	EOR
Mach number	-	0	0	0	0	0.82	0.82	0.25
Altitude	m	0	0	0	0	10700	10700	0
Deviation from ISA	K	0	0	0	0	10	0	15
Thrust	kN	236.2	200.8	70.8	16.5	49.99	32.56	183.4
Humidity factor e^H	–	1.000	1.000	1.000	1.000	1.125	1.125	0.832
Fuel Flow	kg/s	3.10	2.50	0.82	0.27	1.36	0.90	3.25
EI NOx (corrected)	g/kg	43.6	32.7	10.7	5.7	31.0	15.1	46.9
Duration	s	42	132	240	1560	per minute of operation		
Mass NO_x	kg	8.11	10.79	2.11	2.40	2.53	0.82	9.15

Table 36 compares the Dp/Foo results with CAEP limits. Since the LRTF2000 OPR at the LTO-cycle T/O condition (π_{oo}) is 35.79, then the Dp/Foo NO_x limit for CAEP/2 is 89.25 and for CAEP/8 it is 61.7. Like the SRTF2000, the LRTF2000 is meets the CAEP/2 limit, but would not meet the later CAEP/8 limit.

Table 36 – LTO-cycle NOx Emissions for Year-2000 Long-range Engines

LTO cycle total Dp (kg) LRTF2000	Dp/Foo (g/kN) average engine LRTF2000	Dp/Foo (g/kN) characteristic Trent 772B	Average LRTF2000 re. CAEP/2 limit	Average LRTF2000 re. CAEP/8 limit
23.4	74.0	78.9	82.9%	119.9%

8.6.3 Year-2050 Reference Engine NOx Emissions Assessments

The ULTIMATE project considered that by the year 2050 a geared open rotor powerplant would be a credible solution for aircraft for short to medium ranges, so performance was worked-up for a 'GOR2050' reference engine for the corresponding 'advanced tube and wing' (ATW) short-range aircraft. For the long-range aircraft the 'TF2050' geared-fan turbofan was modelled. Both these engines had performance models created in PROOSIS and reported in ULTIMATE deliverable D2.6 [13]. However, the original TF2050 was later scaled-down to match the reduced thrust requirements of the iterated long-range ATW aircraft design. Thus the TF2050 performance was re-issued by Florian Jacob in a coordination memorandum ULTIMATE-CU-ECM-005 [1].

The author's study has focused on geared turbofan engine configurations, so only the TF2050 performance and emissions assessments are described here. Selected design-point performance parameters are presented in Table 37.

Table 37 – Selected Performance Parameters for the TF2050 Turbofan

Parameter	Units	TOC	CR	EOR
Mach number	-	0.82	0.80	0.20
Altitude	m	10668	11277.6	0
Deviation from ISA day temperature	K	10	0	15
Total net thrust (FN)	kN	49.99	32.56	183.46
SFC	g/kN.s	13.73	12.62	8.28
Engine air inlet mass flow	kg/s	449.0	384.7	1002.2
Bypass ratio	-	16.08	16.84	16.14
OPR	-	75.4	62.1	60.13
Combustor Inlet Temperature (T_3)	K	1011	860	1058
Combustor Outlet Temperature (COT)	K	1890	1540	1921

For the purposes of emissions assessment, additional performance data were generated from the LRTF2000 model to cover the four LTO-cycle ground-level emissions measurement points as shown in Table 38.

Table 38 – Selected LTO-cycle Performance Data for the TF2050 Turbofan

Parameter	Units	T/O	C/O	App	Idle
Mach number	-	0	0	0	0
Altitude	m	0	0	0	0
Deviation from ISA day temperature	K	0	0	0	0
Total net thrust (FN)	kN	236.2	200.8	70.8	16.5
Relative thrust	-	100%	85%	30%	7%
SFC	g/kN.s	6.12	5.80	5.51	7.94
Fuel Flow	kg/s	1.446	1.165	0.390	0.131
Engine air inlet mass flow	kg/s	992.0	916.9	547.6	263.5
Bypass ratio	-	15.89	16.14	19.57	27.60
OPR	-	60.5	52.8	21.8	6.69
Combustor Inlet Temperature (T_3)	K	1004	949	753	577
Combustor Outlet Temperature	K	1839	1704	1327	1127

For reference, the TF2050 combustion efficiency was modelled as a constant 99.95% and the combined combustor with HP compressor diffuser pressure loss as just 3%.

The TF2050 emissions were estimated using the correlation Equation 21 as discussed in section 3.8.7 and the results are shown in Table 39. The LTO-cycle pollutant emissions are summed over the times specified times in Table 7, and for one minute of operation at each of the TOC, CR and EOR conditions. As for the year-2000 baseline engines, humidity corrections are applied to the NOx estimates, assuming 60% relative humidity at sea level for ISA and ISA +15 K days and a 12.5% increase in NOx emissions at high altitudes. Note the higher absolute humidity assumed for the hot day take-off case reduces the

amount of NOx produced relative to the prediction from the uncorrected correlation, but NOx emissions still increase relative to an ISA day.

Table 40 compares the Dp/Foo results with CAEP limits. Since the TF2050 OPR at the LTO-cycle T/O condition (πoo) is 60.49, then the Dp/Foo NOx limit for CAEP/2 is 128.8 and for CAEP/8 it is 111.1. Note these are estimates for average engine emissions, not projected characteristic values. Very significant reductions in NOx emissions are predicted relative to the LRTF2000 at all comparable conditions. At altitude and particularly at top of climb, the NOx reductions are not quite as impressive as those of the GOR2050, but both engines run relatively hot at top of climb because of their low specific thrusts.

Table 39 – NOx Emissions Estimates for the TF2050 Turbofan

Parameter	**Units**	**T/O**	**C/O**	**App**	**Idle**	**TOC**	**CR**	**EOR**
Mach number	-	0	0	0	0	0.78	0.78	0.25
Altitude	m	0	0	0	0	10668	10668	0
Deviation from ISA	K	0	0	0	0	10	10	15
Thrust	kN	236.2	200.8	70.8	16.5	49.99	32.56	183.4
Humidity factor e^H	–	1.000	1.000	1.000	1.000	1.125	1.125	0.832
Fuel Flow	kg/s	1.446	1.165	0.390	0.131	0.686	0.411	1.519
EI NO_x	g/kg	47.9	31.7	6.4	1.4	36.9	12.7	64.0
EI NO_x (corrected)	g/kg	47.9	31.7	6.4	1.4	41.6	14.3	53.2
Duration	s	42	132	240	1560	per minute of operation		
Mass NOx	kg	2.906	4.875	0.599	0.285	1.712	0.353	4.849
NO_x re. LRTF2000	–	-64%	-55%	-72%	-88%	-32%	-57%	-47%

Mission-level emissions assessments are beyond the scope of this study, but they could be made using Equation 21 together with the humidity correction.

Table 40 – LTO-cycle NOx Emissions Compliance for the TF2050 Turbofan

LTO Cycle Dp (kg)	Dp re. SRTF2000	Dp/Foo (g/kN)	Re. CAEP/2 limit	Re. CAEP/8 limit
8.66	-63%	36.7	28.5%	33.0%

Based on the above figures, the year-2050 reference turbofan is estimated to reduce total NOx emissions by 63% in the LTO cycle and by 57% at mid-cruise relative to the year-2000 baseline engine, equivalent to about 60% per ASK at mid-cruise, given that the ATW aircraft capacity is assumed to grow by 8.3%.

For comparison, the year-2050 reference open rotor was estimated to reduce total NOx emissions by 78% in the LTO cycle and by 83% at mid-cruise relative to the year-2000 baseline engine, equivalent to about 86% per ASK at mid-cruise, given that the short-range aircraft capacity is assumed to grow by 20%.

8.6.4 Advanced Cycle Engines NOx Emissions Assessments

The emissions assessments using Equation 21 have only been made for the engine cycles with lean 'constant pressure' combustors. EINOx figures given in Table 41 are just for the primary combustors. For those cycles that also have inter-turbine combustors (#03, #18), it is not obvious whether the overall EINOx would be increased or reduced. As in section 8.6.2 humidity corrections are applied. It is important to note that the intercooled cycles have been matched for best SFC, not for minimum NOx, so for these cycles the higher OPR has outweighed the NOx-reduction benefit from intercooling.

Table 41 – NOx Emissions Estimates for Advanced-Cycle Turbofans

Parameter\Engine Cycle	TF2050	#01	#02	#03	#18
EINOx at TOC (g/kg) at ISA+10 K	41.6	39.6	33.2	34.9	35.6
EINOx at mid-cruise (g/kg) at ISA	14.3	15.2	18.9	22.0	20.5
EINOx at EOR T/O (g/kg) at ISA+15 K	53.2	57.3	60.5	60.2	64.2

Since the engines have the same primary combustor technology and similar combustor exit temperatures, it is not very surprising that they have similar emissions indexes for NOx. For the engines with intra-turbine combustors, the

figures imply that, in proportion to their fuel flows, the second combustors would add as much NOx to the incoming flow as the primary combustors,

8.6.5 Uncertainty in Emissions Estimates

The uncertainty in the emissions estimates is greater than the uncertainty in SFC or fuel burn. For year-2050 study engines without topping cycles or secondary combustion, Equation 21 gives consistent lean-combustor NOx emissions estimates. The correlation predicts credible trends for changes in P3, T3, and T4, so it should at least be capable of ranking different engine designs in a sensible order of severity regarding NOx emissions. It should also be possible to use it in trade studies of NOx emissions v. CO_2 emissions. However, the prediction method cannot be used for engines with topping cycles and cannot be relied upon for cycles including secondary combustion, nor be expected to give very accurate absolute assessments of NOx emissions.

Some further discussion of uncertainties in emissions assessments is given in Appendix B following the investigation of existing and potential new methods for estimating NOx emissions.

8.7 Development Potential

In general it can be said that the advanced-cycle engines with intercooling and closed-circuit bottoming cycles have low overall development risk, since the engine architectures can remain close to the year-2050 reference engine and the same combustor technology can be used. Development of the supercritical-CO_2 bottoming cycle is considered low to medium risk in the 2050 timeframe and should be capable of being developed for earlier entry into service. The ABC might also be located in the tail-cone rather than needing a reverse-flow core arrangement, now that it seems that its heat exchanger is best placed downstream of the last turbine, rather than further upstream in the engine.

The proposed topping cycles using nutating-disc modules rely on significant enabling technology developments in the coming decades. Cycle#06 is the most-complex cycle with highly-turbocharged nutating disc modules. It assumes

relatively-low heat loss from the topping cycle, reducing the average hot-section temperatures by intercooling, but it sets very challenging requirements for the nutating-disc bearings, valves, sealing technologies and associated materials. The heat exchangers and the bottoming cycle turbine are considered to be lower risk.

8.7.1 Potential Hazards associated with the New Technologies

No systematic risk or hazard assessments have been carried out. However, the risk of uncontained turbomachinery or nutating-disc failures is considered low for all the concept engines (no greater than the risk of uncontained failures in conventional-cycle engines). Engine fuel or oil fires should also be a low risk for most of the new technologies, given sufficient attention to detail design.

The nutating-disc modules would add potential new failure modes and the highly-loaded bearings give cause for concern. A transmission system that could isolate and disconnect a module with overheated bearings or other problems might be able to avoid a potential in-flight shutdown, but it would also introduce the risk of inadvertent disconnection of the modules causing a shutdown.

All of the novel technologies will need to be developed to higher TRL and be rigorously assessed at each level during the process to ensure that they will be capable of meeting the required performance, weight, safety and reliability targets and to justify their inclusion in future aero engines.

9 SCENARIOS FOR THE ENVIRONMENTAL IMPACT OF AVIATION

This chapter analyses the potential impact of engine technology improvements, including those targeted by the author's advanced cycle studies, on the fuel burn and CO_2 emissions of the overall future civil airline fleet.[7] It considers factors affecting growth in civil aviation and different economic scenarios up to the year 2075 and beyond. It shows the potential impact of a step-change in fuel economy introduced starting from year 2050, consistent with the successful development of the proposed advanced engine technologies. It assumes the reference aircraft and engines would be available by 2050 and that the original target of a further 15% reduction in fuel burn could be achieved by combinations of advanced technologies. The implications of the study are discussed.

The spreadsheet developed for this study has been described in section 3.6.

9.1 Factors Affecting Growth in Civil Aviation

The design and operation of future aircraft could be significantly affected by consideration of aircraft noise and engine exhaust emission levels, but these factors have not been quantitatively assessed. For noise, the societal impact of the technology improvements is highly dependent on levels of local air traffic and operational procedures. It is anticipated that future aircraft will be quieter than current ones (even if and when open rotor engines are widely introduced) but any quantitative assessment of the impact of aircraft noise on airline market growth and economics is beyond the scope of this study. It is assumed that the long-term sensitivity of the global development of aviation to changing noise footprints and noise-reducing technologies will be relatively small.

Whereas aircraft noise has long been a major concern, more recently public interest has turned back to concerns about local air quality and to the global-warming impact of aircraft emissions. Legal challenges over NOx emissions as

[7] The author participated in the ULTIMATE project's 'Scenario Studies' and wrote the confidential ULTIMATE deliverable D5.5 [104], the main results of which are summarised here.

well as noise may now hinder airport expansion. Assessments should be made of the advanced-cycle-engine exhaust emissions, not only for the certification Landing and Take-off (LTO) cycle that is indicative of emissions in the immediate environment of airports, but also for on-route emissions that may contribute to climate change and stratospheric ozone depletion.

Aircraft operating economics are also considered as part of the scenario studies in sections 9.4 and 9.5. A simple top-down approach has been adopted for the current study, based on the proportion of operating costs attributable to fuel costs, either with or without additional taxation. Economic modelling is applicable to airline operations by both of the year-2050 ULTIMATE reference aircraft. These two aircraft types together are taken to be representative of airline fleet operations as a whole. Airline operations are assessed either for a fleet of aircraft with a fleet-mix typical of the airline aviation fleet as a whole, or for operation of just the latest aircraft and engine types, either with or without ULTIMATE technology. CO_2 emissions are also assessed for the whole civil aviation fleet, not just for passenger airliners and regional aircraft. It is important to distinguish between these different cases.

In order to predict the effects of changes in operating costs on the market for air travel, it is necessary to consider the price elasticity of demand. The price elasticity of demand (PED or $\boldsymbol{e_{(P)}}$) is defined in Equation 22 as the change in the quantity Q 'demand' divided by the change in the 'price' P. No change in unit demand means the elasticity is zero, but if demand reduces, PED is negative.

$$e_{(P)} = \frac{\Delta Q/Q}{\Delta P/P} \qquad \text{Equation 22}$$

The PED is not a constant but varies along the demand curve. It will tend to rise towards zero as the price falls, but this study is more interested in relatively small changes relative to the baseline scenario, typically for the years between 2040 and 2080, so the PED may be considered as a constant. Also, in terms of the elasticity of demand in the market for air travel, it can reasonably be assumed that the total sum that people would be prepared to spend on air travel

would not reduce if air fares increased, but that they would choose to fly less-frequently, so the PED is expected to be between -1 and 0.

A priori, it might be supposed that the number of flights taken should vary in inverse proportion to the square root of the price per km travelled, i.e. that PED is -0.5. Thus a 10% increase in the ticket price would result in about 5% fewer flights being taken, while total airline revenues would increase by about 5%. If airlines planned for this and reduced capacity and operating costs by 5%, then they would be able to accommodate a 10% increase in DOC per mission for the same level of profitability. Alternatively, if they did not reduce capacity they would only be able to accommodate about a 5% increase in DOC per mission. (However, these assumptions are likely to break down for very low prices.)

The actual elasticity of demand is obviously more complicated and will depend on the market sector, the routes, and the circumstances leading to the increase in ticket prices. These include, for example, levels of airline competition and increases in fuel costs, and whether other areas of the economy would also be affected by increased energy prices that might result in changes to disposable incomes. Note ticket sales are not the only source of airline income.

The International Air Transport Association (IATA) published an analysis of the price elasticity for air travel in 2008 [146]. This briefing document includes further useful references, and other more-detailed reports are also available on the IATA website under ‘economics’. The IATA analysis noted that passengers were becoming less sensitive to price, as increasingly lower prices, in real terms, meant that the air travel price itself has become a smaller and less important part of the total cost of a typical journey or trip. This is a trend that is likely to continue, at least in mature markets, though it may be less true in markets that are still rapidly expanding as a result of rising levels of disposable income (typically in the so-called BRICS economies of: Brazil, Russia, India, China and South Africa). Despite some current difficulties, these economies are expected to lead substantial growth in demand up to and beyond 2050, though by that time they might also be considered to be substantially mature markets.

For international travel PED was found to be about -0.6, but for domestic travel, where alternative modes of transport are likely to be available, the PED falls to about -0.8. For routes where there is airline competition, the PED falls still further to around -1.4, meaning that most passengers will be actively seeking-out lower cost options. These figures show that, up to year 2008 at least, demand was still quite cost sensitive. Assuming real disposable incomes will increase faster than real air travel prices, then it seems reasonable to assume PED will rise to -0.5 by year 2050, at least for long-haul flights. However, it makes sense to use a much more negative figure when comparing alternative airline operations and different levels of engine technology on competing routes.

The assumptions regarding air-traffic growth and infrastructure development scenarios were originally agreed in ULTIMATE deliverable D5.2 [106] but were further developed in D5.5 [105] and are summarised in the following sections.

9.2 Different Growth-rate Scenarios

The baseline air-traffic growth scenario assumes 4.5% increase in RPK and ASK per annum from year 1996 up until year 2030 and then modest reductions from 4.5% in each subsequent half-decade, as shown in Figure 70.

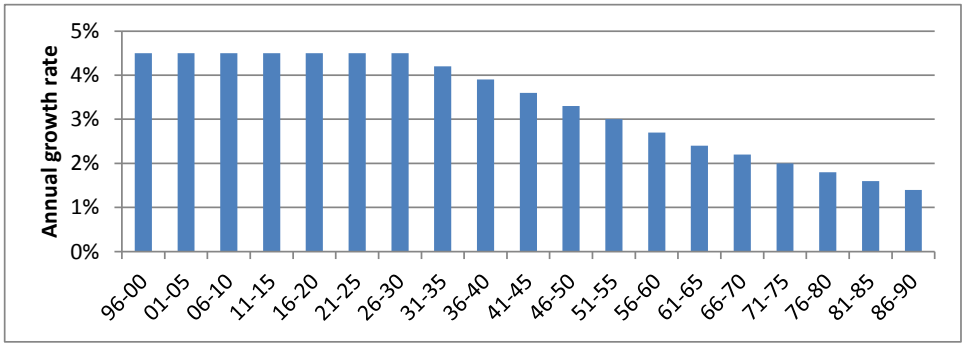

Figure 70 – Assumed Baseline Global Air Traffic Growth Rate (ASK p.a.)

The growth rate for previous years smooths-out the annual variations and may not be very accurate, but the overall level of passenger traffic is datumed to the figures for 2017 so forward projections should have a sound basis. After 2020 the alternative scenarios consider average annual growth rates that are either

1% higher or 1% lower than the baseline. Figure 71 shows the cumulative effect of these different assumptions, normalised against the year 2020 ASK level.

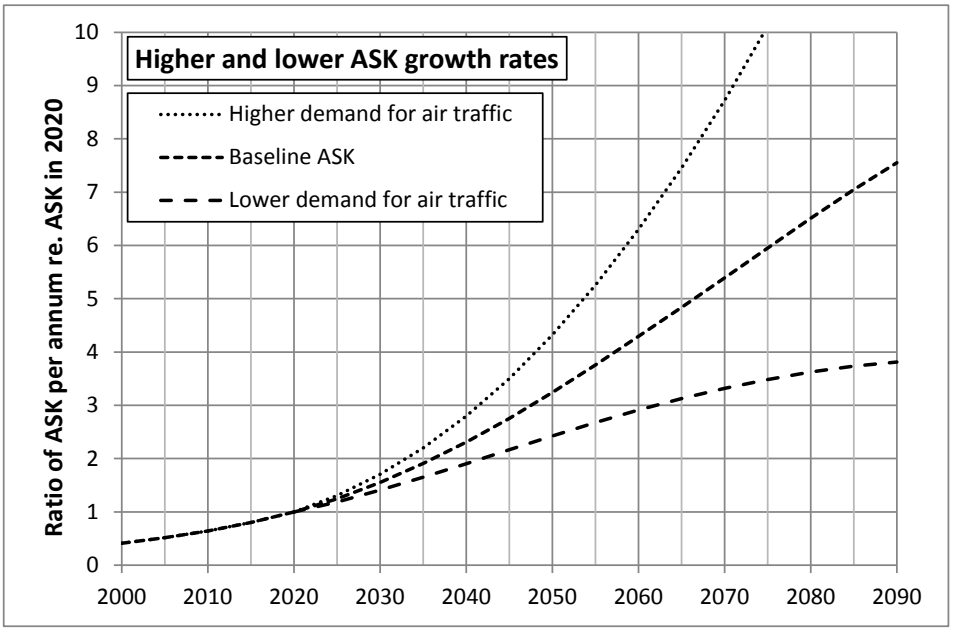

Figure 71 – Effect of Different Growth Rates on Total ASK per Annum

For reference, in year 2020 it is assumed that global passenger airlines will service 3643 billion RPK, 4554 billion ASK. The passenger load factor (PLF), which is the ratio of RPK to ASK, is assumed to remain constant at 80%.

9.3 Fuel-burn and CO_2 Emissions Estimates

Given the preceding methodology and assumptions, the overall civil commercial fleet's fuel consumption and mission-level CO_2 emissions for the baseline year 2000 have been estimated as shown in Table 42 and Table 43.

The factors in Table 42 also apply to the baseline scenario calculations, tables and plots for subsequent years, whereas the factors in Table 43 are specific to the year 2000. In Table 43 the estimated civil fleet fuel-burn figure for the year 2000 is compared to the production of jet fuels in that year.

Table 42 – Benchmark for Fuel-burn and CO_2-emissions Calculations

Parameter	Units	Value	Remarks
Litres per barrel of jet fuel	–	159	US standard barrel
Typical density of jet fuel	kg/m^3	797	From [106]
Typical mass of jet fuel/barrel	kg/barrel	126.7	Product of the two terms
kg of CO_2 per kg of jet fuel burned	–	3.148	As explained above
ASK flown by short-haul aircraft	–	54%	The current-fleet factors as [106] are assumed constant from 1990 onwards
ASK flown by long-haul aircraft	–	46%	
Extra fuel for other operations	–	20%	Estimated
Total RPK in 2017	km/year	7.7×10^{12}	From www.statistica.com
Total ASK in 2017	km/year	9.625×10^{12}	Assumes 80% PLF

Table 43 – Estimation of Fuel-burn and CO_2 Emissions in Year 2000

Parameter	Units	Value	Remarks
Total ASK in 2000	km/year	4.554×10^{12}	$= (9.625 \times 10^{12})/(1.045^{17})$
Baseline short-range fuel burn/seat	g/km	19.64	From [12]
Baseline long-range fuel burn/seat	g/km	22.23	From [12]
New a/c fuel burn per seat in 2000	g/km	20.831	The weighted figure
FB factor allowing for older aircraft	–	1.1586	$= 1/0.98539^{10}$
Fleet fuel burn per seat in 2000	g/km	24.13	Product of the two terms above
FB factor for operations in 2000	–	1.1765	= 1/0.85
FB factor for additional fuel use	–	1.200	Estimated as above
Fleet fuel consumption in 2000	M tonnes	155.2	Estimated as above
Fleet mission-level CO_2 in 2000	M tonnes	489	Conversion using factor 3.148
Jet fuel production/day in 2000	k barrels	4703	From IATA Press Release No. 4
Total jet fuel production in 2000	M tonnes	209	Using the factors in Table 42
Ratio of estimated civil aircraft fuel use to production in 2000	–	74.3%	Note not all jet fuel is used in civil aircraft or in aero engines

The estimated consumption of about 155 million tonnes in the civil aircraft fleet is about 74% of the total. This may well be an underestimate, notwithstanding that significant amounts of fuel would have been used in other types of aircraft

and some also in some gas turbines for power generation and oil pipeline-pumping operations etc.

Calculations for the baseline scenario, summarised in Table 43 for year 2000, were repeated for years 2017, 2020, 2035, 2050 and 2075 and tabulated in [105]. In the baseline scenario, no ULTIMATE technology benefits are claimed before 2050. However a 15% fuel-burn reduction from ULTIMATE technologies is accounted in 2075, assuming that these would be introduced progressively across the fleet between the years 2050 and 2075, and ultimately applied to aircraft accounting for 90% of the total civil-aviation fuel burn.

Figure 72 shows the baseline scenario with projected civil aviation fleet mission-level fuel burn as a function of air traffic growth, ATC and operational improvements, aircraft and engine technology improvement and the original 15% target for ULTIMATE fuel-burn reductions, assuming these are introduced progressively into 90% of the civil fleet over 25 years from the end of 2050. The green dotted line shows the ATAG target for stabilising CO_2 emissions by 2020 and halving them by 2050. The CO_2 reductions to achieve this target might include the use of bio-fuels and synthetic fuels as well as sequestration and other forms of offsetting.

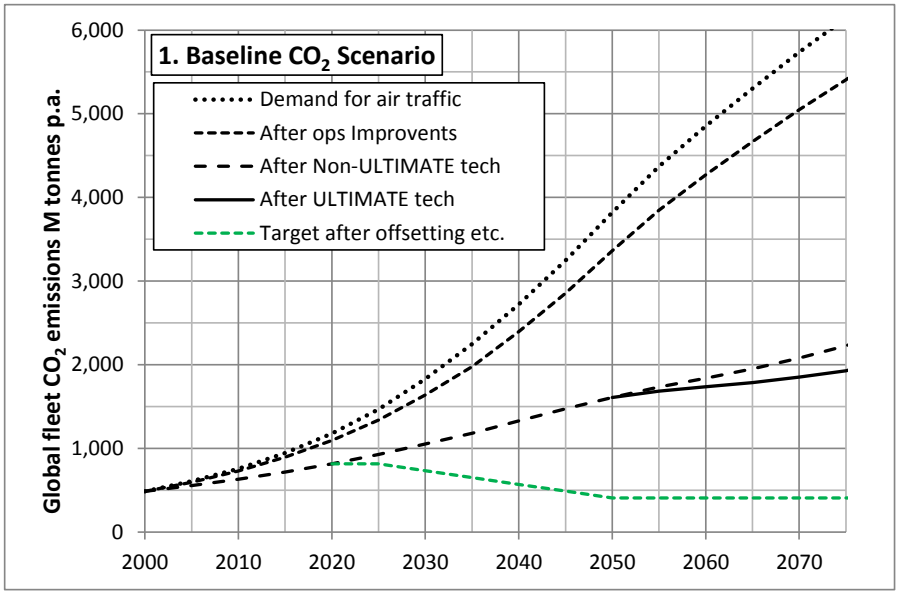

Figure 72 – Baseline Scenario predicting Civil Aviation CO_2 Emissions

The predicted saving from ULTIMATE technologies is over 290 million tonnes of CO_2 per annum by 2075 according to the baseline scenario in Figure 72.

Figure 73 shows how Figure 72 is modified by the higher and lower growth rate scenarios shown in Figure 71. Only in the low-growth scenario do mission-level CO_2 emissions more or less level-off after 2050. For the baseline and high-growth scenarios the CO_2 emissions continue to grow rapidly, accelerating again after 2075, when all the available technology improvements have been rolled-out across the fleet. In the near-term these targets can only be met by offsetting the aviation CO_2 emissions, but in the longer-term biofuels and/or synthetic fuels may help close the gap, but these technologies are beyond the scope of the current study.

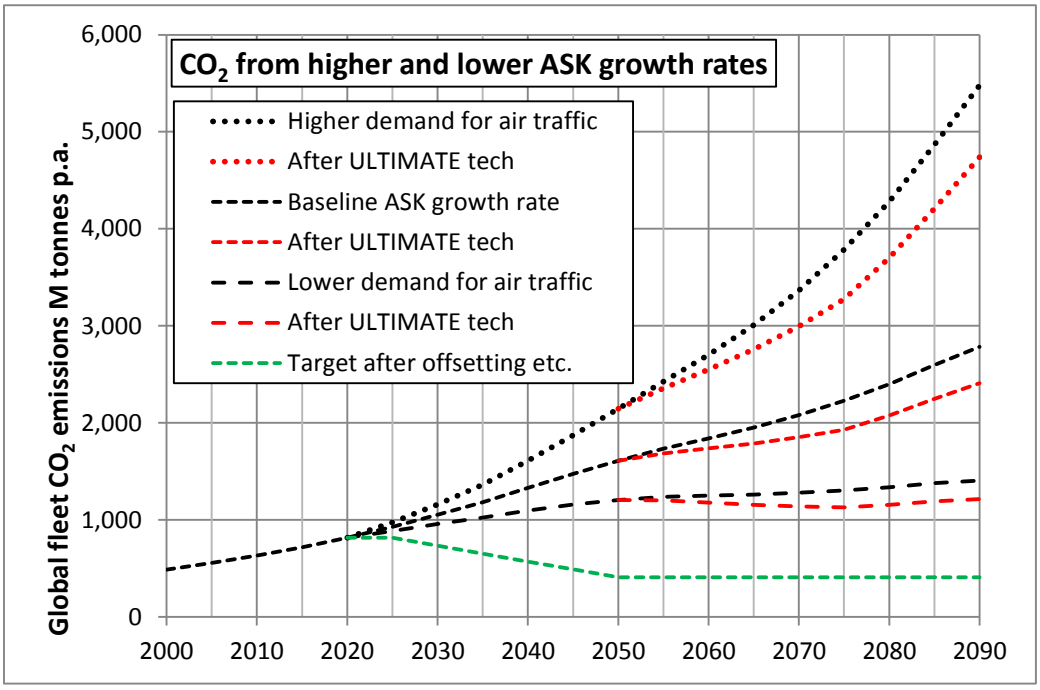

Figure 73 – Effect of ASK Growth Rates on Mission-level CO_2 Emissions for the whole civil aviation fleet

It should also be noted that the year-2050 reference aircraft and engine performance assessments do not take account of potential further benefits of hybrid-electric distributed propulsion and boundary-layer ingestion technology, which might help to close the gap between the performance of the ULTIMATE

year-2050 reference aircraft and engine designs, and the SRIA targets. These additional technologies together with more-radical airframe designs might provide the further ‘non-ULTIMATE’ technology improvements anticipated after 2050. Even though the technologies providing improvements in the 2050–2070 timeframe are highly uncertain, it seems likely that there would still be some.

Further mission-level CO_2 reductions might be achieved with alternative engine fuels such as liquid methane or liquid hydrogen. However, the use of liquid hydrogen in fuel cells to generate auxiliary power on the ground for emissions-free taxiing and to generate secondary power in the air is already assumed in the reference aircraft for year 2050. This contributes to the claimed reference engine technology CO_2 reductions in 2050 relative to year 2000, but the fuel consumption by auxiliary power units prior to year 2050 has not been explicitly accounted. In common with [11] and [12], this study assumes that lower cruise speeds will be used in year 2050 to help reduce CO_2 emissions. Whether fuel cells would actually be used in-flight in primarily-kerosene-fuelled aircraft and whether lower cruise speeds would actually be adopted by airlines to save fuel, are questions very-much open to debate.

No charts are presented for pollutant emissions other than CO_2, though efforts to reduce fuel burn will also tend to reduce overall emissions pro rata for a given combustion technology level. Flightpath 2050, however, sets more demanding targets for disproportionate reductions in emissions of oxides of nitrogen (NOx). Reducing these pollutant emissions is particularly challenging, but necessary in order to minimise the impact of aviation on human health and the environment.

The ULTIMATE study engine cycles and combustion technologies aimed to demonstrate that these further emissions reductions would be possible. With that in mind, the reference engine cycles for year-2050 avoided excessively-high combustor and turbine entry temperatures that would tend to increase NOx emissions, even with advanced lean-burn combustor technology.

Note the CO_2 emissions predicted here for civil aviation are only the emissions from burning fuel in the aircraft. There are further CO_2 emissions associated

with producing fuel and distributing it to airports. These extra emissions (typically adding 15–30% CO_2) may also be attributed to aviation, together with the emissions from airport operations and associated ground traffic.

9.4 Fuel Cost, Taxation and Airline Economics

A large number of assumptions have had to be made to estimate future aviation fuel costs, potential carbon taxes and operating economics. Further to the methodologies described in section 3.6, Figure 74 below, from [106], proposes likely upper, lower and 'most likely' oil prices out to year 2090, based on nearer-term predictions in the public domain. It also considers the possible introduction of a carbon tax increasing progressively after its introduction from year 2050 and effectively adding to the cost of oil. Note the cost of oil is converted to the cost of aviation fuel (in USD/kg) as described in section 3.6.

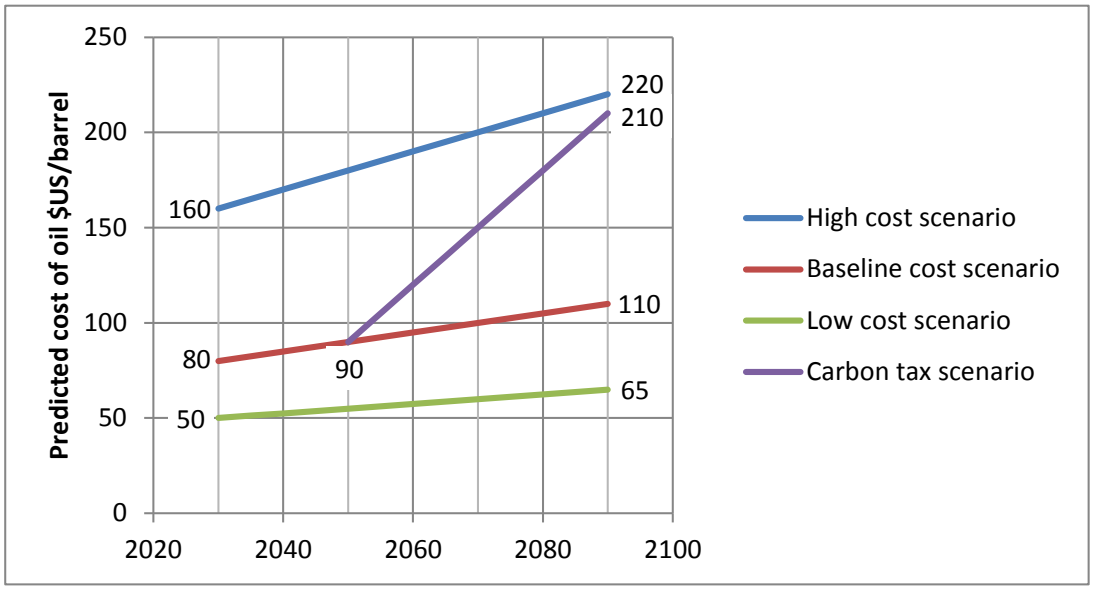

Figure 74 – Suggested Future Oil-price Scenarios [106]

The predicted commercial airline fleet total fuel costs for the high, baseline and low fuel-cost scenarios are shown in Figure 75, assuming no change in demand due to cost of fuel, i.e. assuming the PED is zero. Note the global figures are for airlines only and not for the whole civil aviation fleet.

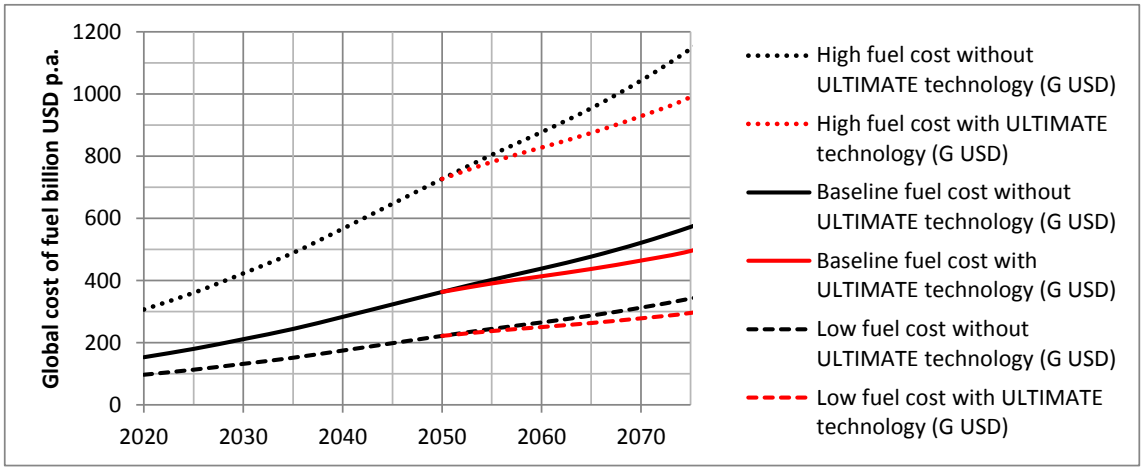

Figure 75 – Total Cost of Fuel for Airlines assuming Demand is Unaffected (ULTIMATE technologies providing 15% fuel savings to 90% of the fleet by 2075)

Airline costs are generally expressed in US cents per ASK. Therefore Figure 76 divides the total cost of fuel to global airlines by ASK. Note the improvement in fuel economy outweighs the anticipated increase in fuel cost. (The slight kink in the curves at year 2035 is because it is assumed that after that date there are no further benefits to come from improvements in operational efficiency.)

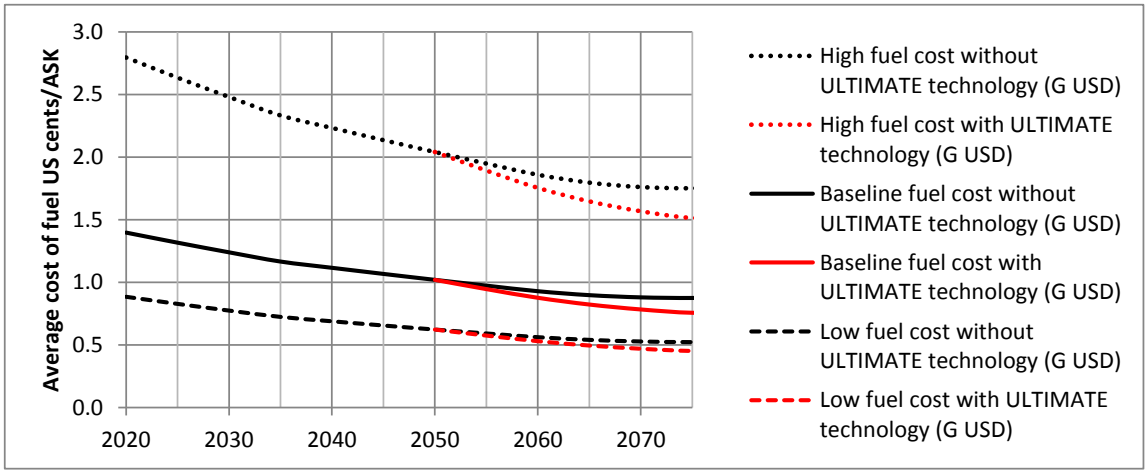

Figure 76 – Airlines' Fuel Cost per ASK assuming Demand is Unaffected (ULTIMATE technologies providing 15% fuel savings to 90% of the fleet by 2075)

To put the cost of fuel into context, it is necessary to consider how other costs may increase. To estimate the effect of fuel price on future direct operating costs it is necessary to take account of inflation as applied to overall airline

operating costs. The assumption here is that inflation rates for aviation services will remain low with respect to the US dollar. Over the last 35 years the general inflation rate in the USA has typically fluctuated between 2% and 5%. It is currently nearer to 2%, which is a figure that may be considered a reasonable target for the foreseeable future. However, air transport costs have not risen at this rate. For example, in the first decade of the 21st century, well after deregulation in the USA, US domestic air fares were still reducing. Even between 2001 and 2017 average US air fares only increased by 8.4% from $320.62 to $347.63, according to the US Bureau of Transportation Statistics. (See: https://www.transtats.bts.gov/AverageFare/)

The slow increase in revenues reflects the increasing productivity of modern airline equipment and operations – trends that are expected to continue. They correspond to an average cost increase per ASK of 0.5% per annum, which is very close to the rate corresponding to the baseline scenario for oil price increases projected from 2030 to 2090. Provided these trends continue, then in the baseline case it may be assumed that total airline costs including acquisition, maintenance and operating costs, will rise by 0.5% per ASK per annum, roughly in proportion to the unit cost of fuel. However, in the baseline scenario the cost of fuel as a proportion of the overall cost is reducing as more efficient engines and aircraft have been introduced into the fleet. Thus 'inflation adjusted' costs will continue to reduce in real terms so that air travel will become increasingly affordable. This will help to sustain the increasing demand predicted for air travel with corresponding growth in RPK and ASK.

9.5 Airline DOC Trends

The derivation of a simple top-down model for airline fleet-average operating costs is described in section 3.6.2. This generated the results given in Table 44. The Cost per Available Seat Kilometre (CASK) in 2017 comes out at about 6 US cents, For comparison, US network airlines had costs approaching 7 US cents/ASK, while low-cost operators had costs from 4 to 5 US cents/ASK, so the aggregate DOC figures therefore are only indicative of average airline costs.

Table 44 – Global Fleet Top-down DOC Figures for 2017

Parameter	Units	Value	Remarks
ASK in 2017	km/year	9.625×10^{12}	From Table 44
Fleet fuel burn per seat in 2017	g/km	18.79	As above
FB factor for operations in 2017	–	1.1061	As above
Fleet fuel consumption in 2017	M tonnes	200.1	Excluding non-airline fuel use
Average cost of oil in 2017	US$/barrel	55	From ULTIMATE D5.2 [106]
Fuel cost in 2017	US$/kg	0.521	= 55 x 0.00947
Fuel cost re. DOC in 2017	–	18.75%	Estimate based on Table 16
Global fuel bill in 2017	$	104.2×10^9	For commercial airlines only
Global overall DOC in 2017	$	556×10^9	As above
DOC per ASK (CASK) in 2017	US$/ASK	0.0577	As above
Inflation rate assumed for all airline costs other than fuel	p.a.	0.5%	Note this is lower than the anticipated general inflation rate

From the simple DOC model it is possible to see how variations in fuel price affect DOC. Figure 77 shows how the CASK figures for the airline industry might increase under different fuel-cost scenarios. As with Figure 75 and Figure 76, this assumes that the baseline air traffic growth is unaffected by DOC changes, i.e. that the PED is zero.

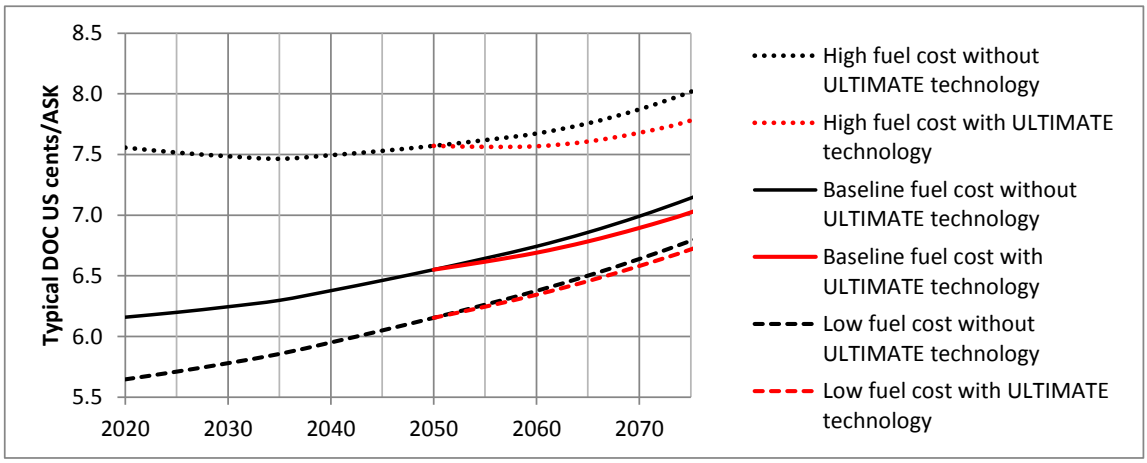

Figure 77 – Effect of Fuel Price on CASK assuming no change in Demand (ULTIMATE technologies providing 15% fuel savings to 90% of the fleet by 2075)

For engines incorporating ULTIMATE technologies it is further assumed that there is no additional increase in acquisition and maintenance costs, which is optimistic. Thus these plots may be taken to represent the upper bound of potential DOC savings for the baseline air traffic growth scenario.

Alternatively, if it is assumed that PED is -0.5, as discussed in section 9.1, and that ticket prices follow DOC, and PLF remains at 80%, then the ASK (or RPK) should vary inversely as the square root of DOC. The effect is shown in Figure 78, which implies that the high fuel-cost scenario could hold back air-traffic growth by two years or more, whereas the low fuel-cost scenario could advance it by about a year. These changes are potentially very significant to the airlines and to the aircraft and engine manufacturers. (The potential benefits of ULTIMATE technologies on market growth are smaller in comparison.)

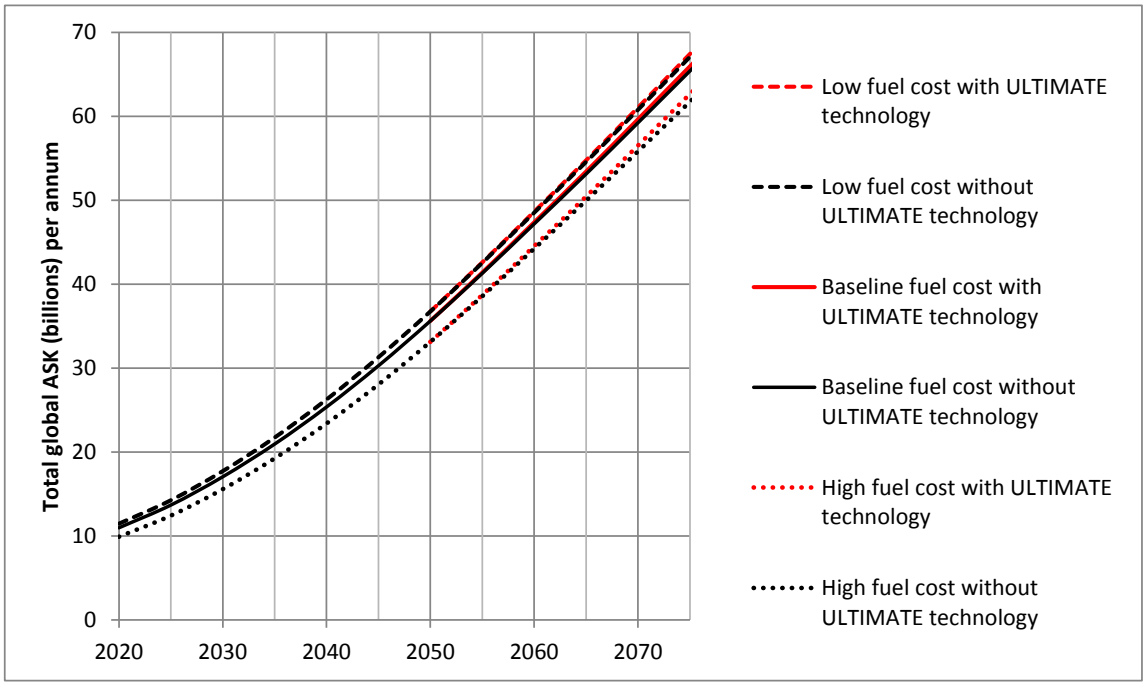

Figure 78 – Effect of Fuel Price and Technology on ASK Growth (assuming PED is -0.5 and ULTIMATE technologies provide 15% fuel savings to 90% of the airline fleet by 2075)

However, if the cost of fuel should oscillate between the upper and lower bounds over periods of a few years, the airlines would in practice try to smooth

out the variations. Initially they can do this by hedging the fuel costs and taking larger or smaller profit margins according to the market conditions. Airlines can also match ASK to the RPK demand by retaining older aircraft for longer or by retiring them earlier (either permanently or just temporarily).

The previous figures are for airlines as a whole, but the fuel costs would be significantly lower for an airline operating only the latest aircraft and engines. The fuel costs would vary as shown in Figure 79, and supposing there would be no change in the non-fuel costs, the CASK would vary as shown in Figure 80.

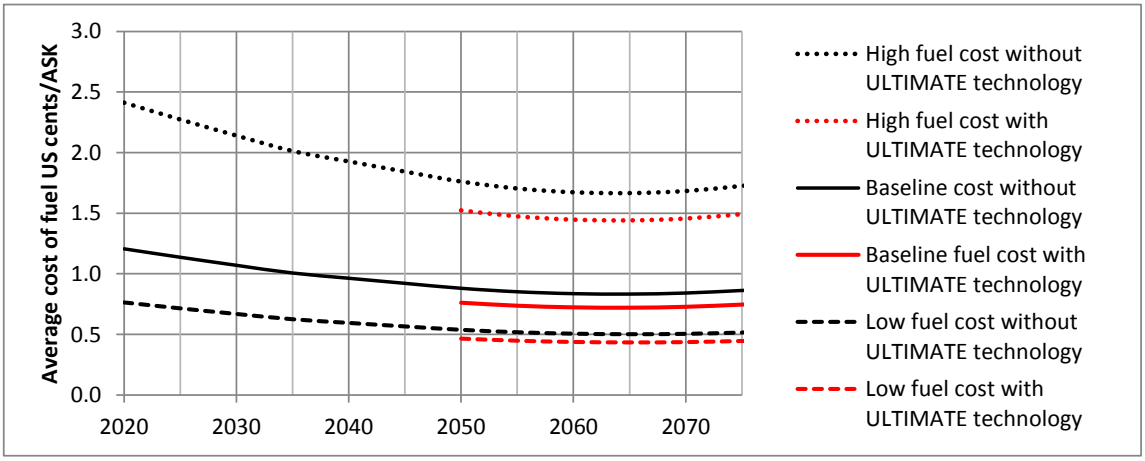

Figure 79 – Cost of Fuel for Airlines only operating the Latest Equipment (ULTIMATE technologies making 15% fuel savings to 90% of its fleet from 2050)

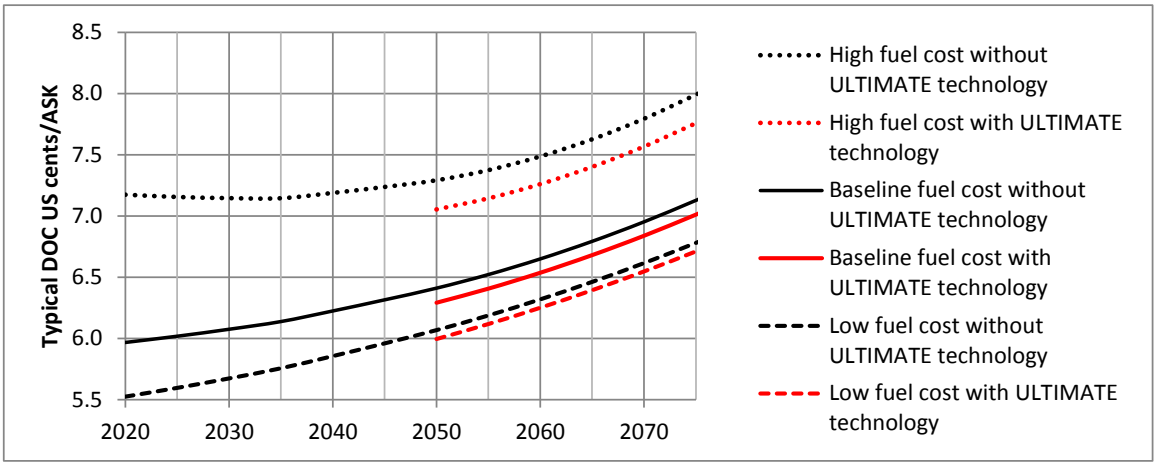

Figure 80 – CASK for an Airline only operating the Latest Equipment (ULTIMATE technologies making 15% fuel savings to 90% of its fleet from 2050)

It is clear that the economic benefit of having more-advanced and fuel-efficient aircraft and engines increases with a higher fuel cost. Relative to the baseline scenario, a sustained higher fuel cost should accelerate research into more-energy-efficient solutions. Conversely, sustained lower fuel costs are likely to delay the development and introduction of new designs.

For an airline choosing whether in year 2050 to acquire new aircraft with ULTIMATE technology engines, or perhaps less-expensive aircraft with year-2050 reference engines, the improvement in fuel burn must be balanced against increases in acquisition and maintenance costs. Considering the cost breakdown in Table 16, after extracting 18.75% for fuel, then acquisition accounts for 6.6% of the remaining costs, and maintenance accounts for 12.6%. Together these make up 19.2% of the non-fuel costs.

Supposing the 15% reduction in fuel burn might be associated with a 7.5% increase in maintenance and acquisition costs; then much of the cost benefit would be eroded. Figure 81 shows how the overall benefit from ULTIMATE technology would then depend on the fuel price, assuming 90% of the new fleet could use the technology. In this case the overall cost saving is greatly reduced for the baseline fuel cost, is non-existent in the low fuel-cost case, but still significant for the high fuel cost scenario.

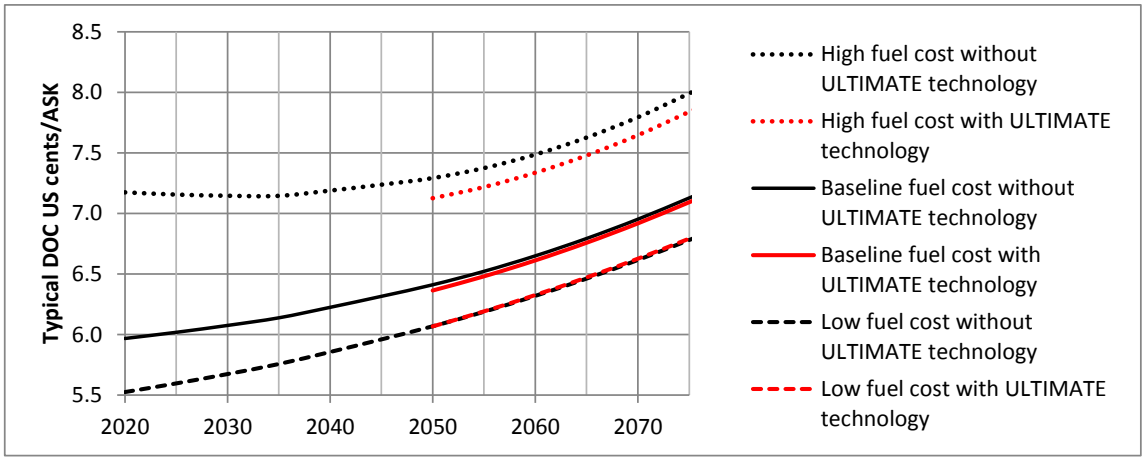

Figure 81 – Effect of a 7.5% increase in Acquisition and Maintenance Costs for acquiring ULTIMATE technologies from year 2050 onwards

9.6 Implications of the Scenario Studies

These studies have attempted to quantify likely future fleet-wide energy and CO_2 savings achievable with and without the benefits of the novel technologies and new engine design concepts researched to TRL 2 in the ULTIMATE project. The future air-traffic growth scenarios from ULTIMATE deliverable D5.2 [106] and deliverable D5.5 [105] account for changes in external forces such as fuel price and environmental regulations. They can be used to predict how the introduction of ULTIMATE technologies could affect the growth in air traffic, the civil air transport fleet's energy needs, and the resultant environmental impact.

Based on these forecasts it is seen that total mission-level CO_2 emissions from the global civil-aviation fleet will probably continue to grow up until the end of this century and, with or without ULTIMATE technology, will only start to level-off in the case of the scenario with the lowest rates of air-traffic growth. Nevertheless ULTIMATE technologies can produce significant reductions in CO_2 emissions. The target of a 15% reduction in fuel burn from engines and aircraft incorporating these technologies seems achievable provided that more than one loss source is targeted and synergistic combinations of technologies are integrated into future engines and powerplant installations.

The ATAG target of stabilising aviation CO_2 emissions by 2020 and of halving them by 2050 can only be met by offsetting in the short to medium term. The predicted quantities needing to be sequestered or otherwise offset in 2050 and 2075 depend on the air-traffic growth scenarios and the whether the CO_2 target for 2075 is the same as for 2050 or zero as shown in Table 45. This table assumes that the target 15% fuel-burn reduction from ULTIMATE technologies is achievable and is implemented across 90% of the civil aviation fleet by energy use. Note these figures make no allowance for the CO_2 generated in the production and distribution of fuel to airports, or for the introduction of biofuels or synthetic fuels to reduce CO_2 emissions.

A recent report by the US National Academies of Sciences, Engineering and Medicine [147] has identified the least-costly options for sequestering CO_2. It

concluded that there are near-term options that can be implemented at costs ranging from around $20 to $100 per tonne. However, the potential capacity of these low-cost options is limited.

Table 45 – Predicted Requirements for the Sequestration of CO_2 Emissions (billions of tonnes p.a.)

Reduction target year \ Scenario	High Growth	Baseline	Low Growth
2050, to 50% of year 2020 emissions	1.74	1.20	0.80
2075, to 50% (or to zero, without ULTIMATE)	3.37 (3.78)	1.82 (2.23)	0.90 (1.31)
2075, to 50% (or to zero, with ULTIMATE)	2.86 (3.27)	1.52 (1.93)	0.72 (1.13)
2075 potential ULTIMATE technology savings	0.51	0.30	0.18

Aviation is not the only industry that will need to offset its CO_2 emissions. (Cement production presents similar problems on an even larger scale.) So, as the quantity of CO_2 to be offset from all industries grows, and the cost of genuinely offsetting these emissions increases, other long-term solutions will be needed. These are likely to require engines to use biofuels or synthetic fuels, since only very-short-range or 'personal-mobility' aircraft will be able to be fully-powered by stored electrical energy that could ultimately be provided by renewable or nuclear energy sources.

Decarbonisation of the aviation industry itself will require the development of new fuels, either biofuels (the production of which still generates some CO_2 emissions) or synthetic fuels. The simplest synthetic fuel is hydrogen, which can be produced by electrolysis of water, but hydrocarbon fuels can also be synthesised from the hydrogen and carbon dioxide extracted from the air or from sea water. This is a very costly way of providing fuel today, but even if the costs come down with the development of renewable energy sources, the proposed advanced-cycle engine technologies would still reduce aircraft energy requirements and have a significant role to play in minimising energy costs and their associated environmental impacts.

10 CONCLUSIONS AND RECOMMENDATIONS

The research objectives outlined in section 1.1.1 included:

- Determining the pros and cons of the novel technologies and combinations of technologies that could improve the thermal efficiency of future engines,
- Identifying a realistic large commercial turbofan engine performance cycle and architecture with potential for a 15% step-change reduction in fuel-burn together with reduced NOx emissions,
- Creating a concept design for a nutating-disc topping-cycle module and assessing its performance and mechanical limitations,
- Quantifying the incremental benefits from potential technologies including intercooling, secondary combustion and topping and bottoming cycles,
- Selecting a method for predicting the NOx emissions of future-engine lean-burn combustion systems,
- Estimating the likely impact of technology improvements on civil-aviation CO_2 emissions for a number of different scenarios up to 2075 and beyond,
- Comparing predicted year-2050 engine emissions with industry targets.

These objectives have almost all been achieved, except that not all the variant cycles of interest have been modelled and quantitative predictions of NOx emissions have not been made for engines including topping cycles. It had also been hoped that the review of recent NASA research on LDI combustors would have enabled an improved method for future LDI combustor NOx emissions estimation to be recommended in preference to Equation 21, but it was not possible to justify a new correlation to supersede it.

10.1 Summary

The potential for year 2050 aero engines combining multiple novel technologies to achieve very high thermal efficiency and very low SFC has been addressed in these studies. It is concluded that a geared turbofan engine cycle that would combine intercooling, topping and bottoming cycles, and secondary combustion

is capable of meeting the ULTIMATE 15% fuel-burn reduction target and merits further study. The logic for combining these four technologies is as follows:

- Topping cycle machines that can also generate power offer the biggest single improvements in thermal efficiency by reducing the exergy losses incurred in combustion,
- Intercooling reduces compression work, increases core specific power, saves weight (in combination with a topping cycle) and can help to limit peak cycle temperatures, thereby reducing NOx emissions,
- Secondary combustion boosts power output to meet take-off and climb thrust requirements without increasing the peak cycle temperatures and potentially without increasing NOx emissions,
- Finally the bottoming cycle extracts additional power from residual heat in the core exhaust.

A geared fan engine architecture that integrates these technologies has been selected and is shown schematically in Figure 26. It has a reverse-flow-core arrangement to avoid compromising the design of the core turbomachinery and it uses an open 'air-cycle' bottoming cycle (ABC) to avoid the need for a pre-cooler. Topping cycle modules are arranged around the core and the intercooler is located at the aft-end of the engine so that the spent cooling air can be exhausted through an efficient centre-line variable-area plug-nozzle. Topping-cycle modules using pairs of nutating discs have been studied, but alternative rotary or piston engine designs might be substituted.

Some simplification of this architecture now seems possible without detriment to SFC or fuel-burn by eliminating the optional HP compressor and relocating the ABC heat exchanger aft of all the core turbine stages.

The methodology and spreadsheet for quantitative performance assessment of potential year-2050 turbofan engines has been described. A conventional Brayton-cycle engine for 2050 EIS has been taken as a starting reference and scaled to the thrust requirements of an advanced year-2050 long-range study aircraft provided by ULTIMATE project partner BHL.

The contribution of each of the four new technologies has been assessed by adding each one in turn. Cycle temperatures have been limited to enable lean combustion systems to achieve low NOx emissions, but emissions from engines including a topping cycle or secondary combustion have not been quantified.

The weights of the study engines have been assessed in order to estimate the fuel-burn benefits when the engines are installed on year-2050 ‘advanced tube and wing’ aircraft. The fuel-burn exchange rates were provided by BHL. The aircraft with more-efficient or lighter engines have thrust requirements that are further reduced for a given mission, compounding their fuel-burn and CO_2 emissions reductions.

Before the year-2050 aircraft thrust requirements and fuel-burn exchange-rates were available, the study engines were sized for year-2000 technology aircraft. Initial engine assessments were made at fixed thrusts and with a mid-cruise specific thrust of 72 m/s. In the later stages of the study the engines were re-sized to match the year-2050 reference aircraft with the year-2050 reference ‘TF2050’ engines. These had approximately 25% lower thrust requirements. The later study engines also had slightly higher specific thrusts, shown by other studies in the ULTIMATE project to give lower fuel burn when weight and nacelle drag were taken into account.

Although predicted to have higher fuel burn, engines having lower specific thrust generally give lower noise and lower LTO NOx emissions. Conversely, engines having higher specific thrust than the fuel-burn optimum may have better overall economics. Therefore further trade-studies might be considered.

The advanced-cycle engines promise significant performance improvements with respect to the reference turbofan, but further research and innovative component design is needed to underwrite the predicted SFC improvements and the associated engine weight and fuel-burn assessments.

10.2 Main Outcomes

Design-point trade studies have indicated that the scaled-down conventional reference turbofan engine cycle for 2050 entry into service is close to optimum for long-range aircraft missions. The take-off temperature limits assumed should enable low NOx emissions to be achieved with lean combustion.

Scaling-down is shown to have significant effects on engine component efficiencies and on turbine cooling-air requirements. To model the major effects on core performance, the HP compressor and turbine efficiencies were adjusted for variations in HP compressor last-stage blade-height. The cooled cooling air mass flows were varied with core mass flow and TET. The non-intercooled study engines were limited on HP compressor delivery temperature, so as efficiencies reduced in scaled-down engines, the OPR also reduced.

In an extreme case of scaling-down to 25% of the original thrust and half the original fan diameter, the OPR for a given HP compressor delivery temperature could reduce by about 13%, increasing SFC by about 7% and reducing thermal efficiency by 6.5%. Intercooling in the larger engines could reduce mid-cruise SFC by about 3% and max climb SFC by nearly 4%, giving 4–5% fuel-burn reduction, but for the smaller engines, the SFC reductions are nearer to 2% because they suffer disproportionately from the scaling-down of their cores.

Axi-centrifugal HP compressors might be substituted for all-axial compressors to improve component efficiency in the smallest cores, but this option has not been modelled in the current study.

Cycles with the lowest mid-cruise SFC may not be the overall optimum cycles, because geared fan engines with slightly lower OPR and smaller core mass flows will tend to be lighter. Practical considerations mean that the fuel burn optimum and economic optimum designs are likely to back-off from cycles with the highest OPR and lowest SFC, made possible by having cooled cooling air and/or intercooling. This applies particularly to smaller thrust-scale engines.

Very high OPR cycles pose particular design challenges including, more highly loaded bearings, compressors and turbines needing extra stages, and more variable stages on each compressor. Without further research and innovative design these challenges could prevent the ambitious 2050 SFC targets being achieved. However intercooling and cooled cooling air technologies provide the core turbomachinery with more benign thermal environments that should help with other issues including component life, heat to oil, and tip clearance control.

10.2.1 SFC, Fuel Burn and CO_2 Reductions

The selected cycle combining intercooling, topping and bottoming cycles, and secondary combustion has been modelled as providing almost 15% lower SFC than the reference year-2050 turbofan at mid-cruise and top of climb conditions. This performance was achieved despite limiting the overall pressure ratio to the nutating-disc accumulators to 80 at top of climb and the pressure to about 70 bar at take-off. Higher pressures could have given better performance, but would have made the nutating-disc bearing loads even higher. The proposed pressures still present the design of the bearings and seals with significant challenges. Alternative topping-cycle technologies, e.g. free-piston core engine modules, might overcome the pressure limitation on performance improvement.

Table 46 shows how the CO_2 savings of the modelled engine designs compare with the SRIA CO_2 emissions target corresponding to a 68% fuel-burn reduction, not allowing for ATC and airline operations improvements.

Table 46 – SFC and Fuel Burn for Selected Engine Cycles

Parameter\Engine Cycle	TF2050	#01	#02	#03	#06	#18
Thrust (kN)	49.99	49.99	49.99	49.99	49.99	49.99
Mid-Cruise SFC (g/kN.s)	12.62	12.63	12.24	11.65	10.76	12.61
Relative SFC (%)	-0.1	datum	-3.1%	-8.2%	-14.8	-0.2
Overall Cruise Efficiency (%)	43.15	43.19	44.57	47.05	50.69	43.26
Fuel Burn (kg)	-	47056	45472	42655	38353	47117
Relative Fuel Burn	-	datum	-3.4%	-9.4%	-18.5%	+0.1%
CO_2 saving re. year 2000 (%)	-	45.5	47.4	50.6	55.6	45.5

A year-2000 baseline-aircraft fuel burn of 86390 kg is implied by [11] so the target of 27645 kg is not yet met. The fuel-burn benefit for the turbofan with the supercritical CO_2 bottoming cycle (cycle#16) modelled by Jacob [62] [9], is similar to that of the year-2050 high-OPR intercooled turbofan engine cycle#02.

10.2.2 Predicting Future Engine NOx Emissions

Lean Direct Injection (LDI) primary combustion systems are proposed for the year-2050 reference engines and all variants without topping cycles. This study has reviewed a wide range of options for estimating LDI combustor exhaust emissions. The NOx emissions targets are particularly challenging because they are to a large extent driven by the minimum residence-time needed to achieve altitude relight, though it is also possible to trade-off NOx emissions against soot, CO and UHC emissions to some extent.

Different approaches to formulating correlations have been investigated and various previously-published and potential new correlations compared and analysed in detail in Appendix B. The conclusions are summarised in the next section. For various reasons, none was found to be entirely satisfactory. A relatively simple and robust NOx emissions correlation was considered most appropriate for the study, so it was decided to continue using an established NASA correlation, Equation 21. This correlation for advanced lean combustors has already been used in previous EU research programmes. This equation is taken to include the benefits of anticipated combustor design improvements minimising hot-spots and reducing the amount of combustor wall-cooling and dilution-air required. The latter would be enabled by using improved combustor materials, such as ceramic matrix composites. Other improvements anticipated for year-2050 include improved fuel injector detail design and sophisticated fuel-scheduling or fuel-staging between multiple fuel injector nozzles.

It is noted that Lean Premixed Prevaporized (LPP) combustion systems, could have combustion temperatures T_c that are more uniform than LDI combustors and potentially produce lower NOx emissions. However these combustors are not proposed for the year-2050 reference engines in this study. This is because

the year-2050 engine cycles have very high combustor inlet temperatures that would present a serious risk of premature ignition and flash-back.

Figure 82 shows how the LTO-cycle Dp/Foo NOx emissions predicted for the ULTIMATE year-2050 short-range (GOR2050) and long-range (TF2050) reference engines compare with the ICAO emissions database figures for two representative year-2000 in-service aircraft engines.

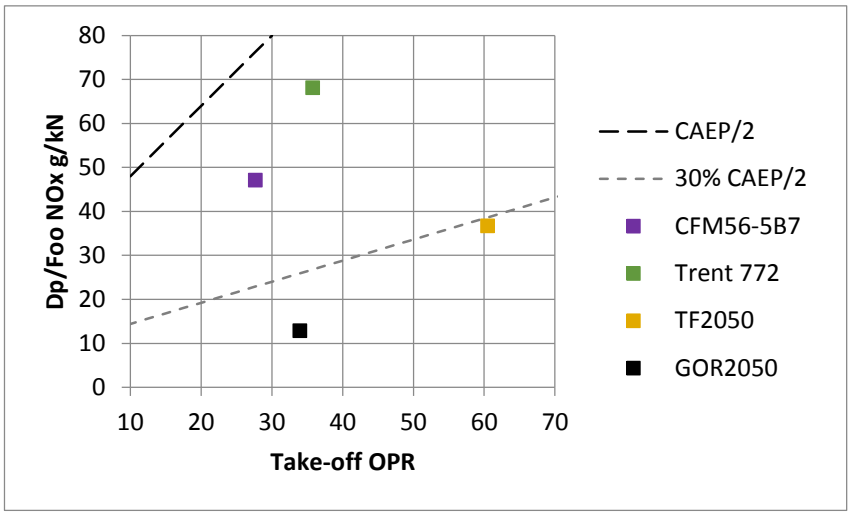

Figure 82 – ULTIMATE Reference Engine NOx Emissions Predictions (Compared with Year-2000 Engines)

10.2.3 Assessment of methods for NOx Emissions Prediction

Alternative methods are reviewed in detail in Appendix B, but the conclusions from the study are summarised here. Given the uncertainty regarding future designs, it was deemed inappropriate to undertake detailed modelling of LDI combustors, so a review of different methods of predicting emissions, and particularly NOx emissions, was made.

- For the currently-in-service rich/quench/lean (RQL) types of combustor, the P3T3 method is recommended for the emissions estimates, where relevant ICAO reference data are available.
- For NOx emissions the ambient humidity is an important factor, but often overlooked when comparing test results obtained at ground level. This omission might be excused when just making comparisons of Dp/Foo

figures for ISA-day sea-level conditions, provided it is assumed they are all for typical days with, for example, consistent 60% relative humidity.

- When considering emissions at high altitudes or for hot or cold days at ground level, humidity corrections for NOx estimates should not be ignored.
- Many of the previously published NOx emissions correlations have been shown to give unrealistic or illogical results when extrapolated beyond limited ranges of operating conditions, so extreme caution is needed if they are to be applied to new engine designs or over wider ranges of conditions.
- Correlations having larger numbers of input parameters are often shown to give a better fit to test data, but this does not mean that their predictions will be any more accurate, since any additional parameters will improve the fit to a finite dataset while tending to make any extrapolation from those results more divergent (Runge's phenomenon).
- The potential to provide a new improved correlation for LDI NOx emissions has been reviewed, but the formulation of any such correlation is greatly complicated by the need to consider: fuel-staging between pilot and main injector nozzles, the multitude of NOx formation mechanisms that are significant at lean-burn combustion temperatures (in contrast to the 'thermal NOx' which predominates at stoichiometric temperatures), the considerable uncertainty regarding time-delays due to fuel droplet evaporation, and uncertainties in the effective NOx formation and combustion residence times in future combustor designs.
- To provide consistent and comparable estimates over a wide range of flight conditions, an existing relatively-simple and often previously used NASA correlation (Equation 21) is recommended for NOx emissions calculations for LDI combustors for the study engines for year 2050, though it may tend to underestimate NOx emissions at idle ratings.
- Previous research in NEWAC suggests LDI combustor designs will be able to meet existing CO and UHC emissions limits with good margins and that visible smoke, CO and UHC emissions can be traded-off against NOx emissions by varying residence time, provided relight requirements are met.

- LDI combustor tests by NASA provide some correlations for CO, but these are very specific to the tested injectors and fuel-staging strategies, and they do not account for optimising combustor residence times.
- No universal correlations can be recommended for CO, UHC or smoke emissions for 2050.
- Fine particulate emissions present a more intractable problem as they relate to the detail composition of the fuel, not least its sulphur content, and so may need to be addressed by tighter limits on fuel specifications, and/or by the introduction of synthetic fuels and/or biofuels in the longer term.

10.3 Recommendations for Further Research and Development

A number of actions are proposed to close-out the reported studies and prepare material for a journal paper to follow-on from [77] by presenting the results from the advanced cycle studies. These include:

- Modelling the mixed-exhaust arrangement and eliminating the minor heat balance errors in the spreadsheet model.
- Modelling cycles #05, #14 and #15 to quantify the benefits of the ABC, intercooling and secondary combustion to cycle#06 that includes all three of these technologies together with the topping cycle.
- Making further parametric studies about cycles #03 and #06 to see if improved matching is possible, including better use of the variable-area nozzles.
- Making more detailed scaled engine and installation layouts for the different cycles to enable comparative assessments of nacelle and afterbody drags to refine the SFC and fuel-burn assessments.
- Investigation of alternative ABC turbine arrangements for integration into a turbofan engine, recognising that the ABC heat exchanger is probably better located downstream of the last core turbine stage.

Further Sankey diagrams could also be constructed to help compare energy flows in the different cycles. These can highlight the features that generate the most entropy and show where this emerges as ‘waste heat’.

In the slightly longer term, a variant of cycle#06 using air-riding free pistons for the topping cycle should be worked-up to see if this would improve on the performance of cycle#06 modelled using nutating-disc modules.

Methods should be developed to estimate NOx emissions from topping cycles and secondary combustion.

The SRIA Flightpath 2050 targets as listed in Table 2 will be very challenging for the aircraft and engine manufacturers to meet. However, more radical airframe designs and improved engine–airframe integration could help. These technologies and should be investigated in future studies.

It would also be interesting to model some of the cycles using liquid methane or hydrogen as fuel.

10.3.1 Routes to Market

Technologies need to be demonstrated to TRL 6 before engine and airframe manufacturers will commit to including them in new products. The necessary steps for maturing the technologies may be summarised as follows:

- TRL 2: potential technology application validated
- TRL 3: design, analysis and experiments for proof of concept
- TRL 4: prototype in lab environment (and route to TRL 6 identified)
- TRL 5: prototype of technology in relevant environment
- TRL 6: validation in a core-engine ‘demonstrator’ that uses the technology

The main analysis elements, prototypes and tests to prepare for a TRL 6 demonstrator programme need to be worked-out by industry partners in collaboration with universities, research institutes, EU and national research-funding bodies.

Despite the promise of double-digit SFC and fuel-burn improvements from nutating-disc technology, the author cannot recommend that this technology be given precedence over alternative pressure-rise combustion technologies that are likely to be developed to similar levels of performance at lower risk. The

wear of unlubricated seals at high temperatures is a particular concern. Opposed-piston and/or free-piston technology seems very promising, and more conventional piston engine technology should not be dismissed. Wave rotor pressure-rise combustion technology also seems worth further consideration.

10.3.2 Potential Benefits from Cryogenic Fuels

The availability of a cryogenic fuel such as liquid hydrogen or liquid methane opens-up new possibilities with regard to intercooling and engine cooling generally. One option could be to use the fuel to help improve the performance of the closed-circuit bottoming cycle as discussed in section 6.4.

Switching from kerosene to liquid methane fuel would produce an immediate reduction in CO_2 emissions that would make the SRIA target of a 68% reduction with year-2050 technology credible, but switching to liquid hydrogen fuel in the longer term would almost-totally eliminate mission-level CO_2 emissions.

10.4 Final Discussion

The engine fuel-burn-reduction target of 15% by year 2050 relative to designs that just develop existing technologies seems to be achievable by combining pressure-rise-combustion topping cycles synergistically with other advanced technologies including intercooling. Intercooling will also help to minimise NOx emissions. Building on other anticipated operational and technological efficiency improvements, and given the baseline scenario for air-traffic growth, the new technologies have the potential to save about 300 million tonnes of CO_2 emissions in operation per annum, when fully realized by 2075. If introduced across all new production aircraft in 2050, these technologies, combined with other improvements are predicted to reduce CO_2 emissions per passenger kilometre by about 59% on average, relative to year-2000 production aircraft and engines, even without improvements in operations. This compares with the SRIA Flightpath 2050 target of 68% reduction from engine and aircraft technologies alone and 75% reduction overall. Further new technologies not

addressed in this study, such as unconventional airframes and distributed propulsion, might help to close the gap to the 68% target.

The ATAG target of stabilising aviation CO_2 emissions by 2020 and halving them by 2050 can only be met in the short to medium term by offsetting, or 'market-based measures'. Since the quantity of CO_2 to be offset is predicted to continue to grow, and the cost of offsetting the CO_2 is almost certain to increase, other longer-term solutions will be needed. These solutions are likely to involve the use of biofuels or synthetic fuels, since realistically only very-short-range aircraft can be powered by stored electrical energy and recharged by electricity from renewable or nuclear energy sources.

The author has made a detailed feasibility study of an advanced-cycle year-2050 engine concept down-selected from 47 possible new technologies and combinations of technologies. The technologies have been assessed for a geared turbofan engine for an intercontinental aircraft. The configuration studied in detail combines intercooling and secondary combustion with an Air Bottoming Cycle and a nutating-disc-technology topping cycle, though alternative topping-cycle technologies may ultimately be preferred and simpler variants have also been assessed. To realize the nutating-disc concept, significant advances in sealing, bearing and materials technologies have needed to be assumed. Nutating disc machines have been shown to have some useful potential benefits relative to alternative topping-cycle technologies, but they also have very severe challenges to meet regarding reliability, durability, seal leakage and the control of ignition and emissions when implemented in very high OPR compound-cycle engines. Fuel injection and spark ignition have been assumed, as the author was not convinced that compression ignition would be viable in the machine when using aviation kerosene as fuel. This was on account of the low Cetane number of Jet-A1, the high rotational speed of the engine giving short residence times for combustion, the modest peak pressures due to bearing constraints in the nutating disc modules, and the complex shape of the pre-combustor and associated expander geometry.

Two different approaches have also been considered in the design of bottoming cycles to extract more power from the core exhaust heat to improve overall thermal efficiency. Supercritical carbon dioxide was studied by Florian Jacob for a closed-circuit option [16], whereas compressed air was used in the alternative open-circuit cycle studied by the author. A closed-circuit design requires two heat exchangers, whereas the open-circuit design only needs one, making it easier to avoid space-constraints when combining a bottoming cycle with intercooling. Though the closed-circuit option has a theoretical performance advantage, in practice this did not seem to translate into better SFC or fuel-burn, despite using compact and light weight supercritical-CO_2 turbomachinery. Relative to the reference year-2050 turbofan, the closed-circuit bottoming cycle design offered improvements of just a few per cent in SFC and fuel burn, even when inter-turbine reheat was added to raise the exhaust gas temperature and reduce the core mass flow needed for the engine.

To integrate the combination of nutating-disc topping cycle modules with intercooling, secondary combustion and an open-circuit bottoming cycle, the turbofan has been proposed with reverse-flow turbines and a mixed exhaust arrangement. This complex engine concept seems to offer the greatest improvements in SFC and fuel-burn in comparison with simpler variants and it is assessed as meeting the 15% CO_2 reduction targeted by ULTIMATE.

The new technologies have demonstrated potential for engine performance improvement, but it is the author's opinion that the technical challenges posed by nutating-disc machinery make it very likely that alternative topping-cycle technologies, such as advanced piston engines or wave-rotors, will offer more attractive long-term design solutions.

11 REFERENCES

1. Jacob F. Engineering Communication Memo ULTIMATE-CU-ECM-005 Update of engine performance of the year 2050 reference engine for intercontinental missions. 2017.

2. Parker R. Challenges of Advanced Propulsion Systems Development for Future Civil Air Transport. General Lecture 1. ICAS-2014-0.2. ICAS Conference 2014. St. Petersburg, Russia: ICAS; 2014.

3. ACARE. Strategic Research & Innovation Agenda, Volume 1, Realising Europe's vision for aviation. 2012. pp. 1–152.

4. ACARE. Strategic Reseach & Innovation Agenda, 2017 Update, Volume 1. 2017. Available at: http://www.acare4europe.org/sites/acare4europe.org/files/document/acare-strategic-research-innovation-volume-1-v2.7-interactive-fin_0.pdf

5. Grönstedt T., Xisto C., Sethi V., Rolt A., Garcia Rosa N., Seitz A., et al. GT2016-56123: Ultra Low Emission Technology Innovations for Mid-Century Aircraft Turbine Engines. Proceedings of ASME Turbo Expo 2016. Seoul, South Korea: ASME; 2016. pp. 1–13.

6. Rolt A., Whurr J. Optimizing propulsive efficiency in aircraft with boundary layer ingesting distributed propulsion. ISABE 2015-20201. Phoenix, USA: ISABE; 2015. pp. 1–10. Available at: DOI:ISABE 2016-20201

7. Salpingidou C., Misirlis D., Vlahostergios Z., Flouros M., Donus F., Yakinthos K. Conceptual design study of a geared turbofan and an open rotor aero engine with intercooled recuperated core. Proceedings of the Institution of Mechanical Engineers, Part G: Journal of Aerospace Engineering. 2018; 0(0): 1–8. Available at: DOI:10.1177/0954410018770883

8. Misirlis D., Vlahostergios Z., Flouros M., Salpingidou C., Donnerhack S., Goulas A., et al. Optimization of Heat Exchangers for Intercooled

Recuperated Aero Engines. Aerospace. 2017; 4(1): 14. Available at: DOI:10.3390/aerospace4010014

9. Jacob F., Rolt AM., Sebastiampillai JM., Sethi V., Belmonte M., Cobas P. Performance of a supercritical CO2 bottoming cycle for aero applications. Applied Sciences (Switzerland). 2017; 7(3). Available at: DOI:10.3390/app7030255

10. Lundbladh A., Grönstedt T., Genrup M., Platell P. High Power Density Work Extraction from Turbofan Exhaust Heat. ISABE-2015-20101. International Society for Air Breathing Engines. Phoenix, USA: ISABE; 2015. pp. 1–18.

11. Heinemann P., Panagiotou P., Vratny P., Kaiser S., Hornung M., Yakinthos K. Advanced Tube and Wing Aircraft for Year 2050 Timeframe. 55th AIAA Aerospace Sciences Meeting. Grapevine, Texas, USA; 2017. pp. 1–25. Available at: DOI:10.2514/6.2017-1390

12. Heinemann P., Panagiotou P., Vratney P., Kaiser S., Vlahostergios Z. ULTIMATE deliverable D2.1 Year 2000 reference aircraft and Year 2050 ATW models for intercontinental long-range and intra-European short-range configurations. 2017.

13. Jacob F., Sebastiampillai J., Rolt A., Sethi V., Grönstedt T., Newton P., et al. ULTIMATE deliverable 2.6 – Year 2000 and initial year 2050 reference configurations. 2017.

14. Sebastiampillai J., Jacob F., Mastropierro FS., Rolt A. GT 2019-90775: Modelling Geared Turbofan and Open Rotor Engine Performance for Year-2050 Long-Range and Short-Range Aircraft. ASME 2019 Turbo Expo. 2019. pp. 1–14.

15. ATAG. Aviation Industry Commitment to Action on Climate Change. 3rd Aviation & Environmental Summit. Geneva, Switzerland; 2008.

16. Jacob F. MSc Thesis – Feasibility Study of Supercritical CO2 Bottoming

Cycles for Aero Application. Cranfield University; 2015.

17. Klingels H. EU patent application: EP2650510A2 Wärmekraftmaschine für Freikolbenverdichter. 2003.

18. Anselmi E., Camilleri W., Laskaridis P., Rolt A. Assessment of the low pressure turbine exhaust challenges in a Geared Intercooled Reversed Flow Cored Engine (ISABE 2015-20200). International Symposium on Air Breathing Engines. Phoenix, USA: ISABE; 2015. pp. 1–8.

19. Rolt A. PhD Study Poster - Combining Advanced Aero Engine Technologies. Cranfield, UK: ULTIMATE Project; 2017. Available at: http://www.ultimate.aero/media/Cranfield_University_2017_ULTIMATE_PhD_Study_Poster_by_Andrew_Rolt.pdf

20. Rolt A., Jacob F., Sebastiampillai J., Sethi V. Cranfield University ULTIMATE Engines Poster for the 2018 Farnborough International Air Show ‘Aiming to meet ACARE Flightpath 2050 fuel-burn and emissions targets with combinations of advanced technologies’. ULTIMATE Project; 2018. p. 1. Available at: http://www.ultimate.aero/media/ULTIMATE A0 Posters/Ultimate_Poster_Cranfield ULTIMATE engines.pdf

21. Robinson D. Giants in the Sky. Foulis; 1973. 23–24 p.

22. Pugh P. The Magic of a Name. The Rolls-Royce Story, Part 1: The First Forty Years. Icon Books Ltd; 2000.

23. Gunston W. Napier Nomad An Engine of Outstanding Efficiency. Flight. April 1954; : 534–552.

24. Korsia J., Spiegeleer G. VITAL, An European R&D program for greener aero-engines (ICAS-2006-612). 25th Congress of International Council of the Aeronautical Sciences. 2006. pp. 1–5. Available at: http://www.icas.org/ICAS_ARCHIVE/ICAS2006/PAPERS/612.PDF

25. Wilfert G., Sieber J., Rolt A., Baker N., Touyeras A., Colantuoni S. New Environmental Friendly Aero Engine Core Concepts. ISABE-2007-1120.

18th International Symposium on Air Breathing Engines. 2007. pp. 1–11.

26. von der Bank R., Cazalens M., Donnerhack S., Lundbladh A., Rae A., Dietz M. GT2014-25040 LEMCOTEC – IMPROVING THE CORE-ENGINE THERMAL EFFICIENCY. ASME 2014 Turbine Expo. Düsseldorf: ASME; 2014. pp. 1–18.

27. ENOVAL High Bypass Ratio Aero Engines - Providing the next step in Engine Technologies. 2018. Available at: http://www.enoval.eu/media/mediablog/files/ENOVAL_Final_Technology_Brochure_2018.pdf

28. Rolt AM., Baker NJ. Intercooled Turbofan Engine Design and Technology Research in the EU Framework 6 NEWAC Programme. International Symposium on Air Breathing Engines. ISABE 2009-1278; 2009. pp. 1–10. Available at: http://www.newac.eu/uploads/media/No._034_RRUK_paper_for_ISABE.pdf

29. Rolt AM., Kyprianidis KG. ICAS-2010-408: Assessment of new aeroengine core concepts and technologies in the EU framework 6 NEWAC programme. 27th Congress of the International Council of the Aeronautical Sciences 2010, ICAS 2010. 2010. pp. 2736–2746.

30. Kyprianidis K., Rolt AM. On the Optimization of a Geared Fan Intercooled Core Engine Design. Journal of Engineering for Gas Turbines and Power. 2015; 137(April 2015): 1–10. Available at: DOI:10.1115/1.4028544

31. Boggia S., Rüd K. Intercooled Recuperated Gas Turbine Engine Concept. 41st AIAA/ASME/SAE/ASEE Joint Propulsion Conference & Exhibit, Joint Propulsion Conferences, (); Available at: http://dx.doi.org/10.2514/6.2005-4192

32. Wilfert G., Kriegl B., Wald L., Johanssen O. CLEAN - Validation of a GTF High Speed Turbine and Integration of Heat Exchanger Technology in an

Environmental Friendly Engine Concept. International Society for Air Breathing Engines. 2005; : 1–8. Available at: DOI:10.1007/s13398-014-0173-7.2

33. Goulas A., Donnerhack S., Flouros M., Misirlis D., Vlahostergios Z., Yakinthos K. Thermodynamics Cycle Analysis, Pressure Loss, and Heat Transfer Assessment of a Recuperative System for Aero-Engines. Journal of Engineering for Gas Turbines and Power. 2015; 137(4): 041205. Available at: DOI:10.1115/1.4028584

34. Misirlis D., Vlahostergios Z., Flouros M., Salpingidou C., Donnerhack S., Goulas A., et al. Intercooled Recuperated Aero Engine: Development and Optimization of Innovative Heat Exchanger Concepts ECATS-37-40. Athens; 2016.

35. Lebre J., Brójo F. Performance of a Turbofan Engine with Intercooling and Regeneration. Engineering and Technology. 2011; 5(6): 359–363.

36. Ito Y., Inokura N., Nagasaki T. Intercooled and Recuperated Jet Engine Using Airfoil Heat Exchangers. ISABE2015-20100. International Society for Air Breathing Engines. 2015. pp. 1–8.

37. Zhao X., Grönstedt T. Aero Engine Intercooling Optimization Using a Variable Flow Path. ISABE-2015-20018. International Society for Air Breathing Engines. 2015. pp. 1–18. Available at: DOI:10.1017/CBO9781107415324.004

38. Camilleri W., Anselmi E., Sethi V., Laskaridis P., Rolt A., Cobas P. Performance characteristics and optimisation of a geared intercooled reversed flow core engine. Proceedings of the Institution of Mechanical Engineers, Part G: Journal of Aerospace Engineering. 2015; 229(2): 269–279. Available at: DOI:10.1177/0954410014530679

39. Camilleri W., Anselmi E., Sethi V., Laskaridis P., Grönstedt T., Zhao X., et al. Concept description and assessment of the main features of a geared

intercooled reversed flow core engine. Proceedings of the Institution of Mechanical Engineers, Part G: Journal of Aerospace Engineering. 2015; 229(9): 1631–1639. Available at: DOI:10.1177/0954410014557369

40. Rolt A., Sethi V., Jacob F., Sebastiampillai J., Xisto C., Grönstedt T., et al. Scale effects on conventional and intercooled turbofan engine performance. The Aeronautical Journal. 2017; (October 2016): 1–24. Available at: DOI:10.1017/aer.2017.38

41. Sieber J. European Technology Programs for Eco-Efficient Ducted Turbofans. International Symposium on Air Breathing Engines. Phoenix, USA: ISABE; 2015. pp. 1–8.

42. Rolt A., Whurr J. Distributed Propulsion Systems to Maximize the Benefits of Boundary Layer Ingestion. ISABE 2015-20288. 2015. pp. 1–10. Available at: https://drc.libraries.uc.edu/bitstream/handle/2374.UC/745833/ISABE2015_CS&A_Andrew Martin Rolt_76_MANUSCRIPT_20288.pdf?sequence=2

43. Raffaelli L., Chung J. OPTIMISATION OF A HIGH BYPASS RATIO TURBOFAN ENGINE USING ENERGY STORAGE. Greener Aviation 2016. Brussels; 2016. pp. 1–10.

44. Kaiser S., Vratny P., Seitz A., Hornung M. GT2016-56313 Unified Thermodynamic Evaluation of Radical Aero Engine Cycles. ASME 2016 Turbine Expo. Seoul, Soth Korea; 2016. pp. 1–16.

45. Jones SM., Haller WJ., Tong MT. NASA/TM - 2017-219501: An N+3 Technology Level Reference Propulsion System. 2017;

46. Moxon J., Winn A., Elliott S., Barrie D. More than a stretch - the SAAB2000 described. Flight International 11-17 December 1991. Available at: https://www.flightglobal.com/pdfarchive/view/1991/1991 - 3227.html

47. Ward CM., Miller RJ. Performance Analysis of an Ejector Enhanced

Pressure Gain Combustion Gas Turbine. 50th AIAA Aerospace Sciences Meeting including the New Horizons Forum and Aerospace Exposition. 2012; (January): 1–11. Available at: DOI:doi:10.2514/6.2012-772

48. Ward CM. DPhil Thesis: Unsteady Ejectors for Pressure Gain Combustion Gas Turbines. Cambridge University; 2013.

49. Matsutomi Y., Meyer S., Wijeyakulasuriya S., Izzy Z., Nalim M., Shimo M., et al. Experimental Investigation on the Wave Rotor Constant Volume Combustor. 46th AIAA/ASME/SAE/ASEE Joint Propulsion Conference & Exhibit. 2010; C(July): 1–12. Available at: DOI:10.2514/6.2010-7043

50. Whurr J. Otto Cycle Core Turbofan Concepts. MSc Thesis. Cranfield University; 1995.

51. Meyer L. United States Patent 5251594: Nutating Internal Combustion Engine. 1993. Available at: DOI:US005485919A

52. Korakianitis T., Meyer L., Boruta M., McCormick HE. Introduction and Performance Prediction of a Nutating-Disk Engine. Journal of Engineering for Gas Turbines and Power. 2004; 126(2): 294. Available at: DOI:10.1115/1.1635394

53. Korakianitis T., Meyer L., Boruta M., McCormick HE. One-Disk Nutating-Engine Performance for Unmanned Aerial Vehicles. Journal of Engineering for Gas Turbines and Power. 2004; 126(3): 475. Available at: DOI:10.1115/1.1496770

54. Korakianitis T., Meyer L., Boruta M., McCormick HE. Alternative Multinutating Disk Engine Configurations for Diverse Applications. Journal of Engineering for Gas Turbines and Power. 2004; 126(3): 482. Available at: DOI:10.1115/1.1688770

55. Mohanarangan R. Cranfield MSc Thesis: Development of a Performance Simulation Model for the Nutating Disk Engine. Cranfield University; 2015.

56. Cochereau J. MSc Thesis: CFD Study of a Nutating Disc Engine. Cranfield University; 2015.

57. Sebastiampillai JM. MSc Thesis: Performance and Preliminary Design of Nutating Disc Topping Cycles for Civil Aer-Engine Applications. Cranfield University; 2018.

58. Kaiser S., Nickl M., Donnerhack S., Klingels H. ISABE-2017-21451 Investigations of Synergistic Combination of the Composite Cycle and Intercooled Recuperation. International Society for Air Breathing Engines. Manchester; 2017. pp. 1–14.

59. Petit O., Xisto C., Zhao X., Grönstedt T. An Outlook for Radical Aero Engine Intercooler Concepts. GT2016-57920. Proceedings of ASME Turbo Expo 2016. 2016. pp. 1–10.

60. Kramer BR., Smith BC., Heid JP., Ng T. DRAG REDUCTION EXPERIMENTS USING BOUNDARY LAYER HEATING 37th AIAA Aerospace Sciences Meeting & Exhibit January 1999 / Reno , NV. 1999;

61. Perullo CA., Mavris DN., Fonseca E. GT2013-95734 An Integrated Assessment of an Organic Rankine Cycle Concept for use in Onboard Aircraft Power Generation. 2013; : 1–8.

62. Rolt A., Sebastiampillai J., Jacob F., Sethi V., Whurr J. ULTIMATE deliverable D4.3 – Optimised Bottoming Cycle and Nutating Disc Combustion Cores. 2018.

63. Beretens Izquierdo M. MSc Thesis: Performance Study of Cryogenic Hydrogen Pre-Coolers for Supercritical Carbon Dioxide Bottoming Cycles for Aero Applications. Cranfield University; 2018.

64. Newton P., Tantot N., Donnerhack S., Lundbladh A. ULTIMATE Deliverable D1.1 – Establish common year 2050 technology level assumptions. 2015.

65. Xisto C., Ali F., Petit O., Grönstedt T., Rolt A., Lundbladh A. GT2017-

63776: Analytical model for the performance estimation of pre-cooled pulse detonation turbofan engines. Proceedings of the ASME Turbo Expo 2017. Charlotte, NC, USA; 2017. Available at: DOI:10.1115/GT2017-63776

66. Xisto C., Petit O., Grönstedt T., Lundbladh A. Assessment of CO2 and NOx Emissions in Intercooled Pulsed Detonation Turbofan Engines. Journal of Engineering for Gas Turbines and Power. 2018; 141(1): 011016. Available at: DOI:10.1115/1.4040741

67. Jacob F., Sebastiampillai J., Rolt A., Sethi V., Xisto C. ULTIMATE deliverable D1.3 – Preferred ULTIMATE Nutating Disc Topping and Bottoming Cycle Configurations. 2017.

68. Kaiser S., Kellermann H., Nickl M., Seitz A. A Composite Cycle Engine Concept for Year 2050. ICAS. 2018.

69. Xisto C. ULTIMATE milestone M1.1 – Intercooler and pulse detonation technology simulators. 2016.

70. Knapp K., Syed K., Stevens M. Fuel Flexibility Capabilities of Alstom's GT24 and GT26 Gas Turbines. PowerGen Asia 2012. Bangkok, Thailand; 2012. pp. 1–19. Available at: http://pennwell.sds06.websds.net/2012/bangkok/pga/papers/T2S4O3-paper.pdf

71. Zahirovic S., Knapp K. GT2017-64289: Ansaldo GT26 Sequential Combustor Performance in Long-term Commercial Operation. ASME Turbo Expo 2017. Charlotte, NC, USA: ASME; 2017. p. 10.

72. Pellegrini A., Nikolaidis T., Pachidis V., Köhler S. On the performance simulation of inter-stage turbine reheat. Applied Thermal Engineering. 2017; 113(February): 544–553. Available at: DOI:10.1016/j.applthermaleng.2016.10.034

73. Zhao D., Gutmark E., de Goey P. A review of cavity-based trapped

vortex, ultra-compact, high-g, inter-turbine combustors. Progress in Energy and Combustion Science. Elsevier Ltd; 2018; 66: 42–82. Available at: DOI:10.1016/j.pecs.2017.12.001

74. Levy Y., Reichel T. AHEAD Deliverable 2.7: Feasibility of the hybrid combustion concept. 2014.

75. Levy Y., Sherbaum V., Erenburg V., Gaissinski I. GT2016-58079 Flameless Oxidation Combustor Development for a Sequential Combustion Hybrid Turbofan Engine. 2016. pp. 1–10.

76. Martinez Bueno V. MSc Thesis: 3D LES - RANS CFD Studies of a Novel Secondary Combustor Concept for Low-NOx Emissions. Cranfield University; 2018.

77. Rolt A., Sebastiampillai J., Jacob F., Sethi V., Xisto C. ISABE-2017-22660: Selecting Combinations of Advanced Aero Engine Technologies. Proceedings of the 27th ISABE Conference. 2017. pp. 1–17.

78. Romanelli M. MSc Thesis - Preliminary Design and Emissions Evaluation of an Aero Engine Secondary Combustor. Cranfield; 2018.

79. EPA. Control of Air Pollution From Aircraft and Aircraft Engines; Emission Standards and Test Procedures; Final Rule. Federal Register USA; 2012 p. 36342. Available at: https://www.gpo.gov/fdsys/pkg/FR-2012-06-18/pdf/2012-13828.pdf%5Cnhttp://www3.epa.gov/otaq/aviation.htm

80. ATR. The Green Power of Tomorrow - ATR Brochure DC/E June 2014. 2014. Available at: http://www.atraircraft.com/datas/download_center/24/brochure_environment_2014_24.pdf

81. Madden P. ICAO / CAEP NOx / nvPM Regulation and Independent Technology Review of Combustion Technology. Rolls-Royce plc; 2017. pp. 1–19. Available at: http://www.forum-ae.eu/system/files/02_caep_emissions_regulations_presentation_for_foru

m_workshop_in_berlin_handout.pdf

82. ICAO. EASA ICAO Aircraft Engine Emissions Database (Version 23b 06/2017). 2017. Available at: https://www.easa.europa.eu/document-library/icao-aircraft-engine-emissions-databank (Accessed: 1 November 2017)

83. Norman PD., Lister DH., Lecht M., Madden P., Park K., Penanhoat O., et al. Development of the technical basis for a New Emissions Parameter covering the whole Aircraft operation: NEPAIR. … Commission, Rept. G4RD-CT-2000-00182. 2003. Available at: http://scholar.google.com/scholar?hl=en&btnG=Search&q=intitle:Development+of+the+technical+basis+for+a+New+Emissions+Parameter+covering+the+whole+AIRcraft+operation#0

84. Madden P., Park K. Methodology for Predicting NOx Emissions at Altitude Conditions from Ground Level Engine Emissions and Performance Test Information, Rolls-Royce Technical Report DNS 90713. 2003.

85. ICAO. ICAO Annex 16 Volume 2. ICAO; 2008. pp. 1–28. Available at: https://www.caa.govt.nz/ICAO/ICAO_Compliance.htm (Accessed: 4 December 2017)

86. Lefebvre AH., Ballal DR. Gas Turbine Combustion, Alternative Fuels and Emissions. 3rd edn. CRC Press; 2010.

87. Lieuwen TC., Yang V. Gas Turbine Emissions. Cambridge University Press. 2013; : 1–368. Available at: DOI:10.2514/1.J053061

88. Young K. Combustor Technology at Rolls-Royce. Forum AE - Technology Meeting - Non-CO2 Mitigation Technology Workshop. Berlin; 2017. Available at: http://www.forum-ae.eu/system/files/06_forum-ae_rr_technology_kenn.pdf (Accessed: 19 September 2017)

89. Liu Y., Sun X., Sethi V., Nalianda D., Li Y-G., Wang L. Review of modern low emissions combustion technologies for aero gas turbine engines.

Progress in Aerospace Sciences. Elsevier Ltd; 2017; 94(November 2016): 12–45. Available at: DOI:10.1016/j.paerosci.2017.08.001

90. Tacina R., Mao C-P., Wey C. AIAA-2004-135 Experimental Investigation of a Multiplex Fuel Injector Module With Discrete Jet Swirlers for Low Emission Combustors. 42nd AIAA Aerospace Sciences Meeting and Exhibit. Reno, Nevada, USA; 2004. pp. 1–13. Available at: DOI:10.2514/6.2004-135

91. Tacina R., Lee P., Wey C. ISABE-2005-1106 A Lean-Direct-Injection Combustor Using a 9 Point Swirl-Venturi Fuel Injector. ISABE. Munich: 17th International Symposium on Air Breathing Engines; 2005. pp. 1–18.

92. Tacina KM., Lee C-M., Wey C. NASA Glenn High Pressure Low NOx Emissions Research. Nasa/Tm. 2008; (February 2008). Available at: https://ntrs.nasa.gov/archive/nasa/casi.ntrs.nasa.gov/20080014197.pdf

93. Tacina KM., Chang C., He ZJ., Lee P., Mongia HC., Dam BK. A Second Generation Swirl-Venturi Lean Direct Injection Combustion Concept. 50th AIAA/ASME/SAE/ASEE Joint Propulsion Conference. 2014; : 2014–3434. Available at: DOI:10.2514/6.2014-3434

94. Tacina KM., Chang CT., Lee P., Mongia H. ISABE-2015-20249 An assessment of combustion dynamics in a low-NOx, second-generation swirl-venturi lean direct injection combustion concept. ISABE. Phoenix, USA: ISABE; 2015. pp. 1–9.

95. Anand MS., Eggels R., Staufer M., Zedda M., Zhu J. GTINDIA2013-3537 An Advanced Unstructured-Grid Finite-Volume Design System for Gas Turbine Combustion Analysis. ASME 2013 Gas Turbine India Conference. Bangalore: ASME; 2013. pp. 1–12.

96. Poutriquet F., von der Bank R., Bourgois S., Tantot N., Gebel G., Donnerhack S., et al. LEMCOTEC: A Key Project to Tackle Pollutant Emissions by Developing New Core Technologies - SP3 Lean Burn

Systems. LEMCOTEC Public Workshop for the Aeronautics Industry, 6 December 2016. Potsdam, Germany; 2016.

97. Rolt A., Sethi V., Jacob F., Sebastiampillai J., Xisto C., Grönstedt T., et al. ISABE 2017-22659 Scale effects on conventional and intercooled turbofan engine performance. ISABE. Manchester, UK; 2017. Available at: DOI:10.1017/aer.2017.38

98. Grönstedt T. PhD thesis - Development of methods for analysis and optimisation of complex jet engine systems. Chalmers University; 2000. Available at: http://publications.lib.chalmers.se/records/fulltext/799.pdf

99. Walsh PP., Fletcher P. Gas Turbine Performance, Second Edition. John Wiley and Sons; 2004. 1–664 p.

100. Sethi V. Advanced performance simulation of gas turbine components and fluid thermodynamic properties. 2008; (April). Available at: http://dspace.lib.cranfield.ac.uk/handle/1826/5654

101. Kyprianidis. KG., Rolt AM. GT2014-26064 ON THE OPTIMISATION OF A GEARED FAN INTERCOOLED CORE ENGINE DESIGN. ASME 2014 Turbine Expo. Düsseldorf: ASME; 2014. pp. 1–13.

102. Lakshminarayana B. Methods of Predicting the Tip Clearance Effects in Axial Flow Turbomachinery. ASME J. Basic Eng. 1992; 92(3): 467–480.

103. Glassman J. Users Manual for Updated Computer Code for Axial Flow Compressor Conceptual Design. Toledo, Ohio, USA; 1992.

104. Jacob F., Sebastiampillai J., Rolt A. ULTIMATE - Installation and use of year 2050 reference engine performance decks. 2017;

105. Rolt A., Whurr J. ULTIMATE deliverable D5.5 – Achievements on SRIA environmental targets. 2018.

106. Whurr J., Rolt A. ULTIMATE deliverable D5.2 Propulsion scenarios: the potential impact of ULTIMATE technology on aviation and the

environment. 2018.

107. The Boeing Company. World Air Cargo Forecast 2018–2037. 2018. Available at: http://www.boeing.com/commercial/market/cargo-forecast/

108. Rolt A., Mastropierro F., Sethi V. ULTIMATE deliverable D2.3 Emissions models for the year 2000 baseline and year 2050 reference engine configurations. 2018.

109. Pervier H. Emissions Modelling for Engine Cycle and Aircraft Trajectory Optimisation. Cranfield; 2013.

110. Celis C. Evaluation and optimisation of environmentally friendly aircraft propulsion systems - PhD thesis. Cranfield University; 2010. Available at: DOI:10.1017/CBO9781107415324.004

111. Eliseo R., Faravelli T., Frassoldati A., Cuoci A., Mehl M. The CRECK Modelling Group. 2018. Available at: http://creckmodeling.chem.polimi.it/index.php (Accessed: 2 February 2018)

112. Zhang X., Toal D., Bressloff NW., Keane AJ., Witham F., Gregory J., et al. GT2014-25886 Prometheus: A Geometry-centric Optimization System for Combustor Design. 2014; : 1–13.

113. Toal DJJ., Zhang X., Keane AJ., Stow S., Zedda M., Witham F., et al. ISABE-2017-21394 Combustor Design Optimization Using the Prometheus Design System. 2017. pp. 1–14.

114. Dumrongsak J., Savill AM. Numerical Analysis and Sensitivity Study of Non-Premixed Combustion Using LES. Prog. Energy Combust. Sci. 2012; 18: 529–552.

115. Chandrasekaran N., Guha A. Study of Prediction Methods for NOx Emission from Turbofan Engines. Journal of Propulsion and Power. 2012; 28(1): 170–180. Available at: DOI:10.2514/1.B34245

116. Jelinek F., Carlier S., Smith J. The Advanced Emission Model (AEM3) - Validation Report - Version 1.5 - Appendices A, B and C. Eurocontrol. Brétigny-sur-Orge; 2004. Available at: https://eurocontrol.int/eec/gallery/content/public/document/eec/report/2001/015_Forecasting_Fuel_Burn_and_Emissions_in_Europe.pdf

117. Baughcum L., Tritz G., Henderson C., Pickett C. Scheduled Civil Aircraft Emission Inventories and Analysis for 1992 : Database Development and Analysis. NASA Cr-4700. 1996; (April 1996).

118. Vömel H. Saturation Vapor Pressure Formulations. 2016. Available at: http://cires1.colorado.edu/~voemel/vp.html (Accessed: 30 October 2017)

119. Deidewig F., Döpelheuer A., Lecht M. Methods to Assess Aircraft Engine Emissions in Flight. Proceedings of the 20th International Council of Aeronautical Sciences Congress, Vol. 1. Reston, Virginia, USA: AIAA; 1996. pp. 131–141.

120. Schaefer M. Methodologies for Aviation Emission Calculation – A comparison of alternative approaches towards 4D global inventories. TU Berlin; 2006. Available at: http://opus4.kobv.de/opus4-tuberlin/files/1383/schaefer_martin.pdf

121. Odgers J., Kretschmer D. The Prediction of Thermal NOX in Gas Turbines. International Journal of Turbo and Jet Engines. 1985; 5(1–4): 1–7. Available at: DOI:10.1515/TJJ.1988.5.1-4.225 (Accessed: 20 November 2017)

122. Rizk NK., Mongia HC. Emissions Predictions of Different Gas Turbine Combustors. 32nd Aerospace Sciences Meeting & Exhibit. 1994; (AIAA 94-0118). Available at: DOI:doi:10.2514/6.1994-118

123. Kyprianidis KG., Nalianda D., Dahlquist E. A NOx Emissions Correlation for Modern RQL Combustors. Energy Procedia. Elsevier B.V.; 2015; 75(x): 2323–2330. Available at: DOI:10.1016/j.egypro.2015.07.433

124. Roffe G., Venkataramani KS. NASA CR-159421 Emission Measurements for a Lean Premixed Propane/Air System at Pressures up to 30 Atmospheres. 1987.

125. Antoine NE., Kroo IM. Framework for Aircraft Conceptual Design and Environmental Performance Studies. AIAA Journal. 2005; 43(10): 2100–2109. Available at: DOI:10.2514/1.13017

126. Lukachko SP., Waitz I a. Effects of Engine aging on aircraft NOx Emissions. IGT&AC&E Orlando, Florida, 1997. pp. 1–15. Available at: DOI:10.1115/97-GT-386

127. Alexiou A., Aretakis N., Mathioudakis K., Roumeliotis I. ASME GT2010-22701: Short and Medium Range Mission Analysis for a Geared Turbofan with Active Core Technologies. ASME Turbo Expo 2010. Glasgow, UK; 2010. pp. 1–8.

128. Jacob F., Sebastiampillai J., Rolt A., Sethi V., Grönstedt T., Fakhre A., et al. ULTIMATE deliverable D2.5 – Multi-objective, multi-disciplinary analysis simulation platform. 2017.

129. Van Nimwegen RR. Design Features of the Garratt ATF3 Turbofan Engine - SAE Technical Paper 710776. National Aeronautical and Space Engineering and Manufacturing Meeting. SAE; 1971. p. 14. Available at: DOI:10.4271/710776

130. Zhao X., Grönstedt T. Conceptual design of a two-pass cross-flow aeroengine intercooler. Proceedings of the Institution of Mechanical Engineers, Part G: Journal of Aerospace Engineering. 2015; 0(0): 1–18. Available at: DOI:10.1177/0954410014563587

131. Peacock N. ANTLE – an Integration of European & National Research Programmes. Aerodays 2006; 2006. Available at: http://www.aerodays2006.org/sessions/A_Sessions/A4/A42.pdf

132. Lu FK., Braun EM. Rotating Detonation Wave Propulsion: Experimental

Challenges, Modeling, and Engine Concepts. Journal of Propulsion and Power. 2014; 30(5): 1125–1142. Available at: DOI:10.2514/1.B34802

133. Gunston W. World Encyclopaedia of Aero Engines: from the pioneers to the present day. 5th edn. 2006.

134. Zhang X., He M., Zhang Y. A review of research on the Kalina cycle. Renewable and Sustainable Energy Reviews. Elsevier; 2012; 16(7): 5309–5318. Available at: DOI:10.1016/j.rser.2012.05.040

135. Meitner PL. The Nutating Engine — Prototype Engine Progress Report and Test Results. 2006; (October): NASA/TM-2006-214342.

136. SKF. On-line Bearing Calculator Tool. Available at: http://www.skf.com/uk/knowledge-centre/engineering-tools/skfbearingcalculator.html

137. Cánovas Ahedo O. MSc Thesis: Investigation and Design of Power Transmission Systems for Novel Propulsion Technologies. Cranfield University; 2016.

138. Kwan P-W., Gillespie DRH., Stieger RD., Rolt AM. Minimising Loss in a Heat Exchanger Installation for an Intercooled Turbofan Engine. ASME 2011 Turbo Expo. 2012. pp. 189–200. Available at: DOI:10.1115/gt2011-45814

139. Lee JM., Kwan PW., Son CM., Ha MY. Characterizations of aerothermal performance of novel cross-corrugated plate heat exchangers for advanced cycle aero-engines. International Journal of Heat and Mass Transfer. 2015; 85. Available at: DOI:10.1016/j.ijheatmasstransfer.2015.01.127

140. Walker AD., Carrotte JF., Rolt AM. GT2009-59612: Duct Aerodynamics for Intercooled Aero Gas Turbines: Constraints, Concepts and Design Methodology. ASME 2009 Turbo Expo. Orlando, Florida: ASME; 2010. pp. 749–758. Available at: DOI:10.1115/gt2009-59612

141. A'Barrow C., Carrotte JF., Walker AD., Rolt AM. Aerodynamic Performance of a Coolant Flow Off-Take Downstream of an Outlet Guide Vane. Journal of Turbomachinery. 2013; 135(1): 011006. Available at: DOI:10.1115/1.4006332

142. Zhao X. PhD Thesis: Aero Engine Intercooling Conceptual design and experimental validation of an aero engine intercooler. Chalmers University of Technology. 2016.

143. Kyprianidis KG., Rolt AM. On the Optimization of a Geared Fan Intercooled Core Engine Design. Journal of Engineering for Gas Turbines and Power. 2015; 137(4). Available at: DOI:10.1115/1.4028544

144. Kyprianidis KG., Rolt AM., Grönstedt T. Multi-disciplinary analysis of a geared fan intercooled core aero-engine. Proceedings of the ASME Turbo Expo. 2013. Available at: DOI:10.1115/GT2013-95474

145. Ali F., Pleguezuelo AM., Grönstedt T. ULTIMATE Deliverable - D2.2 Noise Modelling Capability. 2017.

146. Smyth M (IATA)., Pearce B (IATA). IATA Economics Briefing No. 9: Air Travel Demand. IATA. 2008. Available at: https://www.iata.org/whatwedo/documents/economics/air_travel_demand.pdf

147. National Academies of Sciences Engineering and Medicine. Negative Emissions Technologies and Reliable Sequestration: A Research Agenda. Washington, DC: The National Academies Press; 2018. 369 p. Available at: DOI:10.17226/25259

148. Lam HSH. Residence Time of Atmospheric CO2. Princeton University. 2003. Available at: http://lam.mycpanel.princeton.edu/TauL1b.pdf (Accessed: 7 April 2019)

149. ICAO. ICAO Environmental Report 2016. 2016. Available at: http://www.icao.int/environmental-

protection/Pages/ENV2016.aspx%0Ahttp://www.icao.int/environmental-protection/Documents/ICAO Environmental Report 2016.pdf

150. EUROCONTROL. Open-ALAQS: an open-source local air quality model. Available at: http://www.eurocontrol.int/services/open-alaqs (Accessed: 23 November 2017)

151. ICAO. ICAO Doc 9889, Airport Air Quality Manual. 2011. 1–200 p. Available at: https://www.icao.int/publications/Documents/9889_cons_en.pdf

152. Liu Y., Wilson CW. Investigation into the impact of n-decane, decalin, and isoparaffinic solvent on elastomeric sealing materials. Advances in Mechanical Engineering. 2012; 2012. Available at: DOI:10.1155/2012/127430

153. Li J., Sun X., Liu Y., Sethi V. Preliminary aerodynamic design methodology for aero engine lean direct injection combustors. The Aeronautical Journal. 2017; (x): 1–22. Available at: DOI:10.1017/aer.2017.47

154. Lee C-M., Tacina KM., Wey C. ISABE-2007-1270 High Pressure Low NOx Emissions Research: Recent Progress at NASA Glenn Research Centre. ISABE. 2007. pp. 1–8. Available at: https://ntrs.nasa.gov/archive/nasa/casi.ntrs.nasa.gov/20070022362.pdf

155. Tacina KM., Podboy DP., Branch EC., Lee F., Dam B. Gaseous Emissions Results from a Three-Cup Flametube Test of a Lean Direct Injection Combustion Concept. Proceedings of the 27th ISABE Conference. 2017; (x): 1–19.

156. Mazzola F. MSc Thesis: Trade off studies between liner durability and NOx emissions for a lean direct injection combustor design. Cranfield University; 2017.

157. Gani R. Ideal Temperature Rise for the Constant Pressure Combustion of

Kerosine in Air: TSD 1526. 1963.

158. Khandelwal B. Effect of Fuel Composition on Aircraft Emissions and Local Air Quality. University of Sheffield; 2017. pp. 1–15. Available at: https://auzaniofficial.files.wordpress.com/2017/04/session-5_engine-emissions-and-local-airport-air-quality.pdf

159. Miller JA., Bowman CT. Mechanism and Modeling of Nitrogen Chemistry in Combustion. Progress in Energy and Combustion Science. 1989; 15: 287–338.

160. Tacina R. Low NOx Potential of Gas Turbine Engines, AIAA-90-0550, NASA TM 10242. 28th Aerospace Sciences Meeting. NASA; 1990. p. 20. Available at: DOI:10.2514/6.1990-550

Appendix A THE IMPACT OF AERO ENGINE EXHAUST EMISSIONS

These studies were originally documented in the confidential ULTIMATE project deliverable D2.3 [108]. The deliverable also included a review of engine exhaust emissions prediction methods for ULTIMATE year-2050 reference engines and other engines including the two representative ULTIMATE baseline year-2000 turbofan engine models. Emissions were estimated at design and off-design conditions and for the International Civil Aviation Organisation (ICAO) engine exhaust emissions certification conditions. Assessment methods are described in section 3.7 and section 3.8 and further details are given in Appendix B, where alternative methods are discussed. The nature and effects of aero engine exhaust emissions are reviewed in the following sections.

A.1 Engine Exhaust Pollutants

There are many reasons for wanting to limit both the mission-level emissions from aircraft and the life-cycle emissions from aviation. These include their direct impact on human health, their contribution to climate change and their impact on the ozone layer [10].

Initial emissions legislation was prompted by the large amounts of smoke emitted by early turbojet engines. Improvements to combustor designs quickly reduced the levels of visible smoke, carbon monoxide (CO) and unburned hydrocarbons (HC) in engine exhausts, but reducing the emissions of oxides of nitrogen (NOx) and fine particulates has proven to be more intractable.

Existing legislation has been framed by the ICAO Committee on Aviation Engine Emissions (CAEP) specifically to restrict the aero engine pollutant emissions around airports. Emission Indices (EI) relate the mass of each pollutant generated to the mass of fuel consumed. EICO, EIHC and EINOx relate to the levels of CO, HC and NOx respectively. However, permitted levels of pollutant generation are defined relative to the maximum rated sea-level static thrust (Foo) for each engine. Emissions test measurements on new

engines are summed over a standard Landing and Take-Off (LTO) cycle (as described in section 2.11) and these totals must meet certain limits for the engines to be certificated. Following the introduction of emissions regulations in 1986, progressively tighter limits on NOx emissions have been agreed at the ICAO committee meetings designated CAEP/2, CAEP/4, CAEP/6 and CAEP/8. At the time of writing, the CAEP/8 standard is applied to new engines.

Most aero engine pollutants result from the products of combustion of the fuel, but some also come from engine oil. Oil consumption has been reduced over the last half-century by the introduction of improved sealing arrangements including the use of carbon seals for bearing chambers. This trend should continue, but the prospect of completely oil-free engines still seems very remote and the anticipated wider-adoption of geared fans and open rotors for more efficient and lower specific thrust engines will increase the demands placed on engine oil systems. While exhaust emissions resulting from oil consumption have been researched for diesel engines, they have not been considered significant for aero engines and are not addressed here. Combustor emissions are the main concern and these are addressed in detail.

The emissions of particulate matter (PM), mainly smoke or soot, have hitherto been limited by reference to the smoke number (SN) measured by filter papers sampling the engine exhaust. However, a new system for the measurement of non-volatile particulate matter (nvPM) is being introduced by CAEP/10 and will be mandatory from the start of 2020. The aim is to replace smoke filter paper standards with mass and number standards. In anticipation of this, new emissions measurement equipment is being commissioned [11].

Historically carbon dioxide (CO_2), water, water vapour and ice crystals have not been categorised as pollutants, so they have not been addressed in the certification rules for aircraft emissions. However, there have been attempts in the USA to classify carbon dioxide as a pollutant and there is growing concern over the radiative forcing from persistent contrails and contrail-induced-cirrus cloudiness. Carbon dioxide and water vapour emitted by aero engines are

significant greenhouse gases that, together with contrails, contribute to global warming. Consequently the CAEP/10 meeting in 2016 made recommendations for a new standard for CO_2 emissions to be applicable to new aircraft designs from 2020 and to earlier designs remaining in production in 2023. The impact of emissions at high altitudes is also now under review [12].

Currently no restrictions apply to the en-route emissions from aircraft, though following CAEP/10; some are likely to be introduced in the near future. Stringent targets for the total emissions of CO_2 and NOx are included in the ACARE Flightpath 2050 targets. It can be assumed therefore that global legislation to limit en-route emissions will be introduced by 2050. Exactly what impact this will have on overall engine design is unclear. Some intercooled cycles and intercooled and recuperated cycles propose improving cruise SFC by raising the peak cycle temperatures at cruise, which would tend to increase en-route NOx emissions, so the trade-off between CO_2 and NOx will need to be revisited.

Emissions of oxides of sulphur (SOx) are not monitored since the sulphur content of aviation fuel is very low and quite variable. Sutkus et al. [13] note that jet fuel specifications limit the sulphur content to 0.3%, but that it is generally well below 0.1%. Nevertheless, even trace amounts of sulphur in particulate emissions and aerosols can have a significant effect on atmospheric chemistry and contrail formation, and significant uncertainty remains regarding their indirect effects on climate [14].

A.2 Oxides of Nitrogen (NOx)

The full atmospheric chemistry and photochemistry of the oxides of nitrogen and their reactions with ozone (O_3) and other naturally-occurring and synthetic chemical species are extremely complex and well beyond the scope of this study. However, a wide range of publications from the International Panel on Climate Change (IPPC) have examined atmospheric chemistry in detail [15].

The main species found in the engine exhausts are NO (nitric oxide) and NO_2 (nitrogen dioxide) that collectively comprise NOx. N_2O (nitrous oxide) and other

nitrogen oxides are generally present in smaller quantities in engine exhausts (typically less than 5 ppm) because they decompose rapidly at high flame temperatures [16]. However, the gas N_2O is persistent at ambient temperatures in the atmosphere and is probably the fourth most significant greenhouse gas after water vapour (H_2O), carbon dioxide (CO_2) and methane (CH_4), with a lifetime (τ_L) of 114 years and a Global Warming Potential in the 100-year timeframe (GWP100) 298 times that of CO_2 is quoted [17]. However, these figures are subject to continuing amendment because background CO_2 levels are increasing [18].

Nitrous oxide is also claimed to be responsible for much of the observed ozone depletion in the stratosphere [19], caused when it eventually decomposes to give nitric oxide. Nevertheless, the majority of global N_2O emissions come from nitrifying bacteria and the majority of anthropogenic N_2O comes from agriculture and particularly from the use of fertilizers, and only a small proportion comes from biomass burning and other forms of combustion. N_2O abundance in the atmosphere was 328.9 ppb in 2016, estimated to be a 22% increase since 1750, whereas CO_2 and CH_4 levels are estimated to have increased by 45% and 157% respectively over the same period [20].

Nitric oxide and nitrogen dioxide in the atmosphere are shorter-lived species than nitrous oxide and more easily converted from one to another. At lower ambient temperatures NO_2 can also convert to N_2O_4 (dinitrogen tetroxide). While the combined NO and NO_2 emissions are referred to as NOx (oxides of nitrogen), the sum of all the many possible oxides and acids containing Nitrogen and Oxygen is referred to as NOy. The global warming, or cooling, potential from NOx is hard to define because these gasses are not well-mixed in the atmosphere and they interact with aerosols, ozone and other chemicals. There remains considerable uncertainty, but unlike N_2O, the shorter-lived NOx components found at low altitudes are generally attributed with negative Radiative Forcing (RF) at the global scale, and so are not traditionally labelled as ‘Greenhouse Gasses’ [18]. However, it seems that NOx emitted at very high altitudes by aero engines does contribute to positive RF.

Nitric oxide is the most reactive species and is mostly oxidised to nitrogen dioxide in engine exhausts and fully oxidised for assay purposes during engine emissions measurements.

In the presence of sunlight, NO_2 is photolysed to produce NO and monatomic oxygen. The latter can then react with oxygen molecules to form ozone and this is believed to be the main source of ozone in the troposphere. Conversely, in the stratosphere, the reaction of NO with O_3 produces NO_2 and O_2, which removes some ozone from the 'ozone layer' that otherwise provides useful protection from damaging ultra-violet solar radiation. Increased global NOx levels therefore present a potential health hazard from radiation-induced skin cancers. On the other hand, NOx also helps to remove chlorofluorocarbons (CFC) from the atmosphere and these chemicals are even more damaging to the ozone layer.

Atmospheric nitrogen dioxide is a major constituent of photochemical smog and, together with fine particulates, is the pollutant believed to have the greatest impact on human health. However, these oxides do not persist for very long in the atmosphere and are washed-out by rain. High local concentrations of NOx and/or SOx can result in 'acid rain' which can kill-off plants and aquatic life in lakes and rivers. Typically, it is the slower growing plants that are at risk from excess nitrogen deposition, but nitrogen oxides also have a major role in the Nitrogen Cycle, which is essential for fertilizing soils and maintaining yields from faster-growing food crops. Globally, most of the oxides are generated naturally, not least by lightning in thunderstorms. Nevertheless, background levels of NOx are believed to be increasing globally, as well as locally around cities and industrial plants.

Flightpath 2050 goals include total mission-level NOx emissions limits as well as limits on NOx emissions produced during the LTO cycle.

During combustion, the equilibrium level of NOx is a function of the pressure, temperature, humidity, fuel chemistry and fuel/air ratio or oxygen concentration. It increases rapidly at temperatures above 2000 K. Equilibrium levels are

however rarely achieved because reaction rates are relatively slow, so the residence time at high temperature can be a more significant factor. Then once the hot gasses have been quenched to lower temperatures by dilution, or by expansion through the turbines, the NOx concentration is effectively fixed or 'frozen' by very slow reaction rates, and can only be reduced to lower levels in the engine exhausts by exposure to catalysts and/or reaction with ammonia. (The latter technology is widely used to reduce diesel engine emissions, where the ammonia needed for road vehicles is generally produced by the thermal decomposition of urea.)

At high combustion temperatures, most NOx is generated as 'thermal' NOx via the Zeldovich mechanism, whereby monatomic oxygen O reacts with molecular nitrogen N_2 to produce NO plus monatomic nitrogen N, and then the N reacts with O_2 to give more NO and O. The 'Extended Zeldovich Mechanism' includes reactions with the hydroxyl radical OH. The reaction rates are governed by the Arrhenius law and increase rapidly with increasing temperature. Real NOx emissions may peak at slightly below the stoichiometric fuel/air ratio (FAR), while peak temperatures occur at slightly above the stoichiometric FAR due to dissociation, which is more significant at lower absolute pressures. Dissociation effects are fairly limited in high overall pressure ratio (OPR) gas-turbine-engine primary combustors at sea level.

At relatively-low flame temperatures, other production channels such as 'prompt' NOx and reactions involving N_2O, are relatively more significant [22] [23]. A fourth potential route from 'fuel-bound nitrogen' (FBN) is not significant when the fuel is kerosene. Discussion of all the possible NOx generation routes is beyond the scope of this study, but Nicol et al. compare the main ones [24].

A review of aircraft emissions in the USA and Canada has estimated that their aircraft LTO-cycle NOx emissions were about 73,152 tonnes in 2005, equivalent to just 0.8% of their total anthropogenic NOx emissions in 2002 [25]. However, the proportion is likely to have increased since that study.

A.3 Carbon monoxide (CO) and carbon dioxide (CO_2)

Mission-level carbon dioxide emissions are proportional to fuel burn and contribute to anthropogenic greenhouse-gas emissions that are considered largely responsible for global warming.

Carbon monoxide (CO) results from incomplete combustion. It is an inevitable consequence of the rich-burn combustion of hydrocarbon fuels, but it can also be found where combustion is quenched too quickly, as for example in proximity to a cold wall (which is more typically an issue for piston engines). Significant carbon monoxide emissions in modern aero engines are generally associated with incomplete combustion at low-power or idle conditions and with poor atomisation of the liquid fuel. Real CO emissions are at a minimum when somewhat below the stoichiometric fuel/air ratio.

Through a series of chemical reactions involving the hydroxyl radical (OH-), nitric oxide and sunlight, carbon monoxide contributes to the formation of ozone and photochemical smog. Through the removal of hydroxyl radicals, carbon monoxide increases the residence time of methane in the atmosphere, so it makes an indirect contribution to global warming, though CO itself is only a very weak greenhouse gas [26]. While carbon monoxide is toxic, the emissions from aircraft engines are not considered to be a significant health hazard. There are greater concerns over the more localised CO emissions from ground vehicles, including those operating in and around busy airports.

While the global concentrations of carbon dioxide in the atmosphere are now very well understood, there is greater uncertainty over global levels of carbon monoxide and the overall rates at which the molecules transfer between their various sources and sinks, hence the large uncertainties in the lifetimes of these gasses in the atmosphere. Nevertheless, the rate at which CO_2 is removed (the CO_2 response function) is commonly taken from the 'Revised Bern Carbon Cycle Model' [29] using Equation 23 [30]. This equation predicts an atmospheric CO_2 half-life $t_{1/2}$ of approximately 30.3 years, using coefficients given in Table 47, where R_{CO2} is the fraction remaining after the time t (years)

$$R_{CO2} = a_0 + \sum_{i=1}^{i=3} a_i . e^{-t/\tau_i}$$ Equation 23

Table 47 – Coefficients for Equation 23

Coefficient	a_0	a_{01}	a_{02}	a_{03}	τ_{01} (years)	τ_{02} (years)	τ_{03} (years)
Value	0.217	0.259	0.338	0.186	172.9	18.51	1.186

The mean lifetime τ_m is the average length of time that a molecule of the gas remains in the atmosphere. This is longer than the half-life which is the time taken for half of the molecules to be absorbed into a sink. Assuming exponential decay for the number of molecules, then the relationship between τ_m and $t_{1/2}$ is given by Equation 24 and therefore τ_m would be about 43.7 years.

$$t_{1/2} = \tau_m . \ln(2) = 0.69315 . \tau_m$$ Equation 24

However, as CO_2 levels are rising, the system is not in equilibrium. The rate of removal is not constant and is not increasing pro rata with the rising concentration of CO_2. Thus the long-term 'effective residence times' τ_L for the additional anthropogenic CO_2, inferred by Lam from Nordhaus's model and from more recent climate models [148], are significantly longer than the mean lifetime τ_m.

A.4 Unburned Hydrocarbons (UHC)

Unburned hydrocarbon (UHC or HC) emissions originate from incomplete combustion of the fuel, so the level of emissions is closely related to combustion efficiency and to carbon monoxide emissions. Engine oil consumption also contributes to UHC emissions. These emissions are partly responsible for the odour from gas turbine exhausts. UHC emissions include gases from volatile organic compounds (VOC), and both liquid and solid aerosols.

A.5 Particulate Emissions

Soot and smoke result from the incomplete combustion of hydrocarbon fuels and the pyrolysis of the larger (and hence more persistent) fuel droplets. Particulate emissions tend to increase with combustion at higher pressures, but to a lesser extent where airblast atomisers/airspray burners are used [86]. Currently the only regulation placed on aero-engine particulate emissions is the LTO cycle measurement of visible smoke, recorded as a 'smoke number' (SN). However, concern is growing over the emission of fine particles under 10 micrometres in diameter ($PM_{2.5}$–PM_{10}) that are too small to be visible. These particles seem to be associated with a wide range of human health issues.

A new system for the measurement of non-volatile particulate matter (nvPM) has been proposed by CAEP/10 to become mandatory from 2020 onwards, once approved by the ICAO Council [149]. Initially at least, the new limit was expected to be set at a level where all currently certificated engines would remain compliant [81], but discussions at the CAEP/11 Working Group 3 (WG3) Combustor Technologies meeting in April 2017 were not immediately reported, so the policy remained unclear. When the new test measurements are completed, the results should enable the total LTO nvPM emissions at individual airports to be estimated based on airport operations. Note EUROCONTROL has worked on modelling tools such as the Airport Local Air Quality Studies (ALAQS) model and the more recent Open-ALAQS plug-in to the open-source geographic information system (QGIS) to help facilitate such studies [150] and supplement the guidance provided by ICAO [151].

The composition and size of the particulates is dependent on the detail composition of the fuel and the effectiveness of atomisation by the fuel injectors. A synthetic jet fuel without cyclic aromatic hydrocarbons and sulphur compounds would produce fewer particulate emissions, but might not be a 'drop-in' replacement fuel because those components are believed to be necessary to keep the elastomeric seal materials used in existing aircraft fuel systems 'soft' or 'swollen-up'. Some research has been undertaken into

alternative solvents that could be added to synthetic fuels to keep O-ring seals manufactured in fluorocarbon, flurosilicone and nitrile polymers sufficiently plasticised [152].

It is likely that more stringent nvPM emissions legislation will be introduced by 2050, but apart from ongoing efforts to reduce visible smoke there are no obvious strategies proposed for tackling the emissions of finer particles by aero engines. Particulate traps are now widely used in diesel engine exhaust systems and greatly reduce their emissions, at least for larger particles. In principle, filters and electrostatic precipitators might be used to extract fine particles from aero engine exhausts, though this would come with significant performance, weight and maintenance cost penalties.

Appendix B ALTERNATIVE NOx EMISSIONS PREDICTION METHODS

This appendix provides a detailed review of alternative NOx emissions estimation methods and correlations.[8] A summary has already been given in Chapter 3. The final recommendation was that the older NASA correlation expressed as Equation 21 should continue to be used for year-2050 LDI combustor NOx emissions estimates. This conclusion was only reached after considering various alternatives.

Assessment methods are described in sections 3.7 and 3.8. Section 3.8 is expanded here, providing details of the alternative correlations that were reviewed, including recent correlations based on LDI combustor rig testing, and potential new formulations.

Year-2000 baseline mission-level flight-cycle emissions can be estimated based on the declared Landing and Take-off (LTO) cycle emissions for existing engines. For these baseline mission-level rich-quench-lean (RQL) combustor emissions, the 'P3T3' method described in section 3.8.5 was recommended.

After reviewing alternative methodologies for estimating combustor emissions the author concluded that, in the absence of detail combustor design data, correlations using cycle pressures and temperatures, or related parameters such as fuel/air ratio (FAR) or equivalence ratio Φ, should be able to provide consistent emissions estimates for future designs. Therefore recent research and existing published correlations for lean combustor NOx emissions were reviewed and alternative correlations considered for a range of potential combustor designs. However, no existing correlations were found to be entirely satisfactory for predicting NOx emissions for future lean direct injection (LDI) combustors.

[8] Most of the material in this appendix was also a part of the author's contribution to the ULTIMATE project deliverable D2.3 [106].

Emissions correlations are desired to be robust for lean and staged combustion over a wide range of conditions in both conventional and intercooled engine cycles. For NOx emissions, the correlation should properly separate pressure, temperature and ambient humidity effects in order to be usable throughout the flight envelope. It should also be able to account for advances in technology, such as improved fuel atomisation and the use of new combustor-liner materials that will, by year-2050, require less wall-cooling air. Therefore alternative formulations have been investigated for NOx emissions correlations potentially applicable to future LDI combustors with staged-fuel injection. Suggested new approaches include having separate terms for ‘prompt’ NOx and ‘thermal’ NOx, and accounting for the progress made towards equilibrium NOx levels before those reactions are quenched. Research into these options provides additional insight into combustion processes, but the resulting new correlations discussed here still present difficulties. Insufficient data are currently available to validate them over the full range of engine operating conditions, so they cannot be advocated as superior to the existing published NASA correlations for lean combustors and for specific LDI fuel injector designs.

The results of the different correlations applied to the ULTIMATE year-2050 reference engine cycles are presented in section 8.6.

B.1 NASA Emissions Correlations based on LDI Combustor Research

The difficulty in developing definitive NOx assessment methods for staged LDI combustors is demonstrated with reference to recent research and emissions correlations from NASA Glenn. For example, a recent study by Li et al. [153] has worked-up a preliminary design methodology based on the LDI combustor segment tested by NASA and reported by Tacina et al. in 2014 [93]. The fuel injectors or ‘burners’ each have an array of 13 nozzles in contrast to the injector array with 9 nozzles shown in Figure 14. The methodology considers: air distribution, combustor sizing, and designs for the diffuser, the dilution holes and the swirlers. The LDI combustor NOx emissions are predicted using a

correlation from the NASA studies reported in [93] and reproduced as Equation 25, where Φ_{pilot}, Φ_{m1} and $\Phi_{m2,3}$ are respectively the equivalence ratios for the pilot, first main set, and second and third main sets of LDI fuel injector nozzles. In this case P_3 is in kPa. The factor of 100 in the $(100\Delta P/P_3)^{-0.6}$ term has been inserted because a percentage figure was used for the pressure loss in the original equation.

$$\boldsymbol{EINO_x = P_3^{0.5}\left(e^{(T_3/230)}\right)\left(\frac{100\Delta P}{P_3}\right)^{-0.6}\left(0.0081\Phi_{pilot}^{0.29} + 0.35\Phi_{m1}^{7.15} + 0.369\Phi_{m2,3}^{7.37}\right)}$$

Equation 25

Note the equivalence ratio for the combustion of kerosene can be calculated from the local FAR at the fuel injector divided by the stoichiometric FAR. Taking kerosene to have the nominal composition $C_{12.5}H_{24.4}$ then the ratio of carbon (atomic mass 12.011) to hydrogen (atomic mass 1.008) by mass (the CH_{ratio}) is 6.1043 and the stoichiometric FAR (FAR_{ST}) is given by Equation 26, adapted from formula F5.7.6 in [99], and is found to be 0.06789.

$$FAR_{ST} = 0.087002(CH_{ratio} + 1)/(CH_{ratio} + 3) \qquad \text{Equation 26}$$

But there is a big problem with using Equation 25 to predict NOx emissions.

Unlike some earlier NASA flametube tests that used a moveable cooled sampling-probe to maintain a constant residence time [124], it seems that the correlation given in Equation 25, and those derived from more recent NASA studies, were obtained from rig tests with fixed combustor geometry and probe location. Thus the residence time and non-dimensional flow must have varied with the combustor percentage pressure loss and the selected swirler angles. Increasing the pressure loss across the swirlers helps atomise the fuel and mix it more quickly with the air, but given a fixed combustor volume, it also reduces the residence time roughly in inverse proportion to the square root of $\Delta P/P_3$.

This seems to be the explanation for the magnitude of the pressure ratio coefficients observed in [91] and [93]. The Equation 25 with an R^2 value of 0.95 was derived after simpler equations failed to collapse the experimental data to

give R^2 values any higher than 0.77, but by adding four more coefficients, while analysing a relatively small dataset, it is to be expected that the R^2 figure would improve (just from 'overfitting' of the data, an effect not unrelated to Runge's phenomenon). This means that the relatively-more-complex correlation in Equation 25 might in practice be little or no better at making predictions than one of the simpler correlations that it superseded, like Equation 27 from [93] for example, where T_{ad} is the equilibrium adiabatic flame temperature. In this equation the units are Pa for P_3 and K for T_3 and T_{ad}.

$$EINO_x = 0.0008P_3^{0.46}\left(e^{(T_3/757)}\right)\left(e^{(T_{ad}/355)}\right)\left(\frac{100\Delta P}{P_3}\right)^{-0.647} \qquad \text{Equation 27}$$

Extrapolating from existing data to higher FAR, P_3 or T_{ad} is risky, but necessary where test rigs are unable to simulate the higher-power engine conditions.

From Equation 17 and Figure 22, it is seen that, in rich-quench-lean (RQL) combustors, the NOx emissions are roughly proportional to the formation time spent at peak NOx production. In LDI lean modules the NO_x formation times may be longer, since peak temperatures are generally lower and quenching is less-rapid, but the reaction rates should also be slower. Equation 25 predicts 27.5% more NOx if the design has 2% pressure loss rather than 3% (implying a 22.5% longer residence time) and 15.9% less NOx if it has 4% pressure loss (implying a 13.4% shorter residence time). For a family of combustor designs having the same residence times, but different swirler areas and pressure losses, the $(100\Delta P/P_3)^{-0.6}$ term in Equation 25 might be replaced by a constant, introduced to align the NOx emissions predictions at a typical swirler pressure loss, $\Delta P/P_3$ of 3% say. This would result in Equation 28. This might be reasonably valid for the given percentage pressure loss and residence time, but the latter is not known since residence times are not calculated in [93].

$$EINO_x = P_3^{0.5}\left(e^{(T_3/230)}\right)\left(0.0157\Phi_{pilot}^{0.29} + 0.677\Phi_{m1}^{7.15} + 0.713\Phi_{m2,3}^{7.37}\right) \qquad \text{Equation 28}$$

Also it is not obvious that Equation 28 can still be used when there are large changes in fuel flow distribution and when some sets of injectors are not fuelled. At an equivalence ratio, the figures calculated for the first set of main injectors only differs by a few percentage points from those calculated for the second and third sets. Plotting their contributions to $EINO_x$ against equivalence ratio as in Figure 83 shows the pilot and main injectors' contributions have very different profiles. The three curves intersect at around 0.58 equivalence ratio where each set of injectors makes the same contribution to $EINO_x$ (despite having different fuel and air mass flows).

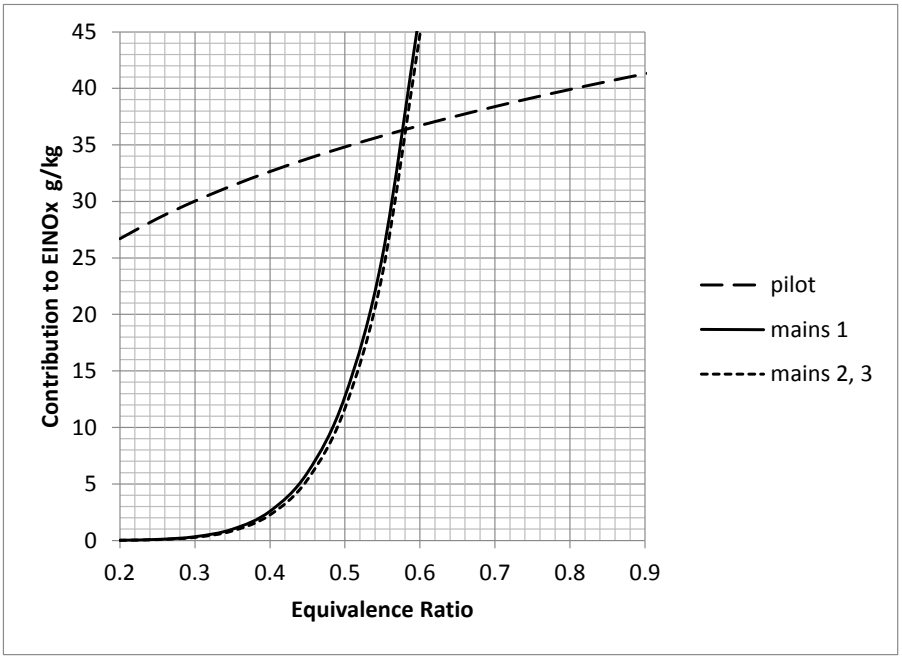

Figure 83 – Contributions of Injectors to $EINO_x$ according to Equation 28 given P3=3810 kPa, T3=870 K

Equation 25 and Equation 28 do not explicitly account for changes in fuel flows between the three streams. For example, if the FAR in the pilot stream is held constant while the main fuel flows are switched on and off, then increasing the total fuel flow can only increase $EINO_x$ according to these equations, whereas firing-up the lean modules would be expected to reduce it, since the overall fuel mass flow has increased and the lean injectors add relatively little NOx.

It is perhaps too simplistic to assume that the NOx generated in each stream is totally independent of the FAR in the adjacent streams, but it would seem more logical to multiply each of the three terms in an equation like Equation 28 by the proportion of the total fuel allocated to each stream. In this way the contribution to the overall emissions index from the pilot stream would reduce when the fuel flows allocated to the main injector nozzles increased, and vice versa. However, implementing this requires even more design parameters to be estimated for a hypothetical future combustor, making this approach too complicated for current purposes. The conclusion drawn is that Equation 26 and Equation 28 may only be valid over a limited range of equivalence ratios, and only for cases where all of the injectors are fuelled.

For high power conditions where fuel is flowing in all the injectors, Li et al. [153] suggest using another NASA study correlation from the earlier Advanced Subsonic Combustion Rig (ASCR) programme using the 9-nozzle array shown in Figure 14. This correlation was published in 2007 by Lee et al. [154] and again in 2008 by Tacina et al. [92], and it is rearranged here as Equation 29. The units for temperature are K and the units for pressure are kPa.

$$EINO_x = 1.359 P_3^{0.595} \left(e^{(T_3/194)}\right) \left(\frac{100\Delta P}{P_3}\right)^{-0.565} (FAR^{1.69}) \qquad \text{Equation 29}$$

It is assumed the *FAR* is not that at combustor exit, but the FAR before the wall cooling or dilution air has been added. Exactly how *FAR* should be calculated is not explained in [153], but in [93] it is stated that 20% of the incoming air could be used for wall cooling. (The percentage is expected to reduce in future designs when a CMC material with higher temperature capability is introduced, making lower NOx emissions achievable.) Lee et al. claim that this correlation fitted both high-pressure and medium-pressure data quite well, though Equation 30 gave a better fit to their more recent high-temperature AST test results [154]. The units are as for Equation 29.

$$EINO_x = 0.104 P_3^{0.68} \left(e^{(T_3/185)}\right) \left(\frac{100\Delta P}{P_3}\right)^{-0.36} (FAR^{1.32}) \qquad \text{Equation 30}$$

As in the earlier example, the pressure-ratio term may be replaced by a constant factor for a given combustor design, assuming a constant combustor pressure loss (which is a reasonable assumption for normal steady-state operation where the downstream nozzles are choked).

For the LTO-cycle emissions estimation, an equation like Equation 28 might be used, with assumed FAR values for each set of fuel injectors. For example, at idle it could be assumed that all the fuel goes to the pilot injector nozzles, so the FAR values for the main injectors are zero. Equation 28 would reduce to an equation like Equation 31, though, as previously discussed, the coefficients should probably be different when only the pilot injectors are fuelled.

$$EINO_x = P_3^{0.5} \left(e^{(T_3/230)}\right) \left(\frac{\Delta P}{P_3}\right)^{-0.1} (0.0157 \Phi_{pilot}^{0.29}) \qquad \text{Equation 31}$$

The next step would be to use the overall combustor FAR and the assumed airflow distribution between the different swirlers to estimate Φ_{pilot}. Taking TF2050 LTO-cycle idle performance as an example, then the emission indexes calculated according to Equation 31 with pilot fuel only would be as in Table 48.

Table 48 – LDI NOx Emissions Estimates at TF2050 LTO-cycle Idle Case

Emissions	Units	Example 1	Example 2	Example 3
T_3	K	596	596	596
P_3	Pa	854135	854135	854135
FAR overall	–	0.00994	0.00994	0.00994
Airflow to pilot injector	–	10%	15%	20%
FAR local	–	0.0994	0.0663	0.0497
Φ_{pilot}	–	1.464	0.976	0.732
$\mathrm{EINO_x}$	g/kg	1.83	1.62	1.49

$EINO_x$ is predicted to increase as the primary zone around the pilot burner becomes more fuel-rich. It should peak at some equivalence ratio, but according to Equation 31, it never does. Such a correlation might still be valid for a limited range of equivalence ratios, but as discussed below, the $EINO_x$ figures in Table 48 are considered optimistic, so this is really the 'negative proof' that Equation 31 should *not* be used.

The most recent correlations from NASA Glenn are for the NOx emissions from a third-generation swirl-venturi LDI injector as reported in [155]. In this case the flow area to the pilot burners is quoted as 12% of the total swirler area, though Tacina et al. argue that it probably should have been increased (and as discussed in their paper, perhaps it actually was higher at the end of the test).

The 'Fit 2' correlation in that paper is reproduced as Equation 32, where $T_{ad,p}$ is the primary injector adiabatic flame temperature, and $T_{ad,mi}$ is the 'i^{th}' main injector-set's adiabatic flame temperature. The coefficients d_p, d_m, e_p and e_m are listed in Table 49. The equation and its coefficients are specific to the particular design with three sets of main swirlers. Like the earlier equations, it does not explicitly account for the distribution of fuel flow between the different fuel injector elements.

$$EINO_x = P_3^{0.931}\left(e^{(T_3/234)}\right)\left(\frac{100\Delta P}{P_3}\right)^{-0.829}\left[d_p e^{T_{ad,p}/e_p} + \sum_{m1}^{m3} d_m e^{T_{ad,mi}/e_m}\right]$$

Equation 32

Table 49 – Coefficients for the Correlation given by Equation 32

Coefficient	d_p	e_p	d_m	e_m
Fit 2	4.97×10^{-6}	246	7.36×10^{-7}	187

B.1.1 Applying and comparing NASA's LDI NOx correlations

Despite the significant reservations noted above, predictions from several of the NASA correlations for $EINO_x$ have been compared, at high-power conditions and also at low-power conditions where some or all of the main injectors would not be fuelled.

In [155] Tacina et al. apply the Equation 32 correlation to the Advanced Air Transport Technology (AATT) 'N+3 Technology Reference Propulsion System' (TRPS) which is the projected future turbofan with CFM56 thrust levels and a geared fan giving very low specific-thrust, as discussed in section 2.4. Helpfully the authors provided a table of some key performance parameters for this engine at climb, cruise and take-off, and at the four LTO-cycle performance points. They also referenced the paper by Jones et al. [45] which provides further details of the climb, cruise and take-off performance, tabulating data from the NPSS performance model. The latter tabulations do not however include the ISA-day SLS LTO-cycle cases, so the fuel flows, needed to calculate Dp/Foo figures have had to be estimated for those cases. Also, it was noted that the adiabatic flame temperature and the combustor exit and 'adiabatic' equivalence ratios quoted in [155] for the top-of-climb (TOC) case seem to be in error, whereas the TOC P_3 figure is in rough agreement with [45]. The data are reproduced in Table 50 with corrections from [45] to the TOC equivalence ratios, and an estimate of the correct T_{ad} figure for the TOC case.

The engine's combustor is assumed to use 20% of the inlet air for combustor liner wall cooling, increasing the engine combustion-zone FAR and equivalence ratio Φ_{ad} by 25% relative to combustor exit. In subsequent calculations for the 100% and 85% thrust cases, the combustion zones behind each type of fuel injector are assumed to have equal FAR, equivalence ratio and adiabatic flame temperature, with the injectors fuelled pro rata. However, for the 30% and 7% thrust cases the figures in Table 50 are the average values and cannot be used directly in the NOx emissions correlation.

Table 50 – NASA N+3 TRPS Turbofan LTO-cycle Performance

Condition	***FN*** kN	***FF*** kg/s	T_3 K	P_3 bar	T_4 K	T_{ad} K	Φ_4	Φ_{ad}	FAR_{ad}
LTO cycle 100%	127.3	0.607[2]	870	38.1	1650[2]	1832	0.354	0.442	0.030
LTO cycle 85%	108.2	0.494[2]	835	32.8	1558[2]	1727	0.325	0.402[4]	0.027
LTO cycle 30%	38.2	0.143[2]	661	14.1	1123[2]	1231	0.186	0.233	0.015
LTO cycle 7%	8.9	0.047[2]	553	7.1	826[2]	890	0.103	0.128	0.008
EOR take-off ISA+15K	101.4	0.8304	957	44.3	1889	2107	0.446	0.558	0.037
TOC 35,000 ft, ISA	27.0	0.3548	851	19.4	1750[3]	1958[3]	0.417[3]	0.521[3]	0.035
Cruise 35,000 ft, ISA[1]	24.3	0.3198	827	18.3	1686	1887	0.392	0.490	0.033

[1] Note the net thrust FN at cruise is 90% of TOC thrust, i.e. it is 'max cruise', not 'typical cruise'.

[2] These figures are estimated since they are not quoted in either [155] or [45].

[3] These figures have been derived from [45], since the figures tabulated in [155] are inconsistent.

[4] Possibly this figure should have been 0.406, since 0.402 is inconsistent with the Φ_4 figure of 0.325.

Note the thrust for the 100% SLS take-off case is calculated from the 0.25 Mach number ISA+15K end of runway (EOR) net thrust by multiplying the latter by a Boeing Equivalent Thrust (BET) factor of 1.2553, as stated in [45]. It is then assumed the 100% SLS ISA-day thrust is equal to the ISA+15K SLS thrust. However the ISA+15K OPR is 36.63, while the ISA day OPR is quoted as 38.1 in [155]. This suggests the latter study may have assumed a slightly higher SLS thrust.

Different engines with the same BET will have the same EOR thrust and thus have comparable take-off performance. The BET is often quoted in preference to a manufacturer's nominal static thrust figure when wanting to compare the take-off performance of different engines. The inverse of the BET factor gives a typical historical reduction in rated thrust with increased forward speed at EOR.

The BET factor has not normally been used to define an actual static take-off thrust rating. While modern aircraft almost invariably start the take-off roll before the engines have reached full thrust, the full static take-off thrust rating is generally set such that, for a given day temperature, a stabilised HP TET is held

roughly constant while the aircraft accelerates along the runway. In quoting a 100% SLS thrust for ICAO emissions tests, the maximum certificated take-off thrust at this ISA-day EOR TET would normally be quoted.

Note some engines with a common bill of materials are supplied with several different take-off thrust ratings, each with its own declared set of characteristic emissions figures. Typically these lower thrust ratings match aircraft variants certificated with lower maximum take-off weights. For NOx emissions, the lower thrusts consistently provide lower dP/Foo figures and larger margins relative to the CAEP/2 limit. However, the limits for CAEP/4, CAEP/6 and CAEP/8 are constructed such that the Dp/Foo margins are more-nearly constant when the '100%' SLS thrust rating is varied and the OPR and TET change. Relative to current NOx limits, there seems little benefit to be gained from reducing the declared static take-off thrust, unless taxation were to be based on the Dp figure. It is possible though that the development of lower-specific-thrust engines will bring about changes to current practice, in order to avoid unrepresentatively high static thrusts being used in future Dp/Foo assessments.

The LTO-cycle 30% and 7% thrust conditions for the N+3 TRPS-cycle combustor were reproduced directly in the NASA rig tests, resulting in $EINO_x$ figures of 6.25 and 4.3 g/kg respectively. For the 85% and 100% thrust conditions the full operating pressures could not be reproduced on the rig, so it was necessary to apply a pressure correction to the measured results.

Table 51 shows the LTO-cycle NO_x re-calculated using Equation 32 for the high-power conditions and taking data from Table 50 and the measured $EINO_x$ figures for the low-power cases. The 85% and 100% thrust NOx emissions indexes calculated here agree with those in [155] to within 1%. The dP/Foo figure is 16.3% of the CAEP/6 limit, compared with the NASA N+3 target of 20%. However, these calculations do not substantiate the 85-89% NOx reduction relative to CAEP/6 claimed in the paper. Tacina et al. noted that the air mass flow through the pilot-burner swirler varied during testing, due to the opening-up of a crack, which explained a progressive reduction observed in the

pilot-only NOx emissions measured over several days of testing. They took the lowest figures from the last day of testing and argued that, for the 7% thrust case, the NOx emissions could have been further reduced if the mass flow of air to the pilot burner had (by design) been further increased. (The cracking was attributed to not having selected the best material for the rig-test component.)

Table 51 – LTO-cycle NOx measured and correlated for the N+3 TRPS (20% wall-cooling, 4% ∆P/P)

Condition	**FN** kN	**OPR**	**EINOx** g/kg	**Time** s	**Dp NOx** g	**Dp/Foo** g/kN
LTO cycle 100%	127.3	38.1	18.65	42	475	12.1
LTO cycle 85%	–	–	8.17	132	533	–
LTO cycle 30%	–	–	6.25	240	215	–
LTO cycle 7%	–	–	4.30	1560	315	–

Since the engine combustor design was assumed to reserve 20% of the inlet air for the combustor liner's wall cooling, the local FAR figures are increased by 25% relative to combustor exit. (The test rig, though, had uncooled ceramic walls.) However, the 20% figure seems an over-estimate by Tacina et al. of the cooling requirement for future combustors. A study by Mazzola has shown that increasing wall cooling flows beyond a critical level is counter-productive, not only for NOx emissions, but also for cooling, since the increase in flame temperature with increasing equivalence ratio at a TET greatly increases the radiative heat transfer to the liner wall [156]. In that Cranfield University study the critical wall-cooling flow was shown to be less than 20%.

Table 51 lists the measured NOx emissions at the 7% and 30% thrust conditions instead of applying the correlation given by Equation 32 for these cases. For these cases the assumption of equal FAR, equivalence ratio and T_{ad} for the pilot injector and all of the main injectors cannot be used, but it is still possible to use the correlation if estimated local flame temperatures are substituted.

For the N+3 TRPS, only the pilot injector is lit at 7% thrust, and [155] states that it receives 12% of the swirler air flow. Thus the local equivalence ratio is increased from the overall figure of 0.128 to 1.067 and the local FAR is 0.0724. Given T_3 is 553 K, the temperature rise is estimated to be 1881 K, making the local flame temperature ($T_{ad,l}$) 2434 K. The resulting $EINO_x$ value calculated from Equation 32 is 2.06 g/kg when the contribution from the main injectors is set to zero. This is significantly lower than the reported measured emissions index values determined by gas analysis, but is not unexpected given that, as discussed above, the correlation should not be accurate at both high-power and low-power conditions. Other possible factors are that the 'adiabatic' flame temperatures used to create the correlation did not account for dissociation, or were affected by varying ambient humidity. It is worth noting that, during testing, some discrepancies were observed between the equivalence ratios determined by the fuel and air flow measurements and those determined by gas analysis. These discrepancies were particularly large for measurements relating to the 30% thrust conditions.

At 30% thrust, the best test results were obtained with only the pilot injector and one of the three sets of main injectors lit, but Tacina et al. commented that it was 'hard to find a "good" fuel staging'. If it is assumed that the lit injectors receive 41.4% of the swirler air flow, and their equivalence ratios are equal, then these local equivalence ratios are increased from the overall figure of 0.233 to 0.563 and the local FAR is 0.0382. Given that T_3 is 661 K, then the local temperature rise is estimated to be 1233 K, making $T_{ad,l}$ 1894 K. The resulting $EINO_x$ value predicted by Equation 32 is 1.84 g/kg when the contribution from two-thirds of the main injectors is set to zero. This figure is also significantly lower than the directly measured emissions at conditions corresponding to the 30% thrust case.

Table 52 modifies Table 51 using the new figures for the 30% and 7% thrust cases and predicts a new figure of 9.6 g/kg for Dp/Foo (NOx). This new figure is 13% of the CAEP/6 limit, corresponding to an 87% reduction, which is in the middle of the 85%–89% range of reductions claimed in [155].

Table 52 – Equation 32 LTO-cycle NOx calculations for N+3 TRPS

(20% wall-cooling, 4% dP/P)

Condition	***FN*** kN	**$\Phi_{ad,I}$**	***$T_{ad,I}$*** K	**EINOx** g/kg	**Time** s	**Dp NOx** g	**Dp/Foo** g/kN
LTO cycle 100%	127.3	0.442	1833	18.65	42	478	9.8 overall
LTO cycle 85%	–	0.402	1737	8.25	132	561	–
LTO cycle 30%	–	0.563	1894	1.84	240	261	–
LTO cycle 7%	–	1.067	2432	2.04	1560	449	–

The assumption that only the pilot injectors are fuelled for the 7% thrust case, and that the pilot and one-third of the main injectors are fuelled in the 30% thrust case, seems applicable to most engines. However, the ULTIMATE year-2050 Geared Open Rotor combustor temperature-rise and its overall fuel/air ratios are unusually high, so a different fuel staging will be assumed for this engine. In applying Equation 32 it is assumed that the FAR, equivalence ratio and flame temperature behind each lit injector are equal, whereas in practice the pilot injector might well be expected to run richer.

Various different methods have been tried to estimate combustion temperatures with liquid kerosene fuel. Walsh and Fletcher [99], for example, provide equations relating FAR to T3, T4, fuel heating value (LHV) and combustion efficiency, but for higher temperatures, other methods might be used to take account of the effects of pressure on dissociation. To compare the method from Gani in [157] used to estimate $T_{ad,I}$ in Table 52 for the 7% and 30% thrust cases, with the unspecified method used in [155], the N+3 TRPS cruise and EOR $T_{ad,I}$ temperatures were recalculated from the quoted T3 and $\Phi_{ad,I}$. figures. The cruise temperature was found to be 1889 K, or 2K hotter than quoted in [155] and Table 50, which is within the range of rounding errors, but the recalculated EOR temperature was 2129 K, a 22 K, or 2%, higher combustor temperature rise. This would increase $EINO_x$ by 16% according to Equation 32. At these temperatures the pressure effects on temperature rise are still modest,

so it is possible the different calculation methods would diverge by even more at higher temperatures, though in LDI combustors these temperatures should only be found behind the pilot injectors. A discrepancy in $T_{ad,l}$ is just one of several potential uncertainties discussed further in section B.6. The method of [157] that accounts for pressure might provide more conservative emissions estimates when applied to other engines.

The NASA correlation for advanced lean-burn combustors given by Equation 21 just using P3, T3 and T4, is much simpler, making its application much less ambiguous than Equation 32. Although it was not originally formulated for LDI combustors, Equation 21 provides an alternative assessment for the overall NASA N+3 TRPS NOx emissions. Table 53 shows that Equation 21 yields a fairly similar dP/Foo (NOx) figure of 11.7 g/kN vs 9.8 g/kN from Equation 32 in Table 52.

Table 53 – Equation 21 LTO-cycle NOx calculations for the N+3 TRPS

Condition	**FN** kN	**P3** kPa	**T3** K	**T4** K	**EINOx** g/kg	**FF** kg/s	**Dp NOx** g	**Dp/Foo** g/kN
LTO cycle 100%	127.3	3810	870	1833	17.86	0.607	455	11.7 overall
LTO cycle 85%	–	3280	835	1737	13.29	0.494	867	–
LTO cycle 30%	–	1410	661	1894	2.83	0.143	97	–
LTO cycle 7%	–	710	553	2432	0.92	0.047	67	–

It seems that, given suitable guidelines, Equation 32 might be used to predict at least the high-power $EINO_x$ figures for year-2050 engines with advanced LDI combustors. (The under-prediction of $EINO_x$ at low-power conditions would not have a big effect on overall Dp/Foo.) However, it must be assumed the residence times that future combustors will need to meet altitude relight requirements are consistent with the correlation and with its assumed swirler pressure loss. The overall combustor pressure loss quoted for the N+3 TRPS engine is 4%, but if the swirler pressure loss is taken to be 3% (allowing 1% for loss in the preceding diffuser), then all the NOx emissions predicted by

Equation 32 would increase by 27%. This is partly due to increased residence time in the flame-tube and partly due to less-vigorous mixing and fuel atomisation. The more appropriate figure is not obvious.

Even with very-advanced CMC liner materials, it seems unlikely that combustor walls would be completely uncooled. Some air is also likely to be needed for pre-filming the HP NGV inner and outer platforms and to control the outlet radial traverse of the combustor. However the figure of 20% wall cooling air seems unduly pessimistic for future CMC combustor liners. Table 54 shows the effect of reducing the cooling air flows to a more realistic 10% of combustor inlet flow for a year-2050 design, with NOx emissions calculated using Equation 32.

The reduction in Dp/Foo to 6.5 g/kN or 9% of the CAEP/6 limit is quite significant. However, reducing swirler pressure loss to 3% would raise Dp/Foo (NOx) to 8.2 g/kN (11% of the CAEP/6 limit).

Table 54 – Equation 32 LTO-cycle NOx calculations for N+3 TRPS (10% wall-cooling, 4% dP/P)

Condition	FN kN	$\Phi_{ad,l}$	T_{ad} K	EINOx g/kg	Time s	Dp NOx g	Dp/Foo g/kN
LTO cycle 100%	127.3	0.393	1740	11.65	42	297	6.5 overall
LTO cycle 85%	–	0.361	1649	5.49	132	358	–
LTO cycle 30%	–	0.500	1779	1.06	240	36	–
LTO cycle 7%	–	0.948	2402	1.81	1560	132	–

When Equation 32 is applied to the TF2050, the results are less impressive, predicting a Dp/Foo NOx figure of 44.4 g/kN when assessed with 4% swirler pressure loss and 10% wall cooling air. These results are shown in Table 55. The margin with respect to CAEP/6 is reduced, but not pro rata, because the OPR of the TF2050 engine at 100% SLS thrust is 60.5 and this increases the CAEP/6 regulatory limit to 119.96 g/kN. The predicted Dp/Foo for the TF2050 is thus 37% of the CAEP/6 limit, a 63% margin, not even close to the 80% margin targeted by NASA. Relative to CAEP/8, the predicted margin is 60%.

Given that the TF2050 cycle has higher combustor temperatures and FAR than the N+3 TRPS engine, it is possible that two-thirds of the main burners could remain lit at the 30% thrust case to reduce NOx levels at that condition. The proportion of air provided to the pilot burner might also be increased to minimise smoke at 7% of thrust. However, these changes will make little difference to the NOx Dp/Foo assessment, since 95% of the NOx is predicted to be produced at the 85% and 100% thrust conditions. It seems that, as performance cycles become more aggressive, the proportion of NOx generated at the high-power conditions becomes more significant, suggesting that a simpler correlation focussing on those conditions might provide sufficiently accurate Dp/Foo predictions.

Table 55 – Equation 32 LTO-cycle NOx calculations for TF2050 (10% wall-cooling, 4% dP/P)

Condition	FN kN	$\Phi_{ad,l}$	T_{ad} K	EINOx g/kg	Time s	Dp NOx g	Dp/Foo g/kN
LTO cycle 100%	236.2	0.429	1915	78.8	42	4785	44.4 overall
LTO cycle 85%	–	0.380	1778	27.2	132	4185	–
LTO cycle 30%	–	0.648	2113	12.3	240	93.6	–
LTO cycle 7%	–	1.500	2254	1.7	1560	357	–

The Dp/Foo NOx assessment for the TF2050 in Table 55 is higher than that predicted in Table 56 using the earlier NASA correlation Equation 21, and higher also than the estimate from Rolls-Royce for the comparable LEMCOTEC LTF study engine [96].

The same two NASA correlations have also been applied to the GOR2050 engine performance and the results are given in Table 57 for Equation 32 and in Table 58 for Equation 21. In the former case the swirler pressure loss was taken as 4% and the wall-cooling flow was taken to be 10% of combustor entry, consistent with the previously assumed year-2050 technology level.

Table 56 – Equation 21 LTO-cycle NOx calculations for the TF2050

Condition	FN kN	P3 kPa	T3 K	T4 K	EINOx g/kg	FF kg/s	Dp NOx g	Dp/Foo g/kN
LTO cycle 100%	236.2	6129	1004	1839	47.86	1.446	2906	36.7 overall
LTO cycle 85%	–	5353	949	1704	31.66	1.165	4871	–
LTO cycle 30%	–	2211	753	1327	6.39	0.390	599	–
LTO cycle 7%	–	678	577	1127	1.39	0.131	285	–

Table 57 – Equation 32 LTO-cycle NO_x calculations for GOR2050 (10% wall-cooling, 4% dP/P).

Condition	FN kN	$\Phi_{ad,l}$	T_{ad} K	EINOx g/kg	Time s	Dp NOx g	Dp/Foo g/kN
LTO cycle 100%	104.8	0.563	2024	39.7	42	811	20.3 overall
LTO cycle 85%	–	0.532	1952	21.8	132	1171	–
LTO cycle 30%	–	0.944[1]	1592	2.06	240	77	–
LTO cycle 7%	–	0.419[2]	1189	0.97	1560	74	–

[1] To avoid an equivalence ratio approaching unity, which would produce high NOx levels, it is assumed that two sets of main injectors as well as the pilot injector would continue to be fuelled at this approach rating.

[2] To avoid an equivalence ratio in excess of two, which would generate lots of smoke, it is assumed that one set of main injectors would also continue to be fuelled at this idle thrust rating. Alternatively, the burner might be redesigned so the proportion of combustor inlet air provided to the pilot injector would be increased.

Table 58 – Equation 21 LTO-cycle NOx calculations for the GOR2050

Condition	FN kN	P3 kPa	T3 K	T4 K	EINOx g/kg	FF kg/s	Dp NOx g	Dp/Foo g/kN
LTO cycle 100%	104.8	3411	839	1928	17.08	0.486	349	12.9 overall
LTO cycle 85%	–	2964	817	1858	13.90	0.407	747	–
LTO cycle 30%	–	1378	690	1502	4.36	0.156	163	–
LTO cycle 7%	–	593	550	1127	1.16	0.049	88	–

In comparison to the TF2050 and GOR2050, the smaller NASA N+3 TRPS has a less aggressive cycle. It also benefits from an unrealistically-low specific thrust and being assessed with a reduced TET for the '100%' static thrust case, relative to the genuine EOR take-off rating TET. The GOR2050 also benefits from its very low specific thrust, which helps to reduce Dp/Foo relative to $EINO_x$.

Figure 84 compares various aero engine Dp/Foo NOx predictions, including those using Equation 21 (labelled as NASA T4) and Equation 32 (labelled as NASA LDI), with NASA and LEMCOTEC targets.

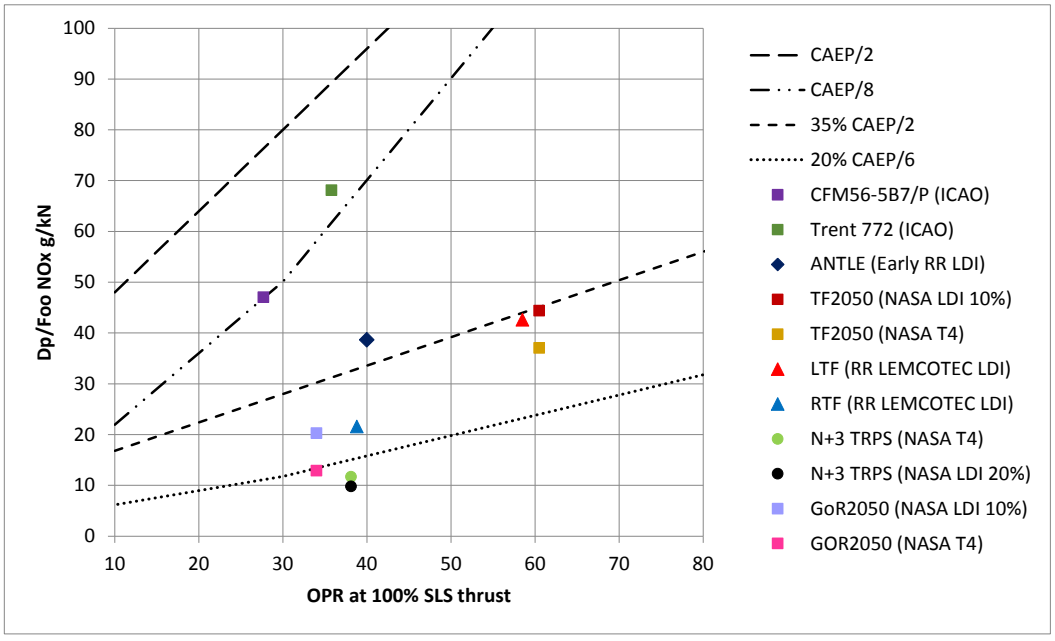

Figure 84 – Average Dp/Foo NOx Predictions from NASA Correlations vs ANTLE and LEMCOTEC assessments and typical year-2000 in-service engine ICAO database figures

All the assessments made using Equation 32 assume 4% combustor pressure loss. The percentage wall-cooling air assumed is as indicated in the legend. Given the N+3 TRPS engine cycle, the LDI combustor concept described in [155] appears to meet the NASA N+3 NOx target of an 80% reduction relative to CAEP/6. However, the technology appears incapable of meeting the NASA target in engines with more-realistic year-2050 performance cycles.

All these assessments of the recent study engines meet the LEMCOTEC LDI target of 'CAEP/2 -65%'.

B.2 Analysis of Existing NOx Correlations

Despite tending to produce broadly similar predictions, none of the foregoing correlations seems entirely satisfactory for predicting the NOx emissions of the year-2050 ULTIMATE reference engines having LDI combustors. Humidity is not taken into account and the equations do not address staged combustion in a logical way. Equation 25, Equation 28 and Equation 32 can account for different equivalence ratios for each set of injectors, but they still do not seem to correctly account for staging. These equations add extra complexity considering the original requirement to be able to make simple and consistent estimates of year-2050 reference engine combustor emissions. The most recent NASA correlation Equation 32, as interpreted here, underestimates NOx emissions at the low power conditions and gives higher emissions estimates for the more aggressive cycles in comparison with the NASA 'T4 correlation' Equation 21, though the latter was probably intended for pre-mixed pre-vaporised double-annular combustor designs. Double-annular designs are now less-favoured, and pre-mixed designs are unlikely to be feasible in engines with very high compressor delivery temperatures.

Another approach to emissions assessment might be to provide separate correlations, similar to Equation 27, Equation 29, Equation 30 or Equation 31 for each fuel-staging mode of the LDI combustor operation, though at part-power conditions, the fuel distribution between the injector nozzles might still be varied within a single mode of operation.

Alternatively a single correlation could ‘smear-out’ the fuel-staging changes. This has been attempted before by fitting a fifth-order order polynomial curve fit to experimental $EINO_x$ measurements plotted against a suitable function of pressure, temperature and FAR (or equivalence ratio), but the shape of this curve would still be specific to a particular strategy for fuel-staging in the combustor.

The most powerful factors determining NOx emissions are pressure, residence time at temperature and local flame temperature, (or associated performance parameters such as T_3 plus FAR), but other factors may also need to be considered.

B.2.1 Equilibrium levels of NOx

As a function of air/fuel ratio (AFR) at a T_3, the levels of NOx (and CO and UHC) vary as shown schematically in Figure 85. Given sufficient residence time, the level of NOx will stabilise in a mixture of combustion products held at a fixed temperature and pressure. For a primary combustor this generally provides an upper limit on $EINO_x$ that is a function of the temperature, pressure and equivalence ratio of the gasses. The last factor is significant, because as the equivalence ratio approaches unity, the remaining oxygen is preferentially scavenged by the hydrogen and carbon from the fuel. However, NOx levels do not immediately fall to zero when the equivalence ratio exceeds one.

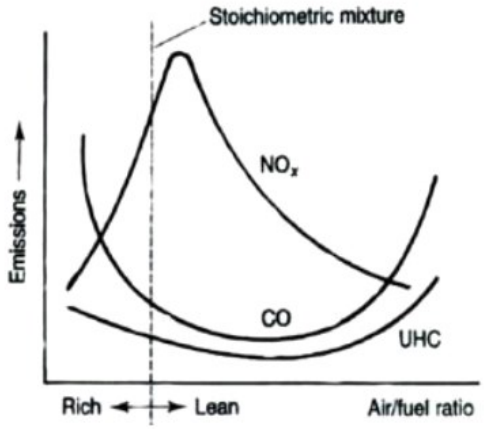

Figure 85 – Effect of AFR on Emissions [158]

The equilibrium NOx levels are seen to peak just on the lean side of stoichiometric conditions, at an equivalence ratio less than one, though flame temperatures peak slightly on the rich side. At lower equivalence ratios, or at higher AFR, the equilibrium NOx levels are seen to reduce rapidly, but this is largely because the temperature of the combustion products reduces.

Figure 85 does not mean that the rate of NOx generation necessarily peaks in lean mixtures. On the contrary, Miller and Bowman [159] show that for shorter time periods NO levels may peak at around 1.2 equivalence ratio as a result of prompt NOx reactions associated with HCN. They even show that under some conditions the amount of prompt NOx produced can exceed the equilibrium levels mediated by thermal NOx, so that extending the residence time might actually reduce NOx. Their charts demonstrate that NO is not in fact generated at a steady rate during combustion, as implied by Equation 17 and Figure 22, and that this assumption is only really applicable to generation of thermal NOx.

B.2.2 Staged combustion

Staging the fuel flow to different injector nozzles enables mostly-lean combustion at high overall FAR when all of the nozzles have fuel flowing, while avoiding lean extinction at lower overall FAR by concentrating the fuel in a sub-set of potential combustion zones. It is generally reasonable to assume that only the pilot nozzles will be fuelled at idle and that all the injectors will be fuelled at take-off and climb conditions, but the optimum distribution of fuel flow at cruise and approach conditions is less obvious. Allegedly, some early double-annular combustors just ran on their pilot injectors at cruise conditions at altitude, but future designs are likely to have at least some of the lean injector nozzles operating together with the pilot injector nozzles at cruise and approach conditions. Managing the transitions between the different operating modes, through various transient and steady-state conditions, presents a significant challenge to the fuel and control systems. The exact arrangements that would be used in future designs cannot be known, so simplifying assumptions must be made.

One possible assumption is that in the future, fuel flows will be optimized between the potential zones of combustion, so that once the overall fuel flow is adequate to support at least one or two lean-burn fuel nozzles, they would be individually switched-on. In a typical combustor with a dozen or more fuel-injectors, the serial introduction of additional combustion zones could provide an almost seamless transition from pilot-only operation to the start of full-burner operation. The variation of the emissions index might therefore be represented reasonably well by a third-order polynomial correlation curve fit against overall FAR, with appropriate additional factors for inlet pressure and temperature.

NASA LDI combustor studies have adopted various approaches to generating $EINO_x$ correlations and attempted to assess the NOx generated behind pilot and main injectors separately before summing them. Early NASA LDI pilot and LDI main injector designs were similar 'simplex' designs, though more recently 'filming' or air-spray/air-blast atomisers have been used for the main injectors.

It is important to properly separate the pressure and temperature effects before constructing any new correlations for year-2050 staged LDI combustors. This is because the correlations would be used in intercooled engine cycles as well as in conventional Brayton-cycle engines, and it should be applicable not only at SLS ISA conditions, but also throughout the full flight envelope as an alternative to the traditional P3T3 method.

B.2.3 Pressure effects

Pressure effects have been modelled variously in existing correlations. Some indices applied to the combustion chamber pressure are noted in Table 59.

There are large variations in the indices on pressure, as noted by Lefebvre and Ballal [86]. Lefebvre's index in Equation 16 is much higher than the others, and Risk & Mongia and Roffe & Venkataramani's figures are lower, implying in the latter cases that that pressure has little or no effect on NOx emissions.

The high index on pressure in Lefebvre's Equation 16 can be explained when it is considered that $EINO_x$ is largely proportional to the residence time. Given that

the mean temperature in the combustor is proportional to T_{st} and T_{pz}, then the residence time is also proportional to $V_C/(P.\dot{m}_A)$ or inversely proportional to P for a given V_C and $\dot{m}_A$. Thus if the residence time is held constant, the power of P is effectively reduced from 1.25 to 0.25. Thus the index 1.25 is no longer to be considered anomalously high.

Table 59 – Indexes for the variation of EINO$_x$ with Pressure (P_3 or P_{31})

Research Papers	Index	Remarks
Norman et al. [83]	0.3-0.5	Range observed in rig testing. For the P3T3 method
	0.34	An average exponent derived from engine testing
	0.50	Exponent 'from NOx formation theory'
	0.20	Possible exponent for low-NOx combustion, where the primary zone is weaker than stoichiometric at take-off
Madden & Park [84]	0.40	For use in the absence of an engine-specific figure
Lefebvre, quoted in [109]	1.25	Equation 16 with combustor volume and mass flow
Odgers & Kretschmer [121]	0.66	Equation 17
Risk & Mongia [122]	-0.05	Equation 18
Kyprianidis et al. [123]	0.40	Equation 19 for new RQL combustors
Roffe & Venkataramani [124]	0.00	Implied by Equation 20 (independent of pressure)
Quoted by Antoine et al. [125]	0.37	Equation 21
Tacina et al. [93]	0.50	Equation 25 and Equation 28
Tacina et al. [92]	0.595	Equation 29
Lee et al. [154]	0.68	Equation 30
Tacina et al. [155]	0.931	Equation 32

Increasing pressure is also associated with increased fuel flow, and because the fuel is an almost incompressible liquid, the fuel nozzle pressure increases faster than the air pressure. This affects fuel atomisation which also has an effect on emissions.

Rig-testing of the MLDI ‘flat dome’ 13-nozzle array at NASA Glenn showed clear trends of increasing NOx emissions with increasing pressure at constant T_3, particularly when tested at 650 K and 860 K, but less so at intermediate temperatures [93]. In these high-T_{ad} tests all the nozzles were fuelled and ran lean with similar FARs. The resulting P_3 indexes were in the range 0.5 to 0.68.

To understand the main effect of pressure, it should be understood that in the combustor both pressure and temperature affect the density of the air and combustion products and hence the mean free path length between the molecules. The frequency of collisions depends on the mean free path length and on the velocities of the molecules, which are proportional to the square root of temperature. Thus the frequency of collisions is roughly proportional to the static pressure and inversely proportional to the square root of the static temperature.

Few collisions, even at high temperatures, have sufficient energy to generate the monatomic oxygen needed for the Zeldovich mechanism, so the rate of formation of thermal NOx is relatively slow. If the residence times would be long enough for the NOx levels to approach thermal equilibrium, then the index on pressure might approach zero (i.e. $EINO_x$ would be independent of pressure). However, when reaction rates are slower, and residence times relatively short, the thermal NOx does not reach equilibrium levels and the rate of NOx accumulation is almost linear, as implied by Figure 22. In this case the index on pressure for a given flame temperature and for a given residence time should be closer to one, in inverse proportion to the reduction in mean free path length between molecules.

For a given T_3 and *FAR*, the combustion temperatures are reduced by dissociation. Since increasing pressure suppresses dissociation, it favours conversion of NO to NO_2 and CO to CO_2, but it also raises the temperature of the combustion products, favouring NO formation. However, the monatomic oxygen needed for the Zeldovich mechanism is produced by dissociation, so its levels are reduced at higher pressures. (A denser gas also favours the reverse

reaction, by disproportionately increasing the number of 3-way collisions that can recombine the oxygen, or nitrogen, atoms). This may help to explain why the pressure indexes for NOx production are lower than unity, though it also seems possible that it is mostly because NOx levels were closer to equilibrium conditions during some of the testing.

Peak flame temperatures are significantly reduced in lean combustors, particularly when operating at part-power, so the thermal NOx reactions proceed more slowly. Equilibrium levels are also reduced. On the other hand, more time is spent at or near the peak flame temperatures in a lean combustor.

Below about 1850K, more NOx is generated as 'prompt' NOx or as 'N_2O-intermediated' NOx rather than as thermal NOx, and this may also account for reduced dependency on pressure. Prompt NOx (or prompt NO) is generated by reactions occurring in parallel with the breakdown of hydrocarbon fuel molecules during combustion. The mechanisms are described by Miller and Bowman [159]. The higher the pressure, the faster the combustion reactions, so less time is available for prompt NOx to form. Increasing pressure might not increase the amount formed in this case and thermal NOx may build-up too slowly after combustion to be significant. So low indexes on pressure might also be consistent with low flame temperatures where thermal NOx is less significant. Thus it is far from obvious that a single index can adequately reflect the effects of pressure over a wide range of combustor operating conditions, including fuel-staging between pilot and main injectors [83].

B.2.4 Combustor pressure loss

In the more recent NASA rig tests, the percentage pressure ratio across the swirlers has a big effect on $EINO_x$, independent of the absolute pressure. Higher pressure ratio gives higher velocities, and for fixed combustor geometry, lower residence time, so for a linear rate of NOx generation $EINO_x$ might be expected to be inversely proportional to the square root of the pressure ratio (i.e. index -0.5). Conversely, if the NOx generation rate is slowing, then the index might be expected to be closer to zero. However, in these tests the

observed sensitivity to swirler pressure ratio typically gave indexes in the range of -0.56 to -0.695, suggesting that additional factors were in play [93] [155].

In real aero engine combustor designs the residence time is largely dictated by the fixed HP turbine nozzle capacity and by the combustor volume, which is largely determined by altitude relight requirements. Thus it seems preferable to exclude most *rig-derived* indexes for pressure ratio from correlations used for $EINO_x$ in new combustor designs.

The minimum swirler pressure loss and the pressure differential across the combustor liner walls is commonly dictated by the need to have a pressure margin for film-cooling the leading edges of the HP turbine nozzle guide vanes, but by 2050 ceramic matrix composite materials may remove the requirement for film cooling. The minimum pressure differential might then depend more on being able to adequately atomise the fuel so that the droplets have a sufficiently small Sauter Mean Diameter (SMD) for successful relight. However the SMD also depends on surface tension and viscosity, and hence on the temperature of the fuel and on the design of the injectors (swirl-venturi or airblast/airspray). The literature suggests that relatively less NOx is generated behind airblast injectors when operating at higher pressures, since the fuel is transported by the air rather than by the ejected fuel-droplet momentum (which is rapidly counteracted by denser air). Assuming the minimum combustor pressure ratio requirements are met, then the resulting SMD and the time taken for fuel to be fully vaporized under normal operating conditions will have further effects on combustor emissions, but these are effects that defy simple analysis.

B.2.5 Temperatures used in NOx correlations

Traditionally, all NOx emissions correlations have used at least one temperature, but there are many different approaches to using temperatures, and, as for P_3, many different indexes have been proposed. The combustor entry temperature T_3 has been considered particularly useful, as to a first approximation it correlates with the stoichiometric flame temperature (with pressure only having a second-order effect). For RQL combustors and other

designs with rich primary zones, most of the NOx is generated at close to stoichiometric conditions. However, in LDI combustors this only applies to combustion occurring behind the pilot fuel injectors and theoretically in a 100% pre-mixed combustion system it does not apply at all. Thus it is at first sight surprising that T_3 appears in Equation 21 for lean-burn combustion systems, given that Equation 21 also includes T_4. The inclusion of T_3 may be justified however, because practical combustors include pilot fuel injectors that run rich.

Ideally, an emissions correlation would use the actual flame or combustion temperatures combined with NOx formation times and static pressure, but apart from the stoichiometric flame temperature T_{st} these temperatures can be difficult to assess and can vary widely, both spatially and temporally throughout the combustor. The combustor exit temperature T_4 is not by itself an adequate indicator of an actual lean-combustor flame temperature, because the latter depends on the distribution of the fuel and the amount of wall-cooling and dilution air that the combustor uses. Equation 21 does not include any handle to account for changes in these secondary air flows resulting from new materials and wall-cooling technology.

For a given technology level, increasing T_3 should require more cooling air to be used, but for a given T_4 and an amount of wall-cooling air, increasing T_3 would reduce the mean FAR inside the combustor. When CMC materials are introduced, therefore, the tendency of increasing T_3 to increase NOx production for a given T_4 in a lean combustion zone should reduce, or even tend to zero. This is counter to the effect of T_3 in Equation 21, where it is still very powerful.

B.3 Potential New Correlations for LDI Combustor NOx Emissions in 2050

Existing correlations generally include P_3, a temperature and either a second temperature, a FAR or an equivalence ratio. For a given fuel, either FAR or equivalence ratio can be used, but the combustion temperature depends on the level of dissociation and is therefore also pressure dependent. Provided the fuel remains kerosene, this argues in favour of using FAR or equivalence ratio,

since simple performance models frequently neglect the effects of dissociation on combustion temperatures.

The FAR can be estimated in the zone where most NOx is produced, so account can be taken of the amount of cooling and/or dilution air that bypasses the combustion zone. Then as combustor liner material technology improves, and less wall-cooling air is needed, lower levels of NOx should be produced. However, for the assumed proportions of cooling air, the combustor exit or turbine entry FAR can be factored-up appropriately.

In these studies, new formulations for correlations were investigated in order to try to make the $EINO_x$ assessments less specific to particular combustor geometries and applicable to a wider range of engine performance cycles. Two approaches are explored in the following sections, though it is argued that both need to be combined in order to reflect the underlying physics and chemistry regarding the formation of both prompt NOx and thermal NOx. At high combustion temperatures thermal NOx predominates and NOx levels increase almost pro rata with formation time, but at lower temperatures most NOx is prompt NOx and longer formation times only provide a relatively small increase in final NOx levels [160].

However, while new equations give some interesting insights into LDI NOx emissions, their use cannot yet be recommended, because the data needed to validate them are contradictory.

B.3.1 A focus on NOx Formation Mechanisms

In a staged LDI combustor there is a particular problem of estimating NOx emissions at intermediate and low power settings, where prompt NOx and N_2O-intermediated NOx become more significant.

Equation 28 has separate terms for each set of injectors, but an alternative approach would be to have separate terms for different NOx formation mechanisms, assuming that equilibrium will not be reached. The idea is to extend the range of combustion temperatures over which the correlation is

valid. This might perhaps be realized by an equation like Equation 33, where the constants and indexes *a*, *b*, *c*, *d*, *g* and *h* would need to be determined:

$$EINO_x = P_3^a \left(e^{(T_3/b)} \right) (c.FAR_{Zeldovich}^d + g.FAR_{Prompt+N_2O}^h) \qquad \text{Equation 33}$$

Unlike Equation 28, the *FAR* figures in Equation 33 might both refer to the overall FAR, or FAR prior to the addition of wall-cooling air, rather than the FAR in specific combustion zones. The two different indexes applied to FAR would account for the high temperature (Zeldovich) and low temperature (prompt and N_2O-intermediated) NOx formation mechanisms. Both FAR terms are multiplied by the same pressure and temperature terms in this equation, though it could be argued that the different NOx formation mechanisms should have different pressure and temperature dependencies. A humidity correction should probably also be added to this equation, but for simplicity it has been omitted.

Comparison with previous correlations places probable upper and lower bounds on the indexes, as shown in Table 60. If the proposed values of the indexes in Table 60 would be accepted, based on previous correlations, then the remaining constants *c* and *g* could be chosen to match the anticipated NOx emissions from an advanced year-2050 LDI combustor, based on recent emissions testing.

However this proposed new correlation is still open to criticism on account of relying on selecting six constants or indexes, while being validated against a limited set of relevant measurements.

Table 60 – Possible indexes for the variation of $EINO_x$ with pressure, temperature and FAR

Index	Upper bound	Lower bound	Proposed value
a	0.6 (from Table 59)	0.2 (from Table 59)	0.25
b	757 (from Equation 27)	122 (from Eq.5-7)	250
d	7.4 (from Equation 30)	1.7 (from Equation 29)	5
e	–	–	2.71828
h	1.7 (from Equation 29)	0.3 (from Equation 30)	0.5

A more definitive assessment of the constants and indices in Equation 33 was therefore abandoned in favour of the option described in the next section.

B.3.2 A focus on NOx Formation Rates and Times

This second approach focusses on the formation of NOx, particularly at the relatively high-power conditions in a LDI design. It is argued that the level of NOx depends firstly on the equilibrium level of NOx (that for lean mixtures is primarily a function of the peak temperature), and secondly on the progress made towards that equilibrium level, which is a function of the residence or formation time and the reaction rates. This is the approach taken by Odgers and Kretschmer that resulted in Equation 17 [121], though as already noted, that should only really be applicable to thermal NOx. Thermal NOx is still assumed to be significant at 85% SLS thrust on an ISA day, though the combustion temperatures are quite modest in the lean modules of the LDI combustor, so the validity of this assumption needs to be tested and the contribution of N_2O-intermediated and prompt NOx still needs to be addressed.

Equation 17, introduced a time-constant of 250 Hz, which means that it would take 4 ms to reach equilibrium if the initial rate of NO formation held steady. However the time-constant for thermal NOx should really be a function of temperature, pressure and equivalence ratio. Recognising this, Odgers and Kretschmer proposed a second equation (18) in [121] for partially-premixed prevaporized combustors, with a variable time-constant as seen in Equation 34. This correlation exhibited lower 'root mean square' (rms) deviation from its experimental dataset than Equation 17, but that was to be expected as it used more input parameters. Also the vaporisation and mixing time-delay problem is absent in such systems. The stated units are K for T_3 and the combustion temperature T_c, Pa for P_3, and s for the time τ and Pa for P_3 (though as is discussed later, the stated units for P_3 might possibly be in error). It is assumed $EINO_x$ is in g/kg, while the equivalence ratio Φ_c, at the combustion temperature, is dimensionless. The constants and indices derived by Odgers and Kretschmer are listed in Table 61.

$$EINO_x = \left(e^{(A-B/T_c)}\right).tanh(C.P_3^D.T_3^E.\Phi_c^F.\tau)\ ) \qquad \text{Equation 34}$$

Table 61 – Constants and Indices proposed for use in Equation 34 [121]

A	*B*	*C*	*D*	*E*	*F*
10.5	17752 K	9.081×10^{-14}	0.8687	3.96	-0.7038

The first term in Equation 34 is interpreted as providing the equilibrium emissions index for NOx, while the second '*tanh'* term quantifies the proportion of the equilibrium level generated in time τ.

The second term recognises that the thermal NOx production rate and equilibrium NOx concentration are functions of the pressure, equivalence ratio, Φ, and temperature. Compressor delivery temperature T_3 is the chosen temperature, but combined with the equivalence ratio it also implies a combustion temperature. Note the maximum value of the '*tanh'* function is unity, implying that the forward and reverse reactions have reached equilibrium.

Figure 86 compares the function $(1-e^{-x})$ used in Equation 17 with the new function *tanh(x)* used in Equation 34.

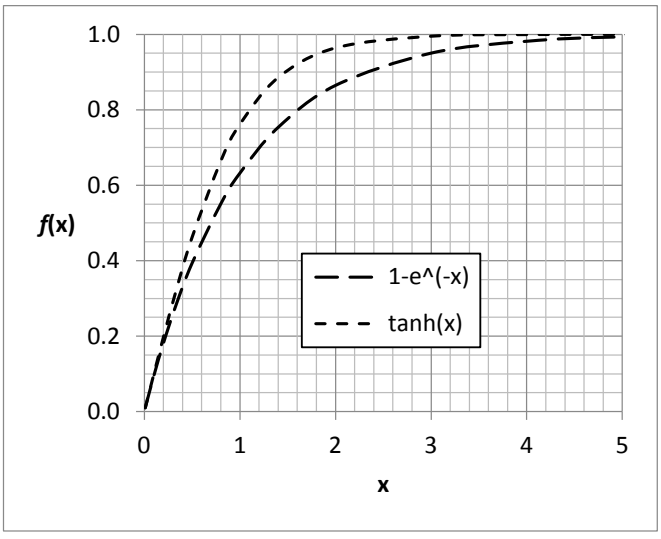

Figure 86 – Comparison of Functions representing Progress towards Complete Reaction

For small values of *x* the gradients approximate to unity and the differences are negligible, but then they reduce and for values of *x* between about 0.5 and 1.5, the *tanh(x)* gradient remains significantly steeper. Considering both the forward and reverse reaction rates, then the *tanh(x)* function (where *x* represents the elapsed time since the reaction started divided by the initial reaction rate) seems to provide a more typical representation of the accumulation of reaction products over time than the $(1 - e^x)$ function. However, since the real chemical reactions are more complicated than N_2+O_2=2NO, the *tanh* function can still only be considered an approximation.

The frequency of molecular collisions at a temperature is proportional to pressure, but increasing the pressure will tend to reduce the abundance of the free O and N atoms that facilitate the Zeldovich mechanism, so it seems reasonable to suppose that the initial rate of reaction will be proportional to pressure raised to a power of slightly less than one. Assuming pressure has little effect on the equilibrium level of NOx (since NO is diatomic) then the power of 0.8687 specified in Table 61 would seem to be reasonable. For comparison, the P_3 index for overall $EINO_x$ is 0.931, according to the 'fit 2' correlation of Tacina et al. in the recent NASA study [155].

The equivalence ratio Φ is expected to have significant effects on the equilibrium NOx concentration and on the rate of formation of NO. In rich mixtures the CO will be competing with N_2 for any available oxygen atoms and will be winning-out, since the carbon-oxygen bonds are stronger, but in lean mixtures this competition is less significant and other reactions may predominate once levels of the intermediate products that support prompt NO_x have reduced. According to Table 61, Φ is raised to the power of -0.7038 in the second term of Equation 34. Figure 87 compares the shape of that function with the function (1-tanh(Φ)), normalising the former to give the same value at $\Phi = 1$ or at $\Phi = 0.5$.

The relative slopes of the two curves are seen to be very similar at around 0.5 equivalence ratio, but over the wider range, the (1-tanh(Φ)) function provides a

more credible representation of the likely effect of the decreasing atomic oxygen concentration on the rate of formation of thermal NOx by the Zeldovich mechanism. The effect of equivalence ratio on the equilibrium concentration of NOx is likely to be similar to its effect on the rate of formation. However, Odgers and Kretschmer neglected the effect of equivalence ratio on the equilibrium level of NOx in the first term of Equation 34. Perhaps that was not unreasonable for the low equivalence ratios typically found in pre-mixed combustion systems, given that Φ already appeared in the second term, but it can be argued that the (1-tanh(Φ)) function would be better applied to the first term instead. However, another potential reason for including Φ in the second term of Equation 34 would be to make it sensitive to the combustion temperature, because T_3 is the only temperature currently input to the second term. T_3 seems a poor proxy for T_c when considering thermal NOx, but the preference for T_3 in the second term might perhaps be justified when considering the ignition delay and prompt NOx formation.

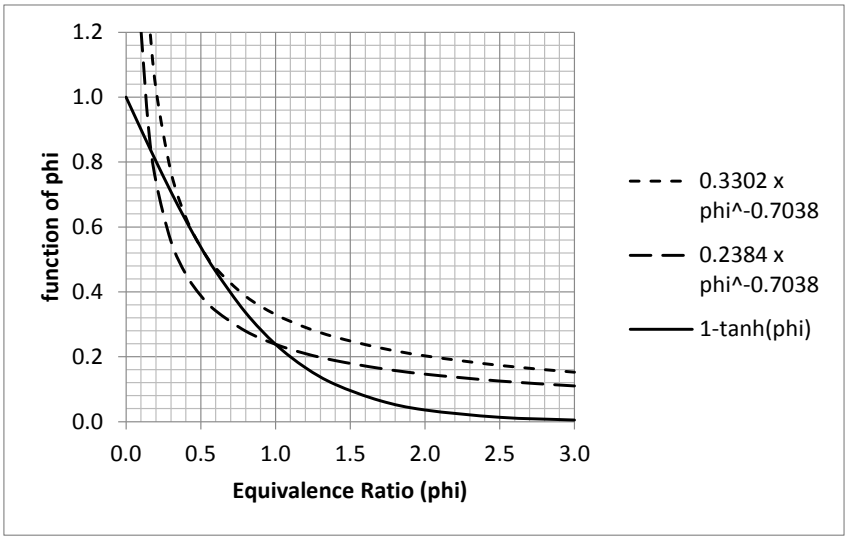

Figure 87 – Comparison of Functions representing Equivalence Ratio Effects on the NOx Formation Rate

Odgers and Kretschmer state that the experimental data, from which the constants and indexes in the Equation 34 correlation were derived, came from an analysis of 172 data points for pre-mixed combustors [121]. These had

formation times of 1 to 3 ms and covered a wide range of conditions with P_3 from 5 to 30 atmospheres, T_3 from 800 to 1000 K, flame temperatures from 1620 to 2395 K, and equivalence ratios from 0.34 to 0.86. They gave $EINO_x$ figures up to 56.5 g/kg.

The equilibrium $EINO_x$ figure should be a function of the equivalence ratio as well as the temperature, but the first term in Equation 34 predicts the equilibrium level of thermal NOx just as a function of the combustion temperature. This function is plotted out in Figure 88, using both linear and log scales for $EINO_x$.

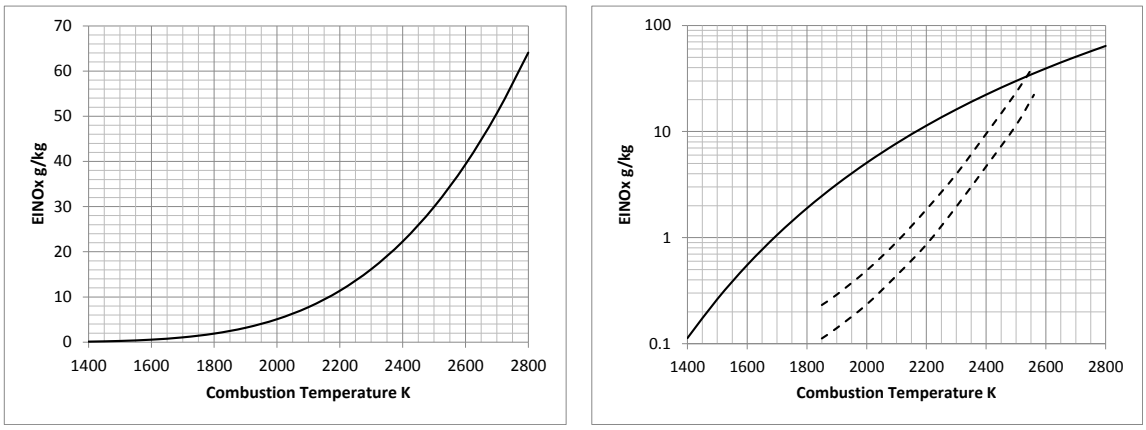

Figure 88 – Equilibrium Level of $EINO_x$ from Equation 34 compared with Typical Emissions (dotted lines)

The dotted lines on the latter plot indicate an actual range of pre-mixed combustor $EINO_x$ values obtained from various pre-mixed combustion systems, with and without water or steam injection. The lines come from an earlier paper by Kretschmer and Odgers who reproduced them in their figure 1 in [121]. Odgers and Kretschmer did not, however, state how parameters other than the combustion temperature T_c were assumed to vary as T_c varied.

By comparing the solid and dotted lines in Figure 88, it would appear that in practice 100% progress towards equilibrium is only achieved when the combustion temperature approaches 2500–2600 K, while at temperatures around 2200 K only about 7–17% of the equilibrium level of NOx is generated. Below 1850 K the solid and dotted lines start to converge again. This could be explained by the thermal NOx mechanism no-longer being the predominant

source of NOx at lower temperatures. There is no logic, however, for the solid and dotted lines crossing-over at the highest temperatures. Differently shaped curves that merged at the highest temperatures would be more credible. Since the correlation was based on data that only extended up to 2375 K, the solid line may be unrepresentative in this region, but it also seems likely that the gradients of the dotted lines should stop accelerating when equilibrium conditions are approached.

B.3.3 Problems with conflicting data

Unfortunately, when the correlation in Equation 34 was applied to engine cycles previously analysed in this study, it gave results that were not credible, with the second term predicting virtually 100% progress towards equilibrium in every case where a sensible NOx formation time was assumed. For example, the 85% SLS ISA condition for the NASA N+3 TRPS has modest temperatures (T_c = 1727 K), but in order to get the *tanh* term below 99%, NOx formation times of less than 0.1 ms had to be specified. This strongly suggested an error in the second term of the equation as published in [121] or in its assessed constants reproduced in Table 61, or in the specified units.

Figure 89 suggests that more credible results might be achieved if the units for pressure P_3 would have been specified as kPa, rather than Pa.

This possible revision has been investigated, but in other cases, where T_3 is lower, the revision implies that there would be negligible progress towards equilibrium in any credible NOx formation time. A more likely explanation for the anomalies is that the index of 3.96 applied to the T_3 term in Equation 34 is too high; resulting in unrealistic predictions of progress towards equilibrium when applied outside of a narrow band of T_3 values.

Given the uncertainty regarding the validity of both terms in Equation 34, some comparisons have been made with other sources of information regarding equilibrium levels of NOx and NOx formation rates.

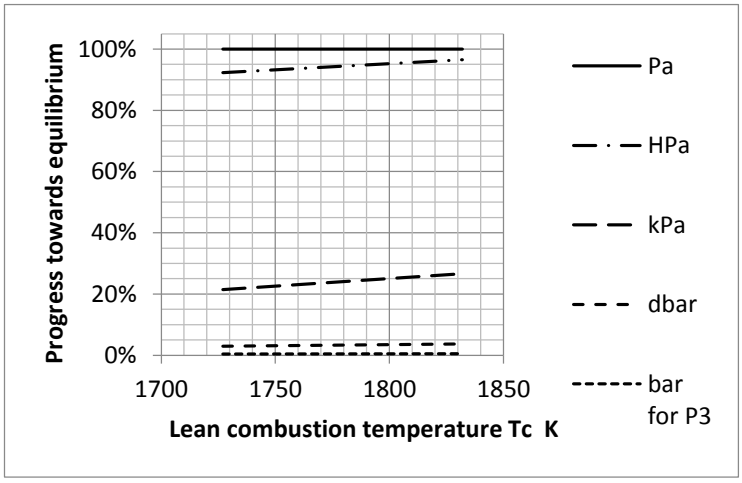

Figure 89 – Progress towards Equilibrium NOx (for NASA N+3 TRPS at SLS ISA, after 3 ms, according to Equation 34, but depending on the units assumed for P_3)

Figure 90 taken from [86] shows NOx formation rates and equilibrium levels, however it has no provenance, and must be treated with extreme caution.

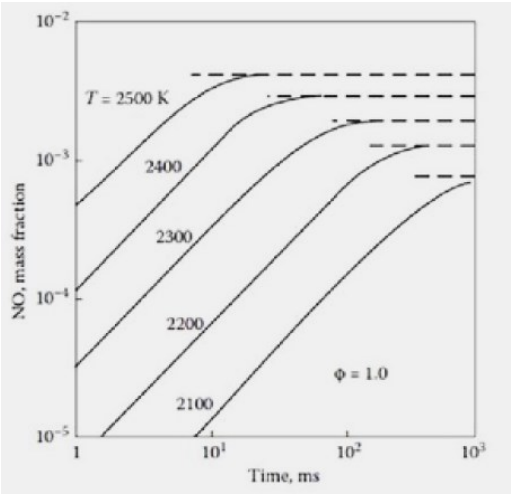

Figure 90 – NOx formation Rates at 10 bar, from Figure 9.6 in [86].

Figure 90 claims to be for an equivalence ratio of one, but the inlet air temperature for the 2200K line would need to be around 200K and that for the 2100K line would need to be colder still, so it appears that this last curve, at least, has been extrapolated. Most probably only a small region of this chart is reasonably accurate.

Since Figure 90 covers temperatures above 2100K, and relatively long formation times, it seems reasonable to assume that it applies to thermal NOx. It is seen that rate of NO formation increases by roughly an order of magnitude for a 160K increase in flame temperature at constant pressure. However, this does not mean that the rate of progress towards complete reaction increases at this rate, since the final concentration of NO also increases with temperature. The time taken to approach equilibrium only reduces by an order of magnitude for about a 250K increase in temperature.

These reaction rates seem slow, with only about 15% of the equilibrium NOx generated at around 2200K after 30 ms. At 1800K the reaction rates would be expected to be slower still. However, the thermal NOx formation rates would be relatively slow at an equivalence ratio of one, due to fewer oxygen atoms being available for the Zeldovich mechanism. The pressure of 10 bar is also relatively low for a gas turbine combustor at sea level and this will also tend to slow-down the reactions. It is also possible that Figure 90 was for the combustion of methane or propane rather than kerosene.

Equation 17 has a time-constant of 250 Hz or 4 ms. At first sight Figure 90 suggests that this reaction rate requires a NOx formation temperature of over 2500 K. However, for the reasons given above, a 4 ms time-constant might be achieved at a significantly lower temperature when the combustor inlet pressure and temperature are increased.

Nevertheless the strong temperature dependence of the NO formation rate in Figure 90 does confirm that time-constants should be a function of combustion temperature, pressure and equivalence ratio, at least for thermal NOx generation. In practice, the time-constant in Equation 17 was likely to have been a compromise, determined not only by typical thermal NOx formation rates, but also for the faster formation rates for prompt NOx, and possibly also N_2O-intermediated NOx.

The NOx formation times in LDI combustors are expected to be longer and the combustion temperatures lower than in RQL combustors. For example the

recent LDI combustor design study by Li et al. [153] found a residence time of 12 ms at design-point appropriate to meet altitude relight requirements. At design-point the NOx formation time should be similar to the residence time for lean combustion.

Taking it at face value, Figure 90 can provide data regarding the equilibrium levels of NOx, as well as reaction rates. In order to make a comparison with other predictions, it is necessary to convert the NO concentrations of Figure 90 to $EINO_x$ values. The first step is to factor-up the NO figures by 46/30 (the ratio of the molecular weights of NO_2 and NO). This conversion is necessary since NO is assayed as NO_2 in emissions testing and also when quoting NOx figures. The second step requires the FAR to be known at each temperature. It is stated that Figure 90 is plotted for an equivalence ratio of one, so the FAR is about 0.06789 for kerosene. Table 62 lists the data digitized from Figure 90 and converts the results to $EINO_x$ values.

Table 62 – Selected Data and $EINO_x$ Estimates obtained from Figure 90

T_c *K*	τ ms	**NO** (mass fraction)	**Equivalent NO_2** (mass fraction)	**FAR**	**$EINO_x$** g/kg
2500	∞	0.417%	0.639%	0.06789	94.1
2400	∞	0.290%	0.445%	0.06789	65.5
2300	∞	0.194%	0.297%	0.06789	43.7
2200	∞	0.130%	0.199%	0.06789	29.3
2100	∞	0.081%	0.124%	0.06789	18.3

These equilibrium $EINO_x$ values for stoichiometric combustion are indeed lower at a combustion temperature T_c than those obtained from lean pre-mixed pre-vaporised combustion systems, but they are actually higher than the equilibrium values obtained from Equation 34 and plotted in Figure 88 and Figure 91. Figure 91 compares the predicted equilibrium NOx concentrations obtained from Equation 17, Equation 34 and Figure 90 (Table 62). The equilibrium concentration term in Equation 17 includes a strong pressure dependency, so it

is plotted for both 10 bar and 40 bar. The trends observed with Equation 17 match the trend obtained with the data from Figure 90, but the NOx predictions of Equation 17 at 10 bar are only about half of those shown in Figure 90.

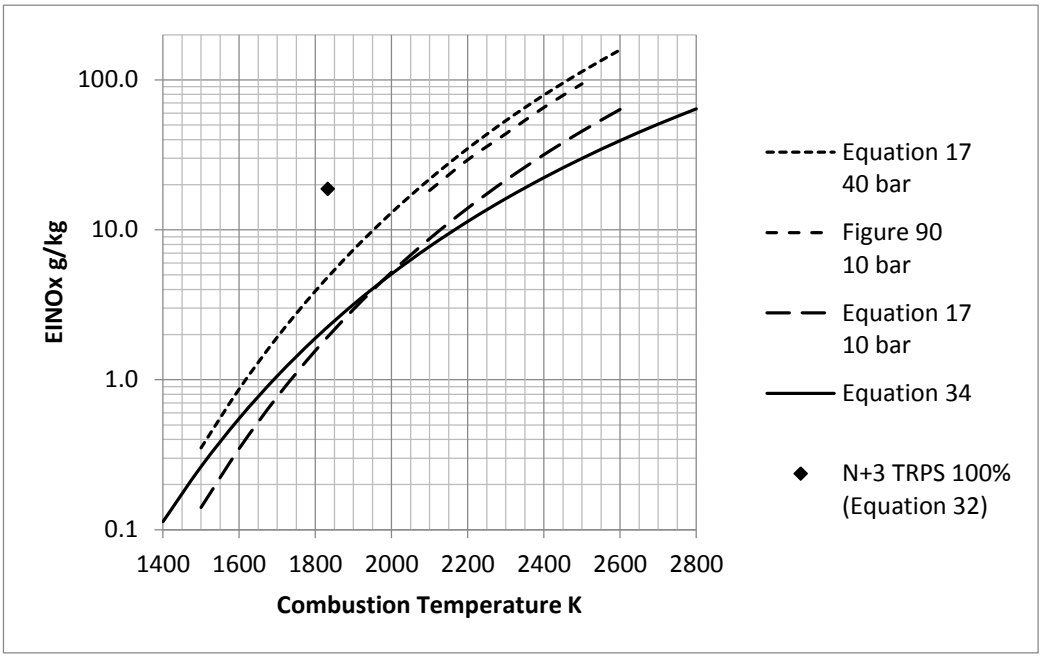

Figure 91 – Comparison of Equations for Equilibrium $EINO_x$ Predictions

In Figure 91 the Equation 34 line and the 10 bar line from Equation 17 intersect at around 2000K. A significant difference between these two equations is that Equation 17 accounts for the pressure dependency in the equilibrium term, while Equation 34 accounts for it in the formation-time-dependent term. Arguably the pressure dependency should apply to both terms, but in the author's opinion it should have a bigger impact on the NOx formation rate. This might also help to explain why different researchers have derived such widely-different indexes to be applied to P_3.

Figure 91 also includes an extra point corresponding to the NASA N+3 TRPS 100% SLS ISA take-off case, previously assessed in section B.2.2 using Equation 32 derived from the latest NASA testing on the triple-cup LDI combustor injector array. The engine operates at 38 bar, but its NOx emissions are predicted well above all of the 'equilibrium NOx' curves. Furthermore it

seems unlikely the NOx formation time in the TRPS LDI combustor would be long enough to closely approach equilibrium.

These higher $EINO_x$ figures might be explained by the lower equivalence ratio having increased the equilibrium NOx concentration, or by the temperature T_{ad} derived from the FAR_{ad} in applying Equation 32 not being representative of local-peak flame-front temperatures. It seems very likely that inhomogeneity in the local equivalence ratios in the LDI combustor (in comparison to those in a well-premixed prevaporized system) would contribute to higher emissions. While generally providing an improvement over RQL designs, it seems unrealistic to expect a LDI combustor to match the very low NOx of a pre-mixed pre-vaporised system at the same average NOx formation temperature.

Regarding Equation 17, the rate should be roughly proportional to pressure, since this reduces the free-path length and the time between molecular collisions. Pressure and temperature effects were not taken into account by Odgers and Kretschmer when validating their original 250 Hz time-constant. Their 59 collated experimental data points covered the range of inlet temperatures from 600 to 1000 K, flame temperatures from 1825 to 2375 K, pressures from 5 to 20 atmospheres and residence times of 1 to 3 ms [121]. Typical conditions may therefore be taken to be: P_3 = 1000 kPa, T_3 = 800K, T_c = 2100 K and FAR_c = 0.0196. The 250 Hz time-constant '*B*' was noted by Odgers and Kretschmer to be most accurate at the mid-temperature condition.

To attempt to 'correct' *B* for other conditions, Equation 35 is proposed (P_3 in kPa, T_c in K, *B* in Hz). It assumes the rate of progress towards equilibrium is proportional to pressure and has the same sensitivity to temperature as displayed in Figure 90.

$$B = 0.25.P_3.10^{T_c/250}/10^{8.4} \qquad \text{Equation 35}$$

For P_3 = 1000 kPa and T_c = 2100 K, *B* = 250 Hz, as originally proposed in Equation 17, and Figure 83 showed that for 0.8 ms residence time, 18.13% of

the equilibrium NOx should be generated. However, for the LDI combustor the NOx formation times are much longer when the main injectors are all lit.

In Figure 92 the time-constant for different NO_x formation correlations, and from Figure 90, are plotted against the combustion temperature. It corresponds to the time it would take to reach equilibrium if the initial formation rate were to be held constant. As the differences are large, it is necessary to plot the results on a log scale.

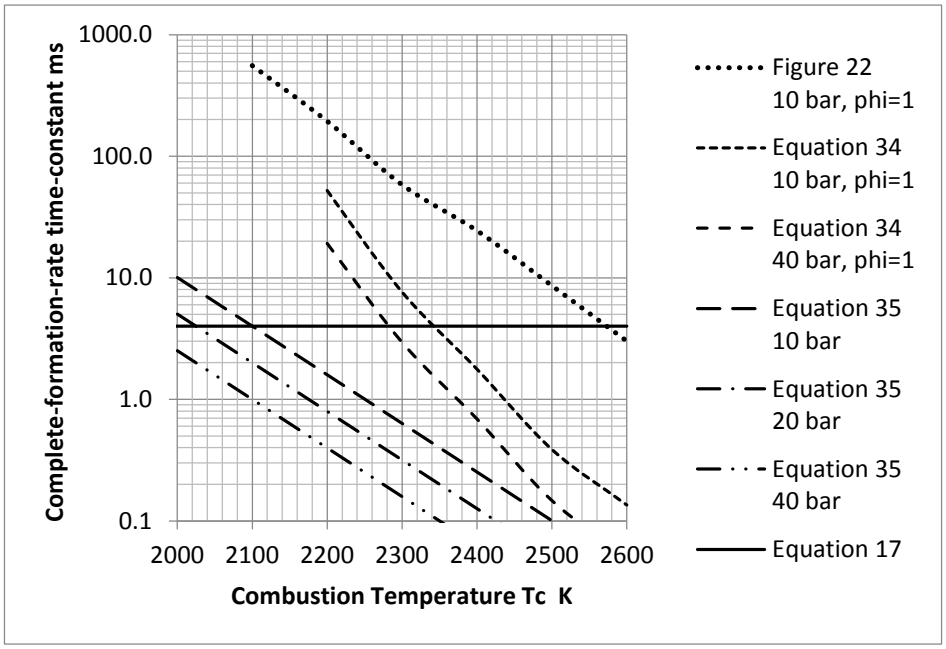

Figure 92 – Comparison of Initial Rates of Progress to Equilibrium NOx

v. Temperature T_c

It is clear that there are *very* large differences in the time-constants obtained from these different equations and from Figure 22. Part of the difference could be accounted for by different equivalence ratios. Equation 34 features T_3 and Φ in the progress term, which would tend to reduce the rate of increase in its time-constant plotted in Figure 92 as T_c reduces, bringing the gradients for the Equation 34 curves more into line with the others, but that still leaves big discrepancies with up to two orders of magnitude difference in time-constants between Equation 34 and Figure 22 on the one hand, and Equation 35 on the other.

Where $\Phi = 1$, as in Figure 90, the inlet temperature T_3 reduces rapidly as T_c reduces, but in most situations in a real engine, T_3 would vary more closely to pro rata with T_c, and in lean combustors Φ would also reduce. Because pressure and dissociation effects on temperature-rise are significant at very high temperatures, the method of [157] has been used to calculate the T_3 figures to go with T_c, in cases where an equivalence ratio of one has been specified.

B.3.4 Possible modifications to formation-rate correlations

As previously noted, NOx formation times and overall residence times in a combustor do not remain constant off-design. The overall residence time reduces at high temperature conditions since the velocity of the gas is proportional to the speed of sound, which is proportional to the square root of a representative temperature. If the total residence time is specified for the reference design-point temperature, this could be factored by $\sqrt{(T_{3,ref}/T_3)}$, for example, for other conditions, but the actual NOx formation time may not scale in the same way, on account of changes to fuel atomisation and the associated time delay before combustion starts. However, for simplicity, the NOx formation time τ may, to a first approximation, be considered a constant for the advanced LDI combustor designs at all conditions.

Substituting the Equation 35 for the time-constant B into Equation 17 gives Equation 36 (with P_3 in kPa, T_c in K, τ in s).

$$\boldsymbol{EINO_x = 29e^{(-21670/T_c)}.(1000.P_3)^{0.66}.(1 - e^{-(0.25.P_3.\tau(10^{T_c/250}/10^{8.4})})}$$

Equation 36

Equation 36 generates some interesting results. For P_3 = 1000 kPa and T_c = 2100 K, then B = 250 Hz, as originally proposed, and Figure 22 showed that for 0.8 ms residence time, 18.13% of the equilibrium NOx should be generated. For T = 1900 K only 2% is generated, but if P_3 increases to 60 bar, 70% is

generated. At 2300 K almost 100% of the equilibrium NOx is produced. While the increases in reaction rates seem credible, the author had not thought that NOx levels so close to equilibrium would be achieved at these pressures and temperatures.

It seems that the first pressure term in Equation 36 may be too strong now that pressure is also included in the last term in the expression for the time-constant. Where slow rates of reaction are limiting NOx production, the effect pressure has on speeding-up reaction rates will predominate, whereas when NOx levels are approaching equilibrium they will be less sensitive to pressure. Since NO has the same number of atoms as N_2 or O_2, it might be expected that its concentration would be largely insensitive to pressure. However the level of NO *is* sensitive to the equivalence ratio (and hence to the FAR) as illustrated in Figure 85.

As noted in section 3.8.6, NOx formation times and overall residence times in a combustor are not constant. The overall residence time reduces at high temperature conditions since the velocity of the gas is proportional to the speed of sound, which is proportional to the square root of a representative temperature. If the total residence time is specified for the reference design-point temperature, this could be factored by $\sqrt{(T_{3,ref}/T_3)}$, for example, for other conditions, but the actual NOx formation time may not scale in the same way. This is on account of changes to fuel atomisation and the associated time-delay before combustion really starts. For simplicity however, the NOx formation time τ may be considered to be constant for all advanced LDI combustor designs at all conditions.

For Equation 34, Odgers and Kretschmer stated that τ should be interpreted as a total residence time for the combustor, rather than a NOx formation time. The latter is shorter, because it takes some time for the liquid fuel to vaporise and for the combustion process to reach its final temperature. This is part of their justification for raising T_3 to the high power of 3.96 in the second term of the equation, since a low T_3 will delay vaporisation of the fuel. However, it seems

hard to justify giving such high prominence to T_3 in this equation, since doubling T_3 from 450K to 900K, for example, will increase its effect over fifteenfold, whereas dropping the equivalence ratio from 0.85 to 0.55, to give much the same T_c, only reduces the rate by 27%. It would seem better to specify T_c or T_4 directly in the second term, together with the equivalence ratio. Any two of T_3, Φ_c and T_c will enable the third to be calculated at modest temperatures where little dissociation occurs. Also Φ_c can be obtained from Φ_4 by Equation 37, where q is the proportion of combustor inlet air used for wall-cooling.

$$\Phi_c = \Phi_4/(1-q) \qquad \text{Equation 37}$$

The further addition of P_3 will enable the third parameter to be calculated at the highest temperatures. However, it seems desirable to retain Φ_c, as one of the parameters, since there are potentially two solutions if only T_3 and T_c are specified. Strictly therefore, it should only be necessary to input *three* parameters to the correlation, though using four may result in a simpler expression.

The wide range of NOx formation rates predicted by these different methods makes it difficult to select one for the LDI combustor. Not only are the equilibrium NOx emissions under-predicted for typical LDI combustors, but the above methods, apart from Equation 17, would also seem to predict that only a very small proportion of the equilibrium NOx would be generated in any credible formation time at combustion temperatures below 2500K. It is clearly correct that the thermal NOx formation rate should decrease as combustion temperatures reduce, but in any LDI combustor it seems that a proportion of the NOx formation must be assumed to occur at higher than the average temperatures post-combustion. However, those higher temperatures can only apply locally and for less than the average formation time. This presents difficulties in attempting to model NOx generation in terms of the proportion of the equilibrium level produced in a given formation time. If a single combustion temperature T_c is to be used then it seems this must be increased relative to the temperature corresponding to the average FAR, but the amount by which it

should be increased is not obvious. It is also not obvious how the equilibrium level of NOx varies with equivalence ratio. Figures quoted allegedly for the equivalence ratio 1.0 could be very misleading for lean combustion conditions.

The predicted reaction rates are still very slow in comparison with those in Figure 89, whether the pressure in Equation 34 is specified in Pa or in kPa. It is suggested therefore that the (1-tanh(Φ)) function would offer a potential improvement to the last term of Equation 36.

B.3.5 A strategy for staged combustion

At high power conditions, all the injector nozzles in the LDI combustor are fuelled and the fuel distribution aims to achieve uniform conditions across the combustor from the initial combustion to upstream of the addition of wall cooling air etc. Thus the average temperature in most of the combustor is relatively easily calculated from the average *FAR* and T_3. This is in contrast to the conditions at 30% and 7% of static thrust, which are dependent on the detail design and fuel scheduling adopted for a future combustor, which are harder to predict with any certainty.

Assuming rapid evaporation and mixing of the fuel at the high-power conditions, most of the combustion should be occurring at close to the computed combustion temperature, which should persist for a relatively long period in the absence of dilution air. A minimum residence time would be 3–4 ms, though in her study Li estimated that 12 ms was needed to meet some altitude relight requirements [153]. These times are in contrast to the 0.8 ms quoted for residence in the rich zone of a RQL combustor, where dilution starts much sooner.

The following scenario is suggested for idealized year-2050 LDI combustors:

- At high power conditions, all injectors are fuelled and run with similar FAR_c, Φ_c, and T_c.
- As power is reduced, all injectors remain fuelled until a critical T_c is reached

- As power is further reduced, fuel is sequentially switched-off for the multiple 'main' injectors so that T_c for the remaining operating fuel injectors is held nearly constant
- At just above the SLS ISA day 7% idle thrust rating, only the pilot injectors remain fuelled
- Below the point where only the pilot injectors are fuelled, T_c in the pilot zone is allowed to reduce below the previous minimum level

Note that since T_3 reduces as the power reduces, the FAR_c and Φ_c of the remaining fuelled injectors will slightly increase. This should help to ensure a good margin against lean extinction. This scenario is a simplification of the probable fuel-staging strategy, but it has the merit that at any condition, only one value FAR_c, T_c or Φ_c needs to be considered. Assuming 100% combustion efficiency, the values of FAR_c and Φ_c can be determined if P_3, T_3 and T_4 or Φ_4 are known, using relatively simple calculations.

Under this scenario, prompt NOx is generated during the combustion process, but when combustion is substantially complete, thermal NOx continues to be produced. The amount of thermal NOx generated depends on the equilibrium level of NOx, which is primarily a function of T_c, Φ_c, and humidity h, and then also on the rate of NOx formation, which is a function of T_c, Φ_c, P_3 and h, and on the formation time τ, which is a function of the design residence time τ_{design}, T_4, $T_{4,design}$ and also T_3. The last term should logically include T_3 because low T_3 will delay fuel vaporization, but this time-delay is likely to be quite small for high values of T_3, and prompt NOx will be more significant at low values of T_3, so to a first approximation the T_3 effects might be ignored.

Since prompt NOx will be more significant than thermal NOx at low temperatures, an additional term must be included in the correlation to account for this. For simplicity, it may be assumed that this contribution is independent of pressure and temperature. However, for RQL combustors, Kyprianidis et al. [123] concluded that a similar constant (*a* in Equation 19 and Table 18) should

be factored by the combustor pressure and temperature rise terms (as well as the humidity correction).

B.3.6 A possible $EINO_x$ correlation for the LDI combustor

Given the above arguments, the new correlation should take the form of Equation 38:

$$EINO_x = \left(a + f_1(T_c, \Phi_c).f_2\left(\tau, \Phi_c, T_c, P_{3,}\right)\right).f_3(h) \qquad \text{Equation 38}$$

The correct forms of the three functions (f_1, f_2 and f_3) now need to be determined. There is general consensus that the function f_3 of the humidity h or $\boldsymbol{\omega}$ should be e^H where H is the humidity correction factor calculated according to Equation 12 or Equation 13, but even the humidity function presents some difficulties when making and presenting $EINO_x$ assessments. Its application is further discussed in sections and B.4.2 and B.6. The equations for the other functions are more speculative.

Figure 91 compared different equations for equilibrium NOx. Equation 34 only considered the combustion temperature, whereas Equation 17 identifies a significant sensitivity to pressure. While high pressure might be expected to favour the formation of NO_2 and N_2O, NO is the main product at high temperatures, and it is not obvious that increased pressure will favour its formation. Low levels of oxygen should however be expected to limit the equilibrium level of NO. Thus, Equation 39 is suggested, based on Equation 17, where k is a constant and T_c is in K.

$$f_1 = \ k.e^{\left(-\frac{21670}{Tc}\right)}.(1-\tanh(\Phi_c))/(1-\tanh(1)) \qquad \text{Equation 39}$$

Taking function f_1 to match the $EINO_x$ from Equation 17 when T_c = 2700K, P_3 = 40 bar, Φ_c = 1, τ = ∞, and $EINO_x$ = 167.9, then Equation 37 can be rewritten as Equation 40.

$$f_1 = \ 2154540.e^{\left(-\frac{21670}{Tc}\right)}.(1-\tanh(\Phi_c)) \qquad \text{Equation 40}$$

Equation 41 is proposed for function f_2 based on the reaction rates derived from Figure 22, where k is a constant, T_c is in K, P_3 is in kPa and τ is in s.

$$f_2 = \tanh(k.\tau.(1-\tanh(\Phi_c)).(\frac{T_c}{2600})^{24.29}.(\frac{P_3}{1000})^{0.9} \qquad \text{Equation 41}$$

Taking the function f_2 to match the rate derived from Figure 22 when T_c = 2600 K, P_3 = 1000 kPa, and Φ_c = 1, then k is 1310. Finally it is necessary to define a in Equation 36. Based on the emissions figures quoted for various different engines at idle, a is taken to be 2.0. There seems no reason why LDI combustors should have worse idle emissions than existing engines. The complete expression for $EINO_x$ is therefore given by Equation 42.

$$EINO_x = \left(2.0 + \left(2154540.e^{(-\frac{21670}{T_C})}.(1-\tanh(\Phi_c))\right).\left(\tanh(1310.\tau.(1-\tanh(\Phi_c)).(\frac{T_c}{2600})^{24.29}.(\frac{P_3}{1000})^{0.9})\right)\right).H$$

Equation 42

These equations might still be underestimating the effect of equivalence ratio on the equilibrium value of $EINO_x$, particularly where it exceeds unity. One option would be to substitute Φ_c^n for Φ_c in Equation 37, so that n would determine the sensitivity to Φ. Figure 93 shows the effect of varying the index n in the term $(1-\tanh(\Phi_c^n))$.

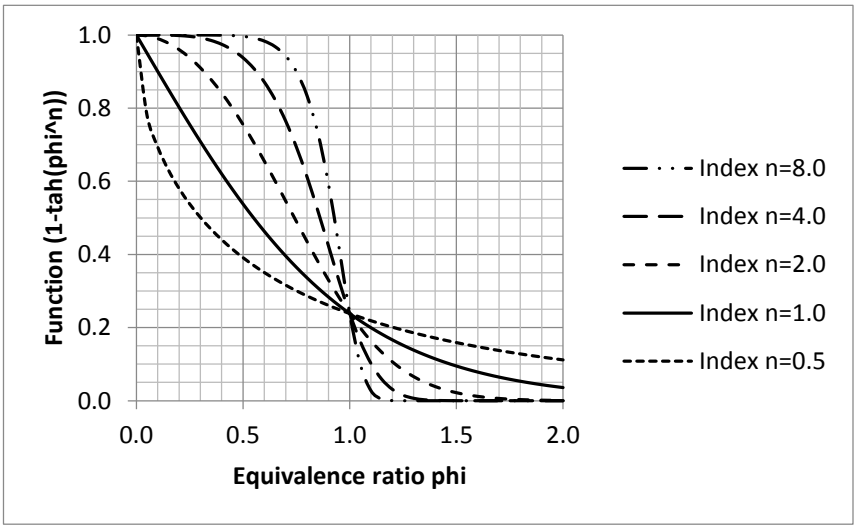

Figure 93 – The Effect of raising Φ to the Power n for Equation 37 and Equation 40

For simplicity, however, it is proposed to keep the value of *n* as one. This seems consistent with the residual oxygen concentration being the significant factor affecting equilibrium NOx levels in lean mixtures. Conversely, higher values of *n* might be more appropriate where CO and UHC are competing for the available oxygen at equivalence ratios greater than one.

To illustrate the results that can be obtained from Equation 42, Figure 94 plots typical $EINO_x$ predictions vs combustion temperature for different thermal NO_x formation times from 1 to 125 ms. The estimates assume P_3 is a constant 3810 kPa, and that Φ_c increases linearly from 0.442 at Tc = 1833K, to 0.842 at Tc = 2633K.

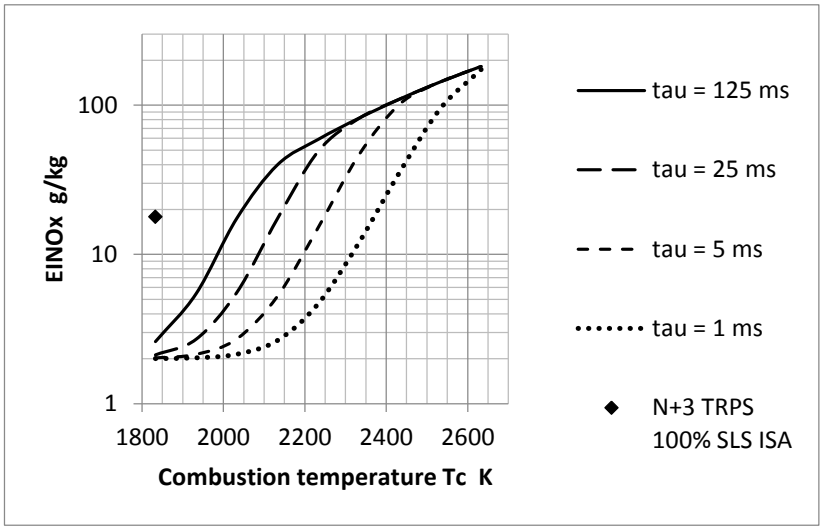

Figure 94 – EINOx Estimates from Equation 42
compared with the NASA estimate for the N+3 TRPS.

For reference, the SLS ISA $EINO_x$ estimate by Tacina et al. for the NASA N+3 TRPS is also shown. It is clear that Equation 42 cannot come close to matching the NASA assessment of its LDI combustor's NOx emissions. There would seem to be several possible explanations:

- Thermal NOx formation rates are underestimated for lean mixtures at moderate temperatures
- Equilibrium NOx levels are underestimated for lean mixtures at moderate temperatures

- Formation routes other than thermal NOx are more significant than assumed in Equation 42
- The average combustion temperatures and formation times are unrepresentative of the real conditions under which NOx forms in LDI combustors
- Existing LDI combustor designs, such as those tested at NASA, have so far failed to demonstrate the full potential of the technology for reducing NOx emissions.

Quite probably the first four explanations are all contributing to the underestimation of typical LDI combustor NOx emissions, but it seems most likely that the major factors are underestimation of the effective combustion temperatures and underestimation of the NOx formation rates in lean mixtures.

Consideration was given to amending Equation 42 to try to account for the above factors, but, with little data available to substantiate such changes, it was concluded that this approach cannot be defended. It was therefore strongly recommended that the more traditionally-formulated NASA correlations and particularly Equation 21 should be used in the ULTIMATE project studies.

Nevertheless this study has shed light on a range of factors that influence NOx formation and it may help to show the way towards the formulation of more-physics-based correlations in future research.

B.4 Applying the Emissions Correlations

B.4.1 Estimating combustion temperatures

For many of the foregoing correlations, temperatures need to be estimated in one or more combustor zones. Where some NASA reports refer to 'adiabatic combustion temperatures' T_{ad}, these are interpreted in the same way as 'combustion temperatures' T_c in other reports, and both are calculated based on T_3 and the *FAR* or Φ of the zone in question. They are theoretical adiabatic temperatures because they are calculated assuming 100% combustion efficiency and neglecting radiant heat loss etc. They are not quite the same as

'stoichiometric flame temperatures' T_{st} used in Equation 16 and Equation 18, though $T_{pz,}$ the primary zone temperature, used in Equation 16, is interpreted in the same way as $T_{ad,}$ $T_{ad,l}$ and T_c. The calculated temperatures are all assumed to be computed for dry air.

The first step is to calculate the FAR_c *or* FAR_{ad} for the zone in question, using Equation 43 for example, where FAR_4 is the FAR at combustor exit and *q* is the proportion of wall-cooling air for the combustor. T_{ad} is obtained in the same manner as in section B.2.2. Thus the only user inputs needed for the correlation are P_3, T_3, FAR_4 and *q*. For year-2050 combustor designs using CMC materials *q* may typically be taken to be 10%.

$$FAR_{ad} = FAR_4/(1-q) \qquad \text{Equation 43}$$

For typical lean combustor conditions encountered on an ISA day, the pressure corrections to the temperature rise are taken to be negligible (though this may not be true for hot-day take-off or for 'type-test' conditions). Thus the formulas 'F3.37-F3.40' of Walsh and Fletcher [99], can be used to calculate T_4 or T_{ad} from FAR_4 or FAR_{ad}, but using these equations directly requires some iteration. The results are claimed to be accurate to within 0.25% for kerosene with LHV 43124 kJ/kg, but above 0.07 FAR or 2100 K they are likely to be significantly less accurate: in part on account of the pressure-related dissociation effects. To avoid the need for iteration and to simplify the calculation while retaining acceptable accuracy in the range of interest, a second-order polynomial curve fit to the Walsh and Fletcher correlations may be used. This is provided by Equation 44, where the three coefficients *a*, *b* and *c* are given by Equation 45, Equation 46 and Equation 47 respectively

$$T_c - T_3 = a.FAR^2 + b.FAR + c \qquad \text{Equation 44}$$

$$a = 0.003178.T_3^2 - 6.922.T_3 - 187410 \qquad \text{Equation 45}$$

$$b = -0.0002741.T_3^2 - 7.063.T_3 + 43598 \qquad \text{Equation 46}$$

$$c = 0.000004618.T_3^2 - 0.006734.T_3 + 7.1$$ Equation 47

The method can be applied at any realistic combustion temperature T_c and at any *FAR* up to about 0.07. For higher FAR, another method should be used. (The temperatures predicted by these equations typically deviate by less than 0.3 K from those derived iteratively from the Walsh and Fletcher equations.)

B.4.2 Applying humidity corrections to $EINO_x$

Humidity corrections should, with few exceptions, be applied to all NOx emissions calculations using the factor e^H where H is defined by Equation 12 as described on Figure 20 in section 3.8.2. However, it has also been noted that humidity corrections have often been ignored by previous researchers.

The corrections are necessary, in large part, because engine performance is commonly modelled assuming dry air, which tends to overestimate the highest engine gas temperatures (at a thrust) when compared with more accurate performance calculations taking humidity into account. Near the ground there is usually a significant amount of water vapour in the air and Equation 12 is formulated assuming a reference level of 60% relative humidity on an ISA day at sea level; equivalent to an absolute specific humidity of about 0.64%.

In practice the specific humidity reduces rapidly with increasing altitude, so for on-route emissions assessments it is generally reasonable to assume that the air above 30,000 ft will effectively be dry and a factor of 1.125 can be applied as indicated on Figure 20. The LTO cycle only extends up to 3000 ft, however, so the humidity correction that should be applied on an ISA day would typically only increases the estimate by 1% and so may be considered negligible for 60% relative humidity.

For hot-day or cold-day take-offs however, the levels of humidity assumed can make quite large differences to the predicted NOx emissions.

B.5 Combustion efficiency, CO and UHC

Combustion efficiency generally improves with increasing pressure and temperature, but at the highest temperatures approaching stoichiometric combustion (in a pilot zone for example) the levels of CO increase, partly due to dissociation effects, but also with the increasing FAR as shown schematically in Figure 85.

As the gasses exiting the combustor expand and cool through the turbines, the CO will continue to oxidise to CO_2, so the final combustion efficiency will tend to be higher than that achieved in the combustor itself and may be higher than that measured in some combustor testing. This effect was noted at NASA Glenn by Tacina et al. in [155]. These researchers therefore generated 'corrected CO emissions' by subtracting the equilibrium CO from the measured CO in order to estimate the combustion efficiencies associated with their rig test measurements. However, it is not obvious that this correction is fully justified, or that any other research groups follow the same practice.

In their reported flame-tube testing on a third-generation swirl-venturi LDI burner array, the UHC emissions were not measured. However, based on experience, Tacina et al. estimated the UHC emissions index would be less than 20% of the CO emissions index, and most probably less than 10% of the CO emissions index.

B.6 Uncertainty in Emissions Predictions

It is fairly obvious from all the foregoing discussions that emissions prediction for future combustor designs is not yet an exact science. Even for a fixed combustor design, it is well known that there will be measurement errors and actual variations from test to test, and from engine to engine, and this is reflected in the ICAO emissions assessments that require a margin between average measurements and characteristic levels declared on the basis of limited testing. Significant error bars should be, and commonly are, attached to

test results. Predicting the emissions performance of combustors thirty years into the future is even more uncertain.

Very few test facilities have the capability to make tests at the full inlet pressures and temperatures achieved in high OPR engines at take-off. The ASCR at NASA Glenn is one such facility, with the capability to run at up to 60 bar [92], but the more recently reported flame-tube tests from NASA Glenn have been restricted to 19 bar operation, so the results have needed to be extrapolated to higher pressures, introducing more uncertainty [155].

Furthermore, for NOx emissions, the uncertainty in how to correct for humidity, or even whether to correct for humidity, and even how to correctly calculate specific humidity, have compounded the uncertainty. The NASA Glenn papers do not report the ambient temperature and humidity during tests, or state whether the incoming air has been dried. Most probably the ambient relative humidity would have been about 60%, so that the NOx emissions correlations should be representative for LTO cycle assessments, but they should have a humidity correction applied for the altitude cases. Tacina et al. do estimate altitude NOx emissions in [155], but they still make no mention of humidity corrections. It seems possible that some of the day-to-day variation observed in their NOx measurements could be due to varying ambient humidity.

Additional test-result variability might also be attributed to variable fuel composition.

Some indication of the likely uncertainties is provided by comparing the predictions obtained by different methods. Results obtained from various methods have been compared and discussed in previous sections.

B.7 Conclusions regarding emissions assessment methods

The conclusions from this study are provided in section 10.2.3.

Emissions assessments are given in section 8.6.

Appendix C EXAMPLE ENGINE PERFORMANCE SPREADSHEET

As examples: Figure 95 shows typical output data for the initial year-2050 reference turbofan and Figure 96 shows how data are input and iteration is managed in the spreadsheet.

Design Point Station Data (static stations in blue):

Station data	FAR	W	T	P	WrtT/P	H	H*W	Cp	γ	FT	PR re.	dS	dS total	Mn	Q	A (functional)	
Blue figures are static cases		lb/s	K	psi		CHU/lb	CHU	CHU/lb.K		CHU/lb.K	5.380	CHU/lb.K	CHU/K		imperial	in^2	
Ambient static		1555.58	228.8080	3.458	6804.59	155.54	241963.1	0.239325	1.4015	-0.34341	0.643	0.00000	0.000	-	-	-	
Intake inlet		1555.58	259.6863	5.380	4659.61	162.94	253460.5	0.239421	1.4013	-0.31311	1.000	0.00000	0.000	-	-	-	
Core inlet		72.60	259.69	5.364	218.14	162.94	11829.9	0.239421	1.4013	-0.31311	0.997	0.00021	0.015	-	-	-	
LPC exit		72.60	365.84	15.984	86.88	188.42	13680.0	0.240990	1.3976	-0.23086	2.971	0.00760	0.551	-	-	-	
IC inlet		72.60	365.84	15.984	86.88	188.42	13680.0	0.240990	1.3976	-0.23086	2.971	0.00760	0.551	-	-	-	
IC exit = HPC inlet		72.60	365.84	15.557	89.27	188.42	13680.0	0.240990	1.3976	-0.23086	2.892	0.00945	0.686	-	-	-	
HPC exit static *		71.12	982.37	386.723	5.57	345.93	24601.3	0.271750	1.3374	-	71.884	-	-	0.24350	0.1574	35.37	
HPC exit		66.76	992.18	402.276	5.23	348.60	23272.3	0.272203	1.3367	0.02162	74.775	0.03893	2.599	-	-	-	
HX inlet		66.76	992.18	402.276	5.23	348.60	23272.3	0.272203	1.3367	0.02162	74.775	0.03893	2.599	-	-	-	
HX exit		66.76	992.18	402.276	5.23	348.60	23272.3	0.272203	1.3367	0.02162	74.775	0.03893	2.599		-	-	
Combustor 1 in		66.76	992.18	402.276	5.23	348.60	23272.3	0.272203	1.3367	0.02162	74.775	0.03893	2.599	-	-	-	
Combustor 1 exit	0.03094	68.83	1890.00	390.208	7.67	650.29	44756.6	0.315439	1.2777	0.24853	72.532	0.26792	18.440	-	-	-	
HPT 1 NGV throat	0.03094	68.83	1890.00	390.208	7.67	650.29	44756.6	0.315439	1.2777	0.24853	72.532	0.26792	18.440	-	-	-	SOT
HPT 1 NGV throat	0.03094	68.83	1659.56	214.532	7.67	569.41	39189.8	0.310364	1.2835	-	39.877	-	-	1.00000	0.3845	19.94	
HPT 1 in	0.03094	68.83	1890.00	390.208	7.67	650.29	44756.6	0.315439	1.2777	0.24853	72.532	0.26792	18.440	-	-	-	RIT
HPT 1 exit	0.03094	68.83	1397.22	72.334	35.57	481.98	33172.1	0.302939	1.2925	0.15506	13.445	0.29001	19.960	-	-	-	
Combustor 2 in	0.02904	73.18	1371.57	72.334	37.47	472.55	34582.2	0.301120	1.2948	0.14723	13.445	0.28217	20.650	-	-	-	
Combustor 2 exit	0.02904	73.18	1371.57	72.334	37.47	472.55	34582.2	0.301120	1.2948	0.14723	13.445	0.28217	20.650	-	-	-	
HPT 2 in	0.02904	73.18	1371.57	72.334	37.47	472.55	34582.2	0.301120	1.2948	0.14723	13.445	0.28217	20.650	-	-	-	
HPT2 NGV throat	0.02904	73.18	1195.37	39.543	37.47	417.22	30532.8	0.294543	1.3034	-	7.350	-	-	1.00000	0.3865	96.93	
HPT 2 exit	0.02904	73.18	1371.57	72.334	37.47	472.55	34582.2	0.301120	1.2948	0.14723	13.445	0.28217	20.650	-	-	-	
LPT 1 in	0.02875	73.91	1365.77	72.334	37.76	470.52	34775.3	0.300776	1.2952	0.14561	13.445	0.28055	20.735	-	-	-	
LPT1 NGV throat	0.02875	73.91	1190.09	39.537	37.76	415.47	30706.6	0.294185	1.3039	-	7.349	-	-	1.00000	0.3866	97.67	
Spare																	
LPT 1 exit	0.02875	73.91	797.58	5.535	377.08	300.76	22228.5	0.273435	1.3346	-0.00896	1.029	0.30220	22.335	-	-	-	
HX inlet	0.02875	73.91	797.58	5.535	377.08	300.76	22228.5	0.273435	1.3346	-0.00896	1.029	0.30220	22.335	-	-	-	
HX exit	0.02875	73.91	797.58	5.535	377.08	300.76	22228.5	0.273435	1.3346	-0.00896	1.029	0.30220	22.335	-	-	-	
LPT2 in	0.02875	73.91	797.58	5.5354	377.08	300.76	22228.5	0.273435	1.33465	-0.00896	1.029	0.30220	22.335	-	-	-	
LPT2 NGV throat	0.02875	73.91	776.78	4.982	377.08	295.03	21805.0	0.272107	1.33683	-	0.926	-	-	0.40000	0.2439	1545.80	
LPT2 exit	0.02875	73.91	797.58	5.535	377.08	300.76	22228.5	0.273435	1.33465	-0.00896	1.029	0.30220	22.335	-	-	-	
LPT OGV exit	0.02845	74.67	793.58	5.502	382.30	299.61	22372.2	0.273067	1.3352	-0.01062	1.023	0.30095	22.472	-	-	-	
Core noz choked	0.02845	74.67	675.88	2.903	382.30	267.72	-	0.265410	1.3483	-	0.540	-	-	1.00000	0.3911	977.54	
Core exit static	0.02845	74.67	705.98	3.458	382.30	275.77	20591.4	0.267388	1.3448	-0.04222	0.643	0.30119	22.490	0.85863	0.3837	996.34	
Fan bypass inlet		1482.98	259.69	5.364	4455.50	162.94	241630.6	0.239421	1.4013	-0.31311	0.997	0.00021	0.305	-	-	-	
Fan tip exit		1482.98	289.64	7.647	3300.32	170.11	252271.2	0.239657	1.4007	-0.28696	1.421	0.00204	3.020	-	-	-	
Bypass inlet		1481.67	289.64	7.647	3297.41	170.11	252048.9	0.239657	1.4007	-0.28696	1.421	0.00204	3.017	-	-	-	
Bypass exit		1481.67	289.64	7.571	3330.72	170.11	252048.9	0.239657	1.4007	-0.28696	1.407	0.00273	4.038	-	-	-	
Bypass noz choked		1481.67	241.22	3.994	3330.72	158.52	-	0.239348	1.4014	-	0.742	-	-	1.00000	0.3964	8401.38	
Bypass exit static		1481.67	231.43	3.458	3330.72	156.17	231396.1	0.239328	1.4015	-0.34069	0.643	0.00273	4.040	1.11977	0.3920	8495.90	
IC cooling inlet		0.00	289.64	7.647	0.00	170.11	0.0	0.239657	1.4007	-0.28696	1.421	0.00204	0.000	-	-	-	
IC cooling exit		0.00	289.64	7.647	0.00	170.11	0.0	0.239657	1.4007	-0.28696	1.421	0.00204	0.000	-	-	-	
IC Cool noz choke		0.00	241.22	4.035	0.00	158.52	-	0.239348	1.4014	-	0.750	-	-	1.00000	0.3964	0.00	
IC Cool exit static		0.00	230.76	3.458	0.00	156.01	0.0	0.239328	1.4015	-0.34137	0.643	0.00204	0.000	1.12777	0.3915	0.00	
CCACA port inlet		1.31	289.64	7.647	2.91	170.11	222.3	0.239657	1.4007	-0.28696	1.421	0.00204	0.003	-	-	-	
CCACA port exit		1.31	627.58	7.265	4.51	252.82	330.4	0.252488	1.3728	-0.09836	1.350	0.19416	0.254	-	-	-	
CCACA noz choke		1.31	526.49	3.805	7.88	227.57	-	0.247100	1.3840	-	0.707	-	-	1.00000	0.3947	19.97	
CCACA exit static		1.31	511.71	3.458	8.55	223.92	292.6	0.246386	1.3856	-0.14923	0.643	0.19418	0.254	1.09281	0.3921	21.80	
HP bleed port		0.00	679.01	109.202	0.00	265.88	0.0	0.255427	1.3669	-0.07836	20.298	-	-	-	-	-	
HP bleed noz choke		0.00	570.79	57.191	0.00	238.57	0.0	0.249370	1.3792	-0.12215	10.631	-	-	1.00000	0.3942	0.00	
HP bleed exit static		0.00	258.88	3.458	0.00	162.74	0.0	0.239417	1.4013	-0.31385	0.643	-	-	2.89403	0.1000	0.00	
LP bleed port		0.00	365.84	15.984	0.00	188.42	0.0	0.240990	1.3976	-0.23086	2.971	-	-	-	-	-	
LP bleed noz choke		0.00	304.83	8.417	0.00	173.75	0.0	0.239836	1.4003	-0.27471	1.565	-	-	1.00000	0.3963	0.00	
LP bleed exit static		0.00	236.21	3.458	0.00	157.32	0.0	0.239336	1.4015	-0.33579	0.643	-	-	1.65628	0.3054	0.00	
	* W includes bleeds not extracted before HPC exit, gamma based on T exit not t, to avoid need for iteration																

Example Component Data Tabulation:

Combustors	Efficiency	Guess FF	WH	FF from	dT ref.	FAR in	W in	H*W in	H cooled	H*W Tref	dH*W	FAR out	W out	H*W out	H @ Tref	H*W Tref
		lb/s	CHU	DH lb/s	K		lb/s	CHU	to Tref		cooling		lb/s	CHU		
Combustor 1	1.0000	2.0653	21484.3	2.0653	897.82	0.00000	66.760	23272.3	172.151	11492.8	11779.6	0.03094	68.825	44756.6	172.406	11865.9
Combustor 2	1.0000	0.0000	0.0	0.0000	0.00	0.02904	73.181	34582.2	172.391	12615.8	21966.4	0.02904	73.181	34582.2	172.391	12615.8
Combined	-	2.0653	21484.3	2.0653	897.82	-	-	-	-	-	-	-	-	-	-	-

Figure 95 – Excel Model showing Typical Detailed Output Data

User general inputs:

General Inputs			Note user inputs have red text		
Fuel Lower Heating Value	CHU/lb	10222	MJ/kg	42.797	
Ref Fuel Temperature	K	298.15			
Fuel CP	CHU/lb.K	0.4777	kJ/kg.K	2.00	
Datum HPC last blade height	mm	13.00	for efficiency corrections		
HPC exit hub/tip ratio		0.925	see actual blade height below		
Cooled cooling air T3+ critical	K	900	set high to switch CCA off		
Index for scaling cooling air flow		0.65	set to 1, or to between 0.5		
Number of HP1 turbine stages		2	and 0.8 for scaling		

Iteration monitoring:

To iterate to a solution, copy values of bold blue cells below into bold red cells and repeat (function F4) until converged, or create a macro to do the same

For non-zero parameters, do not start with very small or "zero" guesses

Converged Models ?

	Climb	Cruise	Takeoff	
Overall	***YES***	***YES***	***YES***	
Tolerance on errors	0.0030%	0.0030%	0.0030%	
Iteration errors	0.0000%	0.0000%	0.0000%	
Mass flow error	0.00000	0.00000	0.00000	lb/s
Mass flow error	0.0000%	0.0000%	0.0000%	
Heat balance error	0.338	0.000	0.301	CHU
Heat balance error	0.0016%	0.0000%	0.0006%	

Mass flow error is re. total fan flow

Heat balance error is re. enthalpy in fuel

Top of the list of case specific inputs:

Cases	Climb	Cruise	Takeoff	Notes
Altitude ft	35000	35000	0	Geopotential altitude
Mach	0.82	0.82	0.25	
Dtamb deg. C	10	0	15	
Power offtake kW	260	260	260	from HPT

Iteration variables for design point:

Climb				Suggested
Design Point	**Guesses**	**Calculated**	**Errors**	**First Guesses**
γ fan mean	1.40102	1.40102	0.0000%	1.40
γ LPC mean	1.39984	1.39984	0.0000%	1.39
γ HPC mean	1.36628	1.36628	0.0000%	1.38
γ pre-comp mean	1.40141	1.40141	0.0000%	1.40
γ hot nozzle mean	1.33659	1.33659	0.0000%	1.36
γ cold nozzle mean	1.40120	1.40120	0.0000%	1.40
γ IC cool nozzle me'	1.40121	1.40121	0.0000%	1.40
γ CCACA nozzle me'	1.37923	1.37923	0.0000%	1.40
γ HP bleed mean	1.38753	1.38753	0.0000%	1.39
γ LP bleed mean	1.40011	1.40011	0.0000%	1.39
γ hot nozzle choked	1.34829	1.34829	0.0000%	1.36
γ cold nozzle choke'	1.40144	1.40144	0.0000%	1.40
γ IC cool nozzle ch'	1.40144	1.40144	0.0000%	1.40
γ CCACA nozzle ch'	1.38401	1.38401	0.0000%	1.40
γ HP bleed nozzle c'	1.37919	1.37919	0.0000%	1.39
γ LP bleed nozzle c'	1.40030	1.40030	0.0000%	1.39
dT HPT1	492.776	492.776	0.0000%	200
dT HPT2	0.000	0.000	0.0000%	0
dT LPT 1	568.194	568.194	0.0000%	400
dT LPT 2	0.000	0.000	0.0000%	0
dT c/a	0.0000	0.0000	0.0000%	0
dT c/a	0.0000	0.0000	0.0000%	0
dT c/a	-25.6491	-25.6491	0.0000%	-30
dT c/a	-5.8034	-5.8034	0.0000%	-4
dT c/a	0.0000	0.0000	0.0000%	0
dT c/a	-3.9988	-3.9988	0.0000%	-2
dT IC coolant	0.000	0.000	0.0000%	0
dT CCA coolant	337.940	337.940	0.0000%	50
dT HX	0.000	0.000	0.0000%	0
FF 1	2.0653	2.0653	0.0000%	1.45
FF 2	0.0000	0.0000	0.0000%	0.36
LPC dH*W	1850.08	1850.08	0.0000%	1452
HPC eta correction	0.0140	0.0140	0.0000%	0.00
CCA Flow	0.0600	0.0600	0.0000%	0.06
Sum of errors			0.0000%	

Iteration variables for off-design case:

				Suggested
Cruise	**Calculated**	**Calculated**	**Errors**	**First Guesses**
γ fan mean	1.40126	1.40126	0.0000%	1.40
γ LPC mean	1.40009	1.40009	0.0000%	1.39
γ HPC mean	1.37251	1.37251	0.0000%	1.38
γ pre-comp mean	1.40147	1.40147	0.0000%	1.40
γ hot nozzle mean	1.36446	1.36446	0.0000%	1.36
γ cold nozzle mean	1.40137	1.40137	0.0000%	1.40
γ IC cool nozzle me'	1.40138	1.40138	0.0000%	1.40
γ CCACA nozzle me'	1.40137	1.40137	0.0000%	1.40
γ HP bleed mean	1.39103	1.39103	0.0000%	1.39
γ LP bleed mean	1.40032	1.40032	0.0000%	1.39
γ hot nozzle choked	1.37150	1.37150	0.0000%	1.36
γ cold nozzle choke'	1.40150	1.40150	0.0000%	1.40
γ IC cool nozzle ch'	1.40150	1.40150	0.0000%	1.40
γ CCACA nozzle ch'	1.40150	1.40150	0.0000%	1.40
γ HP bleed nozzle c'	1.38468	1.38468	0.0000%	1.39
γ LP bleed nozzle c'	1.40044	1.40044	0.0000%	1.39
dT HPT1	449.483	449.483	0.0000%	200.00
dT HPT2	0.000	0.000	0.0000%	0.00
dT LPT 1	491.732	491.732	0.0000%	400.00
dT LPT 2	0.000	0.000	0.0000%	0.00
dT c/a	0.0000	0.0000	0.0000%	0.00
dT c/a	0.0000	0.0000	0.0000%	0.00
dT c/a	-13.8702	-13.8702	0.0000%	-30.00
dT c/a	-4.4319	-4.4319	0.0000%	-4.00
dT c/a	0.0000	0.0000	0.0000%	0.00
dT c/a	-2.5450	-2.5450	0.0000%	-2.10
dT IC coolant	0.000	0.000	0.0000%	0.00
dT CCA coolant	0.000	0.000	0.0000%	50
dT HX	0.000	0.000	0.0000%	0.00
FF 1	1.3917	1.3917	0.0000%	1.73
FF 2	0.0000	0.0000	0.0000%	0.35
LPC dH*W	1854.67	1854.67	0.0000%	1382.12
Core mass flow	69.11	69.11	0.0000%	72.61
Fan mass flow	1499.20	1499.20	0.0000%	1555.61
HPC pressure ratio	19.991	19.991	0.0000%	25.858
Fan pressure ratio	1.330	1.330	0.0000%	1.426
HPC exit Mn	0.2540	0.2540	0.0000%	0.25
Sum of errors			0.0000%	

Figure 96 – Excel Model Typical Input Data and Iteration Control

Appendix D THE TRUE MOTION OF A NUTATING DISC

The exact motion of a nutating disc depends on the constraint applied to it to prevent it from rotating, so a model was created using the 'Proper Euler Angles' method to accurately compute the true motions of a disc. Figure 97 shows the correct motions of five representative points on the rim of a nutating disc plotted through a complete cycle of nutation. In this example, nutation of a disc with axis X is constrained from rotation by a pin sliding in a slot in the z=0 plane in the static frame of reference (x, y, z). The angle of nutation α between the axes x and X is 30° (which exaggerates the displacements relative to a more practical angle of around 20° for the proposed topping-cycle modules).

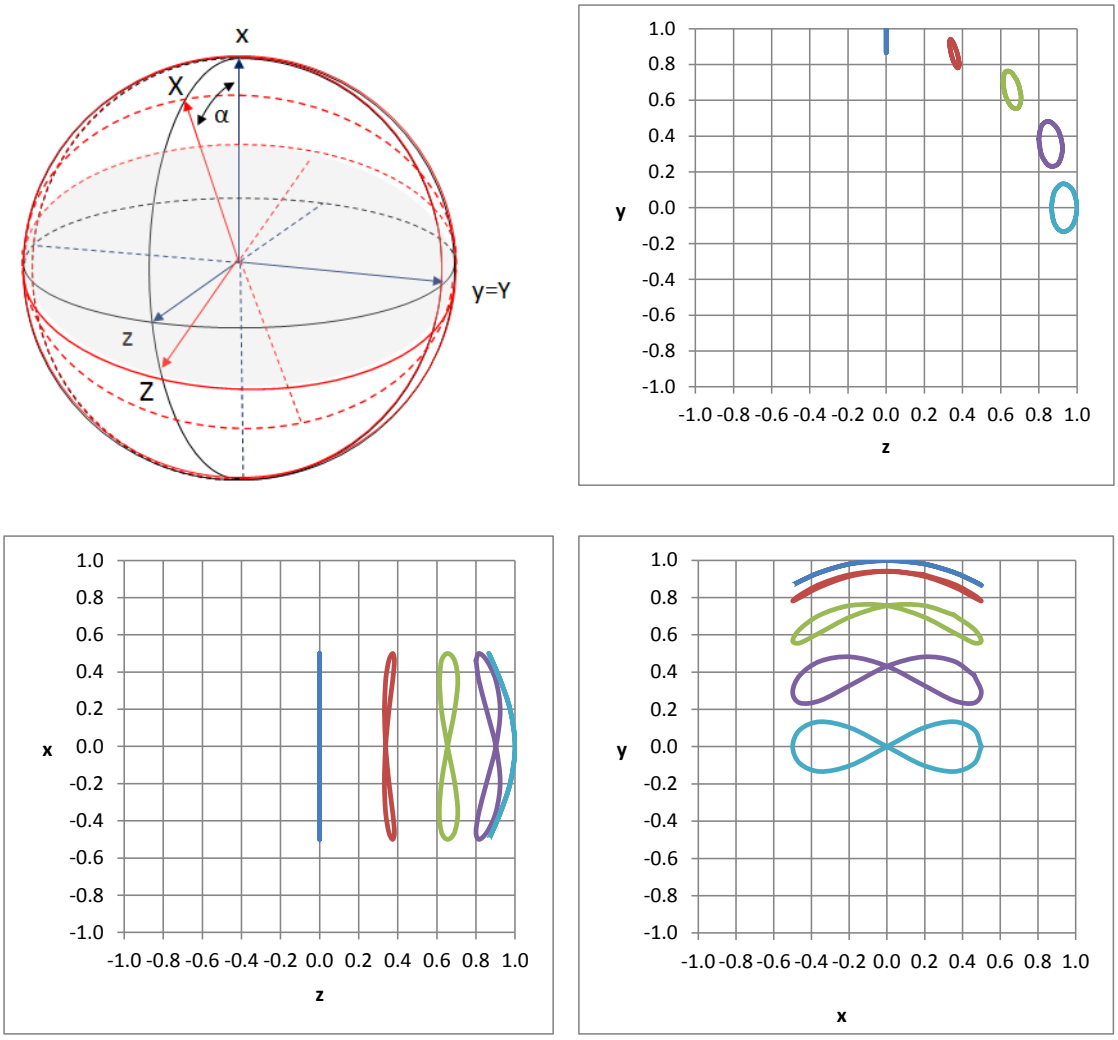

Figure 97 – True Paths of Points on the Rim of a Nutating Disc